A STUDY OF DEMODULATION TECHNIQUES IN FM PULSE COMPRESSION COMMUNICATIONS SYSTEMS, WITH EMPHASIS ON SIZE/WEIGHT ECONOMY

by

MICHAEL LESLIE RANCE, B.Sc.

A Thesis submitted to the University of London in support of an application for the degree of Doctor of Philosophy in Electrical Engineering.

Imperial College of Science and Technology.

Place of research: Royal Aircraft Establishment, Farnborough.

To my wife, Lynda

ABSTRACT

A study of demodulation techniques in FM pulse compression communications systems, with emphasis on size/weight economy

by

M.L.Rance

The investigations undertaken were into means of significantly reducing the physical size of the dispersive network used in the demodulation process in a chirp satellite communications system. Non-linear FM waveforms were examined and their performance assessed in terms of compressed and dispersed pulse responses. A novel technique for using a cascade arrangement of identical passive networks to more efficiently use the delay characteristic of such networks was studied both theoretically and by means of a practical demonstration.

Digital filter techniques were also studied. In particular, and by extension of the passive network ideas, a cascade arrangement of identical first order digital all-pass filters was proposed. Performance characteristics such as compressed and dispersed pulse shapes and error rate performance in the presence of noise were examined. The effects of quantization of input data, coefficients and multiplier outputs were studied and the differences between truncation and rounding in multi-section cascaded all-pass filters examined.

A practical simulation of pulse compression using a 42 section digital filter employing signal recirculation was undertaken and exact agreement was obtained with computer simulations employing 2's complement arithmetic and multiplier output truncation.

Finally a highly simplified digital filter solution was proposed which could be realised using a minimum number of MOS IC chips. The significant advance was to remove the necessity for complex digital multipliers and replace them with a simple interconnection scheme.

LIST OF CONTENTS

		Page
List of Figures		v
List of Symbols		vi
Chapter 1 :	Chirp Modulation	
1.1	Introduction	1
1.2	The chirp signal	1
1.3	The spectrum of a chirp signal	2
1.4	The concept of pulse compression	3
1.5	Matched filter response	6
1.6	Chirp communications	7
1.7	Error rates in the presence of noise	11
Chapter 2 :	Description of the problem with possible solutions	
2.1	Introduction	12
2.2	The all-pass time delay network	12
2.3	Conventional dispersive network design	16
2.4	Construction of dispersive network	19
2.5	Linear delay approximation methods	22
2.6	All-pass active networks	23
2.7	Digital filter methods	26
2.8	Summary of proposed investigations	28
Chapter 3 :	Nonlinear FM Systems	
3.1	Introduction	30
3.2	Design criteria	30
3.3	Power law frequency functions	31
3.4	Modified power law functions	36
3.5	Power law functions with all-pass filter	38
3.6	Logarithmic phase signals	40
3.7	Exponential phase signals	42
3.8	Dispersed pulses for nonlinear FM signals	44
3.9	Comparison of nonlinear functions	45
Chapter 4 :	Identical Section Passive Filter Method	
4.1	Introduction	47
4.2	Basic ideas	47
4.3	Signal design	49

Page

4.4 Complete demodulator 53

4.5 Implications and discussion 54

4.6 Further developments 57

Chapter 5 : An experimental identical section LC filter pulse compression system

5.1 Introduction 60

5.2 Bridged-T network design 60

5.3 Signal generation 61

5.4 Demonstration of pulse compression 62

5.5 Complete system 63

5.6 Summary and discussion 64

5.7 Conclusions 65

Chapter 6 : A Digital Filter Technique employing Cascaded Identical Sections

6.1 Introduction 66

6.2 State of the art 66

6.3 Brief summary of digital filter theory 67

6.4 Principles of pulse compression system using digital all-pass sections 72

6.5 Signals, spectra and conditions 72

6.6 Centre frequency of signal 74

6.7 The complete system 75

6.8 Quantisation and word length 76

6.9 Computer simulations 81

6.10 Probability of error 82

6.11 Discussion 87

Chapter 7 : An Experimental All-pass Digital Filter and Demonstration of Pulse Compression

7.1 Introduction 89

7.2 Serial arithmetic 89

7.3 Arithmetic units 90

7.4 Multiplexing 95

7.5 Additional circuits 96

7.6 Filter testing 97

7.7 Demonstration of pulse compression 100

7.8 Conclusions 103

Page

Chapter 8 : Summary, Conclusions and further Developments

8.1 Summary of achievements 104

8.2 Further developments 105

8.2.1 Simplest conceivable multiplier 106

8.2.2 Complete first order section 107

8.2.3 Operating speed 107

8.2.4 Performance aspects 108

8.2.5 Summary 109

Appendix A : The Spectrum of a chirp pulse 110

Appendix B : The principle of stationary phase 112

Appendix C : Error rate for chirp system employing an ideal synchronised demodulator 116

Appendix D : Nonlinear FM - derivation of dispersed pulse expressions 118

Appendix E : Envelope of compressed pulse in digital filter system 124

Appendix F : Comparison between truncation and rounding in the multi-section digital filter solution 126

Figures

References

Acknowledgements

LIST OF FIGURES

Chapter 1

1.1 The chirp signal

1.2 Amplitude spectrum of a chirp pulse

1.3 Phase Spectrum of a chirp signal - difference between exact expression and stationary phase approximation

1.4 Group delay specification of a chirp filter

1.5 Output of a chirp matched filter

1.6 Chirp demodulator

1.7 Error rates of binary data transmission systems

Chapter 2

2.1 Second order all-pass lattice and its pole-zero locations

2.2 Group delay of second order all-pass network

2.3 Bridged-T all-pass network

2.4 Linear delay/frequency response obtained by adding responses of second order sections

2.5 Placing of second order sections with centre frequencies at unit area intervals

2.6 Use of resistive hybrid network to halve the size of a dispersive delay network

2.7 Bridged-T network including stray capacitances

2.8 Open and short-circuit impedances of the bridged-T network

2.9 Active all-pass networks due to Holt and Gray, and Deliyannis

Chapter 3

3.1 Typical nonlinear delay vs frequency response

3.2 Power law signals - frequency vs time

3.3 Power law signals - stationary phase spectra

3.4 Quadratic FM - exact spectrum

3.5 Compressed pulse envelope - power law signal, matched filter

3.6 Modified power law signals - frequency vs time

3.7 Modified power law signals - stationary phase spectra

3.8 Compressed pulse envelope - modified power law signal, matched filter

3.9 Compressed pulse envelope - power law signal, all-pass filter

3.10 Compressed pulse envelope - modified power law signal, all-pass filter

3.11 Logarithmic phase signals - frequency vs time

3.12 Logarithmic phase signals - stationary phase spectra

3.13 Compressed pulse envelope - logarithmic phase signal, matched filter

3.14 Compressed pulse envelope – logarithmic phase signal, all-pass filter

3.15 Exponential phase signals – frequency vs time

3.16 Exponential phase signals – stationary phase spectra

3.17 Compressed pulse envelope – exponential phase signal, matched filter

3.18 Compressed pulse envelope – exponential phase signal, all-pass filter

3.19 Dispersed pulse envelope – logarithmic phase signal, matched filter

3.20 Nonlinear FM signals – delay area to be synthesised as a percentage of linear chirp filter area

Chapter 4

4.1 Group delay of second order all-pass section using approximate expression

4.2 Illustration of dispersive delay response using cascaded identical sections

4.3 Instantaneous frequency of a {1,0} bit pattern (before demodulator)

4.4 Relationship between the number of identical sections and their Q_e factor

4.5 Stationary phase spectra of signals matched to identical section dispersive filter

4.6 Compressed pulse envelope – identical section dispersive system, matched filter

4.7 Compressed pulse envelope – identical section dispersive system, all-pass filter

4.8 Dispersed pulse – identical section dispersive system, matched filter

4.9 Dispersed pulse – identical section dispersive system, all-pass filter (n = 40,60)

4.10 Dispersed pulse – identical section dispersive system, all-pass filter (n = 48,70)

4.11 Block diagram of complete demodulator

4.12 Magnitude and delay response of 7th order low pass elliptic function filter

4.13 Group delay difference between exact and simplified expressions

4.14 Identical section dispersive system (n = 48) – exact spectrum

4.15 Identical section dispersive system FT = 38.88, F = 46.66, n = 56 – spectrum magnitude

Chapter 5

5.1 Comparison of measured and theoretical delay response of 12 section network

5.2 Technique for generation of stepped modulating waveform

5.3 Oscilloscope photograph of stepped modulating waveform

5.4 Block diagram of {1,0} sequence generator

5.5 Oscilloscope photograph of {1,0} modulating waveform

5.6 Experimental arrangement for pulse compression demonstration

5.7 Oscilloscope photographs of compressed pulses

5.8 Block diagram of complete experimental arrangement

5.9 Oscilloscope photographs of signals and spectra at input and output of dispersive network

5.10 Oscilloscope photographs of signals and spectra at output of high pass and low pass filters

5.11 Oscilloscope photographs of spectra

Chapter 6

6.1 Layout of generalised digital filter - direct form

6.2 Recursive realisation of generalised digital filter

6.3 Parallel and cascade forms of digital filters

6.4 Group delay response of first order digital all-pass delay network

6.5 Different realisations of first order digital delay network

6.6 Relationship between number of identical sections and coefficient of each one

6.7 Demonstration of maximum "jitter" on rectified output

6.8 Demonstration of maximum "jitter" for sampled system with $2fo/F = 1$

6.9 Scheme for obtaining output envelope

6.10 Complete digital filter pulse compression demodulator

6.11 Overall phase error of 42 sections for various coefficient word lengths

6.12 Effect of coefficient quantization on compressed pulse envelope ($N = 42$, $a = 0.34860$, 14 bit binary 0.01011001001111)

6.13 Typical output errors for 9 and 11 bit input quantization (exact filtering) ($N = 30$, $a = 0.445362$)

6.14 Typical output errors for 9 and 11 bit multiplier rounding ($N = 30$, $a = 0.445362$)

6.15 Multiplicative round off error - rms output noise as a function of number of identical sections

6.16 Compressed pulse envelopes - exact computation, no quantization ($\phi_{in}(t = o) = 0$)

6.17 Compressed pulse envelopes - exact computation, no quantization ($\phi_{in}(t = o) = 0$)

6.18 Dispersed pulse envelope - digital system $N = 34$

6.19 Uniform Gaussian noise containing no frequencies higher than F, synthesised from random samples

6.20 Error probability for 42 section digital system (synchronised) FT = 33.33

6.21 Error probability for various gating times ($N = 42$)

Chapter 7

7.1 Practical serial adder

7.2 Practical two's complementer

7.3 Serial/parallel multiplier scheme

7.4 Timing diagram for serial/parallel multiplier

7.5 Multiplexed or recirculating first order digital delay section

7.6 Multiplier truncation circuit

7.7 Multiplier sign bit detection and extension circuit (E) and control waveforms

7.8 Sample sequences generated by test signal generator

7.9 Block diagram of test signal generator

7.10 Test signal generator - word gating waveforms

7.11 Test signal generator - word signal control waveforms

7.12 Test signal generator - timing and control waveform circuit

7.13 Test signal generator - sign control circuit

7.14 Test signal generator - word gating waveform circuit

7.15 Test signal generator - stored samples and output shift registers

7.16 Test signal generator - sign selection circuit

7.17 Practical digital to analogue converter

7.18 Oscilloscope photographs of filter response to constant frequency sampled waveforms from test signal generator

7.19 Approximate sampled waveform generated as input to digital pulse compression filter

7.20 Simulation of 42 section filter using 14 times recirculation, with control waveforms

7.21 Output from 42 sections - response to approximated swept waveform (Fig 7.19) - computed response, true truncation

7.22 Oscilloscope photographs of approximate sweep and compressed pulse

7.23 Output from 42 sections - response to approximated swept waveform (Fig 7.19) - computed response, 2's complement truncation

Chapter 8

8.1 One's complement parallel adder

8.2 Single section first order digital delay, a = 0.25, using parallel one's complement arithmetic

8.3 Proposed scheme for 9 times recirculation of signal

8.4 Compressed pulse envelope for N = 63, a = 0.25

Appendix E

E1 Stationary phase spectrum of signal matched to 42 section digital filter response

Appendix F

F1 Probability density functions of multiplier errors for rounding and 2's complement truncation

F2 Compressed pulse envelopes (N = 50) showing effect of rounding and truncation with 7 and 11 bit quantization

LIST OF SYMBOLS

a	constant; digital filter coefficient
a_k, b_k	digital filter coefficients
$\alpha(\omega)$, β	phase function
C_A, C_B, L_A, L_B, C_a, C_b	capacitances and inductances in bridged-T network
$C_2(y)$, $S_2(y)$	Fresnel Integrals
C_1, C_2, C_3	capacitances in RC active network
Δt	sampling interval
ε	quantising interval
$f_1, f_2, f(t), f_o, f_c, f_d, f_s$	various frequencies - constants, functions of time, Hz
F	nominal sweep bandwidth, Hz
g_1, g_2	conductances in RC active network
$g(t)$	output signal
$G(\omega)$, $G(t)$	output spectrum
$H(\omega)$, $H(f)$	frequency response of a filter
$h(t)$	impulse response of a filter
$\theta(t)$, θ_c, $\theta'(t)$, $\theta''(t)$	phase angles; functions of time, derivatives, constants
$\Phi(\omega)$, $\Phi(f)$	phase spectrum
$\theta(f)$	phase response of filter
k	normalising constant
n, N	number of sections in filter (passive, digital)
Q_e	effective Q-factor of group delay network
Q	loss factor of inductor
s	imaginary frequency variable
σ_o, $\bar{\omega}_o$	poles and zeros
$\tau(\omega)$, $\tau(f)$	group delay function, seconds
ϕ	insertion phase of network
u_n, v_n	input, output samples of digital filter
$U(z)$, $V(z)$	z-transform of u_n, v_n
σ^2	power spectral density
D	dispersion factor
T	bit period
$y(nT)$, $x(nT)$	output, input samples of digital filter
Z_a, Z_b, Z_A, Z_B, Z_s	impedances
Y_p	admittance
V_1, V_2	voltage
$s(t)$	signal
$S(\omega)$, $S(f)$	spectrum of $s(t)$

Chapter 1

CHIRP MODULATION

1.1 Introduction

The concept of pulse compression occurred to several independent workers during the course of World War II as a means of overcoming transmitter power limitations in radar systems. Furthermore, the wide-band signals envisaged improved both range and velocity resolution as well as reducing the effects of many types of interference.

Development of the ideas continued after the war until the techniques began to be applied in many types of radar, especially where transmitters were peak power limited. Most of the early work concentrated on the linearly swept FM signal[1], and most new work uses it as a means of comparison. The word 'chirp' was coined by B M Oliver[2], as a description of the linear FM signal. The practical methods have for the most part centred on linear FM, and it is a part of the purpose of this work to investigate other waveforms, and to show how practical considerations can influence signal design in cases where optimum signals based on radar criteria are not necessary.

However, first we shall examine chirp modulation and pulse compression, leaving practical matters until the next chapter. For the purposes of illustration, signal parameters where quoted will refer to work performed[3] in Radio Department at the Royal Aircraft Establishment, Farnborough which has been aimed at an airborne communications application.

1.2 The chirp signal

The chirp signal is a swept FM waveform in which the instantaneous frequency sweeps linearly with time between frequency limits f_1 Hz and f_2 Hz, during a time period T seconds. So, the instantaneous frequency, $f(t)$, may be expressed as:

$$f(t) = f_1 + \left(\frac{f_2 - f_1}{T}\right) t \qquad 0 \leqslant t < T \ . \qquad (1\text{-}1)$$

The difference $|f_2 - f_1|$ Hz will be referred to as the nominal sweep bandwidth, F Hz. The chirp signal, $s(t)$, is then expressed as:

$$s(t) = a(t) \sin\left\{\theta(t) + \theta_c\right\} \qquad 0 \leqslant t < T \ , \qquad (1\text{-}2)$$

where $a(t)$ is the time dependent amplitude function, here considered to be a constant equal to unity,

$\theta(t)$ is the time dependent phase function,

and θ_c is a constant phase angle.

The time dependent phase, or instantaneous phase angle is related to the instantaneous frequency by the relation:

$$2\pi f(t) = \frac{d\theta(t)}{dt} \ , \qquad (1\text{-}3)$$

which gives the following on substitution in equation (1-2):

$$s(t) = \left\{\sin 2\pi\left[f_1 t + \frac{Ft^2}{2T}\right] + \theta_c\right\} \ , \qquad (1\text{-}4)$$

General signal and frequency functions are illustrated in Fig.1.1 for an upward going sweep (i.e. $f_2 > f_1$). In radar applications the above equations are sufficient to define the chirp signal, but for communications it should be mentioned that a similar signal is defined when $f_2 < f_1$. This is a downward sweep within the same nominal sweep bandwidth and of the same duration; a binary scheme is achieved with an upward sweep representing a one, and a downward sweep representing a zero.

1.3 The spectrum of a chirp signal

It will be necessary at a later stage to have expressions available for the spectrum of chirp signals, and of other swept FM waveforms as they arise. An exact derivation has been published elsewhere[4], but for completeness, some details are given in Appendix A. The spectrum $S(f)$, of a time limited signal, $s(t)$, is given by the Fourier integral:

$$S(f) = \int_0^T s(t) e^{-j2\pi ft} dt \ . \qquad (1\text{-}5)$$

As Appendix A shows, exact solutions of the integral take the form of tabulated functions; no analytic solution is possible, and the expressions do not allow easily for further manipulation. However, for many purposes, including the design of new signals, there exists a useful approximation to the problem of spectrum calculations. This is the principle of stationary phase[5] (explained briefly in Appendix B) which gives approximate formulae for the spectra of signals which have large values of the time-bandwidth product, FT . The larger the value of FT , the better is the approximation.

With this approximation, the power spectrum of a chirp signal is rectangular between the frequency limits f_1 and f_2 . This is obviously a simplification, since time limited functions cannot have frequency limited spectra, but comparison with the exact spectrum as derived in Appendix A, (see Fig.1.2) shows that the approximation is likely to be valid for practical purposes.

Thus:

$$|S(f)| \doteqdot \begin{cases} \frac{1}{2}\sqrt{\frac{T}{F}} & f_1 < f < f_2 \\ 0 & \text{elsewhere} . \end{cases}$$

Similarly, the phase spectrum $\Phi(f)$, is given approximately, by:

$$\Phi(f) \doteqdot -\frac{\pi T}{F}(f_0 - f)^2 \quad , \qquad (1\text{-}6)$$

where $f_0 = (f_1 + f_2)/2$ is the centre frequency of the sweep. Fig.1.3 is the difference between the exact phase spectrum and this approximate expression; the difference is essentially a constant phase angle.

Both Figs.1.2 and 1.3 illustrate spectra of a chirp signal with $FT = 33.3$, which is the value used in the Royal Aircraft Establishment work.

1.4 The concept of pulse compression

Pulse compression can only occur when the waveform to be compressed has phase dispersion, defined as the part of its phase spectrum which varies non-linearly with frequency. To understand this, consider two pulses having identical amplitude spectra, one with phase dispersion and the other without. The pulse with no phase dispersion has all frequency components of the same phase, and so the magnitude of its envelope, being the vector sum of all components, cannot be greater. However, since the

frequency components of the phase dispersed pulse are not all the same, the magnitude of its envelope must be smaller than the magnitude of the other pulse. It follows that, removal of the phase dispersion from a pulse increases its amplitude, and consequently decreases its duration, by conservation of energy.

The chirp signal, with an approximately parabolic phase spectrum, evidently fulfils the condition for a signal to be pulse compressed. Since the phase dispersion of the output of a network is the sum of the dispersion of the network and the input waveform, it follows that a pulse compression network must have a phase dispersion equal and opposite in sign to that of the pulse.

The amplitude response of the network, for optimum signal-to-noise ratio, must be equal to the magnitude of the spectrum of the pulse.

These conditions, describing a matched filter, were first derived by North[6] as the properties of the optimum receiver in a white Gaussian noise environment.

Mathematically, the response of the matched filter, $H(\omega)$, to a signal with a spectrum, $S(\omega)$ is:

$$H(\omega) = kS^*(\omega)$$

where the asterisk denotes the complex conjugate and the factor k is a normalizing constant. Thus if:

$$S(\omega) = |S(\omega)|e^{j\Phi(\omega)}$$

then

$$H(\omega) = k|S(\omega)|e^{-j\Phi(\omega)} .$$

The spectrum of the output waveform, $G(\omega)$, is

$$\begin{aligned} G(\omega) &= H(\omega)S(\omega) \\ &= k|S(\omega)|^2 , \end{aligned}$$

i.e. the phase dispersion $\Phi(\omega)$ has been removed.

The output signal, given by the inverse Fourier transform of the output spectrum is:

$$g(t) = k\int_{-\infty}^{\infty} |S(\omega)|^2 e^{j\omega t}\,\frac{d\omega}{2\pi}$$

$$= k\int_{-\infty}^{\infty} |S(f)|^2 e^{j2\pi ft}\,df \quad . \qquad (1\text{-}7)$$

In particular, the network matched to the chirp signal described above has an amplitude response

$$|H(f)| = k|S(f)|$$

$$= \begin{cases} \frac{k}{2}\sqrt{\frac{T}{F}} & f_1 < f < f_2 \\ 0 & \text{elsewhere} \end{cases} \quad . \qquad (1\text{-}8a)$$

Setting $k = 2\sqrt{\frac{F}{T}}$,

$$|H(f)| = \begin{cases} 1 & f_1 < f < f_2 \\ 0 & \text{elsewhere} \end{cases} \quad .$$

Its phase response, $\arg\{H(f)\} = \Theta(f)$, is:

$$\Theta(f) = \frac{\pi T}{F}(f_0 - f)^2 \qquad (1\text{-}8b)$$

and its group delay response, $\tau(f)$ is:

$$\tau(f) = -\frac{d\Theta(f)}{2\pi df}$$

$$= \frac{T}{F}(f_0 - f) \quad . \qquad (1\text{-}8c)$$

To achieve a realisable delay function a constant delay t_c (equivalent to a non-distorting linear phase function) must be added to this expression, giving a linear delay/frequency response as shown in Fig.1.4.

Thus, a 'long' signal with phase varying nonlinearly with time will be compressed in time and increased in amplitude by a network with the properties of a matched filter as defined above. For radar purposes, the design problem is to define the amplitude and phase characteristics of a waveform and its associated filter in order to achieve the best output pulse for the particular purpose. In general, the criteria used in this design process are minimisation of both the time width and the sidelobe level of the compressed pulse[5], together with optimum unambiguous performance in the presence of Doppler shifted signals. The next section examines the output pulse in a chirp system, and outlines the techniques used to obtain optimum waveforms.

1.5 Matched filter responses

1.5.1 Exact response

The time domain relationship, corresponding to the matched filter frequency domain defining equation:

$$H(\omega) = S^*(\omega)$$

states that the impulse response of the matched filter is a replica of the time inverse of the signal. Thus, the impulse response, $h(t)$, of a filter matched to a signal $s(t)$ is:

$$h(t) = ks(-t) .$$

The output signal is given by the convolution integral:

$$g(t) = k\int_0^t s(\tau)s(t-\tau)d\tau$$

which is the autocorrelation function of $s(t)$.

Evaluation of this integral gives the following result:

$$g(t) = \sqrt{FT}\,\frac{\sin\left[\frac{\pi Ft}{T}\left(T - |t|\right)\right]}{\pi Ft}\cos\omega_0 t \qquad (1\text{-}9)$$

the envelope of which (Fig.1.5) closely resembles the $(\sin x/x)$ function.

Equation (1-9) represents the output waveform resulting from the application of a chirp signal (equation (1-4)) to a network which is perfectly matched to it. The following points concerning Fig.1.5 are worth noting:

(a) There are nulls at multiples of $2/F$ seconds, the first nulls being separated by about $2/F$ seconds.

(b) The peak amplitude is $\sqrt{FT}$.

(c) The pulse width at -4 dB from the peak is $2/F$ seconds.

(d) The main lobe of the envelope (between the first nulls) contains $2\,f_0/F$ cycles of carrier (frequency f_0 Hz).

1.5.2 Practical filter response

A truly matched filter would have to match both the exact amplitude spectrum and the exact phase spectrum as given in Appendix A. This is evidently impractical. The most reasonable practical approximation is the response obtained using the simplifying principle of stationary phase: a rectangular amplitude response, ignoring the Fresnel ripples shown in Fig.1.2,and a parabolic phase response ignoring the residual phase angle Fig.1.3.

Forgan[7] has made a detailed analysis of the effect of using a practically realisable dispersive network as an approximation to a matched filter. For the parameters used in the RAE system, there is a reduction in peak amplitude of 0.35 dB, together with a slight broadening of the main lobe.

1.5.3 Response to a mismatched signal

For the purpose of a communication system two waveforms are required to represent the two binary states, and in chirp these two waveforms are defined by the direction of frequency sweep. Therefore, a mismatched signal is one whose sweep direction is opposite to that of the signal to which a network is matched. In a system using orthogonal signals, there would be no output when a mismatched signal is applied to a network. However, an output is obtained in chirp, and its form is calculated in a similar manner to the matched response.

Again, Forgan[7] has derived exact expressions for the mismatched output. In essence, the signal is dispersed over two pulse periods, 2T seconds, and has a mean amplitude of $1/\sqrt{2}$ of the input amplitude. At the decision making stage in the demodulation process, the mismatched output or dispersed pulse, effectively adds to the existing noise in the zeros channel, and consequently degrades the error rate as compared to a system employing orthogonal signals.

1.6 Chirp communications

With the signals and responses so far defined, we are now in a position to describe a complete chirp communication system. The transmitted signal is a series of chirp signals with the direction of sweep depending upon the binary value of the data. Each sweep has a duration of T seconds, and a nominal sweep bandwidth of F Hz. The data rate is 1/T baud and consequently there is no pause between successive sweeps. The centre frequency of the transmitted signal will naturally depend upon the frequency band being used. As far as the RAE experiments are concerned, the VHF, UHF and L-bands have so far been used; L-band

trials are in progress. Whatever radio frequency is chosen, frequency translation is required at the receiver to enable the pulse compression networks to operate in the optimum practicable frequency range.

The transmitted signal is at a constant amplitude level during transmission of a message, and so optimum use is made of any power limitation in the transmitters or relays envisaged in a complete two-way system (e.g. aircraft or satellites).

There are several methods by which the chirp signals can be generated; they are well described elsewhere[1]. The RAE system so far tested employs gated voltage ramps modulating a frequency synthesiser, on a ground to air link. An air to ground link would require special purpose frequency modulators for use in the aircraft.

A typical chirp demodulator is illustrated in block diagram form in Fig.1.6. The receiver output is fed to a pair of frequency changers each of which has a different frequency applied to it; the frequencies of the two oscillators are arranged such that the mixer output in one channel has its sweep direction reversed, whereas the sweep direction in the other channel is left unaltered.

If the centre frequency of the receiver output is f_c and the required centre frequency after mixing is f_0 then the two oscillator frequencies are $(f_c + f_0)$ and $(f_c - f_0)$. The sweep direction of the difference signal is inverted in the first case, and unaltered in the second case.

This technique enables identical pulse compression networks to be used in each channel; in particular, it is easier to design a network whose delay function has a negative slope than one with a positive slope. The output of each dispersive network will consist of a sequence of compressed and dispersed pulses, and it is the purpose of the following circuits to determine which has occurred in which channel.

Amplitude clipping circuits followed by Schmitt trigger and monostable circuits complete the functions of each channel (in the RAE scheme), and a bistable circuit driven by the two monostables, reconstitutes the data. Other alternatives, such as peak-read and store modules after the dispersive networks, have been suggested[7]; they are refinements to the basic system and are not discussed any further here.

1.6.1 RAE system parameters

The chirp system being studied in Radio Department, RAE was designed to operate in the VHF/UHF frequency bands at a data rate of 1200 baud. The nominal sweep bandwidth is 40 kHz, which was chosen to be well within the then extant channel spacing of 50 kHz. The centre frequency, f_0 of the signal during compression and therefore of the dispersive network, was 108 kHz; the reason for this choice will be explained in the next chapter.

A summary of the RAE system parameters is given below.

Data rate		1200 baud
Pulse length	T	833.3 μs
Nominal sweep bandwidth	F	40 kHz
Centre frequency	f_0	108 kHz
Dispersion factor	FT	33 1/3
No. of cycles within main lobe	$\frac{2f_0}{F}$	5.4

1.6.2 Multipath interference effects

Multipath interference occurs when more than one signal path exists between the transmitter and the receiver. In airborne communications using satellite relays the most significant multipath effect is on the aircraft/satellite link where in addition to the direct path, the signal can be reflected from the surface of the earth. The time delay of the reflected signal relative to the direct signal depends on the position of the aircraft relative to the satellite.

On North Atlantic routes this delay varies from 30 to 60 microseconds for typical aircraft altitudes (25000 to 50000 ft), with a geostationary satellite stationed at 30° W. The strength of the reflected signal will vary according to the sea state condition, and will in general be less than the direct signal strength. A reflected signal will give rise to a compressed pulse at the appropriate dispersive network output (and a dispersed pulse in the other channel). Significant interference will occur if the main lobe overlaps the main lobe of the direct pulse; that is, if the delay time is less than 2/F seconds. Less interference occurs for longer delays.

To prevent intersymbol interference, the data period, T, should be large compared with the expected multipath delays.

Since the half-width $2/F$ is 25 μs and the data period is 833 μs, the RAE system meets both conditions for multipath immunity.

1.6.3 Doppler shift effects

The received signal will suffer a Doppler frequency shift dependent upon the relative velocity of the aircraft with respect to the satellite. It can be shown that[7] a chirp pulse Doppler shifted by f_d Hz is equivalent to an unshifted pulse displaced by $(f_d/F)\ T$ seconds and of duration $[1 - |f_d/F|]T$ seconds.

This has the effect of reducing the dispersion factor in a system which expects a standard signal. The effective dispersion factor becomes

$$(FT)' = \left\{1 - \left|\frac{f_d}{F}\right|\right\} FT$$

and the peak amplitude of the compressed pulse is then:

$$\text{peak amplitude} = \left\{1 - \left|\frac{f_d}{F}\right|\right\}^{\frac{1}{2}} \sqrt{FT} \quad .$$

As long as the nominal sweep bandwidth, F Hz, is large compared with the expected Doppler shifts, then the effect is small.

In practice, the maximum Doppler shifts are as follows, for aircraft flying at Mach 2.2:

At VHF	330 Hz
At UHF	880 Hz
At L-band	3500 Hz .

Thus, even at L-band, the maximum loss in peak amplitude is only 0.8 dB. There are plans to increase the bandwidth for L-band operation to 80 kHz, in which case the maximum loss will be less than 0.4 dB.

1.7 Error rates in the presence of noise

Multipath interference and Doppler frequency shifts are effects which a modulation system must be able to cope with on airborne communication links. However, comparison of modulation systems is usually made on the basis of their performance in the presence of noise alone. Conventionally the measure of performance is the probability of error when Gaussian noise is added before the receiver.

Forgan[7] has analysed the chirp system with Gaussian noise. The results are given in Fig.1.7 which compares the chirp results with standard curves, obtained by other workers[8], for the more common binary modulation methods.

For the purposes of the analysis the significant factor determining the error probability is the ratio of compressed pulse peak amplitude to dispersed pulse amplitude. (Appendix C gives a brief description of the relevant expressions in the error rate analysis.)

For a small change in the dispersion factor, results show that the signal to noise ratio required for a given error rate changes by the same amount, in dB. Thus, a reduction of 0.5 dB in the compressed/dispersed pulse ratio yields a corresponding 0.5dB degradation in the signal-to-noise ratio required for a given error rate. This is not true for all dispersion factors, but in the regions of interest it is substantially true. Advantage is taken of this factor in the work described in a later chapter.

The apparently inferior performance of chirp systems compared with other binary schemes perhaps requires further comment. The most significant factor is the non-orthogonality of the signals used to represent a one and a zero, as evidenced by the presence of a dispersed pulse the equivalent of which is not present in an orthogonal system. Second, a truly orthogonal system would be coherent, which the chirp system is not. And third, truly matched filters are impossible to manufacture.

However, accepting this inferior performance in the presence of white noise, it should be noted that performance in the presence of multipath signals and large Doppler shifts were dominant reasons for the choice of chirp for airborne communications studies.

Although detailed comparisons in this environment have not been performed (to the author's knowledge) for the required system parameters, it is generally accepted that most systems are seriously degraded by multipath propagation and large Doppler shifts which vary with time. Chirp modulation offers a solution in such cases.

Chapter 2

DESCRIPTION OF THE PROBLEM WITH POSSIBLE SOLUTIONS

2.1 Introduction

The central problem in the design of chirp communications equipment is the synthesis and implementation of the dispersive network, which performs the compression process on the chirp signal, converting it into a narrow pulse of increased amplitude. The basic response is shown in Fig.1.4 In the radar applications of chirp, many techniques have been developed over the years. These include ultrasonic devices[9], diffraction gratings[10,11], tapped-delay lines[12,13], microwave waveguides[14] and, more recently, acoustic- and elastic-surface waves[15,16] and optical methods[17]. In general these techniques were designed with radar applications in mind where bandwidths of several MHz are required.

However, perhaps the most common technique is equally applicable at 100 kHz as at 100 MHz, in fact in any frequency range where wire-wound inductors are practicable. The technique employs lumped constant filters based on the bridged-T equivalent of the all-pass constant resistance lattice network. Although the other techniques are supplanting the inductor/capacitor (LC) methods in radar, the first attempts in communications have used these ideas, which were originally developed for radar matched filters. In particular, the RAE system uses a design which was frequency scaled from an original radar design[18].

This chapter examines the conventional passive LC filter methods, and the problems of practical implementation; it then summarises the possible alternative approaches indicating the most promising solutions.

2.2 The all-pass time delay network

2.2.1 The second order all-pass lattice

The basic building block of lumped constant dispersive filters is the second order all-pass lattice section shown in Fig.2.1a. The image impedance of the network is

$$Z_i = \sqrt{Z_a Z_b}$$

and the transfer function is

$$\frac{V_2}{V_1} = \frac{1 - \sqrt{Z_a/Z_b}}{1 + \sqrt{Z_a/Z_b}} \quad .$$

If $Z_a Z_b = 1$, then $Z_i = 1$ and

$$\frac{V_2}{V_1} = \frac{1 - Z_a}{1 + Z_a} \quad . \tag{2-1}$$

Further, if Z_a is a pure reactance, $Z_a = jX_a$, then

$$\frac{V_2}{V_1} = \frac{1 - jX_a}{1 + jX_a} = \exp\{- j2 \arctan X_a\} \quad .$$

So, under these conditions the network is all-pass (i.e. the magnitude of V_2/V_1 is unity), and the phase response function, β is

$$\beta = - 2 \arctan X_a \quad . \tag{2-2}$$

This type of network is called a constant resistance ($Z_i = 1$) all-pass delay network.

If the impedance Z_a is a parallel tuned circuit with an inductance, L_a , in parallel with a capacitance, C_a , then

$$Z_a(s) = \frac{sL_a}{1 + s^2 L_a C_a} \quad .$$

With $s = j\omega$ and $s^2 = -\omega^2$, substituting in equation (2-1), the transfer function becomes

$$\frac{V_2}{V_1} = H(s) = \frac{s^2 L_a C_a - sL_a + 1}{s^2 L_a C_a + sL_a + 1} \quad .$$

With the following designations,

$$L_a C_a = \frac{1}{\bar{\omega}_0^2} \qquad \text{and} \qquad C_a = \frac{1}{2\sigma_0}$$

this function becomes

$$H(s) = \frac{s^2 - 2\sigma_0 s + \bar{\omega}_0^2}{s^2 + 2\sigma_0 s + \bar{\omega}_0^2} = \frac{(s - s_1)(s - s_3)}{(s - s_2)(s - s_4)} \qquad (2\text{-}3)$$

where $s_{1,3} = \sigma_0 \pm \sqrt{-\omega_0^2} = \sigma_0 \pm j\omega_0$ are the zeros of $H(s)$, and

$s_{2,4} = -\sigma_0 \pm \sqrt{-\omega_0^2} = -\sigma_0 \pm j\omega_0$ are the poles of $H(s)$.

Also

$$\bar{\omega}_0^2 = \omega_0^2 + \sigma_0^2 \quad . \qquad (2\text{-}4)$$

Fig.2.1b illustrates a pole-zero plot on the complex frequency plane.

The reactance, X_a , of the tuned circuit is

$$X_a = \frac{\omega L_a}{1 - \omega^2 L_a C_a} = \frac{2\sigma_0 \omega}{\bar{\omega}_0^2 - \omega^2}$$

and substituting in equation (2-2), the phase response, $\beta(\omega)$, becomes

$$\beta(\omega) = -2 \arctan \left\{ \frac{2\sigma_0 \omega}{\bar{\omega}_0^2 - \omega^2} \right\} \quad . \qquad (2\text{-}5)$$

Finally, the time delay function $\tau(\omega)$ is obtained as

$$\tau(\omega) = -\frac{d\beta}{d\omega} = \frac{4\sigma_0\left(\bar{\omega}_0^2 + \omega^2\right)}{\left(\bar{\omega}_0^2 - \omega^2\right)^2 + 4\sigma_0^2\omega^2} \quad . \tag{2-6}$$

This function is illustrated in Fig.2.2 for typical combinations of σ_0 and $\bar{\omega}_0$.

2.2.2 The unbalanced bridged-T form

The lattice is an unsatisfactory practical form since it is unbalanced with respect to ground. A more useful form is the unbalanced equivalent shown in Fig.2.3a. The conversion from lattice to bridged-T takes the form of the following relations:

$$\left.\begin{aligned} \frac{1}{2Z_a} &= \frac{1}{Z_A} + \frac{1}{2Z_B} \\ \frac{Z_b}{2} &= Z_C + \frac{Z_B}{2} \end{aligned}\right\} \quad . \tag{2-7}$$

One form of the unbalanced bridged-T equivalent is shown in Fig.2.3b

where Z_A is a parallel LC combination (L_A and C_A)

Z_B is a capacitance (C_B)

Z_C is an inductance (L_B)

and

$$\left.\begin{aligned} L_A &= 2L_a & L_B &= L_b/2 \\ C_A &= (C_a - C_b)/2 & C_B &= C_b \end{aligned}\right\} \quad . \tag{2-8}$$

There are several other possible versions of this network; in particular, one has the capacitors arranged in star form instead of delta form.

The condition for realisability is that $C_a > C_b$, or $\bar{\omega}_0 > 2\sigma_0$, and it will become evident that this condition is easily met for all useful delay functions.

The arrangement shown in Fig.2.3b was the one chosen for the RAE system.

2.3 Conventional dispersive network design

The common method of obtaining a linear delay/frequency response is to add together the responses of cascaded bridged-T networks such that the resultant is an approximation to the required linear function. Fig.2.4a illustrates the technique. There is an infinite number of solutions to the problem depending upon the required tolerance of the delay characteristic, and the constraints imposed on the individual responses by practical considerations. No analytic solution to the delay approximation problem is known, but many authors[19-25] have examined the general problem of phase and delay equalisation with the aim of obtaining the best approximation either of the maximally flat or equal ripple type. The purpose of these approximations has generally been to minimise the number of poles, but usually practical considerations have provided no constraints on the positions of the singularities.

This section describes the techniques used to design the RAE network, and possible limits to the improvement of the design are indicated.

Consider first the area under the delay function given by equation 2-6.

$$\text{area} = \int_{-\infty}^{\infty} \tau(\omega)\,d\omega = [-\beta(\omega)]_{-\infty}^{\infty}$$

$$= \left[-2 \arctan \frac{2\sigma_0\omega}{\bar{\omega}_0^2 - \omega^2}\right]_{-\infty}^{\infty} .$$

First consider the integral in the range $-\infty$ to $\bar{\omega}_0$. Then

$$\text{area}_1 = -2 \left[\arctan\left(\frac{2\sigma_0\omega}{\bar{\omega}_0^2 - \omega^2}\right)\right]_{-\infty}^{\bar{\omega}_0}$$

$$= -2\,[\arctan(0) - \arctan(\infty)]$$

$$= \pi .$$

Similarly area_2 in the range $\bar{\omega}_0$ to ∞ is also π ; therefore, if we measure frequency in Hz ($f = \omega/2\pi$) and delay in seconds, the area under one second-order all-pass delay response is unity.

Examination of the basic linear response to be synthesised shows that the total essential area is $FT/2 = 16.66$ (RAE system parameters). It follows that this is the basic number of second-order sections required, if all the available delay could be packed into the frequency range $f_1 < f < f_2$. Obviously this is a practical (and theoretical) impossibility; all sections have some delay down to dc and up to high frequencies. Therefore more than 16.66 sections are necessary. The problem is to use as few as possible to give the required tolerance, and to keep within practical limits of component realisability. For example, if the range of inductor values is too large, the physical size of the inductors may have to vary, and overall construction becomes difficult. Furthermore, it may not be possible to achieve a large enough Q factor for all values of inductance.

At this stage it is convenient to introduce a parameter which more readily describes the shape of the delay response of the second-order network. It is an effective Q factor, Q_e , which is defined as follows:

$$Q_e = \frac{\bar{\omega}_0}{2\sigma_0} \quad .$$

The delay function, $\tau(\omega)$, then becomes

$$\tau(\omega) = \frac{2\dfrac{Q_e}{\bar{\omega}_0}\left(1 + \dfrac{\bar{\omega}_0^2}{\omega^2}\right)}{1 + Q_e^2\left\{\dfrac{\bar{\omega}_0}{\omega} - \dfrac{\omega}{\bar{\omega}_0}\right\}^2} \quad . \qquad (2\text{-}9)$$

Since the delay function is the sum of two curves centred at positive and negative frequencies, the frequency at which maximum delay occurs, ω_0 , is not in general equal to the resonant frequency $\bar{\omega}_0$, i.e.

$$\omega_0^2 = \bar{\omega}_0^2 - \sigma_0^2$$

i.e.

$$\omega_0^2 = \bar{\omega}_0^2 \left(1 - \frac{1}{4Q_e^2}\right).$$

However, for $Q_e > 2$, the frequencies are approximately the same, and in that case, Q_e may be expressed in terms of the delay response as:

$$Q_e = \frac{\omega_0}{\Delta\omega}$$

where $\Delta\omega$ is the half delay frequency separation. (This 'definition' explains the choice of symbol since it is a similar term to that which describes the shape of a power resonance function.)

The term is useful for describing the delay function, and for obtaining practical guide lines for component design.

2.3.1 Optimisation of the response

The inductor Q factor has a low order effect on the delay response but it has been shown that the higher the required delay factor Q_e, the higher does the inductor Q factor have to be.

A high inductor Q factor means less overall attenuation (which follows a curve rather similar in shape to the overall delay response) and hence less need for an attenuation equalizer.

Work at RAE showed that in order to maintain the input resistance as constant as possible at 600Ω over the frequency range of interest (a requirement which was found to be essential when using a hybrid network to halve the size and weight - see section 2.4.1) the Q/Q_e ratio should be more than 50.

Similarly, stray capacitances cause frequency sensitive distortion of the response which cause more significant effects at higher frequencies.

Thus, practical considerations put limits on the values of Q_e and the centre frequency of the response. The next step is to position the second-order sections such as to give a resultant linear response. Since it is obviously impossible to obtain linearity of response down to zero delay, the linear portion must be raised on a

delay pedestal to account for the delay of sections above f_2 (see Fig.2.4). Then, a first approximation may be obtained by placing sections at unit area intervals along the frequency axis, starting from the high frequency end at one half unit area from f_2 [18] (Fig.2.5).

The resultant is then calculated by summing the responses of the sections at a set of frequencies within the band. This first attempt will undoubtedly not coincide with the specification; the next step is to modify the specification and divide this predistorted function again into unit areas. Then the new response is computed, compared with the original specification, and a new predistorted specification calculated. After several such successive approximations, the process is stopped when the required delay tolerance is achieved.

This technique was used in the original design of the networks which were scaled to give the RAE values. Full details may be found elsewhere[18].

Today, there exist sophisticated computer programs which can perform circuit analysis and optimisation of component values with respect to a desired response. It is likely that these techniques can improve upon the original design, by using fewer sections to achieve the same delay tolerance. However, the practical constraints described above will define a limit to the improvement.

The RAE network consists of 48 bridged-T networks, divided into four identical groups, each with twelve sections. The average Q_e value is 5.6 and the range of component values is as follows:

Minimum inductance	0.279	mH	1:11.3
Maximum inductance	3.16	mH	
Minimum capacitance	388	pF	1:21.9
Maximum capacitance	8510	pF	

2.4 Construction of dispersive network

The RAE design was constructed from standard ranges of ferrite core inductors and polystyrene capacitors. The inductors were 14mm Mullard Vinkor assemblies, wound with multistrand wire to obtain the maximum possible Q , as required by the constraints in section 2.3.1. The capacitors were Suflex polystyrene type, ordered as matched pairs to meet a tolerance of $\frac{1}{2}$%. Each group of twelve sections was mounted on a printed circuit board, with side supports to carry the Vinkors,

and a complete two channel dispersive network therefore comprised eight of these boards, four for each channel.

2.4.1 A hybrid method of size reduction

A practical reduction in size was achieved, however, by the use of a hybrid technique to enable one half of a complete dispersive network to be used twice. The operation of a resistive hybrid is illustrated in Fig.2.6. The input signal path is split between a resistive load and the network input; the signal is then reflected at a short circuit at the end of a one half network, and is operated upon by the network in the reverse direction before being split by the hybrid into two directions, one of which is completely separated from the input. By this means, 24 sections can be made to do the work of 48.

An analysis by Forgan[7] has shown that the action of an ideal hybrid is identical to a complete dispersive network. However, in practice the performance is degraded by impedance mismatches between the actual impedance of a real network and the resistive hybrid. Signal break through occurs between the input and output causing some distortion of the compressed pulse, but the effects can be tolerated in view of the 50% size reduction achieved. Therefore, instead of eight groups, a complete system requires four groups plus two hybrids.

2.4.2 Compensation for stray capacitance

The use of $\frac{1}{2}$% tolerance capacitors is hardly justified when there exist stray capacitances associated with every inductor. In fact, uncompensated component values with stray capacitances cause compressed pulse distortion, amounting to a time shift and a small amplitude reduction (about 0.3 dB). Therefore, it is important to compensate in some way for these extra unwanted capacitances.

The strays associated with a Vinkor assembly are a winding capacitance in parallel with the inductance of about 10 pF (C_0), and a capacitance of about 4 pF (C_a) between each end of the winding and the outer can. Since the cans were all earthed, the overall circuit for a bridged-T network including strays is as shown in Fig.2.7.

Using a compensation technique developed by Marconi and expanded at RAE, the compensated component values are:

$$L'_A = L_A \qquad C'_A \doteq C_A - \frac{1}{4}(5C_0 + C_a)$$

$$L'_B \doteq L_B\left(1 - \frac{C_0 + C_a}{C_B}\right) \qquad C'_B \doteq C_B + \frac{1}{2}(C_0 + C_a) \quad .$$

These expressions are obtained assuming that C_0 and C_a are both very much less than C_B and C_A ; they are calculated at the centre frequency, ω_0 , of each section, but analysis has shown that compensation is adequate across the whole frequency range of interest.

2.4.3 Alignment procedure

Simply putting together an LC circuit, which relies on accurate components, seldom guarantees an accurate response. Such circuits required fine tuning for optimum performance. In this case, as in most similar networks, the capacitors are most easily made accurately, and least easily tuned. Therefore, ½% capacitors are used, with the inductors variable by means of a ferrite tuning slug.

The technique adopted for the RAE system involved tuning both inductors *in situ*, with all strays present.

With the network open circuited, the effective impedance is Z_s in series with an impedance $\frac{1}{4}Y_p$, where Z_s is the impedance of a series tuned circuit comprising L_B and $2C_B$, and Y_p is the admittance of a parallel tuned circuit comprising L_A and $(C_A + C_B/2)$. This impedance is a minimum when L_B is tuned at the centre frequency, ω_s ; the impedance when short circuited is a parallel combination of Y_p and $\frac{1}{4}Z_s$. This is a maximum when L_A is tuned to ω_s (see Fig.2.8).

2.4.4 Inductor losses

The RAE network with $Q_e \sim 5.6$ requires inductor Q factors greater than 300 to minimise distortion. Multistrand wire with as many strands as possible was found to be essential to achieve such high values and care was necessary to make the windings even. Two types of wire were required, one type for L_A and another for L_B ; Q values of 325 were obtained for each inductor.

2.4.5 Conclusions

The problems of large scale manufacture of passive dispersive networks are evident. Ideally, all stray capacitances should be measured and individually compensated; low inductor losses are necessary together with fine tuning of the inductors at accurately determined

frequencies, which are different for each section. Finally, the size and weight of the networks are a large proportion of the overall size and weight of the demodulator.

A reduction of the size of the network would be highly desirable for an airborne application. Furthermore, an improvement in the alignment procedure, preferably none at all, would be an advantage. Passive LC networks would almost certainly require re-tuning at intervals which makes maintenance a further problem.

All these factors point inevitably to an active solution if one can be found. In particular, a digital method would require no tuning and therefore no maintenance problems, since the response cannot drift with time or temperature. Some specific solutions to the problem will be investigated in detail in later sections. Meanwhile, various solutions developed by other authors are examined.

2.5 Linear delay approximation methods

Many authors have approached the problem of obtaining approximations to the constant delay function, and more recently, the approximation of arbitrary delay functions has received attention. Since no analytic solution to the problem has been found, the most efficient solutions have generally involved the estimation of a first set of poles followed by a perturbation technique to minimise the departure of the achieved phase or delay functions from the specification.

In general the problem becomes one of devising the most efficient perturbation algorithm having decided upon the number of delay sections to be used and an initial 'guess' for their poles. Specifically with regard to linear delay approximations the following work is represented in the literature.

O'Meara[26] has used graphical approximation methods to arrive at a set of initial pole locations. Ward[27] employed a potential analogue technique (an electrolytic tank) followed by a computer perturbation. Väland[28] obtained an initial guess by constraining the phase angle to fit the ideal at a set of points equally spaced in phase angle, and by introducing a variable factor in the denominator of the transfer function; again a computer perturbation technique was required to minimise the final errors.

The most complete description of a practical delay approximation technique is given by Crane[29]. The first step is to determine an approximation that coincides with the desired delay on a specified set of points. The second step consists of perturbing these points in an attempt to find an equal ripple solution.

These methods are all basically means of refining an initial estimate to obtain a close fit to a linear delay function. In principle an optimum design for a given network complexity can be obtained. However, none can provide more than a small size reduction compared with the original RAE design. All will require many sections of bridged-T network, some of which will have large Q_e factors, unless the pole locations are constrained in the design process as in the Marconi work, in which case optimum designs (from a delay error viewpoint) cannot be achieved. This practical constraint has not been considered in any of the above methods, but in a system which demands a relatively high centre frequency/bandwidth ratio, it must be an important consideration.

Therefore it was decided not to approach the problem by looking for a more efficient initial choice of pole locations and minimum delay errors, but to attempt more extensive departures from the original design concept in order to find more significant gains.

2.6 All pass active networks

Many authors[30-36] have described active filter configurations which realise the second order all-pass transfer function, equation (2-3). Essentially there are two main approaches: one uses an infinite gain 'computing' amplifier or inverting operational amplifier as the active element (high input impedance low output impedance) while the other employs fixed gain amplifiers in Sallen Key or similar configurations. There are other active network elements often discussed (current amplifiers, negative impedance converters, gyrators) but practically the elements most often used for all-pass network synthesis are amplifiers.

The most promising networks discovered in the literature employ only one differential input operational amplifier. The circuit due to Holt and Gray[30] is shown in Fig.2.9a. It requires five resistors and three capacitors in addition to the differential amplifier.

To realise the transfer function

$$H(s) = \frac{s^2 - as + b}{s^2 + as + b}$$

the following identifications are made ($R_1 = 1$):

$$R_2 = 1+(a^2/b); \quad R_3 = a^2/b; \quad C_1 = a/b; \quad C_2 = (a^2 + b)/ab;$$

$$C_3 = a/b; \quad K = 1/a$$

and the transfer function becomes

$$H(s) = \frac{s^2 - s[(C_2 + C_3 - C_1 - K_1)/KC_1] + 1/KC_1}{s^2 + s[(- C_2 + C_3 + C_1 + K)/KC_1] + 1/KC_1} .$$

Both the poles and zeros depend on differences between component values such that a small percentage error in a component results in a large percentage error in the difference, and hence a component sensitivity problem. However in an application where many sections, tuned to different frequencies are arranged in cascade, the delay error from any one section could be considered as only a small perturbation on the overall response.

Another differential amplifier circuit was described by Deliyannis[31] (Fig.2.9b). This circuit which requires only four resistors and two capacitors has a transfer function given by:

$$H(s) = \frac{1}{1 + K} \frac{s^2 + \left(\frac{g_1 + g_2}{C_1} - K\frac{g_1}{C_2}\right) + \frac{g_1 g_2}{C_1 C_2}}{s^2 + \left(\frac{g_1 + g_2}{C_1}\right)s + \frac{g_1 g_2}{C_1 C_2}} .$$

Its sensitivity characteristics are better than the Holt and Gray circuit but it realises $H(s)$ only to within a constant multiplier $1/(1 + K)$. In a multi-section cascade this is obviously a disadvantage since separate amplifier sections would be necessary to maintain a given signal level.

Many other realisations have been published.

At the time when these possibilities were being considered the major impediment to active filter realisations was the frequency limitations of the integrated circuit operational amplifiers. The application

requires accurate operation, up to frequencies around 100 kHz. For a network (such as that due to Deliyannis) to operate satisfactorily at a frequency of ω_0 the following expression must be satisfied (Budak and Petela[37]):

$$\frac{\omega_0 Q_e k}{A_0 \alpha} \ll 1$$

where the gain of the operational amplifier is

$$- A_0\alpha/(s + \alpha)$$

and $k = (C_1 + C_2)/C_2$ in Fig.2.9b.

Thus for $\omega_0 = 2\pi 10^5$, $Q_e \sim 5$, $A_0\alpha = 10^7$ (roughly typical of present day IC operational amplifiers) we find that

$$k \ll 3 .$$

A further limitation in Deliyannis's circuit is that

$$Q_{e_{max}} \doteq \frac{\sqrt{k - 2}}{2} .$$

This requires a value of $k \sim 100$ which is entirely inconsistent with the frequency limitation (setting $k \ll 3$).

This kind of problem is encountered with all active filter realisations at frequencies $\sim$ 100 kHz, although some are better than others. Furthermore, it is unlikely that these realisations can be easily cascaded without intermediate buffer stages which mean a further increase in complexity, unreliability and power consumption.

A solution to the problem using active filters awaits suitable wideband integrated circuit operational amplifiers which will be able to provide repeatable responses (not requiring tuning) with easily manufactured components (tolerances not better than 1%) at frequencies around 100 kHz.

Active filters were not considered further for these reasons.

2.7 Digital filter methods

Digital filter methods have the potential for reducing the size and weight of many complex filter applications such as dispersive filters. Chapters 6, 7 and 8 describe a technique which is capable of being implemented on only a few MOS/LSI chips.

A digital filter operates arithmetically (by multiplication, addition and pure delay) on sampled and quantized versions of a signal. Thus, the first obvious requirement is an analogue to digital converter (ADC) to sample the incoming signal at the required rate and to convert the samples into n-bit numbers for manipulation by the filter.

Digital all-pass sections could be used to build up a desired delay response in a similar manner to that already described for passive sections. A technique like that described by Kisel[38] could be employed which matches the response of a digital filter to the required phase or delay function at a set of equally spaced frequencies. The delay response of a digital filter is examined in detail in Chapter 5; one of the results is the phase response of an Nth order all-pass digital filter, which is given by

$$\Phi_N(\omega) = -N\omega\Delta t + 2 \arctan \left\{ \frac{\sum_{k=1}^{N} a_k \sin k\omega\Delta t}{1 + \sum_{k=1}^{N} a_k \cos k\omega\Delta t} \right\} .$$

a_k are the so-called coefficients (or constant multipliers); they are in effect the 'component values' of a digital filter which, once having been chosen, determine its response; Δt is the delay time or sampling interval. The a_k can be chosen such that $\Phi_N(\omega)$ matches the required delay, at least at given frequencies, in the following manner.

The nonlinear part of $\Phi_N(\omega)$ is $\alpha(\omega)$, say

i.e.

$$\Phi_N(\omega) = -N\omega\Delta t + \alpha(\omega) .$$

The delay of an Nth order filter is

$$\tau_N(\omega) = + N\Delta t - \frac{d\alpha(\omega)}{d\omega} .$$

The delay function we intend to obtain is given by

$$\tau(f) = \frac{T}{F}(f_0 - f) + T_0 = -\frac{T}{F} f + T_0 + \frac{f_0 T}{F}$$

thus

$$\phi(f) = -2\pi \int \tau(f)df + \text{constant} .$$

Integrating and setting $\phi(0) = 0$ we get

$$\phi(f) = \frac{\pi T}{F} f^2 - 2\pi f\left[T_0 + \frac{f_0 T}{F}\right]$$

$$\phi(f) = \frac{\pi T}{F} f(f - 2f_0) - 2\pi T_0 f = \psi_1(f) - \psi_2(f) .$$

If we match $\psi_1(f)$ with $\alpha(f)$ and choose N and Δt such that $N\Delta t = T_0$ we have synthesised a suitable network. First we choose a set of N frequencies ω_i $(= 2\pi f_i)$ $(i = 0,1,\ldots,N)$ such that

$$\psi_1(\omega_i) = 2 \arctan \left\{ \frac{\sum_{k=0}^{N} a_k \sin k\omega_i \Delta t}{1 + \sum_{k=0}^{N} a_k \cos k\omega_i \Delta t} \right\}$$

which transforms into the system of equations

$$\sum_{k=1}^{N} a_k \sin\left[k\omega_i \Delta t - \frac{1}{2}\psi_1(\omega_i)\right] = \sin \frac{1}{2}\psi_1(\omega_i) \qquad i = 1, 2, \ldots n .$$

the solution of which gives the required a_k .

This method gives an economic solution in the frequency range $0 < f < F$ where $F = 1/2\Delta t$.

Such a solution is theoretically possible but requires a complex recursive structure which is extremely sensitive to round off noise effects in the multipliers requiring high coefficient accuracy and should ideally be factorised into smaller units.

A further digital solution employs a transverse or non-recursive structure similar to a tapped delay line. After sampling and encoding in an A to D converter, the samples are transferred successively to delay elements in series. The outputs from each delay element are multiplied by a constant multiplier and the results of each multiplication are added to produce the output. The values of the multiplier coefficients are equivalent to samples of the time inverse of the input signal.

Thus the output sequence $y(nT)$ is the discrete convolution of the input sequence $x(nT)$ and the impulse response sequence $a_0, a_1, \ldots aN$ formed by the multiplier constants, i.e.

$$y(nT) = \sum_{k=0}^{N} a_k x[(n - k)T] \quad .$$

For adequate resolution of the output compressed pulse, many sections of delay are required (probably up to 600 for the RAE parameters). Thus the filter is extremely complex.

Ash[39] has demonstrated a modified digital transversal solution, employing a delta modulated input signal and resistor implementation of multipliers at outputs of a shift register. Promising results were obtained.

All the above digital methods hold promise for significant weight reduction yet none possess the simplicity which is desirable on the basis of reliability and cost.

2.8 Summary of proposed investigations

2.8.1 The linear delay function has been exhaustively examined by various authors, basically because it is an optimum signal in its class (i.e. optimum from consideration of the ratio of compressed pulse peak to main lobe time width). The class of signals defined by $f(t)$ = function (t) $(-T/2 < t < T/2)$ are all candidates for a pulse compression system, but have not been examined in detail unless in classified work. The next chapter looks at some possible nonlinear FM signals and computes compressed pulse envelopes for comparison with the sin X/X shape obtained with linear FM. The aim is to discover if a significant size/weight advantage can be achieved at the expense of only small performance degradation.

2.8.2 Anticipating for a moment the conclusions of the following chapters, the arguments surrounding nonlinear FM signals directed the work along a different route. Instead of looking for nonlinear signals which gave acceptable results and then having to synthesise the delay required (section 2.5), easily realisable delay functions were examined for their acceptability in pulse compression - a reversal of the usual design process. Chapter 4 describes a system which follows this principle.

2.8.3 A digital filter solution would appear to have the most promising impact on the size and weight of a pulse compression network. Chapters 6, 7 and 8 develop and demonstrate ideas conceived in Chapter 4 in a digital realization and conclude with an extremely simple, small and reliable digital solution for future applications.

Chapter 3

NONLINEAR FM SYSTEMS

3.1 Introduction

Arising out of the previous chapter, a technique for reducing the complexity of a dispersive network could be to design the system around a nonlinear delay response, which has a smaller area and thus requires fewer delay sections. This is not a great departure from the existing system, except that the signal required to match the response is inevitably nonlinear (i.e. its frequency varies nonlinearly with time). Unless this implies an unacceptable loss in terms to be discussed, the size advantage to be gained from such a departure may be a significant factor.

This chapter examines the techniques for evaluating departures from linear FM and looks at some typical signals and their corresponding filter responses.

3.2 Design criteria

In Appendix B some expressions are derived for signals and spectra with large time-bandwidth products, and methods of obtaining matched filter responses. The usual application of these methods is to specify signal frequency vs. time such that the magnitude of the signal spectrum assumes a specified form. In this section a particular signal function will be assumed, and its spectrum obtained; then the compressed pulse shape can be found using the inverse Fourier transform.

The conditions on the signal are:

(1) frequency limits, f_1 and f_2, such that the spectrum is effectively contained within 40 kHz,

(2) its envelope must be rectangular in order to make optimum use of transmitter power.

Otherwise, the criteria refer to the shape of the compressed and dispersed pulses. These criteria are difficult to specify quantitatively; but, in general, as long as the compressed pulse is not too much wider than the 'ideal' sin x/x, and the peak amplitude is not degraded to a great extent the change is acceptable. Nominal values of say 10% and 0.5 dB could be placed on these parameters for the purposes of evaluation.

If small size is the aim, with fewer all-pass sections, a smaller total area under the group delay vs. frequency curve must be achieved. The kind of response necessary is illustrated in Fig.3.1. The smaller the shaded area can be made, the fewer sections of delay network are required to synthesise it. Some practical problems may be created by the necessity for a larger range of delay/frequency slope, and less stringent restrictions on component values may be required.

The effects on the response of reducing the area to be synthesised will be investigated by reference to some particular analytic nonlinearities.

3.3 Power law frequency functions

3.3.1 Signals and spectra

These functions provide a simple method of demonstrating the effect of varying the nonlinearity of the frequency function in a systematic manner. The signals have instantaneous frequency given by

$$f(t) = f_1 + \frac{F}{T^n} (t + T/2)^n \quad . \qquad (3\text{-}1)$$

Here we make the limits of the sweep f_1 and $f_1 + F$ as before, and refer to the functions as linear, quadratic, cubic and quartic FM (n = 1, 2, 3, 4). The functions are illustrated in Fig.3.2.

Using the principle of stationary phase, we can obtain approximate expressions for spectra and delay functions, remembering the restrictions on FT product and centre frequency. From equation (B-2), the instantaneous radian frequency is

$$\omega = \theta'(t) = 2\pi \left\{ f_1 + \frac{F}{T^n} (t + T/2)^n \right\}$$

and the second derivative, $\theta''(t)$ is

$$\theta''(t) = 2\pi n \frac{F}{T^n} (t + T/2)^{n-1} \quad .$$

Substituting from equation (3-1) to remove the t-dependence:

$$\theta''(t) = 2\pi n \frac{F^{1/n}}{T} (f - f_1)^{\frac{n-1}{n}} \quad .$$

Then, an approximate spectrum magnitude function is obtained using equation (B-5) thus:

$$|S(f)_n| \doteq \sqrt{\frac{T}{F}} \frac{1}{\sqrt{n}} \left(\frac{F}{f - f_1}\right)^{\frac{n-1}{2n}} . \qquad (3\text{-}2)$$

Using a similar procedure to remove t-dependence the phase function, $\Phi(f)$, is found to be:

$$\Phi(f) = - 2\pi FT \frac{n}{n+1} \left(\frac{f - f_1}{F}\right)^{\frac{n+1}{n}} + \pi FT\left(\frac{f - f_1}{F}\right) + \frac{\pi}{8} . \qquad (3\text{-}3)$$

Then the group delay function of the signal $f(t)$ is

$$T(f) = - \frac{d\Phi(f)}{2\pi df}$$

$$= - \frac{T}{2} + \frac{T}{F}\left(\frac{f - f_1}{F}\right)^{1/n} . \qquad (3\text{-}4)$$

This can be obtained direct from equation (3-1) using the stationary phase relationship, equation (B-7). The group delay of the filter matched to this function must be the negative of equation (3-4). Thus

$$\tau(f) = \frac{T}{2} - \frac{T}{F}\left(\frac{f - f_1}{F}\right)^{1/n} .$$

Obviously, to make this function realisable, an extra constant delay, greater than T/2 seconds, must be added, but for the purpose of analysis the expression is adequate.

The magnitude spectra of these signals are shown in Fig.3.3. They have been normalised with respect to the linear case for which

$$|S(f)_1| = \sqrt{\frac{T}{F}} \ .$$

So the functions plotted are

$$|S(f)_n| = \frac{1}{\sqrt{n}} \left(\frac{F}{f - f_1} \right)^{\frac{n-1}{2n}} \ . \qquad (3\text{-}5)$$

The alarming feature of these spectra is that

$$\left|S(f)_n\right|_{f \to f_1} \to \infty$$

which poses a serious realisation problem for the matched filter. Since such infinities are unlikely in practice, it is to be expected that a more exact analysis will yield non-infinite spectrum magnitudes. An exact computation of the spectrum of a quadratic signal is shown in Fig.3.4, and compared with the stationary phase spectrum. Although, as expected, the spectrum is finite the nonlinearity is such that there is a range of about 5:1 between the magnitude of the response required at 80 kHz and 120 kHz. This in itself poses a practical problem of amplitude equalisation.

The familiar ripples on the magnitude response are evident; their magnitude is largest near the band edges and smallest near the centre. In this case the minimum occurs near 95 kHz. Further, it may be noted that the ripples have approximately equal positive and negative departures from the stationary phase approximation.

3.3.2 Output signals

The output signals from a matched filter are obtained in approximate form by assuming that the nonlinear part of the phase response is cancelled exactly by the filter phase response, and applying the inverse Fourier transform to the output magnitude spectrum; the response function is given by equation (3-5) (normalised to the n = 1 spectrum). Thus

$$g(t) = \sqrt{\frac{T}{F}}\,\frac{F^{\frac{n-1}{n}}}{n}\int_{f_1}^{f_1+F}\frac{e^{j2\pi ft}}{(f-f_1)^{\frac{n-1}{n}}}\,df$$

$$|g(t)| = \sqrt{FT}\left|\int_0^1 e^{j2\pi Ftx^n}\,dx\right| \qquad (3\text{-}6)$$

where $x = \left(\frac{f-f_1}{F}\right)^{1/n}$.

The only signals in this set which yield relatively simple expressions are the linear and quadratic types (n = 1, 2). The linear case is well-known as chirp, described in Chapter 1. The quadratic case may be expressed in terms of the Fresnel integral.

$$\bar{f}(y) = \frac{1}{\sqrt{2\pi}}\int_0^y \frac{e^{-jx}}{\sqrt{x}}\,dx$$

$$= C_2(y) - jS_2(y) \quad .$$

Noting that $\bar{f}(-y) = \bar{f}(y)$, we obtain the following expression for the output envelope for quadratic FM:

$$g(t) = \frac{1}{2}\sqrt{\frac{T}{t}}\sqrt{\left\{C_2(y)^2 + S_2^2(y)\right\}} \qquad (3\text{-}7)$$

where $y = 2\pi Ft$.

In general, the output envelopes are given by the magnitude of equation (3-6); they are shown in Fig.3.5.

Although the peak amplitude of the compressed pulse is the same for all values of n , there is a successive broadening of the main lobe, and an increase in sidelobe level as the input waveform departs from the linear.

The peak level is determined solely by the FT product of the signal, i.e.

$$|g(t)|_{t=0} = \sqrt{FT} \qquad \text{for all } n \ .$$

Any waveform with the same FT product gives the same peak compressed pulse amplitude when operated upon by a truly matched filter in the manner outlined above.

However, the pulse broadening, with an apparent increase in output signal energy for more nonlinear waveforms, deserves further explanation. The phenomenon occurs due to the necessity for a matched filter to emphasise those parts of the spectrum having higher signal-to-noise ratios (or spectrum amplitude), and to place less weight on the parts having lower signal-to-noise ratios.

Consider, for example, a simple spectrum with a normalised squared magnitude function

$$\left|S_i(f)\right|^2 = 2.5 - f \quad .$$

The power within this spectrum, band limited to the region $1 < f < 2$

$$\int_1^2 \left|S_i(f)\right|^2 df = 1 \quad .$$

The squared magnitude response of a filter matched to this function is identical, which means in this case that frequencies below 1.5 are emphasised more than frequencies above 1.5 in a linear fashion. The spectrum function of the output is the product of the input spectrum and the magnitude response of the filter, i.e.

$$\left|S_0(f)\right|^2 = \left|S_i(f)\right|^4$$

and the power in the output signal is

$$\int_1^2 \left|S_i(f)\right|^4 df = \int_1^2 (2.5 - f)^2 df = 1.0833 \quad .$$

So the power in the output signal is 1/12 greater than in the input. This general argument applies to all nonlinear signals having the same gross properties (bandwidth and FT product). The greater the nonlinearity, the more pronounced is the difference in the power distribution at various frequencies across the band, and the greater is the total power within the compressed pulse envelope.

The preceding discussion indicates a special problem which sets a limit to the acceptable degree of nonlinearity. We cannot put a limit on the total output power since functional differences produce different power distributions; limits must be placed on sidelobe level as well as main lobe broadening and peak amplitude loss. These factors will be brought together in a comparison towards the end of this chapter.

3.4 Modified power law functions

The major disadvantage of the nonlinear functions above was felt to be the infinite spectrum magnitude at $f = f_1$, caused by the fact that the derivative of the instantaneous frequency is zero at $f_1 (t = -T/2)$. A function having $df/dt = 0$ outside $f_1 < f < f_1 + F$ does not have this disadvantage. Such a function can be derived from the power law relation by changing the time scale by a factor 2, and using the middle time portion.

The following instantaneous frequency function is suggested.

$$f(t) = f_1 - \frac{F}{3^n - 1} + \frac{2^n}{3^n - 1} \frac{F}{T^n} (t + T)^n \quad . \qquad (3\text{-}8)$$

The modification, though arbitrary, will serve to demonstrate the effect of having $df/dt \neq 0$; the signals in equation (3-8) are illustrated in Fig.3.6.

Stationary phase analysis gives the following expression for the spectrum magnitude:

$$|S(f)| = \sqrt{\frac{T}{F}} \frac{1}{\sqrt{2^n}} (3^n - 1)^{\frac{1}{2n}} \frac{1}{\left\{x + 1/(3^n - 1)\right\}^{\frac{n-1}{2^n}}} \qquad (3\text{-}9)$$

where $x = \dfrac{f - f_1}{F}$

These spectra are illustrated in Fig.3.7. Exact computation again gives the Fresnel ripples about the average stationary phase approximation; the output pulse, using equation (3-9), illustrated in Fig.3.8, is

$$g(t) = \sqrt{\frac{T}{F}} \frac{1}{2^n} (3^n - 1)^{1/n} \int_{f_1}^{f_1+F} \frac{e^{j2\pi ft}}{\left\{\frac{f - f_1}{F} + \frac{1}{(3^n - 1)}\right\}^{\frac{n-1}{n}}} df \quad .$$

Thus:

$$|g(t)| = \sqrt{FT} \frac{(3^n - 1)^{1/n}}{2^n} \left| \int_0^1 \frac{e^{j2\pi ftx}}{\left\{x + 1/(3^n - 1)\right\}^{\frac{n-1}{n}}} dx \right| . \quad (3\text{-}10)$$

As before

$$|g(t)|_{t=0} = \sqrt{FT} \quad .$$

A different arrangement of this expression yields the following form in terms of the Fresnel integral, as in section (3.3.2)

$$g(t) = \frac{1}{2} \sqrt{\frac{T}{t}} \left\{\bar{f}(x_2) - \bar{f}(x_1)\right\}$$

where $x_1 = 2\pi Ft/(3^n - 1)$

and

$$x_2 = 2\pi Ft3^n/ 3^n - 1)$$

$$|g(t)| = \frac{1}{2} \sqrt{\frac{T}{t}} \sqrt{\left\{C_2(x_2) - C_2(x_1)\right\}^2 + \left\{S_2(x_2) - S_2(x_1)\right\}^2} \quad .$$

The group delay function of the matched filter is

$$\tau(f) \doteq T - \frac{T}{2}\left\{(3^n - 1)\left(\frac{f - f_1}{F} + \frac{1}{3^n - 1}\right)\right\}^{1/n}$$

Although the amplitude response required at $f = f_1$ has been reduced, the compressed pulse shapes are generally similar to the true power law outputs. However, the table below, giving the area under the delay response as a percentage of $FT/2$, shows that for similar gains, a modified cubic or even quartic is necessary to be equivalent to the true quadratic.

Type	% area of FT/2
Quadratic	66.7
Cubic	50.0
Quartic	40.0
Modified quadratic	83.3
Modified cubic	69.2
Modified quartic	58.0

The cubic and quartic matched responses still require careful tailoring with the response at 82 kHz more than twice the response at 118 kHz. The simplification achieved by the reduced area of delay is partially offset by the need for a tailored amplitude response, which could demand several amplitude equalising sections, each of which contributes an unwanted distorting phase function.

A possible route avoiding this difficulty is to depart from the theoretical matched filter which matches both the phase and amplitude spectrum, and to use an all-pass network. The response in this case is

$$1e^{j\varphi(\omega)} \quad \text{instead of} \quad |S(\omega)|e^{j\varphi(\omega)} .$$

3.5 Power law functions with all-pass filter

Using the same signals, the spectra are as before but the output signal becomes

$$g(t) = \sqrt{\frac{T}{F}} \frac{1}{\sqrt{n}} F^{\frac{n-1}{2n}} \int_{f_1}^{f_1+f} \frac{e^{j2\pi ft}}{(f - f_1)^{\frac{n-1}{2n}}} df$$

$$|g(t)| = \sqrt{\frac{FT}{n}} \left| \int_0^1 \frac{e^{j2\pi Ftx}}{x^{\left(\frac{n-1}{2n}\right)}} dx \right| \qquad (3\text{-}11)$$

where $x = \dfrac{f - f_1}{F}$.

Comparison of equations (3-11) and (3-6) shows important functional differences, and it should not be surprising if the envelope shapes are also different, in important respects. Fig.3.9 shows the compressed pulse outputs of the all-pass filter for the signals given by equation (3-1).

In particular the peak amplitude of the compressed pulse is reduced to

$$|g(t)|_{t=0} = \frac{2\sqrt{n}}{1 + n} \sqrt{FT} \quad .$$

Similarly, the modified power law functions give rise to the following output signals (*cf.* equation (3-10))

$$|g(t)| = \sqrt{\frac{FT}{2^n}} (3^n - 1)^{\frac{1}{2}n} \left| \int_0^1 \frac{e^{j2\pi Ftx}}{\left\{x + 1/(3^n - 1)\right\}^{\frac{n-1}{2^n}}} dx \right| . \qquad (3\text{-}12)$$

The peak amplitude is

$$|g(t)|_{t=0} = \frac{1}{1 + n} \sqrt{\frac{2^n}{3^n - 1}} \left(\sqrt{3^{n+1}} - 1 \right) \sqrt{FT} \quad .$$

These are shown in Fig.3.10. The notable features of the all-pass filter outputs, compared with matched outputs, are

(1) reduced peak amplitude, the amount depending on the degree of nonlinearity;

(2) deeper nulls;

(3) reduced absolute amplitude at all times.

These items are quantified in a summary at the end of the chapter.

3.6 Logarithmic phase signals

For a more complete picture of the effect of nonlinear frequency functions, some more examples were examined. Firstly, the logarithmic phase function which has an instantaneous frequency of the form (see Fig.3.11):

$$f(t) = f_0 + \frac{k}{T_1 - t} \qquad -T/2 \leq t < T/2 \quad . \qquad (3\text{-}13)$$

The shape of this function can be altered in a controllable manner by, say, specifying the point at which it crosses the frequency axis as a function of the full sweep, F ; let the curve cross the frequency axis (t = 0) at $f = f_1 + F/\lambda$, where $2 < \lambda < \infty$. Then the parameters f_0 , k and T_1 are:

$$\left.\begin{aligned} f_0 &= f_1 - \frac{F}{\lambda - 2} \\ k &= FT\,\frac{(\lambda - 1)}{(\lambda - 2)^2} \\ T_1 &= \frac{T}{2}\,\frac{\lambda}{(\lambda - 2)} \quad . \end{aligned}\right\}$$

Once again, the stationary phase approximation may be used to obtain the following spectrum function:

$$|S(f)| \doteq \frac{\sqrt{k}}{f - f_0}$$

$$= \sqrt{\frac{T}{F}}\left\{\frac{\sqrt{\lambda - 1}}{1 + (\lambda - 2)(f - f_1)/F}\right\}$$

which is shown in Fig.3.12 for various values of λ . As before, the matched filter output is obtained with an amplitude response:

$$|H(f)| = |S(f)| \Big/ \sqrt{\frac{T}{F}} \quad .$$

Then

$$g(t) = \int_{f_1}^{f_1+F} \frac{|S(f)|^2}{\sqrt{\frac{T}{F}}} e^{j2\pi ft} df$$

therefore

$$\left.\begin{aligned} g(t) &= \sqrt{\frac{F}{T}}\, k e^{j2\pi f_0 t} 2\pi t \int_{x_1}^{x_2} \frac{e^{jx}}{x^2}\, dx \\ \text{where } x_1 &= 2\pi(f_1 - f_0)t = \frac{2\pi f}{\lambda - 2}\, t \\ x_2 &= 2\pi(f_1 - f_0 + F)t = 2\pi\left\{\frac{F}{\lambda - 2} + F\right\} t \quad . \end{aligned}\right\} \qquad (3\text{-}14)$$

This may also be expressed in terms of tabulated functions, as follows.

Consider

$$I = \int_{x_1}^{x_2} \frac{e^{jx}}{x^2}\, dx$$

$$= \frac{e^{jx_1}}{x_1} - \frac{e^{jx_2}}{x_2} + j \int_{x_1}^{x_2} \frac{e^{jx}}{x}\, dx \quad .$$

An alternative formulation is

$$|g(t)| = \sqrt{FT}(\lambda - 1)\left| \int_0^1 \frac{e^{j2\pi Fxt}}{[1 + (\lambda - 2)x]^2}\, dx \right|$$

where $x = \dfrac{f - f_1}{F}$.

The logarithmic phase function is of particular interest since it has been shown to be optimum for the purpose of minimising signal degradation resulting from Doppler distortion effects[40]. It is interesting to note that certain kinds of bats are known to use this optimum nonlinear modulation in their 'sonar'. Although this property has potential for radar signals, the improvement attainable in a communications application is insignificant, especially when the effects of Doppler are so small. In fact, all FM signals with acceptable gross parameters provide sufficient immunity against Doppler effects.

The output pulses for matched and all-pass filters are shown in Figs.3.13 and 3.14. In the all-pass filter case the peak amplitude is

$$|g(t)|_{t=0} = \sqrt{FT}\, \frac{\sqrt{\lambda - 1}}{\lambda - 2} \ln(\lambda - 1) .$$

3.7 Exponential phase signals

A final class of nonlinear signals, called exponential phase, is defined by the relationship (see Fig.3.15):

$$f(t) = ce^{at} + f_\alpha . \qquad (3\text{-}15)$$

Applying the same factor λ to vary the depth of the waveform, we obtain the following identifications:

$$\left.\begin{aligned} f_\alpha &= f_1 - \frac{F}{\lambda(\lambda-2)} \\ c &= F\,\frac{(\lambda-1)}{\lambda(\lambda-2)} \\ a &= \frac{2}{T}\ln(\lambda-1) \end{aligned}\right\} .$$

Substituting these expressions in equation (3-15) we get:

$$f(t) = f_1 + \frac{F}{\lambda(\lambda-2)}\left\{(\lambda-1)^{1+\frac{2t}{T}} - 1\right\} .$$

The spectrum modulus (by stationary phase) is (see Fig.3.16):

$$|S(f)| = \frac{1}{\sqrt{a(f-f_\alpha)}}$$

$$= \sqrt{\frac{T}{F}}\,\frac{1}{\sqrt{2\ln(\lambda-1)\left\{\frac{1}{\lambda(\lambda-2)} + \frac{f-f_1}{F}\right\}}} .$$

The output signal is

$$|g(t)| = \frac{\sqrt{FT}}{2\ln(\lambda-1)}\left|\int_0^1 \frac{e^{j2\pi Fxt}}{k_0 + x}\,dx\right| \qquad (3\text{-}16)$$

where $x = \dfrac{f-f_1}{F}$ and $k_0 = \dfrac{1}{\lambda(\lambda-2)}$

or

$$|g(t)| = \frac{\sqrt{FT}}{2\ln(\lambda-1)}\left|\int_{y_1}^{y_2} \frac{e^{jy}}{y}\,dy\right|$$

where $y_1 = 2\pi Ftk_0$ and $y_2 = y_1 + 2\pi Ft$.

These outputs are illustrated in Fig.3.17; the equivalent all-pass filter outputs are

$$|g(t)| = \frac{\sqrt{FT}}{\sqrt{2\ln(\lambda - 1)}} \left| \int_0^1 \frac{e^{j2\pi Fxt}}{\sqrt{k_0 + x}} \, dx \right|$$

which are illustrated in Fig.3.18. The peak amplitude at the output of the all-pass filter is

$$|g(t)|_{t=0} = \sqrt{FT}\sqrt{\frac{2(\lambda - 2)}{\lambda \ln(\lambda - 1)}} \quad .$$

3.8 Dispersed pulses for nonlinear FM signals

In order to describe completely the performance of nonlinear FM signals it is necessary to examine the response of a filter to a mismatched signal; that is one whose direction of sweep is opposite to the signal to which the filter is matched.

Expressions for the dispersed pulse envelope obtained from the various types of nonlinear waveform considered in this chapter are derived in Appendix D. In all cases numerical integration using a computer was required. The rapidly oscillatory nature of the argument within the integral means that a large number of integration steps is necessary and hence a rather lengthy computer processor time. For this reason the whole of each signal was not computed but a complete computation for a selection was performed in order to examine the trends as described below.

In fact all the dispersed pulses are similar in character, but their magnitudes vary slightly and of course it is the magnitude of the dispersed pulse at its centre point in time (corresponding to the compressed pulse instant in the other channel) which is the parameter of interest. Fig.3.19 illustrates a typical dispersed pulse for log phase signals.

3.9 Comparison of nonlinear functions

None of the waveforms examined exhibit properties with outstanding advantages in a pulse compression communications system. In fact, as indicated in Chapter 2, it is difficult to define strictly quantitatively those properties which are desirable. Although certain parameters are important, a trade-off between them to determine an overall formula for assessment is at best a subjective task. Therefore, the simplest way to compare the possibilities is to construct a table in which all measurable quantities are listed, and from this, if desired, a reasonable choice might be made.

The parameters chosen for the comparison (see Fig.3.23, were

(i) Peak amplitude of compressed pulse, A (wrt unity input amplitude)
(ii) Depth of first null in relation to central peak (in dB)
(iii) First sidelobe in relation to central peak (in dB)
(iv) -4 dB central pulse width (in μs)
(v) Average amplitude of dispersed pulse over central 50 μs.

Table 3.1 below makes the comparison for (i) to (iv).

Table 3.1

COMPARISON OF NONLINEAR FM COMPRESSED PULSES

TYPE	n/λ	PEAK AMPLITUDE		DEPTH OF FIRST NULL dB		FIRST SIDELOBE dB		PULSE WIDTH μs	
		MF	AP	MF	AP	MF	AP	MF	AP
POWER LAW	n								
	2	5.77	5.44	10.93	19.44	8.78	11.67	25.00	24.30
	3	5.77	5.00	7.02	15.92	6.31	10.75	27.50	24.25
	4	5.77	4.64	5.20	14.25	4.85	10.41	31.80	24.25
MODIFIED POWER LAW	n								
	2	5.77	5.74	16.24	22.71	11.53	12.57	25.25	25.00
	3	5.77	5.56	11.03	17.75	9.29	11.61	25.88	25.20
	4	5.77	5.45	7.91	15.74	7.55	11.09	27.00	25.75
LOGARITHMIC	λ								
	2.5	5.77	5.72	17.61	24.02	12.55	13.00	25.75	25.25
	3.5	5.77	5.58	11.09	16.87	9.83	12.20	27.25	25.25
	4.5	5.77	5.41	8.78	14.24	8.66	11.44	28.75	25.25
EXPONENTIAL	λ								
	2.5	5.77	5.72	17.96	24.27	12.36	12.94	25.50	25.25
	3.5	5.77	5.58	11.25	17.43	9.93	11.95	26.50	25.25
	4.5	5.77	5.42	8.86	15.22	8.38	11.22	27.75	25.25

Time and computing finance did not permit the comparison of dispersed pulses to be completed. During the period of study the primary effort was applied to the study of the compressed pulses. Any extension of these studies should examine the compressed-to-dispersed pulse ratio of the contending systems in more detail. An optimum is however unlikely as suggested above.

Another aspect of further study should be a comparison of likely systems having equal delay areas. This implies non-integral power functions, or non-integral values of λ ; Figure 3.20 illustrates. To obtain a response having a delay area to be synthesised equal to 60%, say, of the chirp linear response requires a power law response with $n = 2.33$, a modified power law response with $n = 3.92$, a logarithmic response with $\lambda = 4.52$ and an exponential response with $\lambda = 4.81$. This direct comparison technique was not employed in the work reported on.

Chapter 4

IDENTICAL SECTION PASSIVE FILTER METHOD

4.1 Introduction

The previous chapter examined some nonlinear FM waveforms in order to discover the effect of nonlinearity on the output pulse shapes. For the purposes of reducing the network complexity within certain constraints the effects are all similar in kind but problems of synthesis mean that the apparent advantages are partly illusory.

At this stage in the project, before further work towards choosing and implementing a nonlinear design, as in Chapter 3, was attempted, a new approach was made to the problem. Instead of choosing a nonlinear waveform, only to be confronted with the same synthesis problems as before (Chapter 2), it was considered that the problem could be tackled from the opposite end of the usual design process. By taking a network which is trivial to synthesise and simple to construct and maintain, could its response be used to derive a waveform suitable for the purpose? This essential reversal of the traditional design process would in general lead to inadequate signals for performance reasons but in this case when (as indicated in Chapter 3) performance is relatively insensitive to wave shape it turned out to yield satisfactory performance.

4.2 Basic ideas

The philosophy which gave rise to this system is that the final communications equipment shoul'd be as simple as possible to manufacture and maintain, while avoiding any significant loss of performance. The size and weight should be much less than the existing design. One of the disadvantages of the existing design is that 12 different bridged-T sections are required, each of which has to be separately tuned to a different frequency; in addition there are 24 different inductors and 24 different capacitors, the total design requiring four of each inductor, four of one type of capacitor and eight of the other type: in all, 240 components.

If for example a system could be devised which used only one type of bridged-T network, a considerable practical simplification would be achieved. Several identical sections would be needed, but perhaps not as many as 48.

Consider again the second-order delay response examined in Chapter 2, and illustrated in Fig.2.2. In general, this delay/frequency curve is not symmetrical about the centre frequency owing to the contribution from the tail of the predominantly negative frequency response. However, it has been shown that, under the following conditions;

$$\frac{\omega_0}{\sigma_0} > 3 \qquad \text{and} \qquad |\omega_0 - \omega| < 0.3\omega_0$$

equation (2-6) may be approximated by a symmetrical response, given by

$$\tau'(\omega) = \frac{2/\sigma_0}{1 + \left(\frac{\omega - \omega_0}{\sigma_0}\right)^2} \quad . \qquad (4\text{-}1a)$$

Alternatively, this may be expressed in terms of the effective Q factor, Q_e

$$Q_e = \frac{\omega_0}{2\sigma_0}$$

i.e.

$$\tau'(\omega) = \frac{4Q_e/\omega_0}{1 + \frac{4Q_e^2}{\omega_0^2}(\omega - \omega_0)^2} \quad . \qquad (4\text{-}1b)$$

This relationship is plotted in Fig.4.1 for some typical Q_e values and for $f_0 = 100\text{kHz}$ ($\omega_0 = 2\pi f_0$).

A symmetrical response makes the following ideas possible. It is proposed to use the second-order delay response as the basis for a complete two-channel dispersive network, able to compress both upward and downward sweeps (ones and zeros).

A cascade arrangement of n identical networks has an overall group delay equal to n times the delay of one section, given by equation (4-1). If the parameters n and Q_e are chosen carefully, a differential delay of T seconds can be obtained between frequencies f_0 and $(f_0 + F)$Hz, and this nonlinear response, viewed separately from the other half of the curve, may be considered as a dispersive delay function. Then, a swept frequency signal is envisaged (whose characteristic is derivable from the delay curve) with a frequency/time relationship which exactly matches this n-section response. This signal is nonlinearly swept upwards from f_0 to $(f_0 + F)$Hz in T seconds.

Similarly a downward sweep from f_0 to $(f_0 - F)$Hz in T seconds is arranged to match the lower half of the frequency response.

The attractive feature of the proposal is that the arrangement makes use of the maximum possible amount of delay available, with the synthesised delay not directly usable confined to the area under the pedestal, height t_1 seconds (Fig.4.2), and the tails at $|f_0 - f| > F$. At this stage, it is evident that as Q_e increases, so the usable delay area increases, but, at the same time, the response departs further from a linear delay function. Therefore, a compromise is necessary between the number of sections and the Q_e value, but a choice should be made only when pulse responses have been examined.

The basic philosophy will be expanded into a complete demodulator scheme in a later section. Meanwhile, it will be demonstrated how explicit relationships for signals and spectra may be derived.

4.3 Signal design

Introducing a new parameter, a, defined as

$$a = \frac{\sigma_0}{2\pi} = \frac{f_0}{2Q_e}$$

the (approximate) delay response of n identical sections in cascade is

$$\tau'_n(f) = \frac{n/\pi a}{1 + \left(\frac{f - f_0}{a}\right)^2} \quad . \qquad (4\text{-}2)$$

For a given value of f_0, there is a unique relationship between n and a. To find this relation, the following conditions are required (refer Fig.4.2):

(i) $\tau_n'(f) = T + t_1$ at $f = f_0$

(ii) $\tau_n'(f) = t_1$ at $f = f_0 + F$.

Eliminating t_1 from the two equations obtained, we find

$$n = \pi a T(1 + a^2/F^2) . \qquad (4\text{-}3)$$

Once again, the stationary phase principle is invoked in order to obtain the time/frequency characteristic of the matched input signal

$$t(f) = -\tau_n'(f) + t_1 .$$

After substitution and rearrangement, the instantaneous frequency of the matched signal becomes

$$f_{(1)}(t) = f_0 + a\left\{\frac{T}{t}\left(1 + \frac{a^2}{F^2}\right) - 1\right\}^{-\frac{1}{2}} \qquad 0 < t < T . \quad (4\text{-}3a)$$

Similarly, the signal matched to the low frequency half of the symmetrical response is

$$f_{(0)}(t) = f_0 - a\left\{\frac{T}{t}\left(1 + \frac{a^2}{F^2}\right) - 1\right\}^{-\frac{1}{2}} \qquad 0 < t < T . \quad (4\text{-}3b)$$

The 'one' signal, $f_{(1)}(t)$, occurs in $f_0 < f < f_0 + F$ and the 'zero' signal, $f_{(0)}(t)$ in $f_0 - F < f < f_0$. In practice the signals will have to be transmitted within the same bandwidth F and so a means of separating the signals will have to be devised. A typical transmitted signal of a {1,0} pattern is illustrated in Fig.4.3, and compared with the equivalent chirp signal.

The (n,Q_e) relationship, obtained from equation (4-3), is shown in Fig.4.4. On this curve the number of sections should be compared with

the total number in a two-channel chirp system, since the n sections perform the operations of both channels, as will be demonstrated in the next section. Thus, 30 sections each with a Q_e of 4.7 could do the job of 96 sections in the existing design, if the performance is satisfactory. The qualifying statement about performance must be examined in detail, since as shown in Chapter 3 the performance will degrade as the FM waveform becomes more nonlinear.

In order to obtain manageable expressions for spectra, and to calculate output pulse shapes, the stationary phase approximation is again used. The spectrum magnitude function in its approximate form requires an expression for the first time derivative of the instantaneous frequency function, i.e.

$$2\pi \frac{df(t)}{dt} = \theta''(t) = 2\pi \frac{aT}{2t^2}\left(1 + \frac{a^2}{F^2}\right)\left\{\frac{T}{t}\left(1 + \frac{a^2}{F^2}\right) - 1\right\}^{-\frac{3}{2}}. \quad (4\text{-}4)$$

Making t the subject in equation (4-3a) and substituting in equation (4-4) to remove the t-dependence, the expression for $\theta''(t)$ obtained is substituted in equation (B-5), giving:

$$\left.\begin{aligned} |S_M(f)| &\doteq \sqrt{\frac{nf_0}{\pi Q_e}} \frac{1}{(f - f_0)^{\frac{3}{2}}} \frac{1}{\left\{1 + \frac{1}{4Q_e^2}\left(\frac{f_0}{f - f_0}\right)^2\right\}} \\ &= \sqrt{\frac{2an}{\pi}} \frac{1}{(f - f_0)^{\frac{3}{2}}} \frac{1}{\left\{1 + \left(\frac{a}{f - f_0}\right)^2\right\}} \end{aligned}\right\} \quad f_0 < f < f_0 + F . \quad \ldots\ldots \quad (4\text{-}5)$$

These stationary phase spectra are drawn in Fig.4.5; the important differences to note between these spectra and the uni-directional FM spectra in the previous chapter (Fig.3.3 for example) are that the peak power occurs at a frequency greater than 100kHz (f_1) and that the power at 100kHz is zero, caused by df/dt being infinite at this frequency. The smooth functions appear more readily realisable with simple amplitude equalisers than the sharp transitions encountered before. This could be an advantage if a truly matched filter is found to be necessary.

As before the compressed pulse is obtained from the inverse Fourier transform of the output spectrum. With a matched filter, the output spectrum is

$$G(f)_{MF} = |S(f)|^2 \sqrt{\frac{T}{F}} \quad .$$

With an all-pass filter the output spectrum is

$$G(f)_{AP} = |S(f)|$$

assuming, in accordance with the stationary phase approximation, that the phase spectrum of the input is exactly matched by the phase response of the filter. The matched filter outputs are given in Fig.4.6 and the all-pass outputs in Fig.4.7. The matched outputs are significantly wider than those derived in Chapter 3, and the nulls are very shallow or, for most $n < 60$, even non-existent. The nulls, when they do occur, appear to exist at times up to 5μs later than those previously studied. These phenomena would intuitively imply a reduced bandwidth; examination of the spectra in Fig.4.5, compared with Fig.3.3 say, reveals that the tendency to zero power at f_1 is likely to have this effect on the effective bandwidth. The signal power has been redistributed from the sidelobes to the main lobe which is wider, though still equal to $\sqrt{FT}$ at its peak.

The all-pass output is also wider by about 2μs, again with deeper nulls than the matched outputs but overall lower sidelobe levels. As a response suitable for the present purpose, the all-pass network would appear preferable as a compromise between peak loss and pulse width. (For example, with $n = 48$ the loss is only 0.39dB and the -3dB pulse width 9% greater than the chirp system; the matched pulse has a width 24% greater, and would require an amplitude equaliser.)

The dispersed pulse is obtained when the upward swept signal is operated upon by the left-half response. The output is:

$$g(t) = \sqrt{\frac{F}{T}} \int_{-\infty}^{\infty} |S(f)_1| \; |S(f)_0| e^{j\{\Phi_0(f)-\Phi_1(f)\}} e^{j2\pi ft} df \qquad (4\text{-}5a)$$

in the matched case and

$$g(t) = \int_{-\infty}^{\infty} |S(f)_1| e^{j\{\Phi_0(f)-\Phi_1(f)\}} e^{j2\pi ft} df \qquad (4\text{-}6b)$$

in the all-pass case.

The matched system gives a symmetrical dispersed pulse (see Fig.4.8) which has a maximum amplitude at its centre, whereas the all-pass system gives a non-symmetrical dispersed pulse falling in amplitude with time (see Figs.4.9 and 4.10). If the compression gain is defined as the ratio of the peak amplitude of the compressed pulse to the amplitude of the dispersed pulse at its mid point the difference between the matched and all-pass schemes for $n = 48$ is 0.14dB in favour of the all-pass scheme.

4.4 Complete demodulator

A complete demodulator scheme (Fig.4.11) employing the signals described above begins by accepting a sequence of swept FM signals at the receiver output, centred on an intermediate frequency, say f_c. The upward sweep representing a one is defined by

$$f(t)_1 = f_c - \frac{F}{2} + p(t) \qquad (0 < t < T)$$

and a zero by

$$f(t)_0 = f_c + \frac{F}{2} - p(t) \qquad (0 < t < T)$$

where $p(t) = a\left\{\frac{T}{t}\left(1 + \frac{a^2}{F^2}\right) - 1\right\}^{-\frac{1}{2}}$.

In the chirp system, the two channels are separated using two frequency changers whose attendant oscillator frequencies are arranged such that the sweep direction is inverted in one channel but unaltered in the other, in order that networks of identical design can be used in the two channels. In this proposal, a single network is able to perform the pulse compression required in both channels; however, the signals must be separated in frequency such that the ones are compressed by the response above f_0, and the zeros by the response below f_0. After

frequency changing, without inversion, the signals, in adjacent bands, are added together and passed through the n-section network. The oscillator frequencies which drive the frequency changers are $(f_c - f_0 + F/2)$ and $(f_c - f_0 - F/2)$. The two channels must be separated again after the network, and this may be achieved with two filters, each having a cut-off frequency f_0, one high-pass for the one's channel, the other low-pass for the zero's channel.

The rest of the detection system can be the same as for chirp, the data being recovered by rectifying, clipping and triggering digital decision circuits.

4.5 Implications and discussions

4.5.1 Signal generation

In chirp the FM modulating function is a linear ramp, for which several circuits have been developed for many purposes. In this proposal, the modulating function is unique; certainly there exist no circuits to generate it. Therefore, a special part of the design includes the generation of the nonlinear modulating function, as shown in Fig.4.3. Experience in Radio Department, RAE has shown that for communications purposes the most reliable signal generation technique is to produce a voltage waveform and to modulate a signal source, such as a Schlumberger synthesiser. This is particularly useful in the development phase, and even in practice on the ground-satellite-air link, but a more compact system is essential for the air-ground link.

An elegant standard technique is to use the dispersive network to generate the swept signal, by exciting it with an impulse. This technique is designated passive generation. If the impulse is of the right form a good approximation to the required signal is obtained.

For the purposes of this exercise, a controllable method of generation was required, and in view of the lack of success with the passive method at RAE, an active method was chosen. Practical details will be given in the next chapter. In essence the technique involves approximating the required waveform by adding the weighted outputs of a long shift register which shifts a single pulse along its whole length during each period T seconds. The length (i.e. number of bits) of the shift register and hence the clock rate will depend upon the accuracy to which the waveform must be approximated.

4.5.2 The channel filters

The filters required to separate the two channels after the dispersive network are an added complication to the proposed system compared with standard chirp. Their performance is vital to its successful operation. The overall spectrum of a sequence of upward and downward sweeps presented to the input terminals of each channel filter has a sharp minimum at the centre frequency f_0 . This gives some help to the filtering process, since, at 100kHz the spectra are already 12dB down compared with 90kHz and 110kHz. The contribution to the output pulse shape from the spectra in this interval is likely to be smaller than the remainder, as shown by the apparently smaller effective bandwidth in the output pulse (see section 4.3). Therefore the cut-off frequency of the channel filters can be placed either side of f_0 , such that a less complex filter may be possible than would be necessary if the spectra were more closely spaced near f_0 . A guard band between the two channels was not included since the maximum delay of the bridged-T network occurs at the centre frequency, and a large proportion of the delay would have to be wasted if the centre of the response were not utilised for pulse compression.

To achieve satisfactory channel separation sharp cut-off filters are essential (e.g. elliptic function or Chebyshev types) but it is well-known that such filters exhibit poor phase linearity. This fact is demonstrated in Fig.4.12 which gives the amplitude and time delay response of a seventh order low-pass elliptic function filter (three inductors and seven capacitors) which, while providing good rejection, has an unwanted peak in the delay response near cut-off. As discussed above, the filter response can be so placed as to approximately match (in this case) the high frequency end of the spectrum of a zero. This in conjunction with a second-order low-pass filter (see later) can approximately match the amplitude spectrum, but the delay response is unsatisfactory.

Without unacceptable further complexity which would be necessary if an attempt were made to equalise this undesirable nonlinear delay, the following courses of action are available.

(1) Incorporate the delay response of the channel filter into the matched filter delay response, and modify the signal to match the resultant delay, thus making the best use of a troublesome effect. Since the

signal function can be tailored easily using the tapped shift register technique, this solution is promising in the long run as a means of overcoming delay distortion problems. The distortion is small enough that the output should not be significantly modified by including it in the signal.

(2) Use a higher order but still less discriminating filter (such as a Butterworth or Gaussian type) with better phase linearity but added co-channel interference. The trade-off calculation between phase linearity and amplitude rejection is complicated by a complexity constraint. Any degree of matching can be achieved in theory but must be paid for by added size and weight. Since this constraint is the principle purpose of the project, this solution was not followed up in detail.

(3) The simplest course of action is to ignore the delay perturbation, and accept some degradation of performance. In the short term, and for the purposes of the practical investigation described in a later chapter, this route is recommended, although the first solution above should be adopted in any further development of the system.

4.5.3 Number of sections

Table 4.1 summarises the performance of a likely range of (n,Q_e) combinations, in terms of compression gain, compressed pulse width and a measure of complexity expressed as a percentage of the size of the chirp system. Included in the complexity is an amount for the channel filters, assumed to be equivalent to four bridged-T sections. The high values of compression gain in the matched filter column should be weighed against the increased width of the compressed pulse. It is interesting to note that the width of the all-pass compressed pulse is constant for the range of n values examined. The value chosen will ultimately depend on the relative weights placed on the various performance measures. Size and weight reduction at any cost probably implies an approximately matched system with n less than 40, but a pulse width increase of more than 30%; or an all-pass system with only 10% pulse width increase, but more than 3dB loss in compression gain.

The first column is headed $n/2$ because the hybrid technique explained in chapter 2 is equally applicable to this system, allowing half the design number of sections to be used twice over, with a short circuit after $n/2$ sections.

Another important input to the decision on the number of sections is the value of Q_e required for each sub-network.

For small Q_e values, the symmetrical approximation to the group delay is less accurate. Fig.4.13 shows how the difference between the approximate and exact delay responses varies over the frequency range of interest for Q_e from 2 to 4. The two delay curves equations (2-9) and (4-1b) are compared strictly: i.e.

$$\omega_0^2 = \bar{\omega}_0^2 (1 - 1/4Q_e^2)$$

where $\omega_0 = 2\pi f_0$ and f_0, the maximum delay frequency, is 100kHz.

Furthermore, the practical problems described in Chapter 2 dictate that Q_e should neither be small nor large; all the values in Table 4.1 are acceptable, so this factor has only a small effect on the choice.

The above factors point to an acceptable value in the range 45 to 55; a value of 48 was chosen for the practical work, to emphasise the point that the network complexity had been effectively halved compared with the RAE system. This corresponds to a Q_e value of 3.155 which poses no practical difficulties. Inductor Q values need be no greater than 200.

4.6 Further developments

A further improvement, which has not been investigated practically can be achieved by taking advantage of a reduction in the effective transmitted bandwidth due to df/dt of the signal being infinite at f_0. The effective bandwidth can be variously defined, but assume arbitrarily that it should be between those frequencies at which the power spectrum of the signal is the same as the power spectrum of the equivalent chirp waveform at $f_0 \pm F/2$. Comparing Figs.1.2 and 4.14 (the exact spectrum for $n = 48$) this means that the effective bandwidth of the $n = 48$ system is only $0.85F = F'$. Thus if the value of F is increased (to say F/0.85) better use can be made of the available bandwidth.

A test case simulation was run with the following parameters:-

$\hat{Q}_e$ unchanged (=3.155)

F increased to 46.666kHz

f_0 increased to 116.666kHz

n increased to 56 .

Fig.4.15 shows the exact spectrum magnitude function of this signal.

It may be seen by comparison with Fig.1.2 that the spectrum magnitudes are similar at $f_0 \pm 20$kHz such that roughly equal powers are contained between these limits. (A complete comparison by numerical integration between these limits has not been performed but an approximate 'square counting' process has confirmed this statement.) The compressed pulse is as shown in Fig.4.6 (for n = 48) with the time axis contracted by a factor 6/7 and the peak amplitude increased by a factor $\sqrt{7/6}$.

Since this improvement was not made till a later stage in the project it was not investigated experimentally. However, it is suggested that in any further work on this topic the question of effective bandwidth is carefully considered since beneficial gains can be made.

Table 4.1

COMPARISON BETWEEN POSSIBLE (n,Q_e) COMBINATIONS

$\frac{n}{2}$	Q_e	Peak amplitude of compressed pulse (input amplitude = 1		Matched filter peak/ all-pass (dB)	Compression gain (dB)		-3dB pulse width μs		Size and weight saving %	
		MF	AP		MF	AP	MF	AP	MF	AP
20	3.66	5.77	5.44	0.52	18.32	17.57	29.8	24.5	46.0	50.0
22	3.38	5.77	5.48	0.44	18.10	17.63	28.8	24.5	41.5	46.0
24	3.16	5.77	5.52	0.39	17.84	17.69	28.0	24.5	37.5	41.5
26	2.97	5.77	5.55	0.34	17.60	17.74	27.5	24.5	33.0	37.5
30	2.66	5.77	5.59	0.27	17.38	17.80	27.0	24.5	25.0	29.0
35	2.38	5.77	5.63	0.23	17.16	17.86	26.5	24.5	14.5	19.0
Linear FM (chirp)		5.77	5.77	0.0	18.23	18.23	22.5	22.5	0	0

Chapter 5

AN EXPERIMENTAL IDENTICAL SECTION IC FILTER PULSE COMPRESSION SYSTEM

5.1 Introduction

This chapter describes briefly an experimental demonstration of the non-linear FM principles which were introduced in Chapter 4. The major tasks were to construct the filters and associated hybrid signal splitting circuit, and to find a suitable method of synthesising the required non-linearly swept input signal. These signals were examined for comparison of their spectra with theoretical calculations. The signals were then applied to the networks and output pulse shapes similarly examined.

5.2 Bridged-T network design

The design chosen for the study was the 48 section design where each section has a Q_e value equal to 3.155. The filters are required to have their maximum delay at a frequency of 100 kHz.

i.e. $$\omega_0 = 2\pi\ 10^5 = 2\pi f_0 \ .$$

The frequency $\bar{f}_0$ at which the lattice arms resonate is given by

$$\bar{f}_0 = f_0 \Big/ \sqrt{1 - 1/4Q_e^2}$$

$$= 1.014\ f_0$$

i.e. $$\bar{f}_0 = 101.4 \text{ kHz} \ .$$

Using the expressions given in equation (2.8) the component values for the chosen bridged-T realisation (Figure 2.3b) are

$$L_A = 0.5978 \text{ mH} \qquad C_A = 3718 \text{ pF}$$

$$L_B = 1.4879 \text{ mH} \qquad C_B = 830 \text{ pF} \ .$$

The inductors were constructed from 14 mm Mullard Vinkor assemblies and multistrand copper wire (40/48 gauge for L_A and 16/48 for L_B). The capacitors were purchased from Suflex as matched pairs to $\frac{1}{2}\%$ tolerance; quantities sufficient for 24 complete sections were obtained.

The circuits were assembled on two special purpose printed circuit boards which had been designed for the previous RAE chirp experiments, each of which holds 12 sections.

Each section was adjusted by the method described in section 2.4.3 at the frequency $\bar{f}_0$ before they were connected together.

The phase response of the 12 sections was then measured using a Wiltron phase meter; the delay response derived from these phase requirements is shown in Fig.5.1, and compared with the theoretical response.

5.3 Signal generation

Synthesis of the non-linearly swept FM signal which must match the response as closely as possible was an important aspect of the experiment. The technique chosen is illustrated in Fig.5.2. It consisted of tailoring a stepped voltage ramp waveform which was then applied to a frequency modulator. The stepped ramp was made to approximate as closely as possible to the required continuous waveform, and the size of the step was chosen to minimise the error at each sample consistent with a reasonable limit on the circuit complexity.

It was decided to divide the 833.3 μs data bit period into 64 samples, requiring a basic clock rate of 76.8 kHz. The clock was divided down to give a pulse of duration one clock period every 64 clock periods which was then applied to the input of a 64 bit shift register (serial in, parallel out) driven by the same basic clock. The registers were 13 SN 7496 5 bit devices.

The 64 parallel outputs were connected via 64 specially selected resistors to the inverting input of a summing amplifier (μA702). The resistor values were chosen such that the gain of the amplifier was proportional to the required amplitude at 64 points on the waveform. Fig.5.3 is an oscilloscope photograph of the resulting waveform.

To obtain a (1,0) data pattern a downward sweep was required to alternate with the upward sweep. The modulating waveform for this signal was obtained as shown in Fig.5.4. A gating waveform was obtained from the shift register input signal by dividing by 2; this square wave and its inversion (between +5v and 0v) were modified to MOS levels (- 10v, 0v) in a TTL/MOS interface circuit and applied to the gates of a pair of MOS analogue switches (Plessey ML150 series). The signals to be switched were the sampled ramp and its inverted replica. The switched outputs were summed at the summing junction of a 702 wideband amplifier. The resulting (1,0) modulating signal is shown in Fig.5.5.

5.4 Demonstration of pulse compression

The object of this experiment was to demonstrate the characteristics of pulse compression signals and spectra. The experimental system is illustrated in Fig.5.6.

5.4.1 Hybrid signal splitting network

As in the RAE chirp system a hybrid network was used to halve the size of the dispersive filter. The network consisted of three 600 Ω resistors and a difference amplifier connected as shown in Fig.2.6. The dispersive network with 24 identical sections in series was short circuited at the end.

5.4.2 Output signals

Fig.5.7 shows oscilloscope photographs of compressed pulses obtained when a continuous sequence of unidirectional swept waveforms was applied to the network. The sequence of upward sweeps in $100\ \text{kHz} < f < 140\ \text{kHz}$ gave rise to the output in Fig.5.7.a and the downward sweeps in $60 < f < 100$ kHz gave the output in Fig.5.7.b.

Fig.5.7.c is an expanded version of the low frequency output. There are four cycles of carrier within the main lobe $(= 2f_0/F = 2 \times 80/40)$.

Clearly the signals in the two cases are not identical. This is due to practical alignment problems which make it difficult to produce exactly matched input signals. The factors which affect the shape of the compressed pulse most significantly are:

(a) data rate: this can be controlled by frequency counting either the original clock or the derived ramp waveform

(b) centre frequency: using the Schlumberger waveform synthesiser a centre frequency can be set very accurately but the centre frequency of its output also depends on the symmetry about zero potential of the modulating waveform

(c) bandwidth: this can be adjusted either by varying the amplitude of the ramp or by an adjustment for FM deviation on the Schlumberger front panel. Calibration of the input spectrum is extremely difficult however so it is practically more convenient, as was found in development of the RAE chirp system, to adjust the sweep bandwidth and centre frequency in combination to obtain the "best" compressed pulse shape.

5.5 Complete system

5.5.1 Network response

Fig.5.8 illustrates in block diagram form the experimental arrangement which was used to demonstrate the signals which would be produced in a complete 48 section demodulator utilising high pass and low pass filters at the network output to separate the channels.

Fig.5.9.a shows the signals obtained at the input and output of the dispersive network. The signals contain two sequences of upward/downward sweeps (one centred on 80 kHz and the other on 120 kHz) which were summed before the dispersive network. The output is a continuous sequence of compressed pulses combined with a continuous sequence of dispersed pulses.

Fig.5.9.b shows the spectra of these two signals as measured and displayed on a Tektronix spectrum analyser plugin to the oscilloscope. Some distortion of the magnitude spectrum is evident: some loss (equivalent to about 1.5 dB) is occurring near the centre frequency together with a distortion around 82 kHz. The effects are attributed to

(1) the hybrid network and the necessary short circuit at the output of 24 sections

(2) the loss characteristic of the network

(3) the imperfect match between the signal and the network

(4) the difference amplifier at the output of the hybrid network.

5.5.2 Filter networks

The filters chosen for the channel separation were 7th order elliptic function filters with cut-off frequencies of 101.4 kHz. They were constructed from 14 mm Vinkor assemblies and selected Suflex capacitors.

5.5.3 Filter outputs

Fig.5.10.a shows the spectra at the outputs of the high pass and low pass filters and Fig.5.10.b shows these signals.

Clearly there has been some loss of signal within the pass-band, particularly for the lower frequency signal near 100 kHz. In addition the dispersed pulse in the higher frequency channel is somewhat larger

in amplitude than the dispersed pulse in the low frequency channel. The best measured compressed to dispersed pulse ratios that were obtained by the process of adjustment described in 5.4.2 were

high frequency channel : 15.5 dB

low frequency channel : 16.2 dB.

The theoretical figure for a correctly matched system given perfect channel filtering (i.e. sharp cut-off, linear phase) is 17.7 dB in each case based on the results in Chapter 4.

The effect of the network and the high pass filter on the spectra is illustrated in Fig.5.11 which shows the spectra at the input and the outputs for a continuous sequence of upward sweeps. The losses due to the dispersive network are clearly shown as well as the effect of the high pass filter at the low frequency end of the spectrum.

5.6 Summary and discussion

The ability of an identical section passive dispersive network to operate on a sequence of upward and downward frequency sweeps approximately matched to its response has been demonstrated.

The advantage of the system has been explained in Chapter 4, namely the reduction in size of the network itself by a factor 2.

The weaknesses and difficulties of the system became clearer during the experimental study.

(a) First it is essential that a good match between the input waveform and the delay response of the network is obtained. Further refinements to the non-linear voltage ramp are obviously possible. A step-wise approximation using 64 samples was simple in concept from an experimental viewpoint but further modifications were clearly needed to obtain a closer match, as evidenced by the approximate nature of Fig.5.3.

(b) The channel separation filters are clearly a cause of distortions. Some effect is inevitable since the two channels have no deadband between and co-channel interference to some degree is unavoidable. As suggested in section 4.5.2 the optimum solution is to choose a sharp cut-off filter for the channel separation, determine its

phase and hence delay response, add this to the delay response of the dispersive network and modify the input waveform to match this summed response. Optimum benefit would then be gained from the necessary introduction of the channel filters.

(c) A closer approximation to a matched filter could be made by introducing a low order filter whose magnitude response matches the spectrum of the input signal. Again the phase response could be added into the dispersive network response and the modulating waveform slightly modified accordingly. This would have the primary effect of reducing the level of the dispersed pulse whilst at the same time slightly increasing the compressed pulse peak amplitude, widening the main lobe and reducing the null depth.

5.7 Conclusions

5.7.1 A novel technique for using the response obtained from a cascade of identical all-pass networks as a dispersive network has been demonstrated. Signals which approximately match the response have been generated and compressed and dispersed pulses examined.

5.7.2 In the experimental study a shortfall in performance (compressed to dispersed pulse ratio) was apparent compared to the theoretical predictions. This was attributed to approximations in the modulating waveform and imperfect channel filters. Improvements which should largely overcome this problem have been suggested for any future development of the system.

5.7.3 In comparison with the existing chirp system the technique investigated here possesses many advantages but although the disadvantages can be quite simply overcome it is unlikely that for the given application the size reduction is significant enough to warrant a change. Therefore digital techniques were investigated more thoroughly and the following chapters describe the work undertaken.

Chapter 6

A DIGITAL FILTER TECHNIQUE EMPLOYING CASCADED IDENTICAL SECTIONS

6.1 Introduction

Previous chapters have described some methods which are in essence modifications of established design techniques which enable more economic use to be made of traditionally synthesised delay. However, by retaining passive networks as building blocks an irreducible size limit is reached, at least until a major breakthrough is made in the design of inductors and capacitors of the required range of values. Therefore, alternative techniques were sought in the field of active circuits in the light of ever increasing interest in the development and application of integrated circuits for both linear active filters and digital systems.

In recent years many authors have described active filter realisations of all-pass networks using various types of frequency selective feedback schemes and relying for the gain element upon commonly available linear integrated circuit operational amplifiers such as Fairchild μA709 and μA741. Such an approach to the present problem is possible as discussed in chapter 2 but would primarily involve implementation in the form of say a thick or thin film circuit which was considered to be outside the terms of reference of this study.

Therefore it was decided to consider the problems of dispersive network synthesis using digital filter techniques, which, although unlikely to provide a cheap short term answer, would if successful hold promise for long term integrated circuit development. This chapter deals briefly with general digital filter topics, particularly the all-pass realization, and goes on to develop some ideas already considered in an earlier chapter for use with digital filters. Error probabilities in a communications system employing digital dispersive filters are also derived.

6.2 State of the art

The recent rapid developments in large-scale integration (LSI) of digital circuits has greatly increased the possibility of implementing digital filters directly into hardware. For several years mathematicians and engineers have examined in detail the theoretical aspects of digital filters until the stage has been reached when theory is ready and waiting for a suitable realization technique to appear. To realise the full potential of digital filtering a fast, reliable, inexpensive

form of integrated circuit is required, and only recently has MOS technology reached the stage where all three requirements are becoming available. Custom design of MOS circuits, with the aid of advanced computer aided design techniques at all stages is falling within the scope of many firms who do not even possess their own IC manufacturing capability.

Therefore, the time has come when certain special kinds of filtering operation are ideally suited for implementation in digital form; in particular applications which require banks of filters or multiplexed operations are highly suitable. In due course, even single filter functions will be included, particularly as part of an otherwise entirely digital application.

The solution proposed in this chapter is just such a suitable application since the signal is recirculated through the same hardware several times in different time slots and full use is made of all available circuit speed and maximum packing density.

6.3 Brief summary of digital filter theory

6.3.1 General digital filters

A digital filter is the implementation of a linear constant coefficient difference equation. To realise a linear difference equation the input signal must consist of discrete samples, and it is usual to consider only uniformly spaced samples. The sample amplitudes are quantized and processed by logic circuits and delay elements which perform the required numerical operations.

A linear difference equation with constant coefficients relates the sequence of input samples u_n to the sequence of output samples v_n as follows:

$$v_n = \sum_{k=0}^{M} a_k u_{n-k} - \sum_{k=1}^{N} b_k v_{n-k} \quad . \tag{6-1}$$

Thus the output sample v_n is computed from the current input u_n and a linear combination of past inputs and outputs. The choice of the coefficients a_k and b_k determines the performance of the digital filter.

The z-transform of equation (6-1) may be written:

$$V(z) = \sum_{n=0}^{\infty} v_n z^{-1}$$

$$= \sum_{n=0}^{\infty} \left\{ \sum_{k=0}^{M} a_k u_{n-k} - \sum_{k=1}^{N} b_k v_{n-k} \right\} z^{-n}$$

$$= \sum_{k=0}^{M} a_k z^{-k} U(z) - \sum_{k=1}^{N} b_k z^{-k} V(z) \quad .$$

Thus, the z-transform of the transfer function is

$$H(z) = \frac{V(z)}{U(z)} = \frac{\sum_{k=0}^{M} a_k z^{-k}}{1 + \sum_{k=1}^{N} b_k z^{-k}} \quad . \qquad (6\text{-}2)$$

If the sampling interval is Δt the unit delay operator z^{-1} can be replaced by $\exp\{-j\omega\Delta t\}$ to determine the frequency response of a system with z-transfer function $H(z)$. Thus the frequency response of a digital filter is determined by the values of its transfer function on the unit circle ($|z| = 1$) just as the frequency response of a continuous-time filter is determined by its values on the imaginary axis.

Fig.6.1 represents a machine which implements the linear difference equation (6-1). A circle describing a constant represents multiplication of a variable by a constant and a rectangle with Δt inscribed represents a one-sample delay. A triangle with a summation inscribed is a summing point. All input and output samples u_{n-k}, v_{n-k} are delayed and are available for computation of y_n at any given sample instant.

Equation (6-1) is not the only way of realizing the function $H(z)$. Consider the introduction of an intermediate variable w_n :

$$w_n = u_n - \sum_{k=1}^{M} b_k w_{n-k}$$

$$v_n = \sum_{k=0}^{N} a_k w_{n-k} \quad .$$

This system may be represented in a different form shown in Fig.6.2 which requires only N or M delay elements (depending on which is the larger).

For high order functions accuracy considerations lead to the need to express H(z) either as a partial fraction expansion leading to a parallel form of representation (Fig.6.3a) with

$$H(z) = H_1(z) + H_2(z) + \ldots$$

or as a cascade of factored functions each of which includes a subset of the poles and zeros of H(z), (Fig.6.3b), i.e.

$$H(z) = H_1(z) \times H_2(z) \times H_3(z) \times \ldots \quad .$$

6.3.2 All-pass digital filters

Consider the special case where the numerator and denominator coefficients are related as follows:

$$\left.\begin{aligned} a_n &= b_{N-n} \\ a_N &= 1 \end{aligned}\right\} \quad . \qquad (6\text{-}3)$$

Then H(z) may be written

$$H(z) = z^{-N}\left\{\frac{1 + a_{N-1}z + \ldots + a_1 z^{N-1} + a_0 z^N}{1 + a_{N-1}z^{-1} + \ldots + a_1 z^{-(N-1)} + a_0 z^{-N}}\right\}$$

and replacing z^{-1} by $\exp\{-j\omega\Delta t\}$ to obtain the frequency response, we obtain

$$H(\omega\Delta t) = e^{-jN\omega\Delta t}\left\{\frac{1 + a_{N-1}e^{j\omega\Delta t} + \ldots + a_1 e^{j(N-1)\omega\Delta t} + a_0 e^{jN\omega\Delta t}}{1 + a_{N-1}e^{-j\omega\Delta t} + \ldots + a_1 e^{-j(N-1)\omega\Delta t} + a_0 e^{-jN\omega\Delta t}}\right\}$$

$$= e^{-jN\omega\Delta t}\,\frac{P(\omega\Delta t)}{P^*(\omega\Delta t)}$$

where $P^*(\omega\Delta t)$ is the complex conjugate of $P(\omega\Delta t)$.

Since (by definition) $|P(\omega\Delta t)| = |P^*(\omega\Delta t)|$ then $|H(\omega\Delta t)| = 1$. Thus the coefficients (6-3) define an all-pass filter function. Furthermore, since $\arg\{P^*(\omega\Delta t)\} = -\arg\{P(\omega\Delta t)\}$ then

$$\arg\{H(\omega\Delta t)\} = -N\omega\Delta t + 2\arg\{P(\omega\Delta t)\}$$

thus

$$\Phi_N(\omega) = -N\omega\Delta t + 2\arctan\left\{\frac{\sum_{k=1}^{N} a_k \sin k\omega\Delta t}{1 + \sum_{k=1}^{N} a_k \cos k\omega\Delta t}\right\} . \qquad (6\text{-}4)$$

Equation (6-4) is the phase response of $H(z)$ to a signal of frequency ω sampled at intervals of Δt.

Now consider a first order system ($N = 1$; $a_0 = 1$; $a_1 = b_1 = a$):

$$H(z) = \frac{z^{-1} + a}{1 + az^{-1}} . \qquad (6\text{-}5)$$

The phase response is

$$\Phi_1(\omega) = -\omega\Delta t + 2\arctan\left(\frac{a \sin \omega\Delta t}{1 + a \cos \omega\Delta t}\right) \qquad (6\text{-}6)$$

and the group delay $\tau_1(\omega) = -\dfrac{d\Phi_1(\omega)}{d\omega}$ is

$$\tau_1(\omega) = \frac{\Delta t(1 - a^2)}{1 + a^2 + 2a \cos \omega\Delta t} . \qquad (6\text{-}7)$$

This group delay response is plotted in Fig.6.4 for some typical values of the coefficient a, both positive and negative. The response repeats at frequency intervals equal to the sampling frequency, $f_s = 1/\Delta t$, and is even with respect to frequencies $f = nf_s/2$. (Similarly the phase function $\Phi_1(\omega)$, in fact $\Phi_n(\omega)$ in general, is an odd function with respect to frequencies $f = nf_s/2$.)

The difference equation for the first order all-pass section is

$$v_n = au_n + u_{n-1} - av_{n-1} \qquad (6\text{-}8)$$

i.e.

$$v_n = a(u_n - v_{n-1}) + u_{n-1} . \qquad (6\text{-}9)$$

The direct realisation of this equation is shown in Fig.6.5a which requires two multipliers, one delay element and two summing points. Equation (6-8) suggests a different realisation shown in Fig.6.5b requiring two delays, two adders and one multiplier while Fig.6.5c shows a third possibility (two delays, two adders and two multipliers), and Fig.6.5d a fourth (two delays, one adder, two multipliers).

For practical reasons Fig.6.5b is preferred since only one multiplier is needed and the multiplier is the largest part of the filter in terms of circuit complexity. This arrangement is only possible for all-pass functions (where the coefficients in the numerator of $H(z)$ are the same magnitude as those in the denominator) such that the multiplication can occur after the summation of two numbers.

Since the delay response of a single all-pass delay section will be directly used in what follows it is worth taking a closer look at its characteristics.

(a) $\tau_1(\omega)$ is an even function with respect to the frequencies $\omega = n\omega_s/2$ $(\omega_s = 2\pi/\Delta t)$

(b) $$\int_0^{\omega_s} \tau_1(\omega)d\omega = 2n\pi$$

(c) $$\tau_{max} = \left(\frac{1 + |a|}{1 - |a|}\right)\Delta t$$

(d) in $0 < f < f_s/2$ the response is a mirror image about $f_s/4$ for coefficient values of opposite sign, i.e.

$$\tau(\omega)_{a\ positive} = \tau(\omega_s/2 - \omega)_{a\ negative}\ .$$

This property will be used at a later stage.

It should be emphasised that input signals to digital filters must be band-limited in order to eliminate or at least reduce aliasing effects. That is, the sampling frequency must be at least twice the highest frequency present in the waveform. For example, a signal in the frequency range $f_s < f < 3f_s/2$ (say) when sampled at f_s and passed through a digital filter will be delayed according to the response in $0 < f < f_s/2$ and will appear at the output as a signal in this range.

Having described a building block for digital all-pass network design which holds a similar position in digital systems as the all-pass lattice network in continuous filter systems, the next section suggests how it may be used in a very simple fashion to obtain a useful dispersive delay response.

6.4 Principles of pulse compression system using digital all-pass sections

The ideas developed in Chapter 4 for passive all-pass networks may be transferred in principle to the sampled signal domain using digital networks. It is proposed that the non-linear delay/frequency response of the first order digital section, as described in 6.3.2, be used as the basis of a pulse compression dispersive network.

Consider, in particular, a cascade of several identical sections. The overall delay of the cascade is simply the delay of one section multiplied by the number of cascaded units. The requirement (see Chapter 2) is for a delay differential of T seconds over a bandwidth of F Hz; for a given number of sections, the magnitude of the coefficient, a, can be arranged such that this delay difference is achieved between dc and half the sampling frequency, which is equated to F. (The implications of this 'low pass' type system, with the centre frequency equal to half the bandwidth, will be discussed later.)

The signal, which is arranged to match this response, is inevitably non-linear, and, as in the equivalent passive system, must be carefully tailored. In choosing an optimum system, the number of sections N, say, is a variable which can be minimised according to complexity constraints, but compatible with adequate performance. For a given N there is a unique value for the coefficient, a, in order to meet the requirements for frequency and delay difference.

Before continuing to describe the complete system, and to discuss the associated problems, the mathematical basis will be presented.

6.5 Signals, spectra and conditions

Once again, the principle of stationary phase is invoked to obtain approximations for signals and responses.

The group delay of N identical first order delay sections is

$$\tau(\omega) = N\tau_1(\omega)$$

where $\tau_1(\omega)$ is as given in equation (6-7). The time frequency relationship of a matched signal is (by stationary phase)

$$t_\omega = -\tau(\omega) + \text{constant} \quad .$$

The constant is chosen such that the signal has zero frequency at time $t = 0$; we are considering here an upward sweep to match a response with a negative coefficient, a . Thus:

$$t = N\{t_0 - \tau_1(\omega)\}$$

where t_0 is the delay at zero frequency of a first order section, $\tau_1(0)$. Therefore:

$$t = N\left\{t_0 - \frac{\Delta t(1 - a^2)}{1 + a^2 + 2a \cos \omega\Delta t}\right\} .$$

On rearranging and making ω the subject, we get:

$$\omega(t) = \frac{1}{\Delta t} \arccos\left\{\frac{T_0 + ct}{T_0 - t}\right\} \qquad 0 < t < T \qquad (6\text{–}10)$$

where $T_0 = Nt_0$

and $c = (1 + a^2)/2a$.

Equation (6–10) is the instantaneous frequency of the signal matched to the delay response of N sections each with a coefficient of a . (As yet we have made no statement concerning the magnitude response required.)

The relationship between N and a is obtained as follows. The difference in delay between dc and $f_s/2 = F$ Hz is T seconds, i.e. between $\omega = 0$ and $\omega = \omega_s/2 = \pi/\Delta t$.

Thus:

$$\tau_1(0) = \Delta t\left(\frac{1 - a}{1 + a}\right) \qquad \text{is the delay at zero frequency}$$

$$\tau_1(\pi/\Delta t) = \Delta t\left(\frac{1 + a}{1 - a}\right) \qquad \text{is the delay at frequency } f_s/2$$

and

$$N\{\tau_1(0) - \tau_1(\pi/\Delta t)\} = T$$

therefore

$$N\Delta t\left\{\frac{1 - a}{1 + a} - \frac{1 + a}{1 - a}\right\} = T .$$

This equation solves for the coefficient, a , to give:

$$a = 2N\left(\frac{\Delta t}{T}\right) - \sqrt{1 + 4N^2\left(\frac{\Delta t}{T}\right)^2} .$$

Since $f_s = 2F$ then:

$$\frac{\Delta t}{T} = \frac{1}{f_s T} = \frac{1}{2FT} = \frac{1}{2D}$$

where D is the dispersion factor (time-bandwidth product) then

$$a = \frac{N}{D} - \sqrt{1 + \left(\frac{N}{D}\right)^2} \quad . \tag{6-11}$$

The present system, for which an alternative design is being sought, has $D = 33.33$ and so

$$a = 0.01\left(3N - \sqrt{10^4 + 9N^2}\right) \quad .$$

This relationship is illustrated in Fig.6.6.

The input signal which matches the response of N identical sections is obtained from equation (6-10). The unit amplitude continuous signal is

$$\left.\begin{aligned} f(t) &= \sin\left[\theta(t) + \phi_c\right] \\ \text{where} \qquad \theta(t) &= \int_0^t \omega(t)dt \end{aligned}\right\} \tag{6-12}$$

with $\omega(t)$ as given in equation (6-10). The input to the network is of course a sampled version of this signal, with a sampling frequency of $f_s (= 2F)$.

In order to obtain samples of $f(t)$ for simulation purposes, the expression (6-12) has to be integrated numerically on the computer, in the absence of an analytical solution. The samples obtained can then be operated upon by a 'software' digital filter in a simulation study to determine pulse shapes and to examine quantisation effects (see sections 6.8 and 6.9).

6.6 Centre frequency of signal

In general, from considerations of compressed pulse definition, the centre frequency of a swept FM pulse compression system should be as high as possible compared with the sweep bandwidth. This is because the envelope of the compressed pulse is better defined by a high rather than by a low frequency carrier, since there are more cycles of carrier within the main lobe of the pulse. This effect is illustrated in Fig.6.7.

Instantaneously, the carrier phase can be such that the maximum amplitude of the carrier (after rectification) occurs at equal times either side of the envelope[1] peak (Fig.6.7a). At other times the phase can be such that the peaks coincide (Fig.6.7b), and of course in a random phase situation, the peak of the compressed pulse will 'jitter' between these two extremes, from pulse to pulse. The higher the carrier frequency (i.e. centre frequency of the sweep) the smaller is the jitter obtained.

However, in the digital system under consideration, the centre frequency, f_0, is exactly half the sweep bandwidth, F, and so the number of cycles of 'carrier' within the main lobe is just one ($= 2f_0/F$). Since the sampling frequency is $2F$ Hz, it follows that within the main lobe of the compressed pulse there are only four samples. Under the random input-phase condition, these four samples can be anywhere between the extremes indicated in Fig.6.8, which imply a possible maximum departure of 6 dB from the nominal peak envelope value, which will only rarely be attained itself by a single sample.

This amount of jitter is intolerable; a possible solution, and the one suggested here, is to process another input, obtained as the quadrature of the original (i.e. 90° out of phase with it), in a separate filter, and to obtain a sampled version of the true envelope by squaring, and adding the two outputs. Fig.6.9 illustrates the process and the technique for obtaining the two quadrature signals. The output compressed pulses will still jitter due to random phase inputs, but the magnitude of the jitter is reduced from 6 dB to 0.8 dB.

The input signal is applied to two frequency changers which are driven by oscillators, 90° out of phase. The 'upper side band' can be easily filtered out, and with appropriate choice of oscillator frequency the signals obtained are 90° out of phase in the range $0 < f < F$.

The extra complexity is unfortunate, but the overall advantage of a digital system in terms of size and weight will still outweigh this drawback.

Expressions for the spectrum and compressed pulse envelope are derived in Appendix E.

6.7 The complete system

A complete demodulator must be able to deal with both upward and downward sweeps, representing ones and zeros. The downward sweep is designed to match the response of a filter which is identical to the ones filter in all respects, except the sign of the coefficient, a. A block diagram of the proposed demodulator is shown in Fig.6.10.

Two frequency changers and two analogue-to-digital converters (ADCs) feed four sets of digital filters. The squaring and adding circuits in each channel can be purely digital, since the operations are simply multiplication and addition, and the decision circuit to decide which channel produced the compressed signal can likewise be digital.

Thus, all operations after the ADC can be considered as arithmetic manipulation of n-bit binary numbers. Potentially therefore, the demodulator can be realised entirely with digital integrated circuits.

6.8 Quantization and word length

Having 'designed' a digital filter (i.e. calculated the values of its coefficients), the next problem is the hardware implementation. The problem is analogous to realisation of an LC passive filter from an S-plane transfer function, but much easier. The structure of a digital filter is determined simply by the z-plane transfer function, apart from decisions concerning factorisation into cascaded or paralleled sub-units, which do not affect this particular application.

The problems which remain are hardware oriented, by virtue of their impact on circuit complexity, but also have effects on accuracy and stability. Such a problem is the choice of word length, and the kind of arithmetic to be used.

Since the final manufactured demodulator would contain a large number of units, it is vital to maintain the complexity of each unit at a minimum compatible with satisfactory operation. Therefore, a careful study of word length effects is desirable.

In any digital filter, there are three basic sources of error:

(i) inexact values of coefficients, caused by the necessary word length limitation, or quantization, of the stored coefficient;

(ii) quantization of the input samples, which usually manifests itself as noise, and is caused by approximation as truncation or rounding in the ADC;

(iii) quantization of the results of multiplications, again by truncation or rounding at the output of each multiplier prior to the next operation.

These three effects are analysed now in more detail, with particular reference to a cascaded first-order all-pass configuration.

6.8.1 Inexact values of coefficients

The realisation chosen for investigation, Fig.6.5b uses only one multiplier per section, which ensures that, given a particular coefficient in error, the pole and zero of the network remain reciprocals, and only the phase response is affected. In other words, the same multiplier gives rise to both the pole and the zero, which in a first order arrangement ensures the exactly all-pass nature of the response.

Assuming a small coefficient error, Δa, the phase error may be approximated by

$$\Delta\phi \doteq \frac{\partial\phi}{\partial a}\Delta a \quad .$$

From equation (6-6)

$$\frac{\partial\phi}{\partial a} = \frac{2 \sin \omega\Delta t}{1 + a^2 + 2a \cos \omega\Delta t} \quad .$$

For example, with $N = 42$, $a = (\pm)0.3486$, then

$$\Delta\phi = \frac{-2 \sin \omega\Delta t \, \Delta a}{1.1215 \pm 0.6972 \cos \omega\Delta t} \quad .$$

This has a maximum value of $\Delta\phi_{max} = 2.28\Delta a$ when:

$$\omega\Delta t = \left\{ \begin{matrix} \pi - 0.9 \\ 0.9 \end{matrix} \right\} \text{ radians for } a \left\{ \begin{matrix} \text{positive} \\ \text{negative} \end{matrix} \right\} \quad .$$

In the proposed system, it can be assumed that the coefficient of each section will be stored as exactly the same digits, unless there is a special reason otherwise, in which case, the maximum overall phase error for a 1% error in a is about 19° (i.e. accumulated over 42 sections).

The peculiarity of a digital method is that the value of the coefficients, being generally hardwired, is known exactly to the designer at the outset and the errors can therefore either be designed out or accepted as known but insignificant overall. As an example, Fig.6.11 shows the phase error for a 42 section filter with coefficient word lengths as stated. The maximum delay error is 23.6 μs (5 bit), 4.5 μs (8 bit) and 2.1 μs (11 bit). These values must be weighed against the overall delay across the band (833 μs) and against the effect on the compressed pulse of an inaccurate filter. This effect is illustrated in Fig.6.12 for 5 bit, 8 bit and 10 bit coefficients (0.01011, 0.01011001, and 0.0101100101 respectively).

6.8.2 Quantization of input samples

The analogue-to-digital converter quantizes samples of the input waveform in steps equal to the smallest possible non-zero number, ε, say; in an n-bit fractional number the step size ε is 2^{-n}. Two quantization methods can be distinguished: rounding, where the sample is approximated to the nearest quantization level, and truncation, where the sample is approximated to the highest level that is not greater than the sample. The two methods have different probability density distributions but have the same variance. A uniform statistical distribution is assumed and the error quantities En lie in the interval

$$|En| \leq \varepsilon/2 \quad .$$

For rounding, the distribution has zero mean and variance $\varepsilon^2/12$. Thus, the steady state output component due to En is a zero-mean sequence with power spectral density given by

$$\sigma^2 = H(z)H\left(\frac{1}{z}\right)\frac{\varepsilon^2}{12} \qquad (6\text{-}12a)$$

where $H(z)$ is the transfer function of the filter. Here the effect on the output of coefficient inaccuracy and round-off accumulation has been ignored. For an all-pass filter $H(z)H(1/z) = 1$ and so the power spectral density is the same at the output as at the input, which is as expected for all-pass functions. This effect is illustrated in Fig.6.13 which shows typical output errors for two input word lengths, assuming an ideal filter (i.e. no quantization of coefficients or multiplier outputs). The inputs were rounded.

6.8.3 Multiplicative round-off error

In general, the errors caused by rounding or truncating the products at each multiplication are the most difficult to analyse. Fortunately, however, the analysis is simplified for all-pass networks. Use is made of the result that the output variance of a network subject to a white noise input with a uniform probability density is

$$\sigma^2 = \frac{\varepsilon^2}{12}\sum_{m=0}^{\infty} h^2(m)$$

where $h(m)$ is the network impulse response. (This expression is equivalent to equation (6-12a) since

$$\frac{1}{2\pi j} \oint_{|z|=1} H(z)H\left(\frac{1}{z}\right) \frac{dz}{z} = \sum_{n=0}^{\infty} |h(m)|^2$$

where $H(z)$ is the z-transform of the sequence $h(m)$.)

It is assumed that the white noise is introduced at each multiplier which is considered as a noise generator. Each noise sample is filtered by a cascade combination of the pole of the section in which the noise is generated, and the following all-pass network.

The impulse response of the pole at $z = -a$ is

$$h(m) = (-a)^m \quad .$$

So

$$\sum_{m=0}^{\infty} h^2(m) = \sum_{m=0}^{\infty} a^{2m} = \frac{1}{1 - a^2} \quad .$$

In a cascade of N identical sections, there are N noise generators and the total variance due to multiplication round off error is

$$\sigma^2 = \frac{N\varepsilon^2}{12(1 - a^2)} \quad .$$

When $N = 42$, $|a| = 0.3486$ and so

$$\sigma \doteq 2\varepsilon \quad .$$

That is, the rms noise generated by round-off at the multipliers is equivalent to two quantization levels. Fig.6.14 shows two typical computed output error signals (for $N = 50$) caused by multiplicative round-off (all other arithmetic processes were exact) and indicates the close agreement between the theoretical rms noise figure and computer simulated output errors.

The table below compares the computed values of σ^2 with the theoretical value above for $N = 50$.

No. of bits	$\frac{Nq^2}{12(1 - a^2)}$	From simulations
5	$4.48\ 10^{-3}$	$3.57\ 10^{-3}$
7	$2.80\ 10^{-4}$	$3.08\ 10^{-4}$
9	$1.75\ 10^{-5}$	$1.55\ 10^{-5}$
11	$1.09\ 10^{-6}$	$1.04\ 10^{-6}$

Fig.6.15 plots $\sigma/\varepsilon = \sqrt{N/12(1 - a^2)}$ to show how the multiplicative round-off noise increases almost linearly with the number of identical sections in the filter, but for typical values of N only varies between 1.8 and 2.4.

The table below gives the signal to noise ratio for various possible word lengths and numbers of sections, (the figure quoted is the ratio of peak input signal to rms output noise including the effect of scaling the input signal by a factor 1/7 to prevent multiplier overflow).

No. of sections	S/N ratio (dB)					
	6 bit	7 bit	8 bit	9 bit	10 bit	11 bit
30	14.2	20.2	26.2	32.2	38.2	44.2
40	13.4	19.4	25.4	31.4	37.4	43.4
50	12.6	18.6	24.6	30.6	36.6	42.6
60	11.9	17.9	23.9	29.9	35.9	41.9
70	11.3	17.3	23.3	29.3	35.3	41.3

Although it is naturally desirable to minimise quantization noise to a negligible level, a balance must be found between complexity and performance. Since the system is expected to operate at signal to noise ratios as low as 0 dB (peak signal to mean noise) it is considered justifiable to assume that a quantization effect of 30 dB would have a negligible effect on the performance of the system.

6.9 Computer simulations

As indicated in the previous sections computations were performed to estimate the errors which were to be expected in a practical realisation from the various sources. The computations involved a numerical integration of equation (6-12) to obtain the sampled input signals, followed by a simple implementation of the difference equation (6-9). The signal was 'recirculated' N times (in a program loop), where N is the chosen number of sections, and the constant a is given by equation (6-11). The sources of error can all be simply modelled and their effects computed independently or simultaneously.

During the early stages of this study the effects mentioned above were the only ones considered and as a result a suitable word length of 9 bits (plus sign) and a two's complement realisation were chosen. During design of the hardware (see Chapter 7) the multiplier output quantization method was chosen, for simplicity, to be truncation as opposed to rounding. It was not until the experimental results were seen that the differences between truncation and rounding became apparent. These effects are described in Chapter 7 and in Appendix F which examines the problem from the particular viewpoint of a multi-section cascaded network.

Figs 6.16 and 6.17 illustrate some typical compressed pulses calculated as indicated above, for identical section cascades with 42, 47, 52 and 60 sections. The input waveforms were calculated such that the phase angle was zero and 90° at $t = 0$ - that is, random phase simulations were not performed. The number of sections for simulation was chosen such that the compressed pulse peak occurred near an integer number of sampling intervals. Thus $N = 42, 47, 52$ and 60 show the compressed pulse to best advantage with the maximum sample occurring near the envelope peak.

Fig.6.18 illustrates just one example of a dispersed pulse, in fact for a $N = 34$ system. The characteristics are similar to those of the identical section passive system discussed in chapter 4 and illustrated in Figs 4.9 and 4.10. A curious and anomalous discontinuity is apparent near the centre of the dispersed pulse. This is believed to be due to the fact that the sampled input contains only 66 samples, whereas with $FT = 33.33$ there should be 66.666 samples. Thus the sampled input waveform is not as good a match to the response as it

might be. A slight adjustment of the sampling rate from 80 kHz to 80.4 kHz would correct this allowing then 67.00 samples per bit period. However in the simulation studies and in the practical work the RAE chirp parameters were strictly adhered to although in any further development they could quite easily be modified slightly.

6.10 Probability of error

In spite of special problems such as multipath propagation and Doppler effects which often affect an airborne communications system, one fairly reliable and often used measure of performance, for comparison purposes, is the probability of error in a noisy environment. The system as described in this chapter will be considered, assuming that a Gaussian noise component is presented at the input in addition to the signal.

6.10.1 A model for the signal plus noise

A representation of a band limited noise process suitable for manipulation in a sampled system is illustrated in Fig.6.19, which shows a typical noise waveform containing no frequencies higher than FHz, the bandwidth of the system. This is a series of random Gaussian numbers, mean value zero, separated in time by $1/2F$ seconds, the rest of the waveform interpolated by means of the temporal sampling theorem.

In addition, the following assumptions will be made:

(i) The effect of an all-pass filter on noise samples obeying a Gaussian distribution leaves the distribution unaltered; i.e. the output noise distribution is Gaussian.

(ii) The noise samples at the output of the two quadrature paths are independent.

(iii) The noise samples at the output of the ones and zero channels are independent.

First we consider the samples at a time corresponding to the peak amplitude, R_0, of the compressed pulse. In the ones channel the noisy output is represented by one sample from the two quadrature paths, each including an additive independent Gaussian noise variable. In the zeros channel, the signal envelope value, R_z, is taken as the average value over the two bit periods containing the dispersed pulse.

Let the two samples at the quadrature outputs in the ones channel be u and v; the corresponding values in the zeros channel are p and q.

Then

$$u^2 + v^2 = R_1^2$$

and

$$p^2 + q^2 = R_0^2 \ .$$

At points U and V (Fig.6.10) the amplitude distributions of the two samples coinciding with the compressed pulse peak are

$$p(x) = \frac{1}{\sqrt{2\pi\sigma^2}} e^{-(x-u)^2/2\sigma^2}$$

and

$$p(y) = \frac{1}{\sqrt{2\pi\sigma^2}} e^{-(y-v)^2/2\sigma^2}$$

where σ^2 is the variance of the Gaussian process and x and y are the output random variables in the two paths. In practice the samples are squared and summed, so we must find the probability distribution functions (pdfs) of x^2 and y^2. From the theory of functions of a random variable:

$$p(x^2) = p(X) = \left[\frac{p(x)}{\left|\frac{dX}{dx}\right|}\right]_{x=\sqrt{X}} + \left[\frac{p(x)}{\left|\frac{dX}{dx}\right|}\right]_{x=-\sqrt{X}} \ .$$

Therefore

$$p_1(X) = \frac{1}{\sqrt{2\pi\sigma^2}} \left\{ \frac{e^{-(\sqrt{X}-u)^2/2\sigma^2}}{2\sqrt{X}} + \frac{e^{-(\sqrt{X}+u)^2/2\sigma^2}}{2\sqrt{X}} \right\}$$

$$= \frac{1}{\sqrt{2\pi\sigma^2}} \frac{e^{-(X+u^2)/2\sigma^2}}{\sqrt{X}} \cosh\left(\frac{u\sqrt{X}}{\sigma^2}\right) \ . \qquad (6\text{-}13)$$

Similarly, for the zeros channel:

$$p_0(Y) = \frac{1}{\sqrt{2\pi\sigma^2}} \frac{e^{-(Y+v^2)/2\sigma^2}}{\sqrt{Y}} \cosh\left(\frac{v\sqrt{Y}}{\sigma^2}\right) \qquad (6\text{-}14)$$

where $Y = y^2$.

The pdf of the sum of two random variables X and Y with individual pdfs $p_1(X)$ and $p_2(Y)$ is obtained as the convolution of $p_1(X)$ and $p_2(Y)$:

$$p(\omega) = p(X + Y) = p_1(X) * p_2(Y) \quad .$$

The convolution integral is

$$p(\omega) = \int_0^\omega p_1(\lambda)p_2(\omega - \lambda)d\lambda$$

$$= \frac{1}{2\pi\sigma^2} e^{-(u^2+v^2+\omega)/2\sigma^2} \int_0^\omega \frac{\cosh\left(\frac{u\sqrt{\lambda}}{\sigma^2}\right)\cosh\left(\frac{v\sqrt{\lambda}}{\sigma^2}\right)}{\sqrt{\lambda(\omega - \lambda)}} d\lambda \quad .$$

Unfortunately, an analytic evaluation of this integral is not possible, but it can be rearranged into a form more suitable for numerical integration on the computer using the following substitution:

$$\lambda = \omega \sin^2\theta \quad .$$

Then

$$d\lambda = 2\omega \sin\theta \cos\theta \, d\theta$$

and

$$\sqrt{\lambda(\omega - \lambda)} = \omega \sin\theta \cos\theta \quad .$$

Then

$$p_1(\omega) = \frac{1}{\pi\sigma^2} \exp\left\{-\left(R_1^2 + \omega\right)\Big/2\sigma^2\right\} \int_0^{\pi/2} \cosh\left(\frac{u\sqrt{\omega}}{\sigma^2}\sin\theta\right) \cosh\left(\frac{v\sqrt{\omega}}{\sigma^2}\cos\theta\right)d\theta \,, \qquad (6\text{-}15)$$

where the suffix 1 refers to the ones channel. (0 will refer to the zeros channel.)

A similar expression is obtained for the pdf of the squared and summed output of the zeros channel:

$$p_0(\omega') = \frac{1}{\pi\sigma^2} \exp\left\{-\left(R_0^2 + \omega'\right)\Big/2\sigma^2\right\} \int_0^{\pi/2} \cosh\left(\frac{p\sqrt{\omega}}{\sigma^2}\sin\theta\right) \cosh\left(\frac{q\sqrt{\omega}}{\sigma^2}\cos\theta\right) d\theta \qquad (6\text{-}16)$$

6.10.2 Error probability computation

The probability of bit error is now the probability that the zeros channel output (ω') exceeds the ones channel output (ω):

$$P(\text{error}) = P_\varepsilon = P(\omega' > \omega) = \int_0^\infty \left\{ \int_\omega^\infty p_0(\omega')d\omega' \right\} p_1(\omega)d\omega \ . \qquad (6\text{-}17)$$

The numerical evaluation of these integrals with infinite limits poses some difficulties. However, if we consider finite limits ω_1 and ω_0 such that the integrals

$$I_1 = \int_0^{\omega_1} p_1(\omega)d\omega \ , \qquad \text{and} \qquad I_0 = \int_0^{\omega_0} p_0(\omega')d\omega'$$

are very nearly unity (which they must be by definition), then the values of $p_1(\omega)$ and $p_0(\omega')$ may be normalised to yield exactly unity values integrals, and then the evaluation of equation (6-17) can proceed with negligible error. These normalised expressions for $p_1(\omega)$ and $p_0(\omega')$, indicated by a bar, are obtained as follows

$$\overline{p_1(\omega)} = \frac{p_1(\omega)}{I_1}$$

$$\overline{p_0(\omega')} = \frac{p_0(\omega')}{I_0} \ .$$

Next we note that

$$\int_{\omega}^{\omega_0} \overline{p_0(\omega')}d\omega' = 1 - \int_{0}^{\omega} \overline{p_0(\omega')}d\omega'$$

and so

$$P_\varepsilon = \int_0^{\omega_1} \left\{ 1 - \int_0^{\omega} \overline{p_0(\omega')}d\omega' \right\} p_1(\omega)d\omega$$

$$= 1 - \int_0^{\omega_1} \left\{ \int_0^{\omega} p_0(\omega')d\omega' \right\} p_1(\omega)d\omega \quad .$$

The numerical evaluation of this expression using equations (6-15) and (6-16) is a lengthy process, which has to be repeated for various values of σ, (equal to the rms noise voltage) and the results are shown in Fig.6.20 which gives P_ε against mean signal to noise power ratio, S where

$$S = 10 \log_{10} \frac{\text{mean signal power}}{\text{mean noise power}} \quad \text{dB}$$

$$= 10 \log_{10} (1/2\sigma^2) \quad .$$

therefore

$$S = -20 \log_{10} \sigma - 3 \text{ dB} \quad .$$

It is interesting that the result obtained for a sampled system using the above technique should be identical to that obtained for linear systems with an entirely different approach by Forgan, (Appendix C) when the same compressed and dispersed pulse amplitudes were used. The Forgan approach was to obtain expressions for the pdf of the envelope of a sine wave plus gaussian noise and to integrate the appropriate expressions for error rate. The mathematics were entirely different being relevant to a continuous system. The digital computation confirms our knowledge that there should be no difference between sampled and continuous systems, given certain conditions of equivalence.

In practice it is difficult to attain and maintain synchronisation well enough to enable only one sample per channel to be compared. It implies a gate time of 12.5 μs which is only 1.5% of the data bit period.

A 10% gating time which covers most of the main lobe of the compressed pulse would be more realistic. A simple extension of the results already obtained can predict error probabilities for various gating times, under certain simplifying assumptions:

(a) during the gating time the nominal amplitude of the dispersed pulse samples (without noise) is constant;

(b) the largest sample in the compressed pulse channel will be the peak amplitude. The first assumption is more realistic than the second; however, the second errs on the side of pessimism, since it is quite likely that when a noise pulse reduces the peak sample amplitude, another sample in the compressed channel will exceed it.

Under these assumptions, the error rate can be obtained by simply multiplying the 'one sample' result (Fig.6.20) by the number of samples taken in the gating time. Fig.6.21 shows these answers for various gating times, which also compare well with Forgans.

6.11 Discussion

All the simulations and experimental work have examined the response of all-pass digital networks. For a truly matched response the spectrum magnitude as calculated in Appendix E and shown in Fig.E.1 would have to be approximated by a digital filter to match the amplitude response as well as the delay response.

Similar effects to those shown in Chapter 4 are anticipated. Since the spectrum magnitude is zero at dc and at $f_s/2$ (= F) the "effective" bandwidth of the signal, as discussed in section 4, is significantly less than F. Thus an improvement could be achieved by increasing the frequency spread of the signal, increasing the sampling rate accordingly and achieving a larger compressed pulse whilst still retaining a 40 kHz effective signal bandwidth – i.e. similar energy outside ±20 kHz of the rf carrier frequency compared with the chirp system.

If a magnitude spectrum matching filter were required additional complexity would be introduced as well as an additional delay distortion. The latter could be overcome by adding the extra delay to that produced by the delay network itself and modifying the modulating waveform to match the overall delay characteristic so produced.

By these measures small but possibly significant improvements to the compression gain could be achieved.

The next chapter describes the practical demonstration of a single section digital delay filter and its use in a pulse compression simulation.

Chapter 7

AN EXPERIMENTAL ALL-PASS DIGITAL FILTER AND DEMONSTRATION OF PULSE COMPRESSION

7.1 Introduction

In order to demonstrate the ideas described in Chapter 6, a practical investigation of digital filter techniques was undertaken, with the aim of demonstrating that pulse compression with non-linear sweeps and digital matched filters was possible and to discover some of the practical problems involved.

It was soon appreciated that it was not feasible to build a complete network using TTL components in the laboratory, since the size and cost are prohibitive, but by constructing a building block and using a recirculation technique, a non-real-time simulation can be achieved. Throughout the study a final realization using MOS/LSI was borne in mind, and methods applicable to that technique were used where possible. The first job was to develop suitable practical realizations for the multiplier and adder, and then to build up a first-order all-pass section.

7.2 Serial arithmetic

The choice between serial and parallel arithmetic for hardware digital filters using LSI depends upon several factors. Circuit complexity is the most important in this application, combined with interconnection problems. Parallel multipliers require more complex circuitry than serial multipliers and need many more interconnections. It is vital in LSI realizations to minimise the number of connections between circuits, since the interconnection network is a primary cause of failures.

In parallel multipliers the processing rate is limited by carry-propagation times but with serial arithmetic the rate is limited only by the speed of the basic digital circuits.

Delays are realized simply as single input single output shift registers compared with multi-input/output latches in parallel arithmetic.

The simplicity of the circuitry and the ease with which the units can be multiplexed (by sharing adders and multipliers) are further factors in favour of serial methods. A modular approach is simpler with serial arithmetic and there is more flexibility in the choice of word lengths. For these reasons a serial method was chosen.

7.2.1 Two's complement representation

With serial arithmetic the binary numbers are best represented in two's complement form; in contrast with the one's complement representation, additions and multiplications can proceed with no prior knowledge of the signs of the numbers, and with no corrections to the results. (This decision led to some quantisation problems which are fully discussed later.)

An n-bit-plus-sign number in two's complement form is written as

$$x_0 x_1 x_2 x_3 \cdots x_n$$

which represents a number, X, having a value of:

$$X = -x_0 \sum_{i=1}^{n} x_i 2^{-i}$$

where each x_i is either 0 or 1. Thus, the binary word, X, is assumed to lie in the interval

$$-1 \leq X < 1$$

with the sign of the number given by the last bit in time, x_0.

7.3 Arithmetic units

Having chosen the type of arithmetic to be realized and the word length (9 bits plus sign), the next step was to design the individual elements which make up a filter section. With reference to Fig.6.5.b the elements are an adder, a multiplier and a delay element (The circuits described use TTL components readily available in RAE during 1971. Other more complex components in TTL/MSI were becoming generally available, but were not easily obtainable in RAE.)

7.3.1 Serial adder

A serial adder for two's complement addition is very simple. The IC modules used were an SN7480 gated full adder and an SN7474 dual edge-triggered D-type flip-flop. Fig.7.1 illustrates the arrangement used. The simplicity of the unit emphasises the overall simplicity of serial arithmetic. Addition of two numbers in two's complement form proceeds sequentially from least significant bit (LSB) to most significant bit (MSB), no sign correction being necessary.

e.g.

$$1.0110 - 0.0111 = 1.1101 ,$$

i.e.

$$- 0.625 + 0.4375 = - 0.1875 .$$

7.3.2 Two's complementer

Used to form the negative of $V[(m - 1)\Delta t]$ in the first-order filter, the two's complementer was implemented with a circuit as shown in Fig.7.2. All initial (least significant) bits up to and including the first '1' are passed through, and all succeeding bits are inverted. An SN7472 JK flip-flop with NOR gates and inverters were used.

Thus, to obtain the two's complement of 0.011011100, the first 3 LSBs (100) are unchanged while the remaining digits (0.011011) are inverted (1.100100), giving the result 1.100100100.

7.3.3 Multiplier

The multiplier scheme chosen (perhaps strictly called a serial/parallel multiplier) is shown in Fig.7.3. It is the most complex and important unit in the filter and deserves a detailed description.

The multiplication of the incoming serial word ('multiplier') by the stored coefficient ('multiplicand') is performed by successive addition and shifting. If the specific multiplier bit is a 1, the multiplicand is added to the sum of the previous partial products which is present at the B inputs of the adders; if the multiplier bit is 0, no addition is performed. At the next clock pulse the sum is shifted one position to the right and the next multiplier bit is operated upon. Each multiplier stage consists of a serial adder as described above, followed by a flip-flop to shift the sum digit to the next stage.

The multiplier can deal with an input word of any length as long as a control bit on a separate control line is present to signify the start of the word, and a second pulse is present to indicate the location of the sign bit. With these restrictions, the multiplier can have positive or negative numbers on either input; furthermore, sign correction is performed automatically as long as both inputs are scaled in magnitude to be either less than or greater than unity.

(a) Theory

The theory of the serial/parallel multiplier is as follows. Firstly, it is realized that in the two's complement representation of a fractional binary number, the true value is given if the sign bit is considered equal to -1, i.e.

$$\begin{aligned} 1.1011 &= -1.0000 + 0.1011 \\ &= -(1.0000 - 0.1011) \\ &= -0.0101 \end{aligned}$$

which is the actual value of the number represented in two's complement form as 1.1011. Thus, direct multiplication with the sign bit considered negative gives the correct result.

Consider the two numbers $X = -x_0 + X^*$ and $Y = -y_0 + Y^*$ where x_0 and y_0 are the sign bits (0 positive, 1 negative) and X^*, Y^* are the fractional parts, with

$$X^* = \sum_{i=1}^{m} x_i 2^{-i} \qquad \text{for positive } X$$

and

$$X^* = \sum_{i=1}^{m} \bar{x}_i 2^{-i} \qquad \text{for negative } X$$

(similar expression for Y^*).

The multiplication of X and Y gives:

$$XY = X^*Y^* - x_0Y - y_0X - x_0y_0 \ ,$$

so that the result of the multiplication of the fractional parts X^* and Y^* requires up to three correction terms, depending on the signs of X and Y.

(1) If X is negative ($x_0 = 1$), subtract x_0Y (or add the two's complement of Y).

(2) If Y is negative ($y_0 = 1$), subtract y_0X (or add the two's complement of X).

(3) If <u>both</u> X and Y are negative subtract x_0y_0 (add 1.0000).

As an example, consider the multiplication of the two numbers $X = 1.0111$ $(= -9/16)$ and $Y = 1.0110$ $(= -10/16)$. The desired result is $XY = 0.01011010$ $(= 90/256)$.

First, the fractional parts .0111 and .0110 are multiplied to give $X^*Y^* = 0.00101010$.

Since (1) $x_0 = 1$, we must add the two's complement of $Y = 0.1010$

(2) $y_0 = 1$, we must add the two's complement of $X = 0.1001$

(3) both $x_0 = y_0 = 1$ we must add $x_0y_0 = 1.0000$.

Then, $XY = 0.00101010 + 0.1010 + 0.1001 + 1.000$

$= 0.01011010$, the correct result.

(b) Hardware

In practice, these correction terms are implemented with the following modifications to the basic multiplier circuit.

(1) Circuit E produces the two's complement of X when $y_0 = 1$. The function of circuit E is to locate and detect the sign bit of the multiplier (Y) and, if it is 1, to provide a sequence of ones following it, until the sign bit has been produced at the multiplier output; if the sign bit of Y is zero, then a sequence of zeros is produced to gate the multiplicand. Multiplication by a sequence of ones gives the two's complement of a number; therefore, a sequence of ones following a sign bit of ones gives the two's complement of the multiplicand.

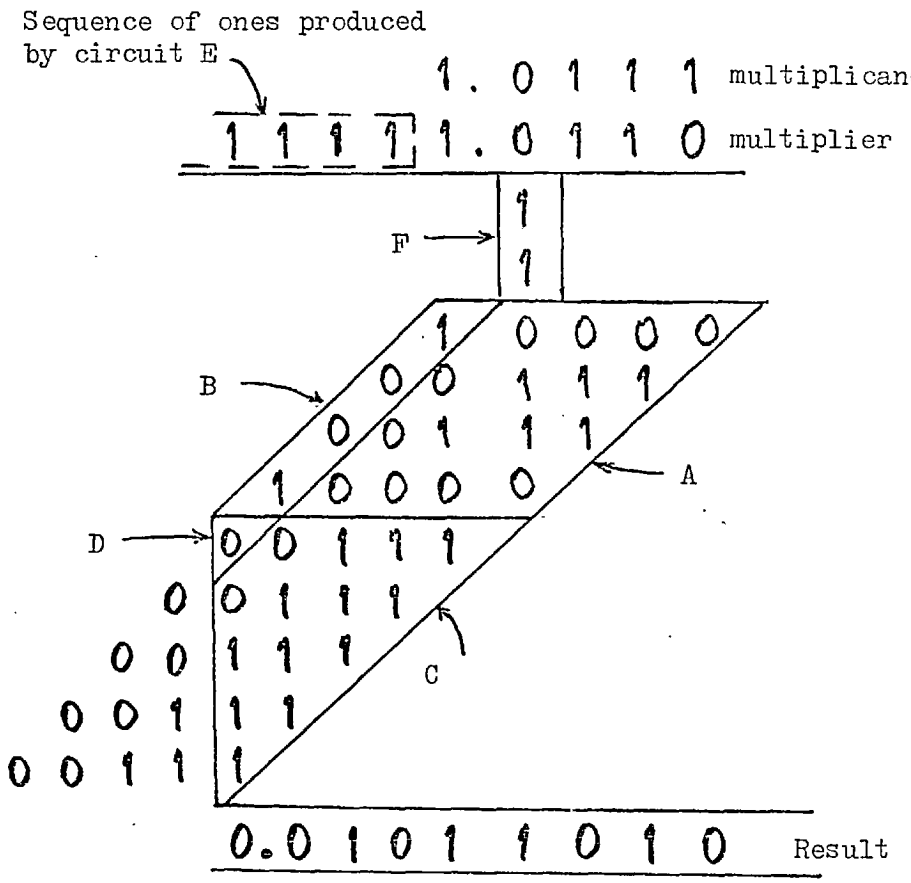
(2) The inverter before the first adder, together with the circuit constraining the B input to the first adder to be 1 during the first clock pulse, produce the two's complement of Y when the multiplicand is negative. The inverted input word appears at the B input to the first adder if the multiplicand sign bit is 1; the two's complement is then formed by adding 1 at the LSB of the input word (equivalent to two ones at the B and C_n inputs of the first adder during the first digit of the input word).

(3) Perhaps more by accident than design, the combination of methods (1) and (2) automatically adds $x_0y_0 = 1.000$ when both numbers are negative.

In this case, the practical circuitry is less complex than a written description.

(c) Illustration

A final illustration may clarify the process. The multiplication of 1.0111 by 1.0110 is illustrated below; the step-by-step addition is omitted, only the final sum is shown.



(1) Box A is simply X*Y* (the product of the fractional parts), formed by standard addition and shifting on the clock transition.

(2) Boxes B + D + F are the two's complement of Y (i.e. $\bar{Y}$ + .00001 + .00001) with the two digits produced at the first digit of the input word

(3) Boxes C + D is the two's complement of X

(4) When X is negative and Y positive, D is 1

When X is positive and Y positive, D is 1

When X is positive and Y negative, D is 1

When X and Y are negative, D is 0.

In effect D is the sum of two ones when both numbers are negative, hence the zero and automatic sign correction.

(d) Timing

If the input data word is M + 1 bits long, and the coefficient has N + 1 bits, the output of the last adder is M + N + 1 bits long; this number will have to be rounded or truncated before passing to the next operation, and since the LSB of the full product appears at the first clock period, there is necessarily a delay of N bits before the most significant M bits appear. This delay must be deducted from the delay which follows the multiplier so that the next operation (addition) is synchronised. This is illustrated in Fig.7.4.

7.3.4 Delay element

The delay required is nominally one period of the sampling frequency, and is realized using single input single output static shift registers (SN7491 8 bit shift registers and some SN7496 5 bit registers were used).

7.4 Multiplexing

In order to make optimum use of the maximum speed available from the circuits, the multipliers and adders can be multiplexed to handle several operations within the basic sampling period, $1/f_s$. The factors which limit the number of channels which can be multiplexed within $T - 1/f_s$ are the speed of the circuits and the time needed to multiply. Fig.7.4 shows that 20 clock periods are required to perform multiplication of a 9 bit + sign number by a 9 bit + sign coefficient, allowing one clock period to clear all flip-flops. That is, 20 clock periods must be allowed between the LSB of successive data words; the minimum nominal delay time allowable is then 20 clock periods. The present application requires a delay time of $\Delta t = 12.5$ seconds and the required clock rate is therefore $f_c = 20 \times 80$ kHz = 1.6 MHz. At the

time of writing, MOS/LSI techniques can provide clock rates up to three times this figure, but achievable clock rates are expected to increase significantly over the next few years. Although TTL can operate faster than this, it was decided to limit the practical demonstration to a three-way multiplex, using a 4.8 MHz clock.

Since we require a cascade of identical sections in this application multiplexing was used to recirculate the signal which had been operated upon once and to reinsert it during the next sub-interval of the basic sampling period. A second reinsertion during the third sub-interval gives an output signal which has been processed three times by the same transfer function.

Fig.7.5 is a block diagram showing the way in which a first order delay section can be arranged to process one sequence of input words three times. The nominal shift register delay is 12.5 μs at 4.8 MHz, i.e. 60 bits. The 69 bit register allows synchronous addition at adder P while the 11 + 40 = 51 bit register allows synchronous addition at adder Q, the deviations from the nominal 60 bits being caused by the 9 bit delay in the multiplier. The gates at the output of the 11 bit register feed back the output (delayed by $\Delta t/3$ = 20 bits) to the input for the first $2\Delta t/3$, and give an output during the final $\Delta t/3$.

7.5 Additional circuits

Apart from the basic multiplier, adder, complementer and shift register, other circuits are needed to complete the filter.

7.5.1 Truncation circuit

The output of the multiplier was truncated from 18 bits plus sign to 9 bits plus sign before being applied to the adder P. The circuit used is shown in Fig.7.6 with associated control waveforms. The output is zero (low) until the start of the sign bit signifier control pulse, after which the word is allowed through unaltered. An interesting consequence of the use of this technique arose during the final stages of the investigation (see section 7.7.3).

7.5.2 Circuit E

Fig.7.7 shows the circuit used to perform the sign function required by the multiplier. If the sign bit of the incoming word is 1, all succeeding output bits are 1 until the clear pulse arrives; if the sign bit is 0, all succeeding bits are 0.

7.5.3 Control waveforms

All sub-units of the filter require control signals to operate properly. These are:

(a) clock waveform, C and occasionally $\overline{C}$

(b) word start signifier, P and occasionally $\overline{P}$

(c) sign bit signifier, S and occasionally $\overline{S}$

(d) clear pulse, T and occasionally $\overline{T}$.

These waveforms are shown in Fig.7.7. In an engineered version of the digital filter technique, the control waveforms would be derived from a basic clock in conjunction with the analogue-to-digital converter and appropriate divider circuits.

In the laboratory model the control waveforms were generated in circuits which were performing the more complex task of providing test signals for the filter.

7.6 Filter testing

In the early stages of practical digital filter work it is essential to be able to test each function in detail before connecting it all together. Even then, a means of response measurement is required, and for these reasons it is useful to have controllable test signal generator so that the progress of each digit can be followed through the various circuits. No such item of test gear was available and so a special purpose signal generator was designed, such that detailed fault-finding could be performed.

7.6.1 Amplitude scaling

At no stage must a word be allowed to exceed unity magnitude for correct functioning of the multipliers. Therefore the amplitude of all input signals must be scaled such that the probability of any word exceeding unity magnitude is extremely small. With no noise at the input, the maximum value of the signal through the compression filter is 5.5 times the input magnitude (at the peak of the compressed pulse). Allowing a reasonable extra 1.5 for possible noise amplitude at this instant, the input amplitude was scaled to a maximum value of 1/7.

7.6.2 Test signals

In order to measure the frequency response of the filter over the required frequency range ($0 < f < f_s/2$) a set of constant frequency signals was synthesised. Nine frequencies were used, and were formed

by suitably gating (and complementing) six stored samples of one quarter cycle of a sine wave. Each stored word was of length 9 bits + sign, and the maximum value ($\equiv \sin \pi/2$) was scaled to 1/7. Thus the maximum valued word is 0.001001001. Table 7.1 below gives the binary value of all six stored words.

Table 7.1

n	$n\pi/10$	Stored word $\equiv$ $(\sin n\pi/10)/7$	Name
0	0	0.000000000	s_0
1	0.1π	0.000010111	s_1
2	0.2π	0.000101011	s_2
3	0.3π	0.000111011	s_3
4	0.4π	0.001000110	s_4
5	0.5π	0.001001001	s_5

As an example, a signal of frequency $f_s/5$ is synthesised by gating the samples s_0, s_2 and s_4 and complementing alternate half cycles to produce the following sequence of numbers:

$$\cdots\cdots \; {}^{-}s_4 s_0 s_4 s_2 {}^{-}s_2 {}^{-}s_4 s_0 \; \cdots\cdots$$

Table 7.2 gives the complete list of sample sequences to synthesise nine frequencies from $0.1(f_s/2)$ to $0.9(f_s/2)$.

Table 7.2

Frequency	Sequence of stored words
$0.1(f_s/2)$	$s_0 s_1 s_2 s_3 s_4 s_5 s_4 s_3 s_2 s_1 s_0 {}^{-}s_1 {}^{-}s_2 {}^{-}s_3 {}^{-}s_4 {}^{-}s_5 {}^{-}s_4 {}^{-}s_3 {}^{-}s_2 {}^{-}s_1 \cdots\cdots$
0.2	$s_0 s_2 s_4 s_4 s_2 s_0 {}^{-}s_2 {}^{-}s_4 {}^{-}s_4 {}^{-}s_2 \cdots\cdots$
0.3	$s_0 s_3 s_4 s_1 {}^{-}s_2 {}^{-}s_5 {}^{-}s_2 s_1 s_4 s_3 s_0 {}^{-}s_3 {}^{-}s_4 {}^{-}s_1 s_2 s_5 s_2 {}^{-}s_1 {}^{-}s_4 {}^{-}s_3 \cdots\cdots$
0.4	$s_0 s_4 s_2 {}^{-}s_2 {}^{-}s_4 \cdots\cdots$
0.5	$s_0 s_5 s_0 {}^{-}s_5 \cdots\cdots$
0.6	$s_0 s_4 {}^{-}s_2 {}^{-}s_2 s_4 s_0 {}^{-}s_4 s_2 s_2 {}^{-}s_4 \cdots\cdots$
0.7	$s_0 s_3 {}^{-}s_4 s_5 s_2 {}^{-}s_5 s_2 s_1 {}^{-}s_4 s_3 s_0 {}^{-}s_3 s_4 {}^{-}s_1 {}^{-}s_2 s_5 {}^{-}s_2 {}^{-}s_1 s_4 {}^{-}s_3 \cdots\cdots$
0.8	$s_0 s_2 {}^{-}s_4 s_4 {}^{-}s_2 \cdots\cdots$
0.9	$s_0 s_1 {}^{-}s_2 s_3 {}^{-}s_4 s_5 {}^{-}s_4 s_3 {}^{-}s_2 s_1 s_0 {}^{-}s_1 s_2 {}^{-}s_3 s_4 {}^{-}s_5 s_4 {}^{-}s_3 s_2 {}^{-}s_1 \cdots\cdots$

and Fig.7.8 illustrates the sampled waveforms represented by the sequences.

7.6.3 Test signal generator

In practice the signal generator turned out to be more complex than the filter itself. Fig.7.9 is a block diagram. The clock generator feeds a network of dividers which provides the control waveforms. Five 10 bit shift registers hold the samples s_1 to s_5 which are clocked out when the appropriate gated clock is applied. These gating waveforms are obtained from the word selector circuit which selects the required words as determined by a selector switch for the desired frequency. Similarly, the sign selector circuit provides waveforms which control the two's complementer. The word gating waveforms are shown in Fig.7.10, and the sign control waveforms in Fig.7.11. The circuit diagrams of the main blocks are given in Fig.7.12 to Fig.7.16. The timing is designed such that one 10 bit word is followed by 50 zeros, giving an interval of 60 clock periods between successive LSBs, as required for recirculation.

An extra board was required to derive all the control waveforms required by the filter and to perform the recirculation gating as shown in Fig.7.5. Essentially, the signal generator with control circuitry filled 6 printed circuit boards each carrying 15 dual-in-line ICs, while the filter itself went on 3 boards. During development and fault finding some changes were required which necessitated using parts of another board.

7.6.4 Digital to analogue converter

The first stage of filter testing involves counting pulses on an oscilloscope screen to discover if the component parts are working correctly. Though essential during development this technique loses its value when further performance investigations are necessary. Furthermore, it is difficult to prove to an observer that digital circuits can indeed filter unless sine waves are displayed. Therefore, special purpose digital to analogue converters were designed and constructed each using 13 TTL circuits and 2μA702 wideband amplifiers (see Fig.7.17).

Fig.7.18 shows some typical input/output waveforms as displayed on a dual trace oscilloscope and photographed with a scope camera. They clearly demonstrate the delaying action of the filter, and close inspection of the outputs confirm the predicted delay/frequency response.

The coefficient 'a' was chosen to be −0.3486 corresponding to a system with 42 such identical sections. The coefficient in binary form is 1.101001110 (9 bits plus sign).

7.7 Demonstration of pulse compression

The initial aim of constructing a digital filter was simply to assess the difficulties and provide some experience for any MOS/LSI developments which might follow. However, having built a working filter some means were sought to demonstrate the pulse compression capability of a multi-section filter. It was clearly impractical on a cost and time basis to build a complete 42 section network, since 14 more units were needed identical to the one already made. Therefore a less direct method was required.

7.7.1 Approximation of input signal

First, an approximation to the matched sweep was needed. The simplest way found was to synthesise samples of an ideal waveform in the correct sequence. The test signal generator already developed was useful for this purpose. The ideal signal was obtained by integration of equation (6-6) as described in section 6.4; sample amplitudes at intervals of $\Delta t = 12.5\ \mu s$ were divided by 7 (amplitude scaling) and the stored level (s_0 to s_5) nearest to this ideal value chosen. The 66 samples chosen are given in Table 7.3.

Table 7.3

1	s_0	18	s_1	35	s_1	52	s_5
2	s_1	19	s_3	36	s_4	53	s_0
3	s_1	20	s_5	37	s_3	54	$-s_5$
4	s_2	21	s_4	38	$-s_1$	55	s_0
5	s_3	22	s_2	39	$-s_4$	56	s_5
6	s_4	23	$-s_1$	40	$-s_3$	57	$-s_1$
7	s_5	24	$-s_3$	41	s_1	58	$-s_4$
8	s_5	25	$-s_5$	42	s_4	59	s_2
9	s_3	26	$-s_3$	43	s_2	60	s_2
10	s_2	27	s_0	44	$-s_2$	61	$-s_5$
11	s_0	28	s_2	45	$-s_5$	62	s_1
12	$-s_1$	29	s_5	46	$-s_1$	63	s_2
13	$-s_3$	30	s_3	47	s_3	64	$-s_5$
14	$-s_4$	31	s_0	48	s_3	65	s_3
15	$-s_5$	32	$-s_3$	49	$-s_2$	66	$-s_1$
16	$-s_3$	33	$-s_5$	50	$-s_4$		
17	$-s_1$	34	$-s_2$	51	$-s_1$		

Fig.7.19 illustrates this synthesised input waveform which is a good approximation to the required matched signal. Suitable gating and sign control waveforms were obtained in a manner similar to before using divider circuits derived from the basic clock and an appropriate arrangement of gates.

7.7.2 Simulation of multi-section response

The 66 sample words were each separated by 50 clock periods to allow for recirculation within the filter three times. The output sequence obtained during the third subinterval $\Delta t/3$ was then fed to the input of a shift register which was long enough to store all 66 words. In fact the register needs to be longer since the filter response of interest is the non-linear portion which is set upon a fixed standing delay; this constant delay must be allowed for, since the compressed pulse will appear during this extra time the sweep is delayed such that the compressed pulse is produced after all components of the input signal. A sufficient time in this case is equivalent to 32 extra words. Thus to handle the complete signal, the shift register needs to be of length $(66 + 32) \times 10 = 980$ bits, and clocked only during the times when the required signal is present (i.e. 10 clock pulses every 60 clock periods). Relative to the previous set of input data the delayed set was fed back to the input exactly 100 words later, (since there is already a two word delay inherent in the recirculation system). The shift registers were General Instrument MTNS static.

Fig.7.20 is a breakdown of the timing system. The above process is repeated 14 times; during the 14th cycle the shift register output is not fed back, since a new 66 word input is being fed in.

The overall system is then a 1/14 real time simulation of a pulse compression system.

7.7.3 Results and discussion

The major difficulty in testing the system with the above arrangement was observing the signals on the oscilloscope and providing appropriate trigger sources so that different parts of the output could be examined. Although it was not possible with the equipment available to examine every word of output at every stage of the compression, some parts could be observed. Computer simulations of the filter with the approximated input waveform were performed in order to check the practical results and an interesting difference came to light. Although the filter compressed the sweep, the shape of the output was not as predicted by the computer simulation. This difference had not been picked up in the

earlier testing phase and was obviously an error which accumulated during the signal's passage through 42 identical sections.

Detailed investigation suggested that the truncation process was the cause of the difference. In the computer simulation the truncation was towards zero; that is, the magnitude of each number at the output of the multiplier was truncated to its 9 bit equivalent. Thus, a negative number was treated as its positive magnitude with an assumed negative sign.

For example, the 18 bit plus sign product of 1.101001110 and 0.000101100 is:

$$1.111110011101101000 \ .$$

Truncation as in the hardware gives the 9 bit answer:

$$1.111110011$$

$$\equiv -0.000001101 \equiv -0.025390625 \quad \text{(decimal)} \ .$$

However, truncation as in the original computer simulation operates on the positive equivalent of the 18 bit product:

$$-0.000001100010011000$$

giving

$$-0.000001100 \equiv -0.0234375 \ .$$

Since this difference only occurs during truncation of negative numbers there is an imbalance causing accumulation of errors which become significant after 42 sections.

In the time available, a modification to the hardware was not feasible but a programming change to simulate the existing practical conditions was made, and the resulting output pulse was as observed in practice. Fig.7.21 is the computed output pulse and Fig.7.22 are photographs of three signals observed in practice. The input waveform is the observed version of Fig.7.19; the middle photograph is the output of 21 sections showing partial compression of the signal and the lower photograph shows the compressed pulse, the observed version of Fig.7.21.

The effect of the small modification of the truncation circuit can be seen by comparing Fig.7.21 with Fig.7.23 which is the pulse shape assuming that truncation was performed as in the computer simulation.

This exercise proved that great care is needed over the details of digital filter design, particularly regarding quantization. The theory developed in Chapter 6 was not strictly correct when applied to the experimental version since the truncation method realized by the hardware involved a bias towards more negative numbers, which introduced an extraneous low frequency component or dc drift towards negative values. This effect can be observed in the photographs of the filter outputs, Fig.7.22.

This effect would usually be negligible in typically complex filters (up to say 10th order).

The effects of truncation and rounding are examined in more detail in Appendix F.

7.8 Conclusions

The practical study undertaken has demonstrated the feasibility of the ideas developed in Chapter 6 for pulse compression using non-linearly swept FM signals and digital dispersive filters. It is clearly not possible or even necessary to demonstrate the complete system with TTL circuits in the laboratory since the demonstration as above is sufficient to solve the basic problems. The practical difficulty lies in the implementation of the technique in integrated circuit form using MOS/LSI. This part of the problem was outside the scope of the present project, although it is believed that the existing state-of-the-art is perfectly capable of converting the circuitry into MOS/LSI. Many companies in the USA and several in the UK are able to do the job without difficulty. The most important advantage of the technique describes here is that only a very small number of different components is required, where a 'component' is considered to be one type of chip. A common method of constructing practical digital filters is to interconnect standard chips (multiplier chips, register chips, adder chips etc) in the desired pattern. However, in the present application, it would probably be more convenient to construct one chip to contain as many complete first order sections as the clock rate, chip size and technology will allow; this reduces to a minimum the number of interconnections and the number of different chip types required. A single control chip to provide control waveforms and recirculation gating waveforms would complete a very simple system.

Chapter 8

SUMMARY, CONCLUSIONS AND FUTURE DEVELOPMENTS

8.1 Summary of achievements

The work reported thus far has covered a variety of solutions to the problem specified in Chapter 2, from a novel adaptation of passive inductor/capacitor delay network techniques with a practical demonstration, to a logical progression of the same ideas into digital techniques and a practical implementation, along with a theoretical examination of non-linear FM signals and their possible application.

The main points to be noted as a result of this work are as follows.

(i) Non-linear FM per se does not give rise to significant advantages on size/weight criteria; nor are there any system performance gains to be made. In fact, any solution employing non-linearly swept signals and non-linear delay dispersive networks inevitably involves compromising on some aspects of system performance, however marginally (Chapter 3).

(ii) If for traditional reasons a passive network LC realisation is desirable then the technique described using cascaded identical bridged-T sections (Chapters 4 and 5) provides a solution which performs slightly less well than the linear chirp baseline solution but which employs far fewer elements and a higher degree of manufacturing and tuning simplicity.

(iii) Digital filter methods promise to make the most significant impact on the size and weight, as well as the cost and necessary maintenance effort of future dispersive network applications. The feasibility of a digital filter solution has been demonstrated by theory and in the laboratory. Section 8.2 below outlines a possible extension of these ideas which holds the greatest promise of fulfilling minimum size requirements.

Other more detailed matters investigated include the following.

(iv) Various non-linear FM waveforms were examined with emphasis given to the nature of the compressed and dispersed pulses obtained in truly matched and phase matched configurations. The detailed results should provide useful reference material for any future work on non-linear chirp-like signals.

(v) Theoretical work on the use of the passive bridged-T second order delay network as a building block for identical section cascaded filters has been performed, and could be applied to other systems requiring different dispersion factors and frequency ranges. The use of the two halves of an easily realisable symmetrical delay function for compression of different signals is novel.

(vi) Error probabilities in a system employing sampled data have been calculated and show good agreement with other work performed on linear systems with the same dispersion factors.

(vii) Detailed simulation and theoretical explanation of truncation effects in multisection cascaded digital delay networks successfully described a practically observed result. The conclusion was that, in multisection cascaded networks, the cumulative effect of multiplier output truncation using two's complement arithmetic is too serious and that, to reduce output errors, quantisation of multiplier outputs should be by rounding.

8.2 Further developments

At a stage in the project which left no time for experimental work, an extension of the above ideas was conceived which could make dramatic improvements to the size and complexity of the digital filter solution.

As a basis the previous theoretical work remains valid. In other words a number N of identical digital filter sections is again used to match the frequency/time relationship of the matched signal as described in Chapter 4.

It is clear from the preceding chapter that in the practical realization the multiplier is the most complex component in the filter, and thus any reduction in the multiplier complexity will have a significant effect on the overall size of the dispersive network.

8.2.1 Simplest conceivable multiplier

The route followed in the previous chapter was to choose a value of N which gave reasonable performance and to accept the coefficient, a, as having to be realized as an n-bit word (9 bits + sign was felt to give sufficient accuracy). However, due to the unique relationship between N and a, and since the performance is not strongly dependent on N, it is clearly feasible to reverse the process and to choose a value of the coefficient which gives a simple realization and accept the value of N which is uniquely determined.

In particular, consider a value of the coefficient equal to 0.25 (0.01 in binary). With $N = 63$ we obtain a value for the dispersion factor D (equation (6-5)) of 33.60. The design figure established in Chapter 2 was 33.33 corresponding to a data rate of 1200 baud and a bandwidth of 40 kHz. If there is any flexibility in these numbers it must be in the bandwidth which is after all a nominal figure corresponding approximately to a channel allocation of 50 kHz; a small increase in the frequency sweep has very little effect on this parameter.

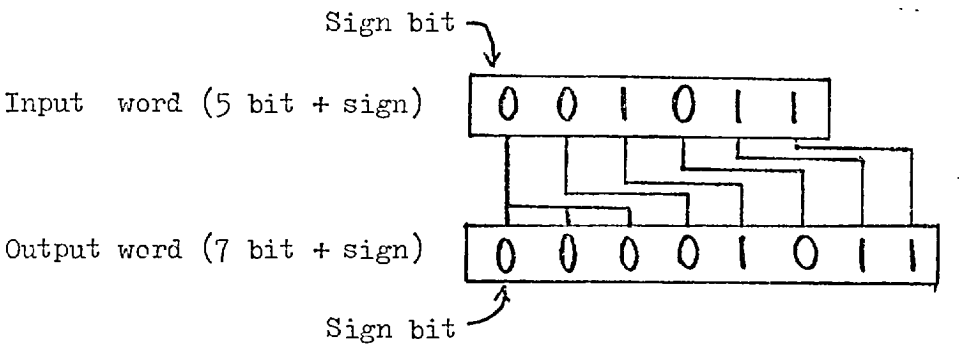
Taking advantage therefore of a slight change from 40 kHz to 40.32 kHz a system with $N = 63$ and $a = 0.25$ should be acceptable.

Immediately it is seen that multiplication by (binary) 0.01 consists simply of a shift in the position of the binary point, i.e.

$$0.01011 \times 0.01 = 0.0001011$$
$$1.11001 \times 0.01 = 1.1111001 .$$

Thus, the complicated shift-add procedure normally required for a multiplier is avoided, and replaced by simple arrangement of input/output connections. A parallel multiplier (by 0.01) is then described below (a 5 bit + sign input word is used for illustration purposes):

X 0.01 Multiplier



Truncation yields 0.00010, rounding yields 0.00011; simplicity suggests that truncation should be chosen since the least significant two digits of the input word are simply ignored.

8.2.2 Complete first order section

Parallel arithmetic is preferred for such a simple system. All delays can be realized by simple flip-flop or latches. The adders are simply realized. The 'end-around-carry' required in ones-complement addition is achieved by connecting the output carry bit of the most significant adder stage to the input carry of the least significant bit (see Fig.8.1).

A block diagram of a single first order delay section is shown in Fig.8.2. The arrangement of modules is the same as was used before; the difference equation which it realizes is (see equation (6-1))

$$v_n = u_{n-1} + a(u_n - v_{n-1}) \quad .$$

8.2.3 Operating speed

The speed of operation of this circuit is determined exclusively by the speed of the logic. Even assuming a relatively slow cycle time of 1 μs it will be clear that a single section with a word sampling

rate of ~40 kHz is capable of being multiplexed more than 12 times. It is considered a simple task to realize seven such sections (say) on one MOS chip; thus recirculation only nine times will provide 63 first order delay functions on one chip. A clock rate of only 9 x 80.64 = 725.8 kHz with seven first order sections on one chip and recirculating nine times achieves the required result – a complete dispersive network on a single integrated circuit.

A proposed recirculation scheme is shown in Fig.8.3. It is conceivable that two complete networks could be realized on one chip. Whatever final complexity can be achieved, it is clear that this system has immense advantages in terms of size and weight.

8.2.4 Performance aspects

An additional advantage of this system is that one source of error usually associated with digital filters – coefficient error – is eliminated. The system is designed around the multiplier coefficient and the fact that its value is 0.25 exactly.

As before the compression process can be simulated on the computer. The results are given in Fig.8.4 which shows a compressed pulse envelope for an $N = 63$, $a = 0.25$ system. Since we are using significantly more sections and the coefficient is smaller than before, the delay response is less non-linear and the compressed pulse more nearly approaches the ideal $\sin x/x$ envelope. Furthermore there is probably room for increasing the input word length beyond 9 bits + sign to a level which makes performance less sensitive to word length quantization and which reduces the consequent noise to an entirely negligible level, as opposed to a just tolerable level; although total complexity depends still on word length, the overall size is now so small that it is no longer necessary to prune the word length to 'minimum acceptable' proportions.

As before all succeeding circuitry – square and add, detector and decision circuits – can be entirely digital employing simple arithmetic functions (add, subtract and multiply).

8.2.5 Summary

The solution described in this section would have a great impact on the size and weight of dispersive delay networks, as long as a degree of sweep non-linearity is acceptable. To achieve the full benefit of the proposed system all filters and associated detection and decision

circuitry should be fully integrated in MOS/LSI, but since the circuits themselves are conceptually and practically simple there should be few problems in implementation by these means.

It is unfortunate that time did not allow this system to be demonstrated in hardware. However the practical system described in Chapter 7 demonstrated the essential features of a multi-section digital filter approach; the practical problems solved in performing that demonstration were more complex than would be the case in a 63 section system with $a = 0.25$. Therefore it is considered that the case for such a system has been adequately demonstrated.

Appendix A

THE SPECTRUM OF A CHIRP PULSE

The spectrum of a chirp signal has been derived by Gott[4]. Using the parameter $\mu = \frac{2\pi F}{T}$, the complete double sided spectrum (*ie* both negative and positive frequencies) is

$$S(\omega) = \frac{1}{2}\sqrt{\frac{\pi}{\mu}}\,|Z(u_1,u_2)|\,\exp j\left\{-\frac{(\omega_0-\omega)^2}{2\mu} + \arctan\frac{S(u_1,u_2)}{C(u_1,u_2)} + \theta_c\right\}$$

$$+ \frac{1}{2}\sqrt{\frac{\pi}{\mu}}\,|Z(v_1,v_2)|\,\exp j\left\{-\frac{(\omega_0+\omega)^2}{2\mu} + \arctan\frac{S(v_1,v_2)}{C(v_1,v_2)} + \theta_c\right\} . \quad \ldots (A\text{-}1)$$

$Z(x_1,x_2)$, $C(x_1,x_2)$ and $S(x_1,x_2)$ are the modified Fresnel integrals given by

$$Z(x_1,x_2) = C(x_1,x_2) + jS(x_1,x_2)$$

$$= \int_{x_1}^{x_2} \exp j\,\frac{\pi}{2}x^2\,dx$$

and

$$\begin{matrix} u_2 \\ u_1 \end{matrix} = \sqrt{\frac{\mu}{\pi}}\left\{\frac{\omega_0-\omega}{\mu} \pm \frac{T}{2}\right\}$$

$$\begin{matrix} v_2 \\ v_1 \end{matrix} = \sqrt{\frac{\mu}{\pi}}\left\{\frac{\omega_0+\omega}{\mu} \pm \frac{T}{2}\right\} .$$

If the contribution from the negative frequency spectrum is small at positive frequencies then the spectrum is given to a good approximation, by the first term in equation (A-1). This condition is substantially true for $f_0 > F$.

Using this approximation, the amplitude spectrum $|S(\omega)|$, is given by

$$|S(\omega)| = \frac{1}{2}\sqrt{\frac{\pi}{\mu}}\,|Z(u_1,u_2)|$$

$$\doteq \frac{1}{2}\sqrt{\frac{T}{F}} \qquad f_1 < f < f_2$$

since the mean value of $|S(u_1,u_2)|$ is $\sqrt{2}$, for $f_1 < f < f_2$.

This approximate result is obtained by very different means using the principle of stationary phase, which is outlined in Appendix B.

The phase spectrum (positive frequencies) is given by

$$\Phi(\omega) = -\frac{(\omega_0 - \omega)^2}{2\mu} + \arctan\frac{S(u_1,u_2)}{C(u_1,u_2)} + \theta_c \quad .$$

Within the nominal sweep bandwidth, the predominant term is the quadratic component. The second term is known as the residual phase spectrum, since it is usually ignored for the purpose of matched filter design.

Fig 1.2 gives the result of a numerical calculation of $|S(\omega)|$ and Fig 1.3 is the same for $\Phi(\omega)$.

Strict band-limiting to $f_1 < f < f_2$ gives rise to a 0.2 dB energy loss compared with an unlimited signal.

Appendix B

THE PRINCIPLE OF STATIONARY PHASE

It is convenient to use the equivalent complex representation of a signal

$$u(t) = a(t) \exp\left[j\theta(t)\right] .$$

The Fourier transform of this function is

$$U(\omega) = \int_{-\infty}^{\infty} a(t) \exp\left[j\{-\omega t + \theta(t)\}\right] dt . \qquad \text{(B-1)}$$

The stationary phase principle states that the major portion of the integral of a rapidly oscillating function is obtained in a region where the phase is stationary, *ie* where

$$\frac{d}{dt}\left[\omega t - \theta(t)\right] = 0$$

or

$$\omega = \theta'(t) . \qquad \text{(B-2)}$$

Expanding the difference $\omega_k t - \theta(t)$ about a time t_k we get the following, ignoring terms of higher order than the second:

$$\omega_k t - \theta(t) = \omega_k t_k - \theta(t_k) + \left[\omega_k - \theta'(t_k)\right](t - t_k) - \frac{\theta''(t_k)}{2!}(t - t_k)^2 . \qquad \text{... (B-3)}$$

Since $\omega_k - \theta'(t_k) = 0$ (equation (B-2)), this reduces to

$$\omega_k t - \theta(t) = \omega_k t_k - \theta(t_k) - \frac{\theta''(t_k)}{2}(t - t_k)^2 .$$

If $a(t)$ is constant in relation to $\theta'(t)$ at t_k then the spectrum, equation (B-1) becomes:

$$U(\omega_k) = a(t)_k \int_{t_k-\delta}^{t_k+\delta} \exp\left[-j\left\{\omega_k t_k - \theta(t_k) - \frac{\theta''(t_k)}{2}(t - t_k)^2\right\}\right] dt$$

since $t - t_k = \pm\,\delta$ (δ small).

Appendix B

The spectrum of a chirp signal (equation (1.1)) can be expressed in complex terms as

$$S(\omega) = \tfrac{1}{2} \int_{-\infty}^{\infty} a(t) \exp j\left[(\omega_0 - \omega)t + \theta(t)\right]dt$$

$$+ \tfrac{1}{2} \int_{-\infty}^{\infty} a(t) \exp j\left[-(\omega_0 + \omega)t - \theta(t)\right]dt$$

$$= S_+(\omega) + S_-(\omega)$$

where S_+ and S_- refer to the positive and negative frequency spectra.

If the overlap is small, the signal is called narrow band and the complex representation is useful

$$U(\omega) = 2S_+(\omega + \omega_0) \quad .$$

The parameter t_k is effectively constant and so we may write:

$$U(\omega) = a(t_k) \exp\left[j\{-\omega t_k + \theta(t_k)\}\right] \int_{t_k-\delta}^{t_k+\delta} \exp\left[j \frac{\theta''(t_k)}{2} (t - t_k)^2\right] dt \quad .$$

Writing $\frac{\theta''(t_k)}{2} \delta^2 = \frac{\pi y^2}{2}$

we get $d\delta = \sqrt{\pi}\left[\theta''(t_k)\right]^{-\frac{1}{2}} dy$

and

$$U(\omega) = 2\sqrt{\pi} \frac{a(t_k)}{\sqrt{\theta''(t_k)}} \exp\left[j\{-\omega t_k + \theta(t_k)\}\right] \int_0^{\delta\sqrt{|\theta''(t_k)|/\pi}} \exp\left[j \frac{\pi y^2}{2}\right] dy \quad .$$

The integral is another form of the Fresnel integral which, for large values of the upper limit, is approximated by

$$\frac{1}{\sqrt{2}} \exp\left[j \frac{\pi}{4}\right] \quad .$$

Thus:

$$U(\omega) = \sqrt{2\pi}\,\frac{a(t_k)}{\sqrt{|\theta''(t_k)|}}\exp\left[j(-\omega t_k + \theta(t_k) + \frac{\pi}{4}\right] . \qquad (B\text{-}4)$$

If the Fresnel approximation holds for all t_k :

$$|U(\omega_t)|^2 \doteq 2\pi\,\frac{a^2(t)}{|\theta''(t)|} . \qquad (B\text{-}5)$$

Similarly, the phase spectrum $\Phi(\omega)$ is obtained from equation (B-4)

$$\Phi(\omega) \doteq -\omega t + \theta(t) + \pi/4 . \qquad (B\text{-}6)$$

Differentiating with respect to ω , we get:

$$\Phi'(\omega) \doteq -t - \left(\omega - \frac{d\theta}{dt}\right)\frac{dt}{d\omega} .$$

Applying condition (B-2):

$$\Phi'(\omega) \doteq -t$$

which is an equivalent relation to equation (B-2) in terms of the phase spectrum rather than the signal phase function. It follows from this (but may also be derived by other means) that:

$$a^2(t_\omega) \doteq \frac{1}{2\pi}\,\frac{|U(\omega)|^2}{|\Phi'(\omega)|} . \qquad (B\text{-}7)$$

Equations (B-5) and (B-6) may be used to obtain approximate expressions for $|U(\omega)|$ (and hence $|S(\omega)|$) and $\Phi(\omega)$ when the signal function is given, or $a(t)$ and $\theta(t)$ when the spectrum is given.

In addition, consider the two stationary phase conditions

$$\omega = \theta'(t) \qquad -t = \Phi'(\omega) .$$

Now $\theta'(t)$ is recognised as the instantaneous frequency, $\omega(t)$:

$$\omega(t) = \theta'(t)$$

and $-\Phi'(\omega)$ as the group delay function, $\tau(\omega)$:

$$\tau(\omega) = -\Phi'(\omega) .$$

Then $\omega = \omega(t)$ and $t = \tau(\omega)$.

Thus:

$$\omega = T^{-1}(t) = \omega(t) \quad . \tag{B-8}$$

So, the instantaneous frequency $\omega(t)$ is the inverse of the group delay function. This gives a simple method of determining the group delay function which must be synthesised in order to match a signal of given phase function.

The stationary phase conditions and the results given above are used in the main text to obtain approximate expressions for spectra, and ultimately for output signals in proposed nonlinear frequency modulation systems.

Appendix C

ERROR RATE FOR CHIRP SYSTEM EMPLOYING AN IDEAL SYNCHRONISED DEMODULATOR

In an ideal demodulator the output envelopes of the two channels are compared at the instant of peak compression gain when each output consists of a sinewave of frequency f_0 plus bandlimited whitenoise.

With a matched signal the output from the dispersive network is

$$S_m(t) = \sqrt{D} \cos(\omega_0 t + \theta_m) + \tfrac{1}{2} n_m(t)$$

where $n_m(t)$ is a noise signal with unity rms amplitude *ie*

$$S_m(t) = R_m \cos(\omega_0 t + \theta_m + \rho_m)$$

The probability distribution of the envelope R_m is

$$p_m(R) = P(R_m = R) = RZ^2 I_0(GRZ^2) \exp\left\{-\tfrac{1}{2}(G^2 + R^2)Z^2\right\}$$

where Z is the signal to noise ratio *ie*

$$Z = \frac{\text{peak input signal voltage}}{\text{rms noise voltage}}$$

and where I_0 is the modified Bessel function of the first kind and order zero for imaginary argument

$$I_0(\mu) = \frac{1}{2\pi} \int_{-\pi}^{\pi} \exp(\mu \cos \alpha)\, \alpha\alpha$$

The dispersed pulse amplitude is approximately $1/\sqrt{2}$ and so the probability distribution of the output envelope of the mismatched network is

$$p_s(R) = P(R_s = R) = RZ^2 I_0\left(\frac{1}{\sqrt{2}} RZ^2\right) \exp\left\{-\tfrac{1}{2}(\tfrac{1}{2} + R^2)Z^2\right\}$$

The probability of error is the probability that the mismatched output exceeds the matched output at the decision instant

Appendix C

$$P(\text{error}) = P(R_s > R_m) = \int_0^\infty P(R_s > R)\, P(R_m = R)\, dR$$

$$= \int_0^\infty \left\{ \int_R^\infty p_s(r)\, dr \right\} p_m(R)\, dR$$

This integral may be expressed in terms of the Q function of radar:

$$P(\text{error}) = \tfrac{1}{2} \left\{ 1 - Q\left(G\,\frac{Z}{\sqrt{2}}\,,\ \frac{Z}{2} \right) + Q\left(\frac{Z}{2}\,,\ G\,\frac{Z}{\sqrt{2}} \right) \right\}$$

where $Q(A,B) = \int_B^\infty W I_0(AW) \exp\left\{ -\tfrac{1}{2}\,(A^2 + \omega^2) \right\} dW$

Appendix D

NONLINEAR FM - DERIVATION OF DISPERSED PULSE EXPRESSIONS

D.1 General

The output of a filter with response function given by

$$H(f)_F = |H(f)_F| \exp j\, \Phi(f)_F$$

when subjected to an input signal with a spectrum given by

$$S(f)_s = |S(f)_s| \exp j\, \Phi(f)_s$$

is

$$g(t) = \int_{-\infty}^{\infty} |S(f)_s||H(f)_F| \exp j\left[\Phi(f)_s + \Phi(f)_F\right] \exp j2\pi ft\, df \qquad (D\text{-}1)$$

For dispersed pulses $S(f)_s$ is the spectrum of (say) a downward directed sweep and $H(f)_F$ is the response of filter matched to an upward directed sweep.

D.2 Power law signals

As described in Chapter 3,

$$|H(f)_s| = \frac{1}{\sqrt{n}} \left(\frac{F}{f - f_1}\right)^{\frac{n-1}{2n}} \qquad (D\text{-}2)$$

$$\Phi(f)_F = + 2\pi FT \left(\frac{n}{n+1}\right) \left(\frac{f - f_1}{F}\right)^{\frac{n+1}{n}} - \pi FT \left(\frac{f - f_1}{F}\right) - \frac{\pi}{8} \qquad (D\text{-}3)$$

with the parameters as defined in section 3.3.1.

The spectrum of the downward sweep is

$$|S(f)| = \sqrt{\frac{T}{F}} \frac{1}{\sqrt{n}} \left(\frac{F}{f_1 + F - f}\right)^{\frac{n-1}{2n}} \qquad (D\text{-}4)$$

$$\Phi(f)_F = + 2\pi FT \left(\frac{n}{n+1}\right) \left(\frac{f_1 + F - f}{F}\right)^{\frac{n+1}{n}} - \pi FT \left(\frac{f_1 + F - f}{F}\right) + \frac{\pi}{8} \,. \qquad (D\text{-}5)$$

Thus the phase term in equation (C-1) is

$$\Phi(f)_s + \Phi(f)_F + 2\pi ft$$

$$= 2\pi FT\left(\frac{n}{n+1}\right)\left\{(1-x)^{\frac{n+1}{n}} + x^{\frac{n+1}{n}}\right\} - \pi FT + 2\pi xFt + 2\pi f_1 t \qquad \text{(D-6)}$$

To determine the envelope of $g(t)$ the constant phase term $-\pi FT$ and the constant carrier frequency term $2\pi f_1 t$ can be ignored. The resultant integral is then

$$|g(t)|_{MF} = \left| \frac{\sqrt{FT}}{n} \int_0^1 \frac{1}{\left\{x(1-x)\right\}^{\frac{n-1}{2n}}} \times \exp j2\pi FT\left\{\frac{n}{n+1}\left[(1-x)^{\frac{n+1}{n}} + x^{\frac{n+1}{n}}\right] + \frac{xt}{T}\right\} dx \right| \qquad \text{(D-7)}$$

the limits being equivalent to $f = f_1 \rightarrow f_1 + F$.

With an all pass filter the magnitude response is unity instead of equation (C-2) and the output dispersed pulse envelope is

$$|g(t)|_{AP} = \left| \frac{\sqrt{FT}}{\sqrt{n}} \int_0^1 \frac{1}{(1-x)^{\frac{n-1}{2n}}} \times \exp j2\,FT\left\{\frac{n}{n+1}\left[(1-x)^{\frac{n+1}{n}} + x^{\frac{n+1}{n}}\right] + \frac{xt}{T}\right\} dx \right| \qquad \text{(D-8)}$$

D.3 Modified power law signals

The expressions equivalent to equations (D-2) to (D-8) for the modified power law signals described in section 3.4 are

$$|H(f)| = \sqrt{\frac{3^n - 1}{n2^n}}\left\{\frac{2^n F/(3^n - 1)}{f - f_1 + F/(3^n - 1)}\right\}^{\frac{n-1}{2n}}$$

$$\Phi(f)_F = 2\pi FT(x + \lambda)\left\{\frac{n}{2(n+1)}\left(\frac{x+\lambda}{\lambda}\right)^{\frac{1}{n}} - 1\right\}$$

where $x = \dfrac{f - f_1}{F}$ and $\lambda = \dfrac{1}{3^n - 1}$

$$|S(f)| = \sqrt{\frac{T}{F}} \sqrt{\frac{3^n - 1}{n2^n}} \left\{ \frac{2^n F/(3^n - 1)}{f_1 + 3^n F/(3^n - 1) - f} \right\}^{\frac{n-1}{2n}}$$

$$\Phi(f)_s = 2\pi FT\ (1 + \lambda - x) \left\{ \frac{n}{2(n+1)} \left(\frac{1 + \lambda - x}{\lambda} \right)^{\frac{1}{n}} - 1 \right\}$$

$$\Phi(f)_F + \Phi(f)_s + 2\pi ft = \pi FT \frac{n}{(n+1)} \left\{ \left(\frac{1 + \lambda - x}{\lambda} \right)^{\frac{1}{n}} + \left(\frac{x + \lambda}{\lambda} \right)^{\frac{1}{n}} \right\}$$

$$- 2\pi FT\ (1 + 2\lambda) + 2\pi Fxt + 2\pi f_1 t$$

$$|g(t)|_{MF} = \frac{\sqrt{FT}}{2} \left(3^n - 1\right)^{\frac{1}{n}} \left| \int_0^1 \frac{1}{\left\{ (x + \lambda)(1 + \lambda - x) \right\}^{\frac{n-1}{2n}}} \right.$$

$$\left. \times \exp j2\pi FT \left[\frac{n}{2(n+1)} \left\{ \left(\frac{1 + \lambda - x}{\lambda} \right)^{\frac{n+1}{n}} + \left(\frac{x + \lambda}{\lambda} \right)^{\frac{n+1}{n}} \right\} + \frac{xt}{T} \right] dx \right|$$

D.4 Logarithmic phase signals

From section 3.6 the response of a filter matched to an upward sweep is

$$|H(f)| = \sqrt{\frac{F}{T}} \left(\frac{\sqrt{k}}{f - f_0} \right)$$

$$\Phi(f)_F = 2\pi (f - f_0) \left\{ T_1 - \frac{k}{f - f_0} \right\} + 2\pi k \ln \left(\frac{k}{f - f_0} \right).$$

Appendix D

The spectrum of a downward sweep, defined by the frequency function

$$f(t) = f_{01} - \frac{k}{T_1 - t}$$

where $f_{01} = f_1 + F\left(\frac{\lambda - 1}{\lambda - 2}\right)$

is

$$|S(f)| = \frac{\sqrt{k}}{f_{01} - f}$$

$$\Phi(f)_s = 2\pi(f_{01} - f)\left\{T_1 - \frac{k}{f_{01} - f}\right\} + 2\pi k \ln\left(\frac{k}{f_{01} - f}\right)$$

The phase term in equation (C-1) is

$$\Phi(f)_s + \Phi(f)_F + 2\pi ft$$

$$= -2\pi\left[k \ln(f - f_0)(f_{01} - f) + 2k - T_1(f_{01} - f_0) - 2k \ln k - ft\right] .$$

Substituting for λ , defined in section 3.6, and putting $x = \frac{f - f_0}{F}$ we get:

$$-2\pi\left[k \ln\left\{x\lambda - x^2(\lambda - 2)\right\} + k \ln \frac{F^2}{\lambda - 2}\right.$$

$$\left. + 2k(1 - \ln k) - T_1(f_{01} - f_0) - Ftx - f_0 t\right] .$$

Again to determine the envelope all terms not including x can be ignored, and finally we get for the dispersed pulse envelope

$$|g(t)|_{MF} = \sqrt{FT}\left(\frac{\lambda - 1}{\lambda - 2}\right)\left| \int_{\frac{1}{\lambda-2}}^{\frac{\lambda-1}{\lambda-2}} \frac{1}{x\{\lambda - x(\lambda - 2)\}} \right.$$

$$\left. \times \exp j2\pi FT\left[-\left(\frac{\lambda - 1}{\lambda - 2^2}\right)\ln x\left\{\lambda - x(\lambda - 2)\right\} + \frac{xt}{T}\right] dx \right| .$$

With an all pass filter the dispersed pulse envelope is

$$|g(t)|_{AP} = \sqrt{FT}\,\frac{(\lambda-1)}{(\lambda-2)}\left|\int_{\frac{1}{\lambda-2}}^{\frac{\lambda-1}{\lambda-2}} \frac{1}{\lambda - x(\lambda-2)} \times \exp\, j2\pi FT\left[-\frac{(\lambda-1)}{(\lambda-2)^2}\ln x\left\{\lambda - x(\lambda-2)\right\} + \frac{xt}{T}\right] dx\right|$$

D.5 Exponential phase signals

The expressions equivalent to those above in this case are

$$|H(f)| = \sqrt{\frac{F}{T}}\,\frac{1}{\sqrt{a(f-f_\alpha)}}$$

$$\Phi(f)_F = \frac{2\pi c}{a}\left(\frac{f-f_\alpha}{c}\right)\ln\left(\frac{f-f_\alpha}{c}\right) - \frac{2\pi c}{a}\left(\frac{f-f_\alpha}{c}\right)$$

$$|S(f)| = \frac{1}{\sqrt{a(f_\beta - f)}}$$

$$\Phi(f)_s = \frac{2c}{a}\left(\frac{f_\beta - 1}{c}\right)\ln\left(\frac{f_\beta - f}{c}\right) - \frac{2\pi c}{a}\left(\frac{f_\beta - f}{c}\right)$$

where $f_\alpha = f_1 - \frac{F}{\lambda(\lambda-2)}$; $f_\beta = f_1 + \frac{F(\lambda-1)^2}{\lambda(\lambda-2)}$

$$\Phi(f)_F + \Phi(f)_s + 2\pi ft = \frac{2\pi c}{a}\left\{\left(x+\frac{1}{\gamma}\right)\ln\left(x-\frac{1}{\gamma}\right) + (\gamma - x)\ln(\gamma - x)\right\} + \frac{2\pi}{a}(f_\alpha - f_\beta) + 2\pi cxt + 2\pi f_1 t$$

where $x = \frac{f - f_1}{c}$ and $\gamma = \lambda - 1$

Appendix D

$$|g(t)|_{MF} = \frac{\sqrt{FT}}{2 \ln \gamma} \left| \int_0^{\gamma - \frac{1}{\gamma}} \frac{1}{\sqrt{\left(x + \frac{1}{\gamma}\right)(\gamma - x)}} \times \exp j \frac{2\pi c}{a} \left\{ \left(x + \frac{1}{\gamma}\right) \ln \left(x + \frac{1}{\gamma}\right) + (\gamma - x) \ln (\gamma - x) + axt \right\} dx \right|$$

$$|g(t)|_{AP} = \sqrt{\frac{FT}{2 \ln \gamma \left(\frac{\gamma}{\gamma^2 - 1}\right)}} \left| \int_0^{\gamma - \frac{1}{\gamma}} \frac{1}{\sqrt{\gamma - x}} \times \exp j \frac{2\pi c}{a} \left\{ \left(x + \frac{1}{\gamma}\right) \ln \left(x + \frac{1}{\gamma}\right) + (\gamma - x) \ln (\gamma - x) + axt \right\} dx \right|$$

Appendix E

ENVELOPE OF COMPRESSED PULSE IN DIGITAL FILTER SYSTEM

As described in section 5.5 the instantaneous radian frequency of the (continuous) upward swept signal matched to the delay response of N identical digital filter sections in

$$\theta'(t) = \omega(t) = \frac{1}{\Delta t} \arccos\left(\frac{T_0 + ct}{T_0 - t}\right)$$

where $T_0 = Nt_0$ and $t_0 = \Delta t \left(\frac{1 - a}{1 + a}\right.$ (a negative) .

To obtain the compressed pulse shape, first the spectrum modulus function must be calculated; by stationary phase,

$$|S(\omega)|^2 = \frac{2\pi}{|\theta''(t)|} .$$

Differentiating equation (F-1) and substituting back to remove the t-dependence, we find

$$|\theta''(t)_{t\omega}| = \frac{1}{\Delta t} \left| \frac{1}{\sin \omega\Delta t} \frac{(1 + a^2 + 2a \cos \omega\Delta t)^2}{2aN\Delta t(1 - a^2)} \right|$$

Thus,

$$|S(\omega)| = 2\Delta t \sqrt{\pi(1 - a^2)|a|} \frac{\sqrt{\sin \omega\Delta t}}{1 + a^2 + 2a \cos \omega\Delta t} .$$

In the system described in Chapters 6 and 7, an all pass filter is used, no attempt being made to implement a true matched filter with a response identical to $|S(\omega)|$ and a linear phase response.

The compressed pulse output envelope is then

$$|g(t)| = \int_0^{2\pi F} |S(\omega)| e^{j\omega t} \frac{d\omega}{2\pi} .$$

Substituting $x = \omega\Delta t$ this expression becomes

$$|g(t)| = \sqrt{\frac{N(1 - a^2)|a|}{\pi}} \left| \int_0^{\pi} \frac{\sqrt{\sin x}}{1 + a^2 + 2a \cos x} \exp\left(\frac{jt\omega}{\Delta t}\right) dx \right| .$$

Appendix F

COMPARISON BETWEEN TRUNCATION AND ROUNDING IN THE MULTI-SECTION DIGITAL FILTER SOLUTION

1 In the experimental demonstration of pulse compression using an identical section digital filter dispersive network (Chapter 6) a significant degradation of the output from the ideal situation, effectively a negative dc shift, was discovered if the multiplier outputs were truncated rather than rounded.

It became apparent that similar effects had been predicted by various authors but that only in multi-section cascaded networks were the differences significant. Practically of course the simple solution to the problem is to quantize by rounding rather than truncation when the mean error is zero. However it is of interest to examine exactly how serious the apparently trivial difference can be by comparing results in the two cases.

2 It has been found convenient to analyse the effect of quantization by representing the error statistically. For fixed point arithmetic and rounding the error e_r is represented as a random variable with a probability density shown in Fig.F.1a. For two's complement truncation the probability density is shown in Fig.F.1b. For rounding the mean error is zero with a variance given by

$$\sigma_r^2 = \frac{\varepsilon}{12}$$

where $\varepsilon = 2^{-n}$ and n is the number of fractional bits in the fixed point realization.

3 For truncation the variance is the same ($\sigma_t = \sigma_r$) but the mean error is $-\varepsilon/2$; the truncation is negative and satisfies

$$0 \geq e_t \geq -(2^{-n_2} - 2^{-n_1})$$

where n_1 and n_2 are the number of bits before and after truncation.

The multiplier output after truncation can be considered as the sum of the true exact number and the error, e_t. The error is then effectively filtered by the pole of the section containing that multiplier and the following cascade of all-pass sections.

4 The impulse response of the pole is $h(m) = (-a)^m$.

Appendix F

The output error at a given instant is the error for the given input sample plus the sum of the previous errors propagated successively through the pole at $z = -a$. If the mean of each multiplier error is $-\varepsilon/2$ then the mean output error at a given instant is

$$\bar{e}_{01} = -\frac{\varepsilon}{2}\sum h(m) = -\frac{\varepsilon}{2(1+a)} .$$

The error e_{01} has a mean value $-\varepsilon/2(1+a)$ and a variance $\varepsilon^2/12(1-a^2)$. The error at the output of the second section has the same properties. The total mean error at the output of the second section is $2\bar{e}_{01}$ thus after N such sections the overall mean error is

$$e_{ON} = -\frac{N\varepsilon}{2(1+a)} .$$

This parameter is tabulated below for various values of N and word lengths, n $(\varepsilon = 2^{-n})$.

Table F.1

n \ N	40	50	60	70
5	0.9797	1.1205	1.2654	1.4130
7	0.2449	0.2801	0.3163	0.3533
9	0.0612	0.0700	0.0791	0.0883
11	0.0153	0.0175	0.0198	0.0221

Overall mean output error (NEGATIVE) due to two's complement truncation

5 Clearly this effect is highly significant when compared with a peak input level of 0.14 and expected peak compressed pulse levels of 0.75.

The choice of a 9 bit realization for the practical demonstration was obviously just acceptable - a 7 bit realization would have run the risk of overflow occurring. But if this negative bias or dc shift of the outputs - all outputs - is tolerable then the system can operate normally.

6 Once the practical observations had been explained a computer simulation was run in which a 50 section response was examined with two's complement truncation and with rounding.

Appendix F

Fig.F.2 shows the computed compressed pulses (two inputs in quadrature, two outputs squared and added) for 7 and 11 bit realizations and for rounding and truncation. Clearly the 7 bit realization for truncation is unacceptable; the mean output error after squaring and adding becomes 0.396 which is far too large as a proportion of the signal. An 11 bit realization gives rise to a mean output error of only 0.025 but rounding is still preferable.

Table F.2 compares the computed mean errors with the data for 50 sections in Table F.1.

Table F.2

n	Theoretical	Computed
5	1.1205	1.018
7	0.2801	0.2506
9	0.0700	0.0628
11	0.0175	0.0158

7 It is interesting to note that the mean output error in this system depends upon the sign of the multiplier coefficient

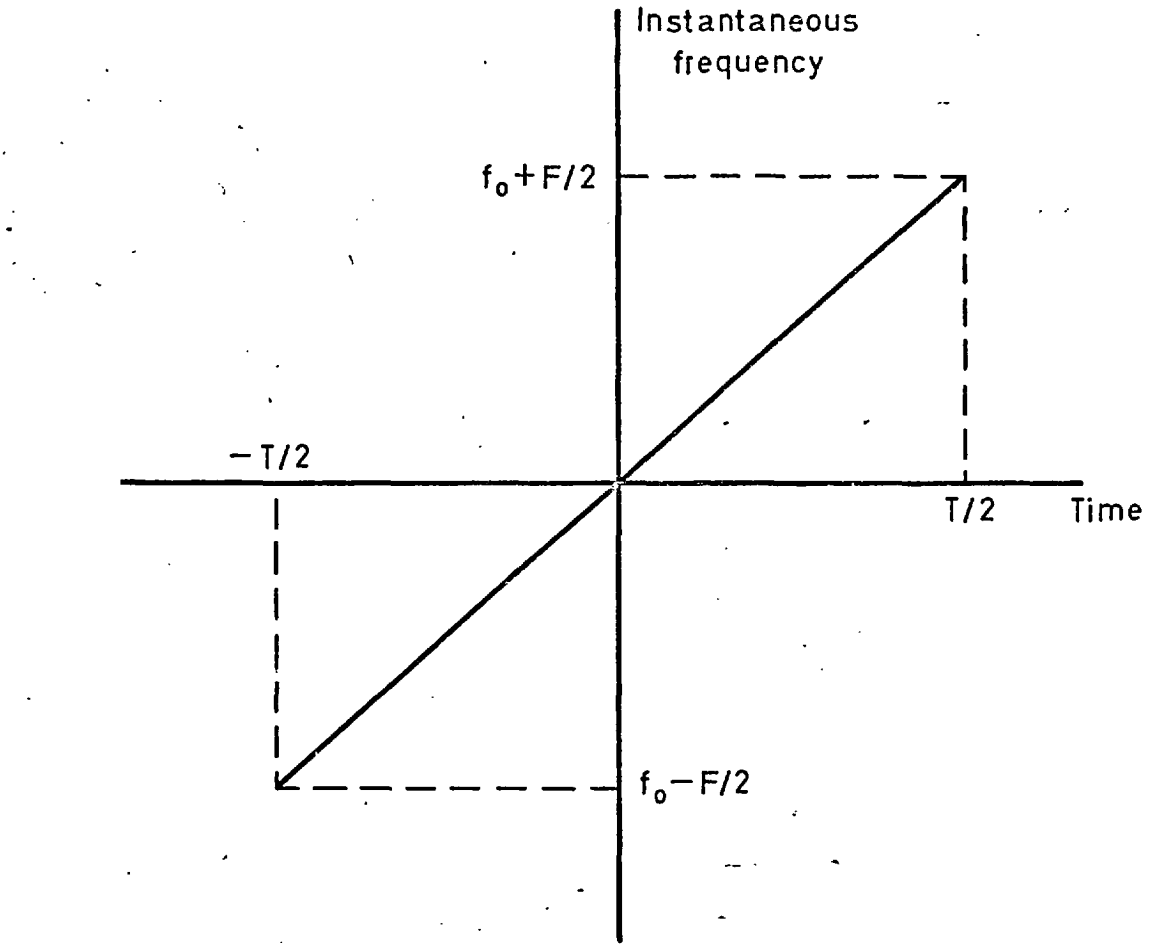
i.e. $$\overline{e_{ON}} \propto \frac{1}{1 + a} \quad .$$

Thus for $N = 50$ $(a = \pm 0.36205)$:

$$\overline{e_{ON}} \propto 1.5676 \qquad \text{a negative}$$

$$\overline{e_{ON}} \propto 0.7342 \qquad \text{a positive}$$

Thus the output signals in the two channels are shifted in amplitude by different amounts if two's complement truncation is employed.



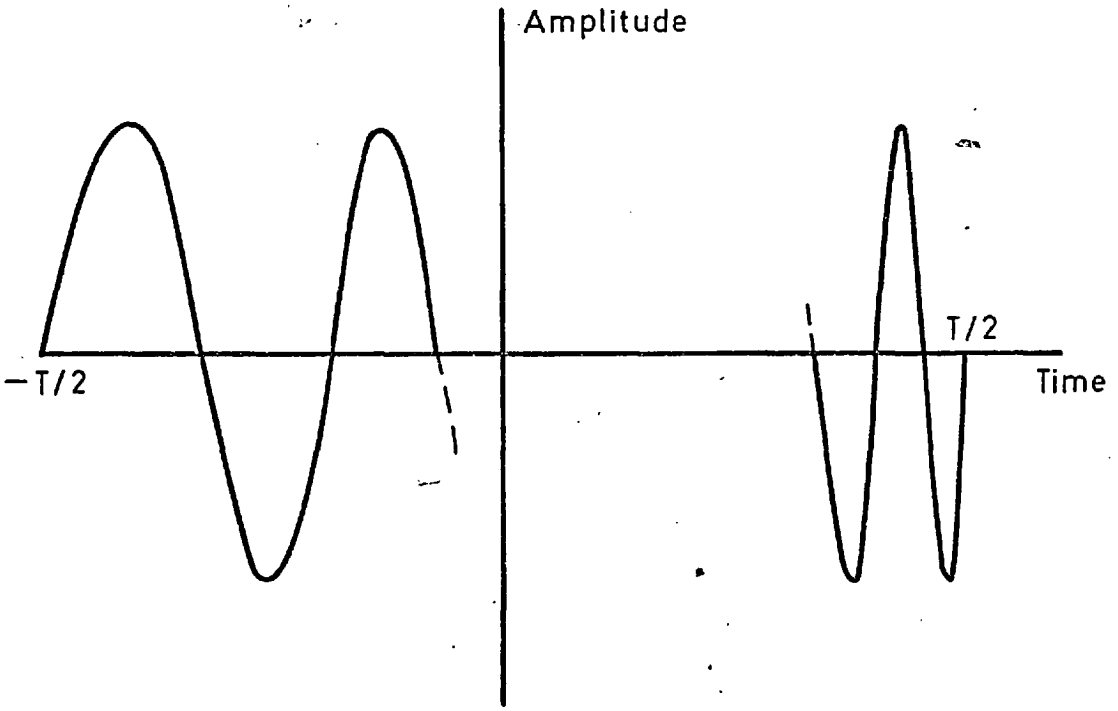


Fig 1.1 The chirp signal

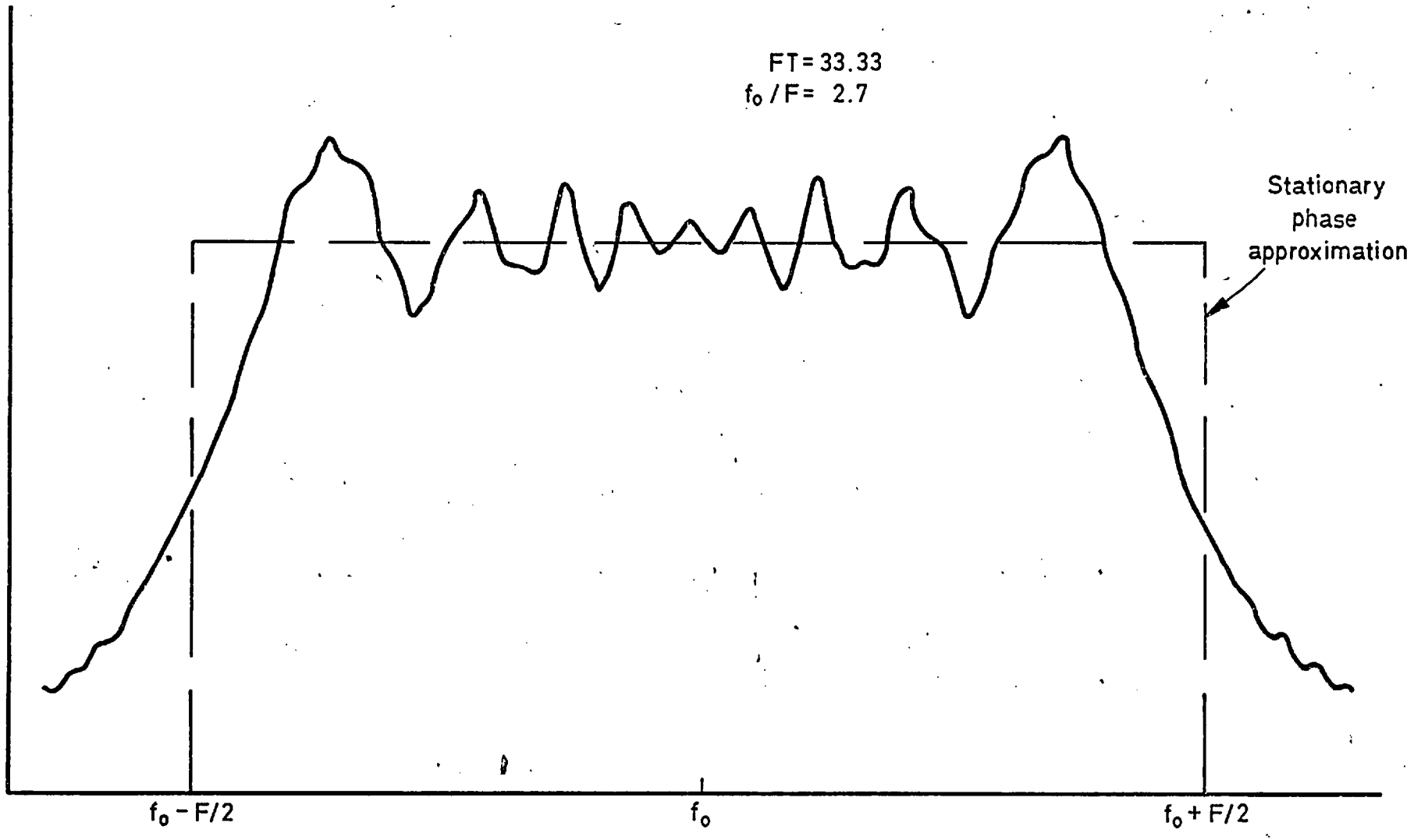


Fig 1.2 Amplitude spectrum of a chirp pulse

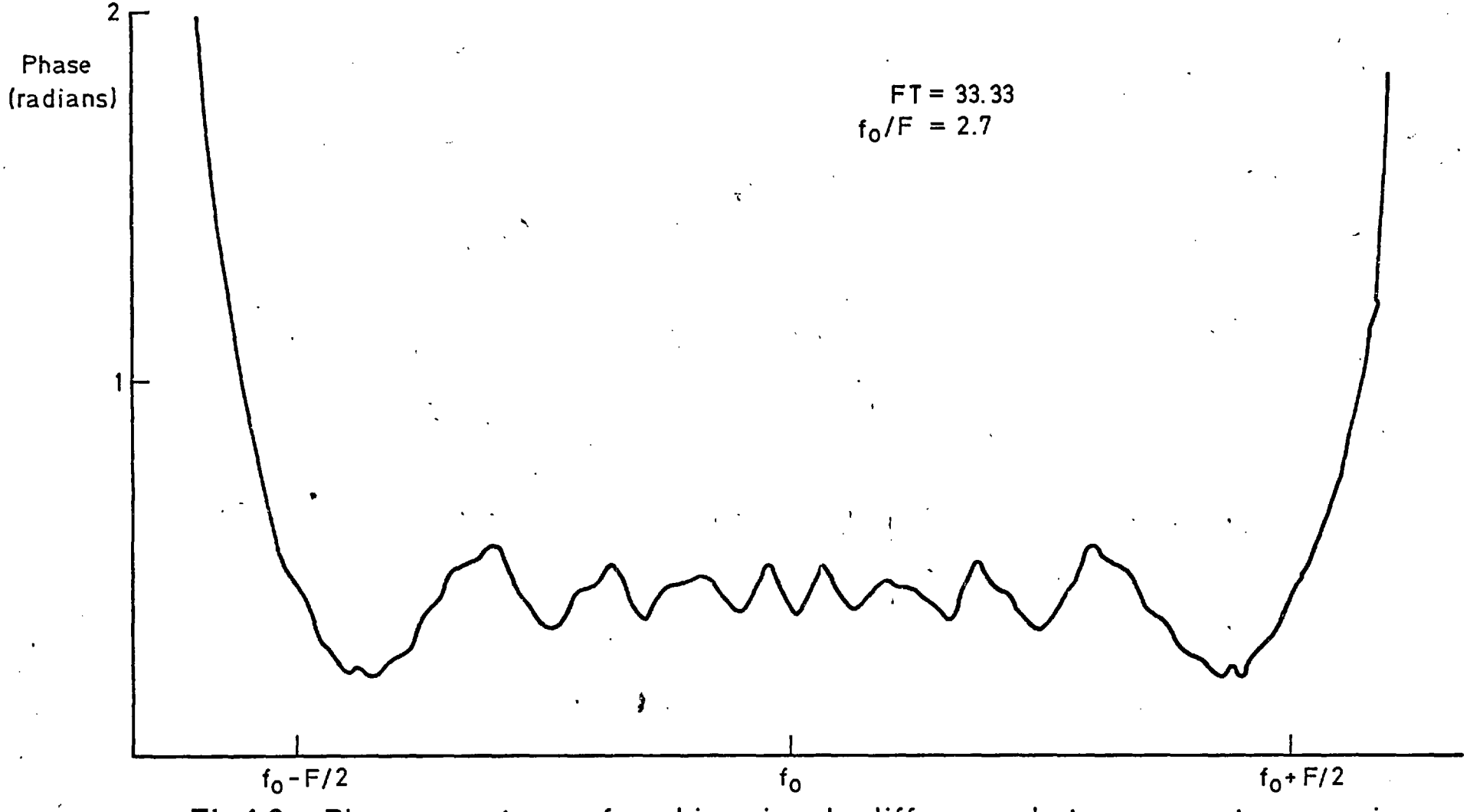


Fig.1.3 Phase spectrum of a chirp signal – difference between exact expression and stationary phase approximation

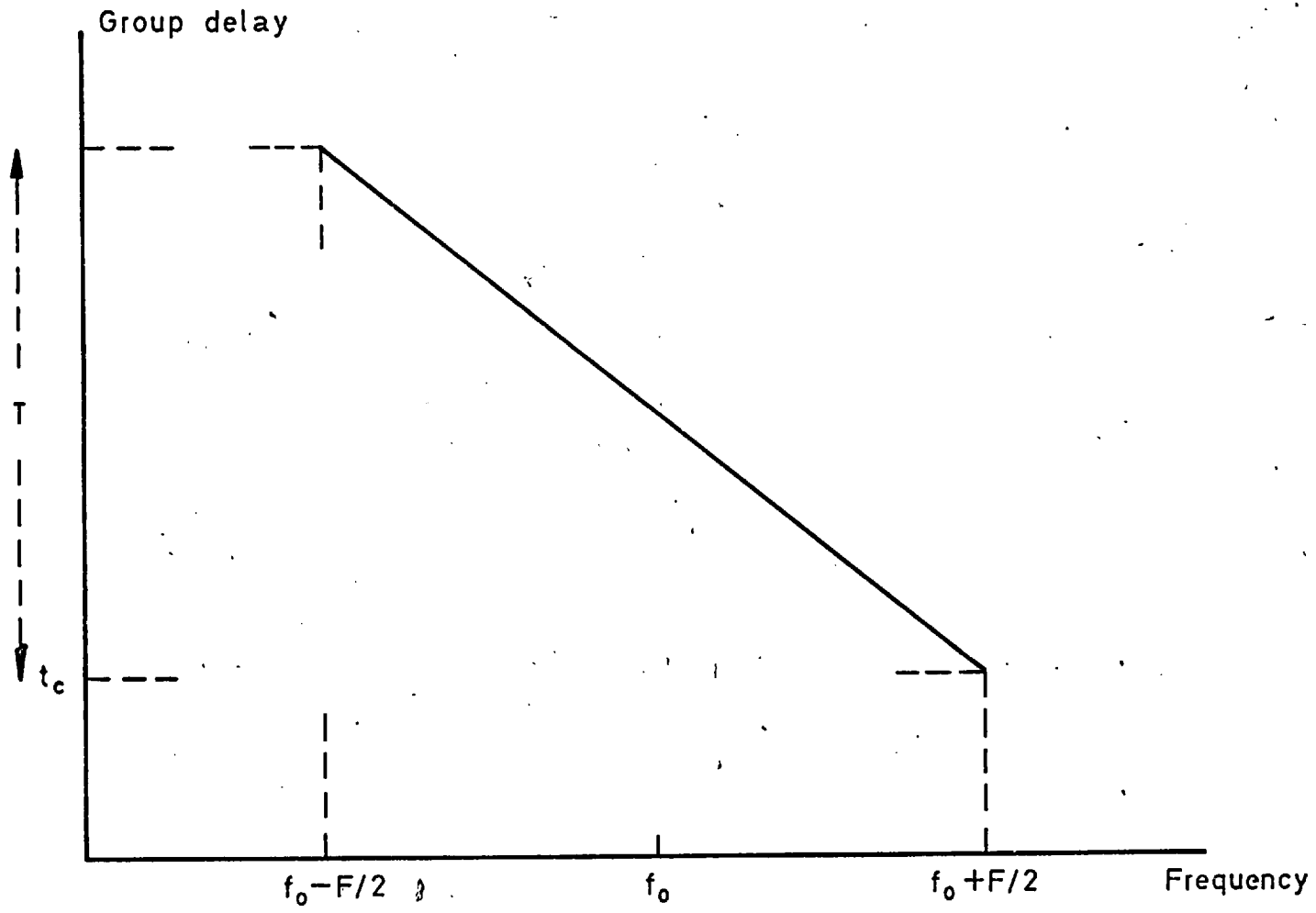


Fig 1.4 Group delay specification of a chirp filter

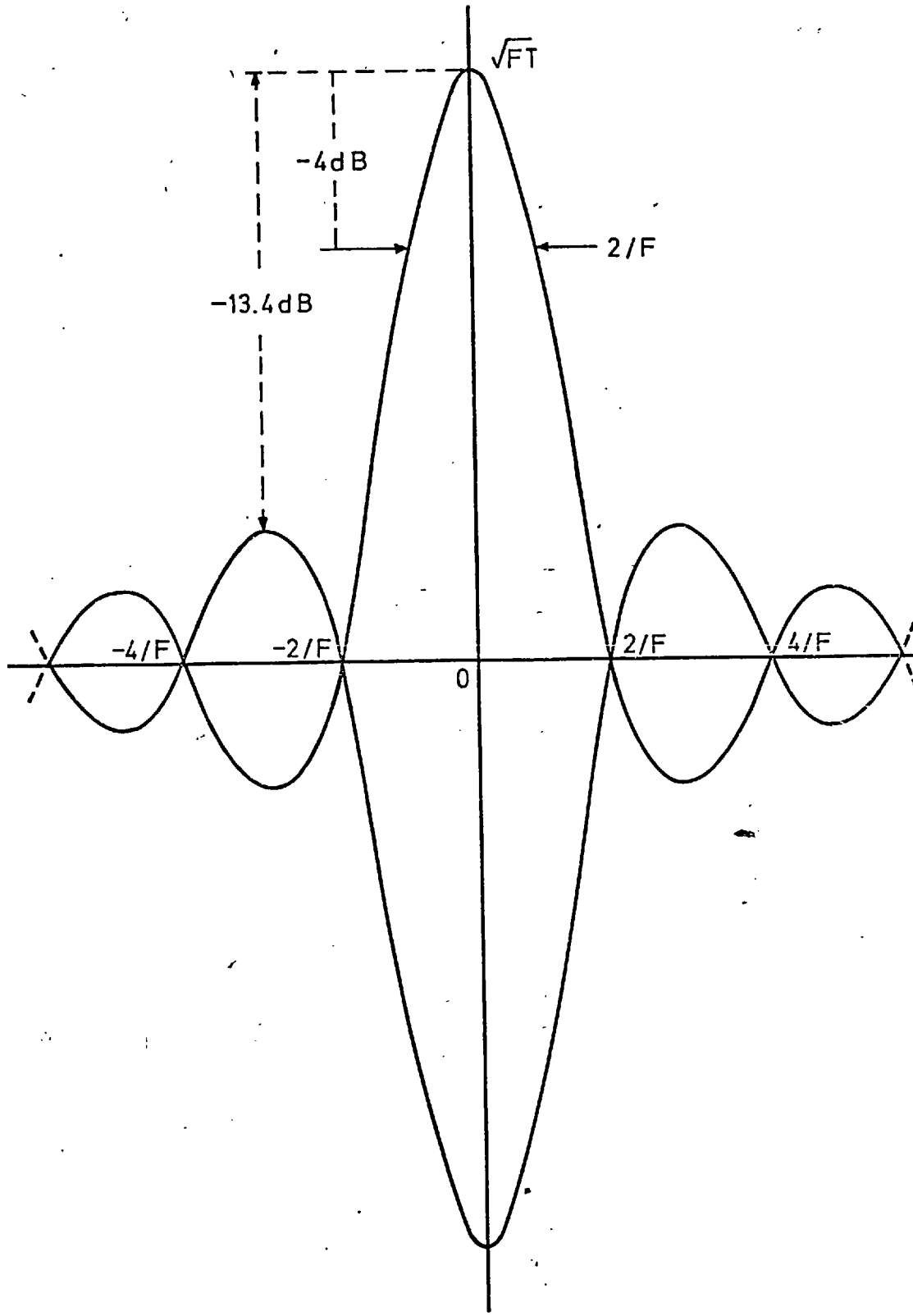


Fig.1.5 Output of a chirp matched filter

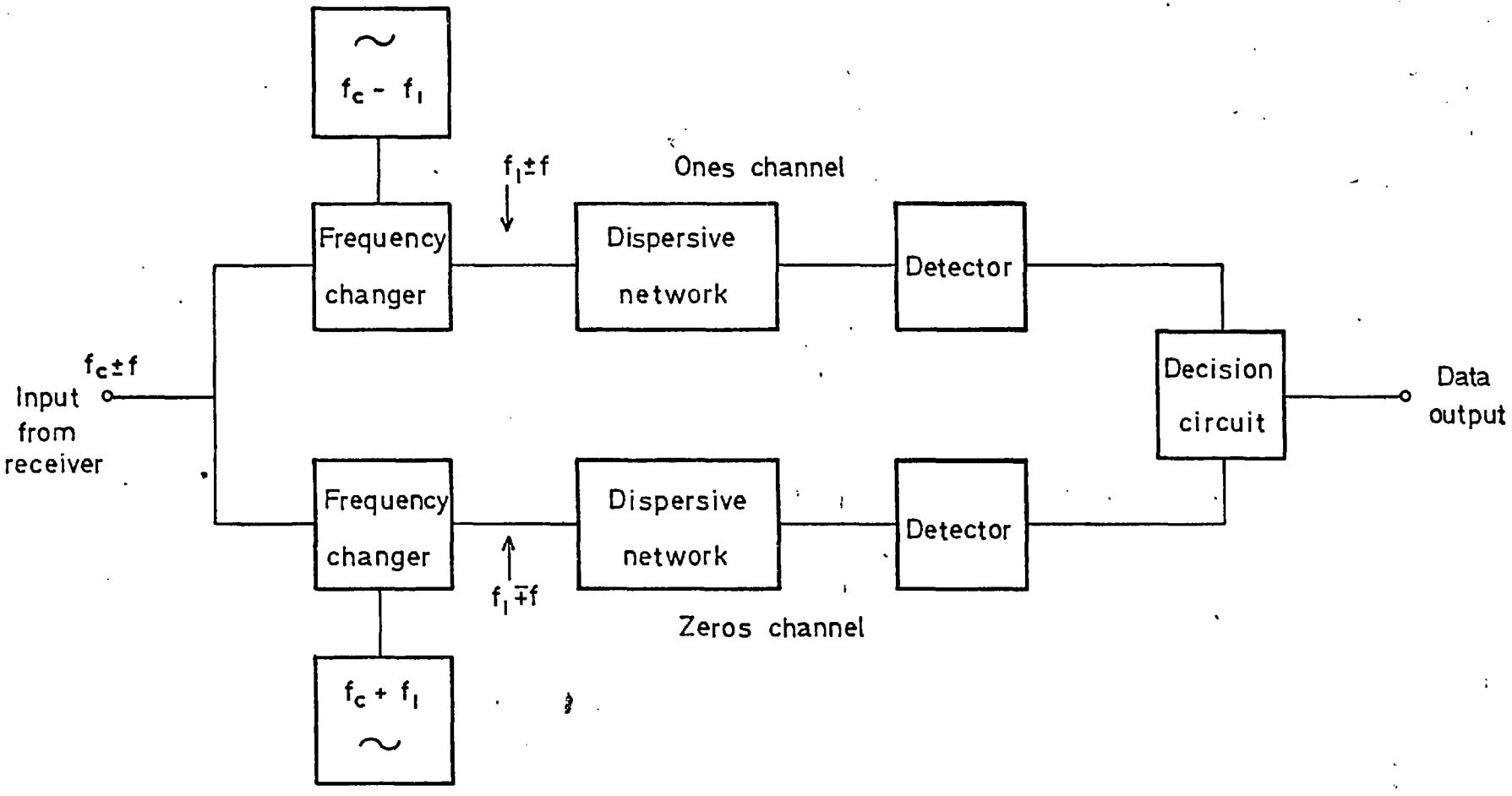


Fig.1.6 Chirp demodulator

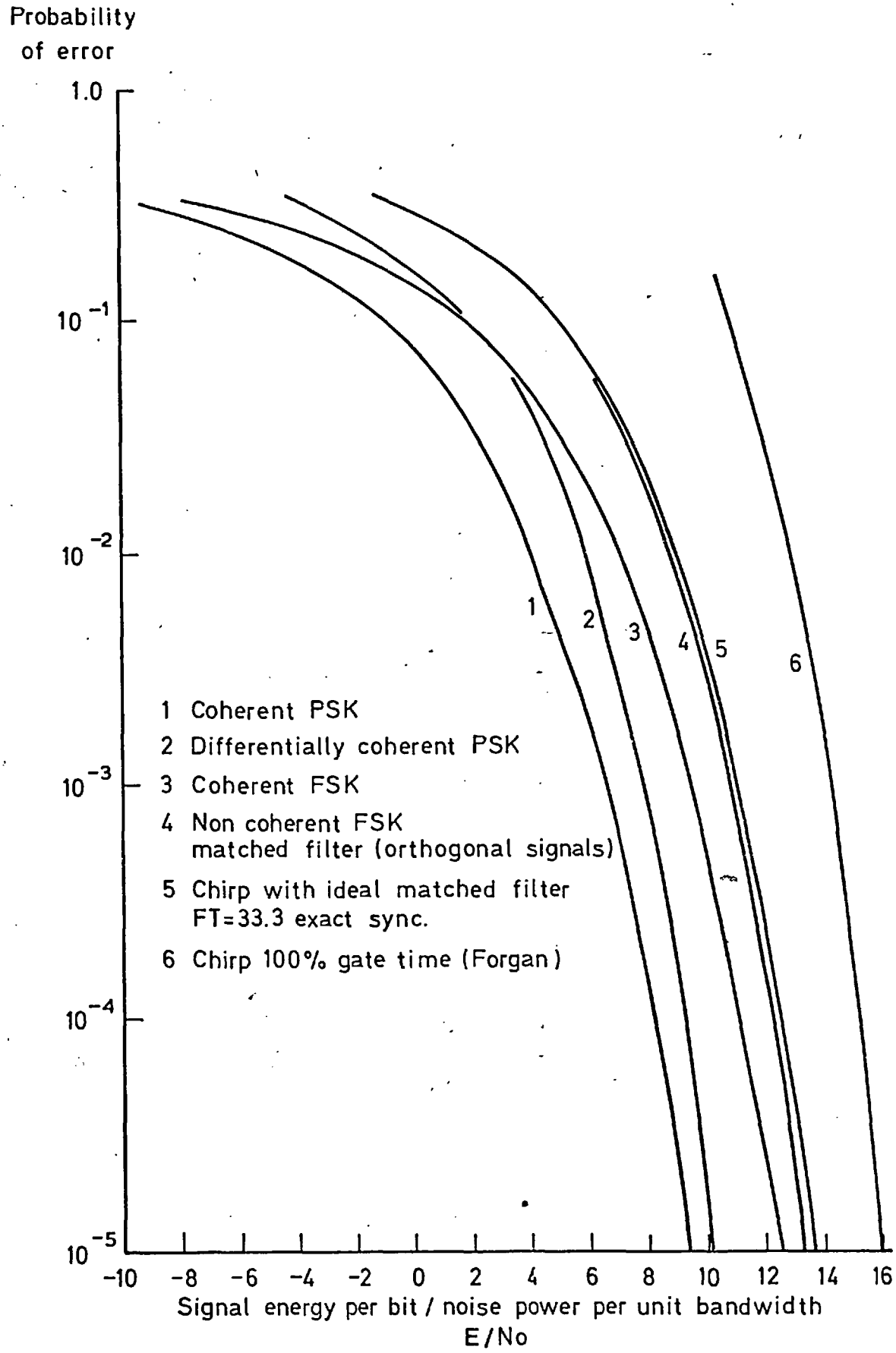


Fig.1.7 Error rates of binary data transmission systems

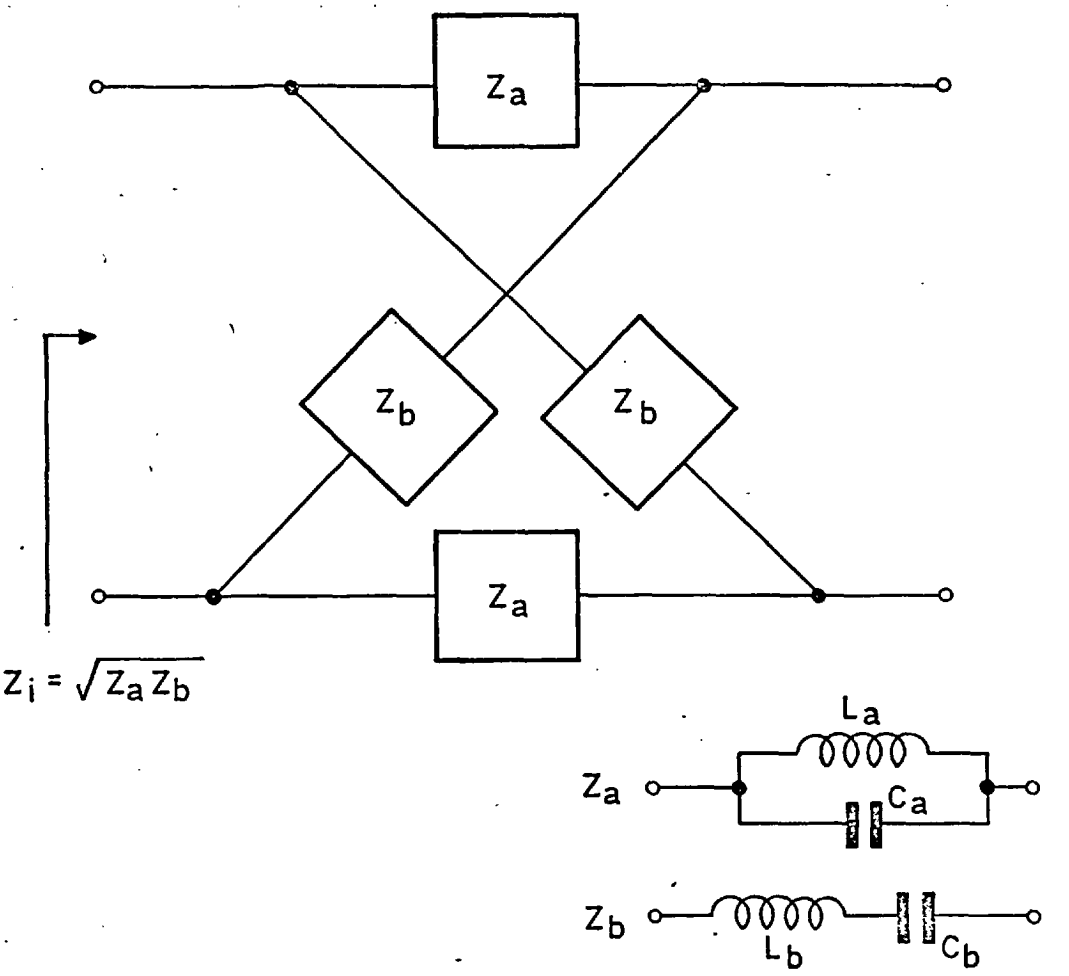


Fig.2.1a Second order all pass lattice

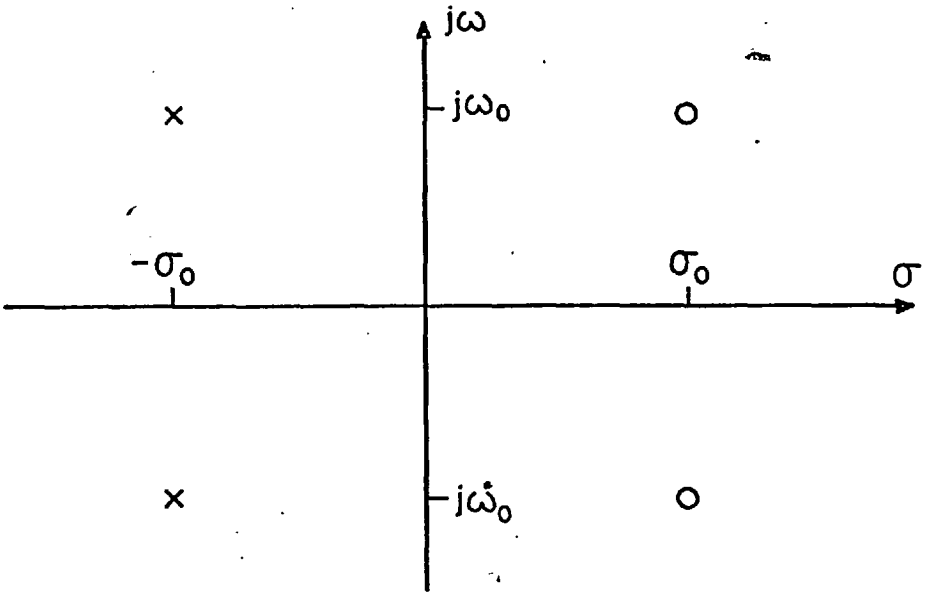


Fig.2.1b Pole-zero locations of second order all pass section

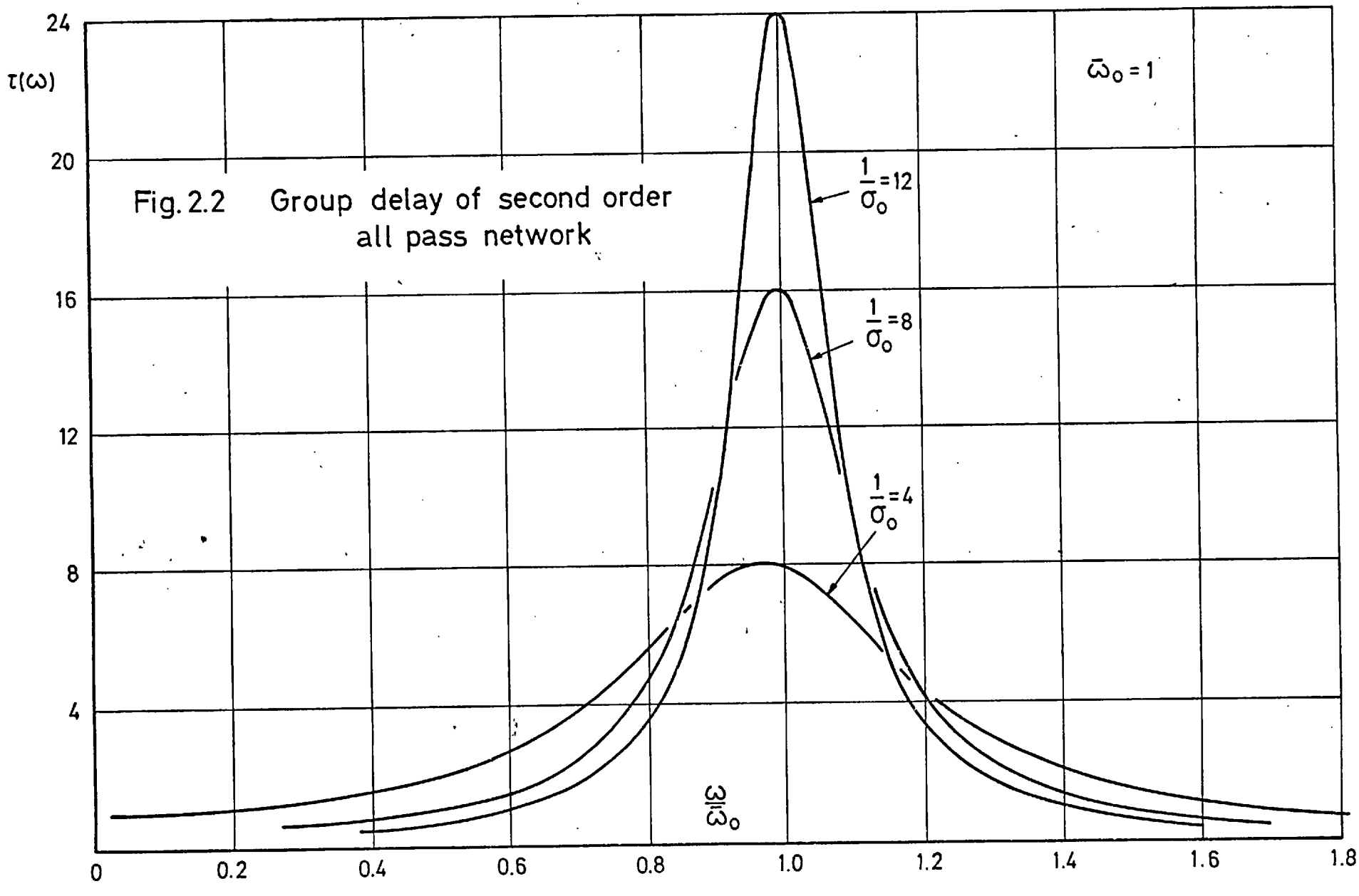


Fig. 2.2 Group delay of second order all pass network

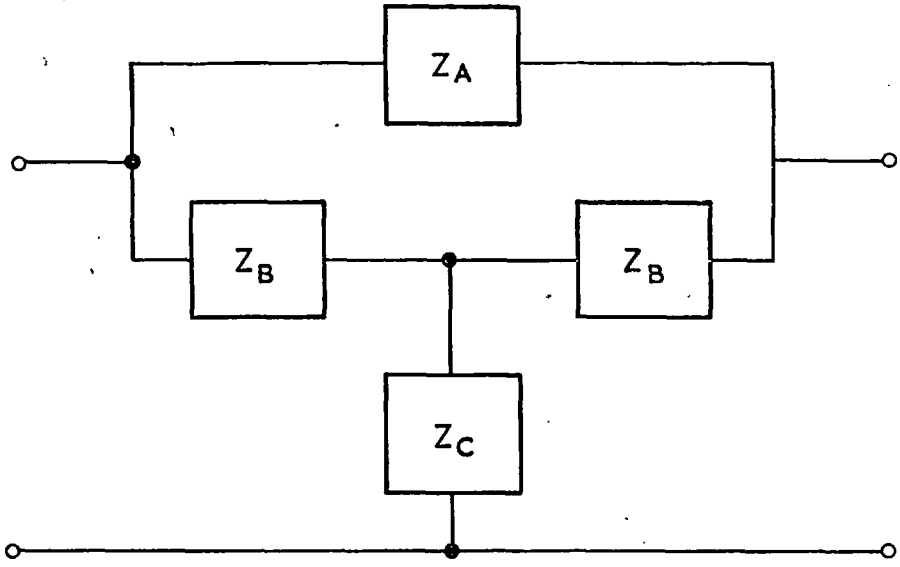


Fig.2.3a Unbalanced bridged-T equivalent of lattice

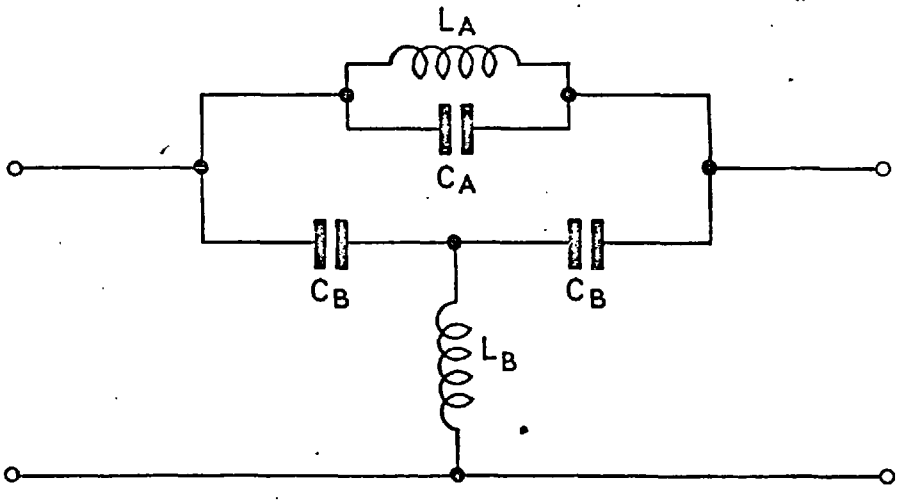


Fig.2.3b Bridged-T all pass network used in RAE system

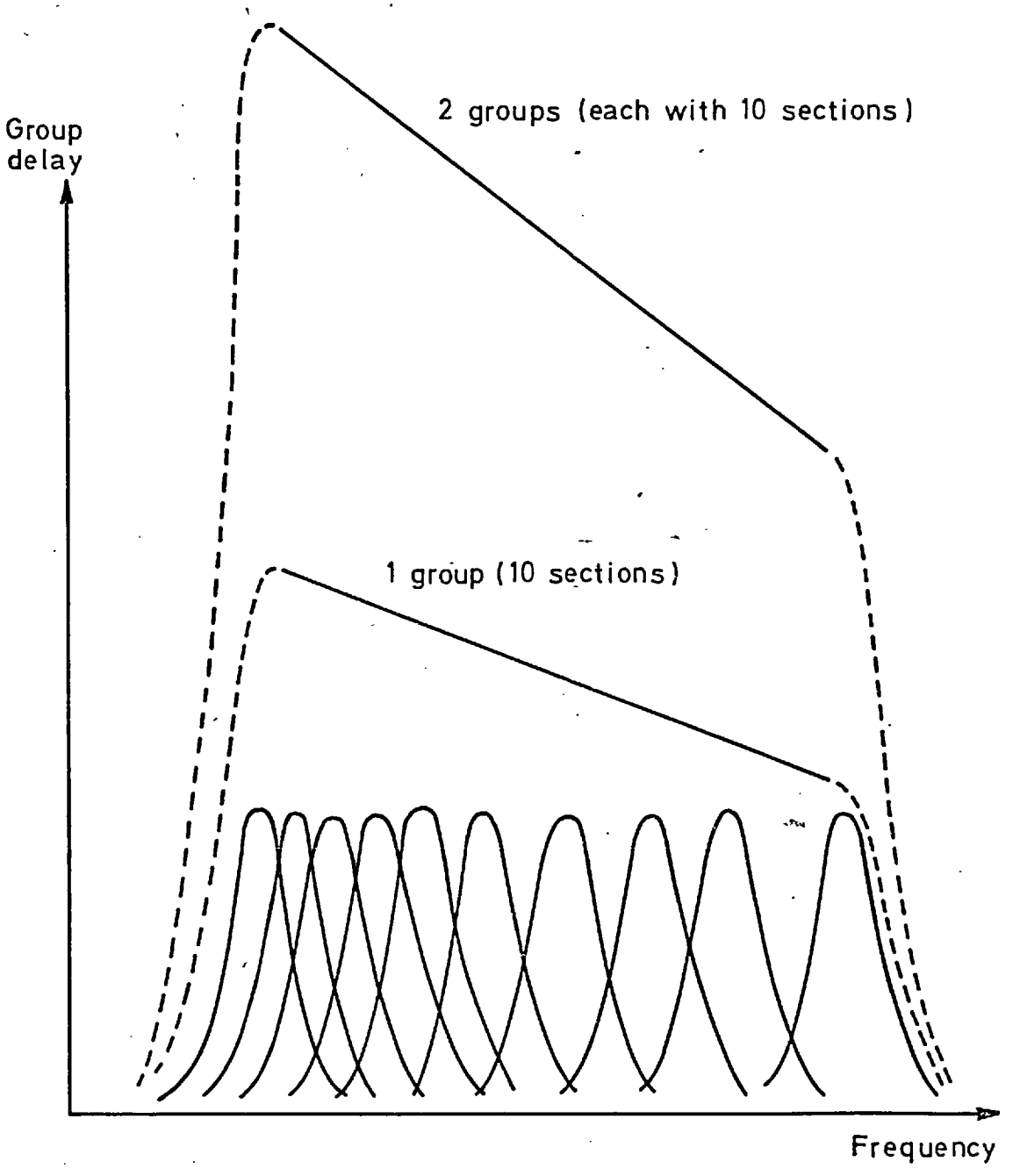


Fig. 2.4 Linear delay/frequency response obtained by adding responses of second order sections

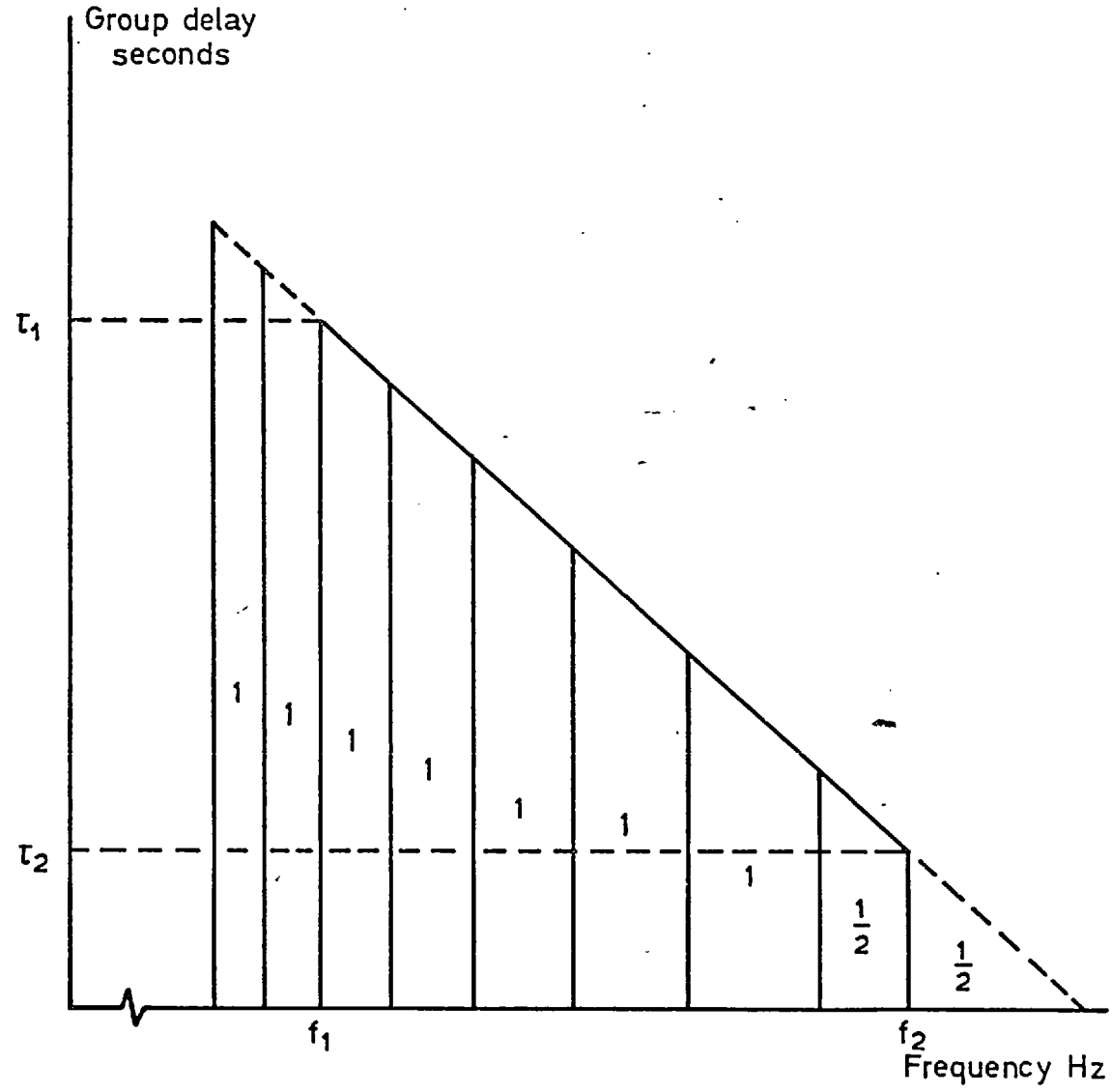


Fig.2.5 Placing of second order sections with centre frequencies at unit area intervals

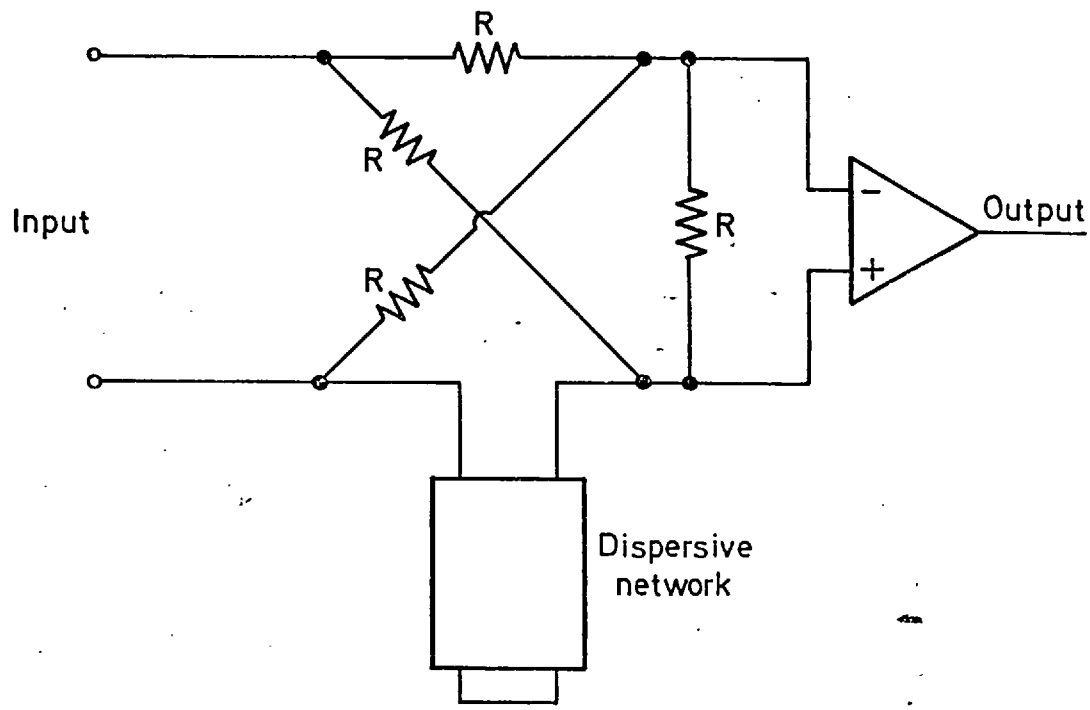


Fig. 2.6 Use of resistive hybrid network to halve the size of a dispersive delay network

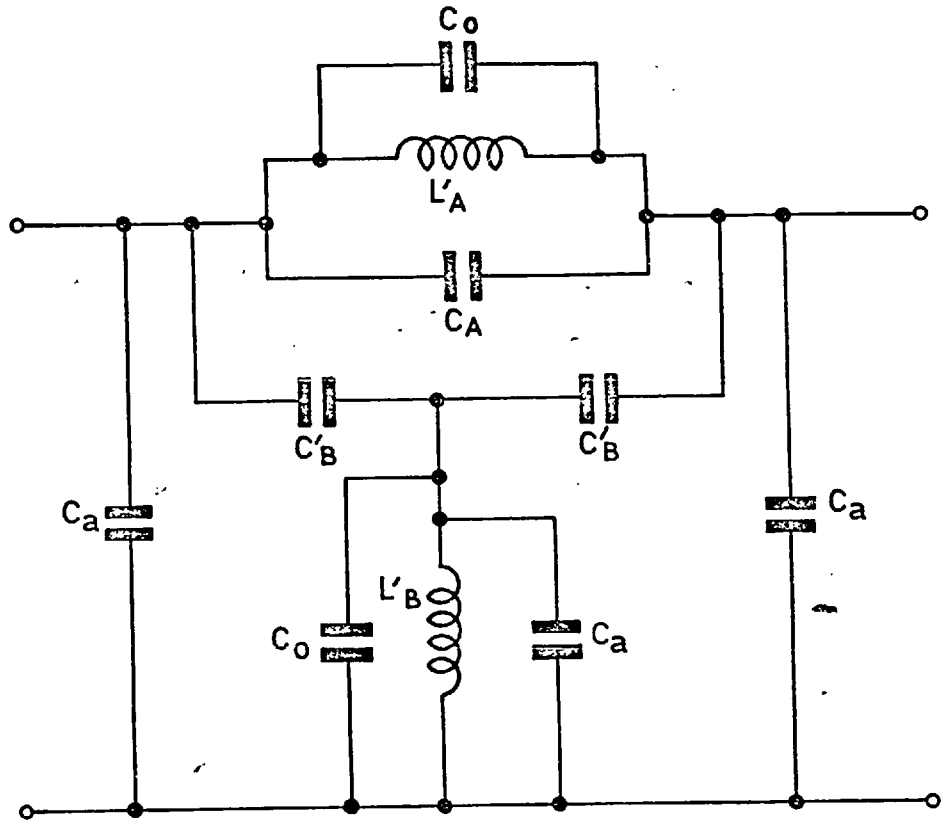


Fig.2.7 Bridged-T network including stray capacitances

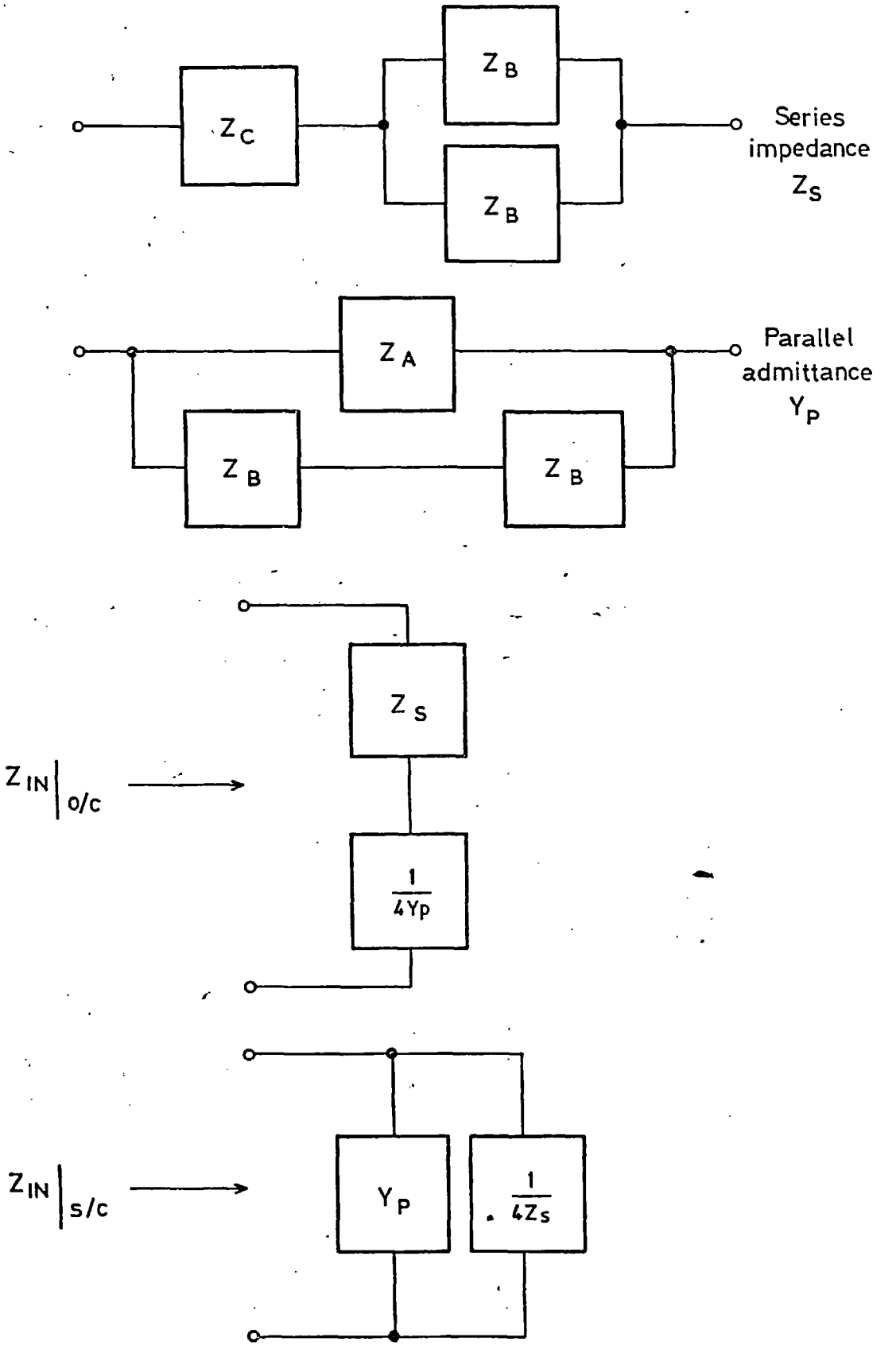


Fig. 2.8 Open-and short-circuit impedances of the bridged-T network

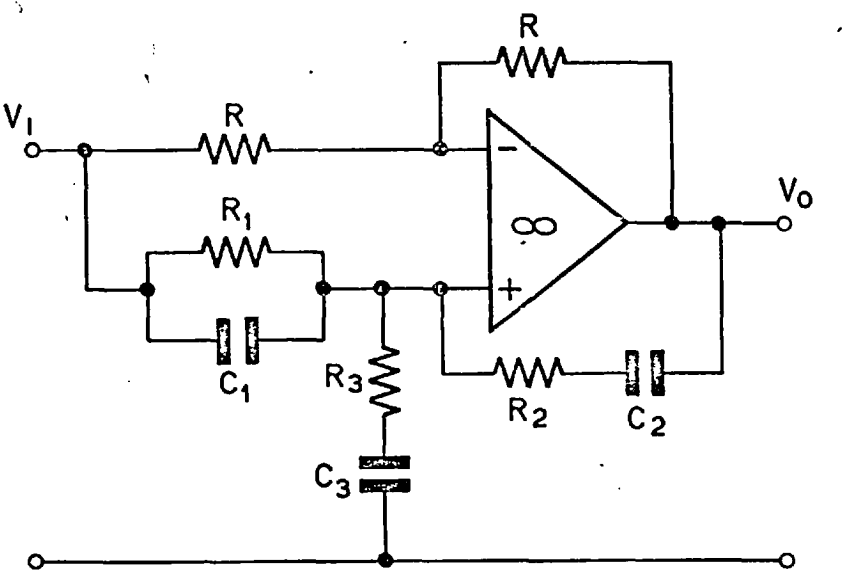


Fig.2.9a Active all-pass network due to Holt and Gray

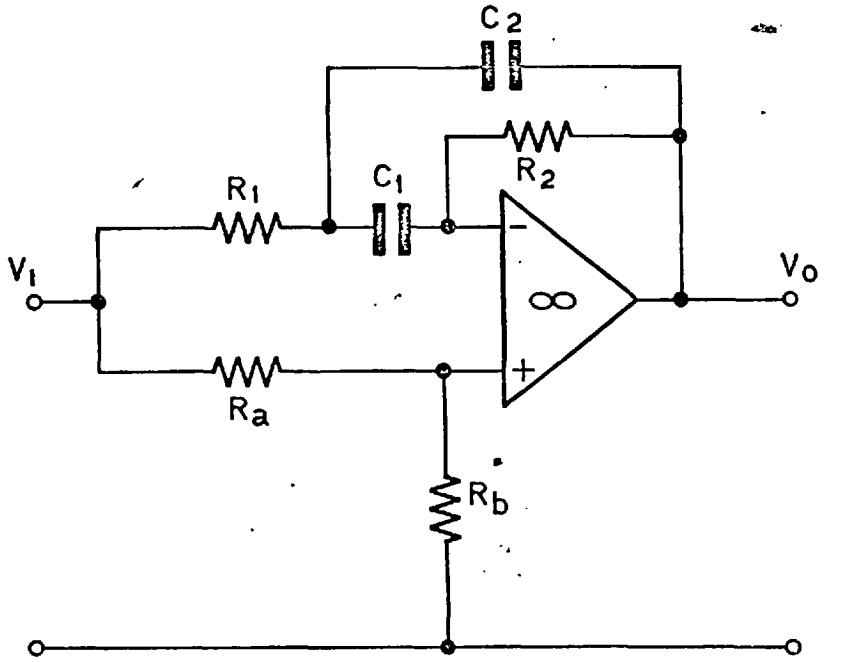


Fig.2.9b Active all-pass network due to Deliyannis

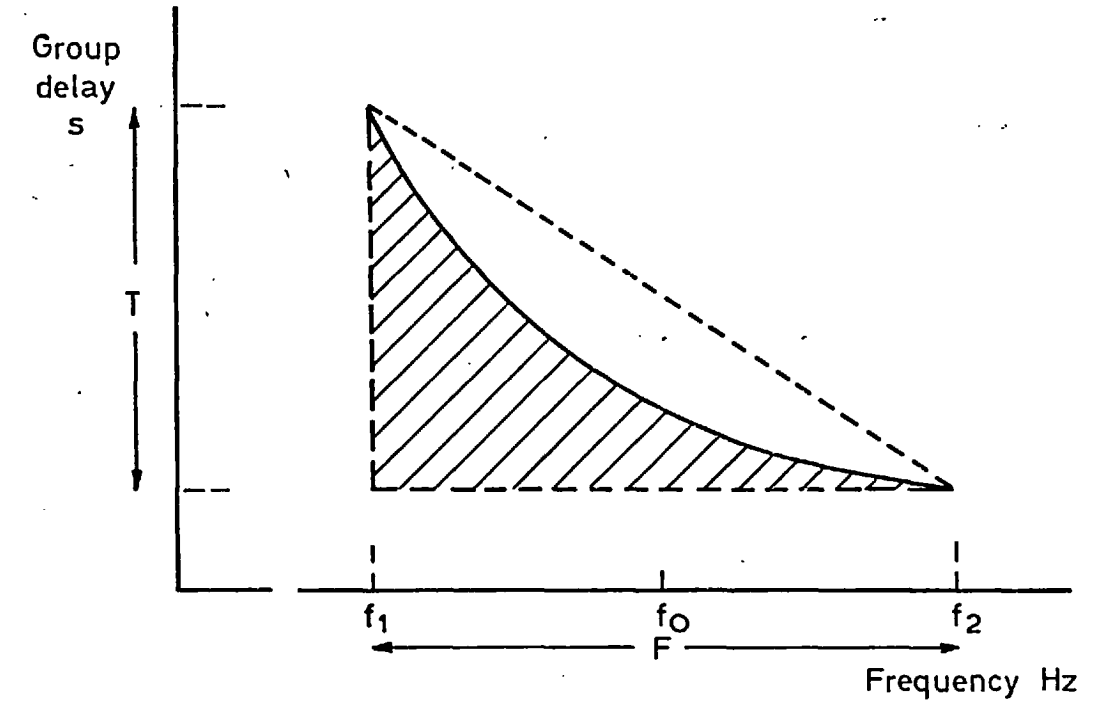


Fig 3.1 Typical non linear delay vs frequency response

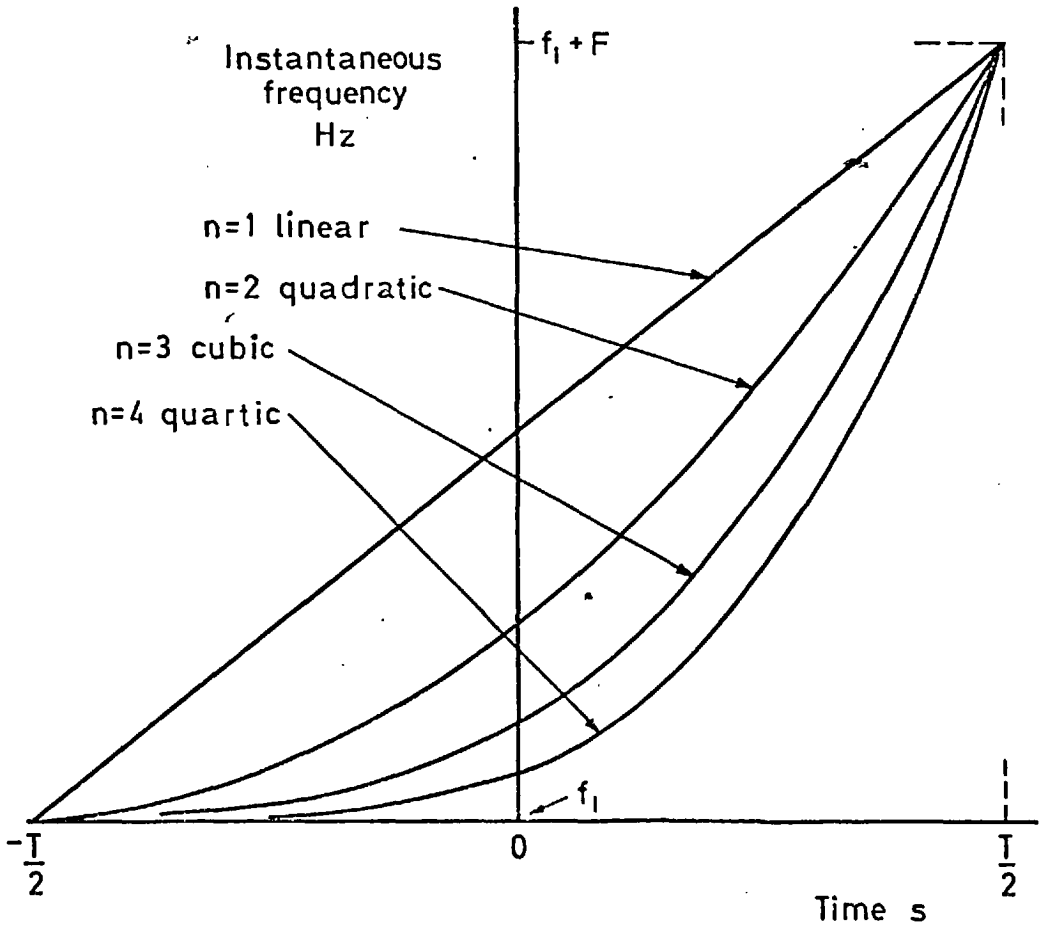


Fig. 3.2 Power law signals-frequency vs time

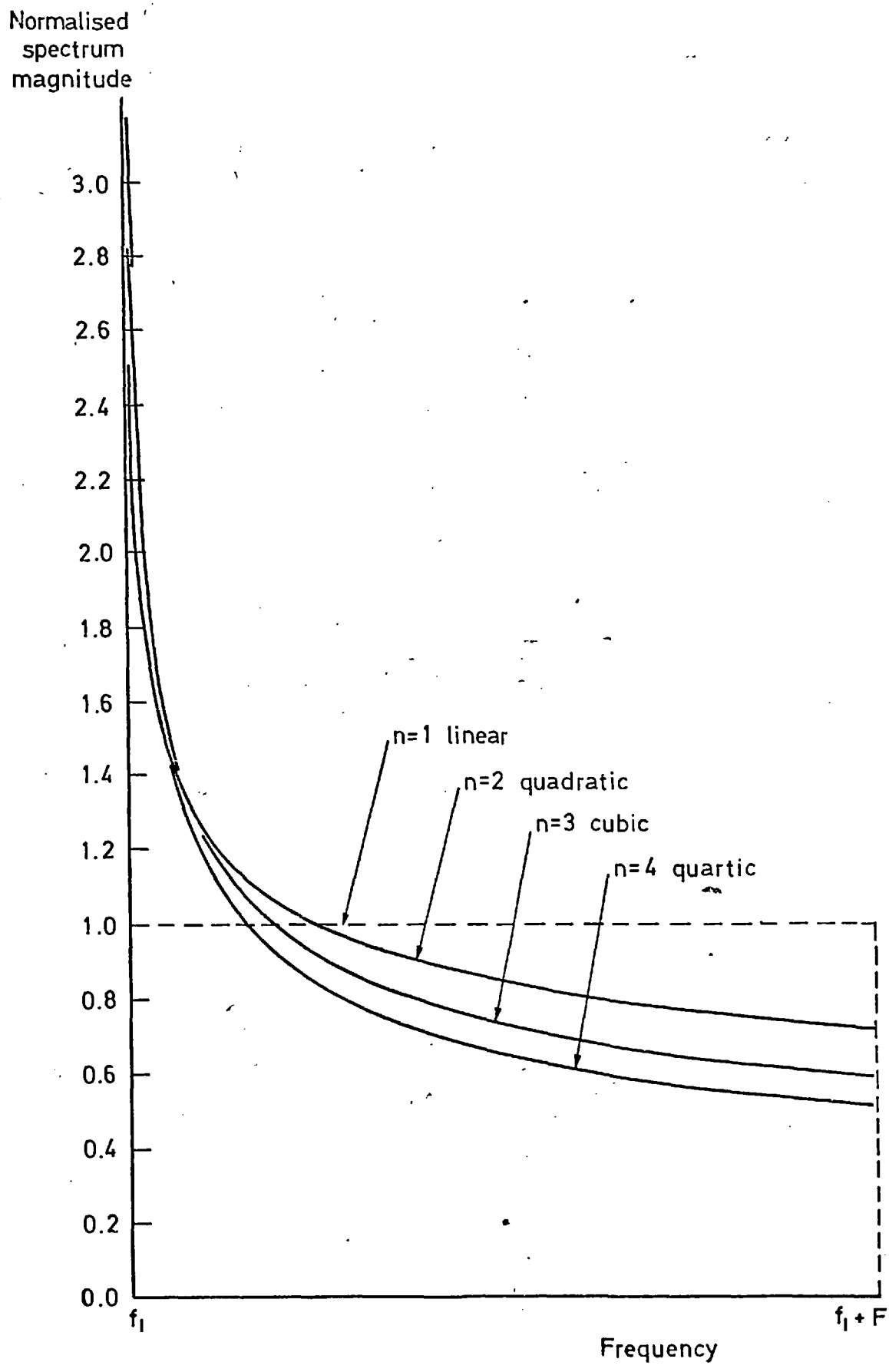


Fig.3.3 Power law signals-stationary phase spectra

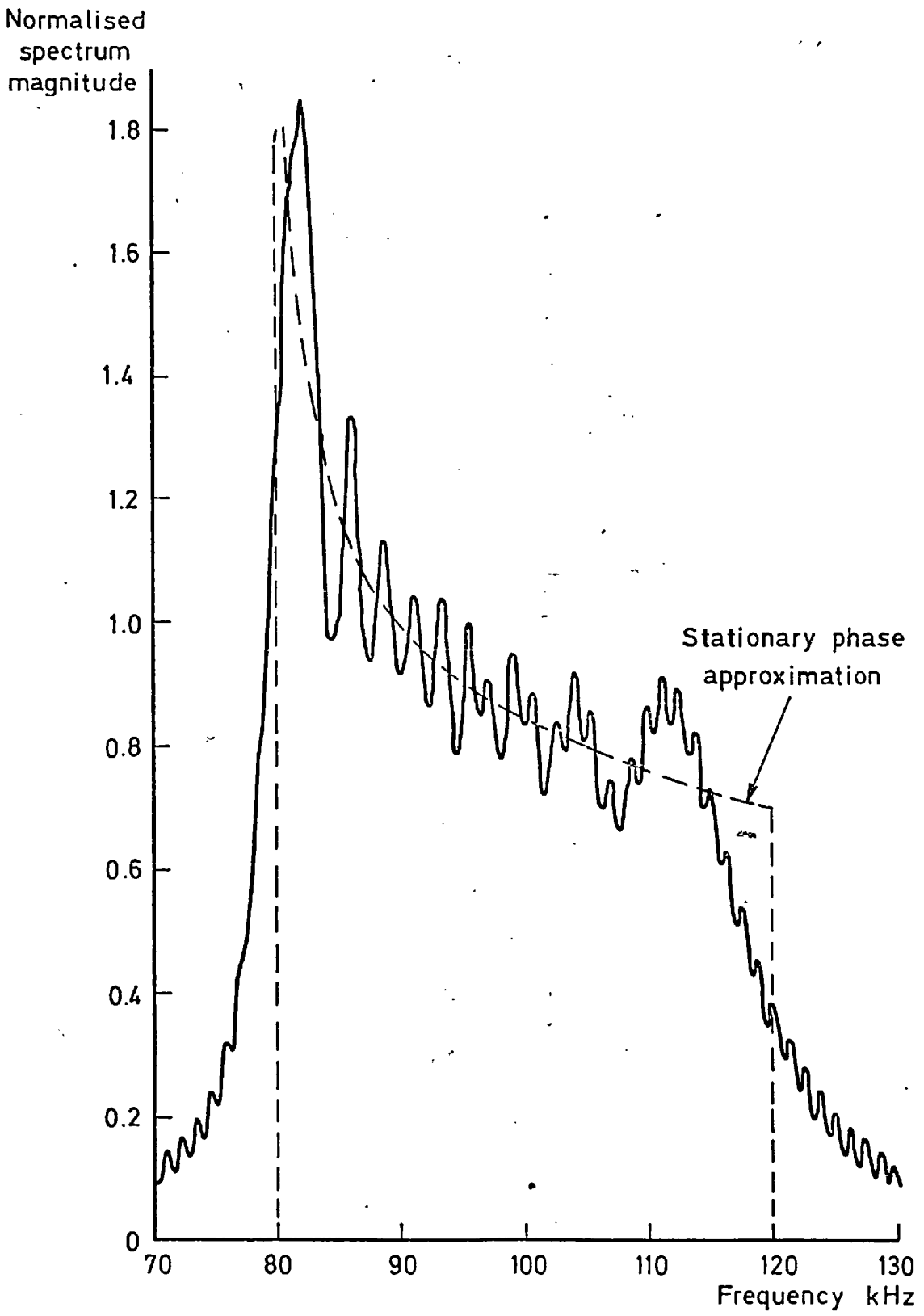


Fig.3.4 Quadratic FM – exact spectrum

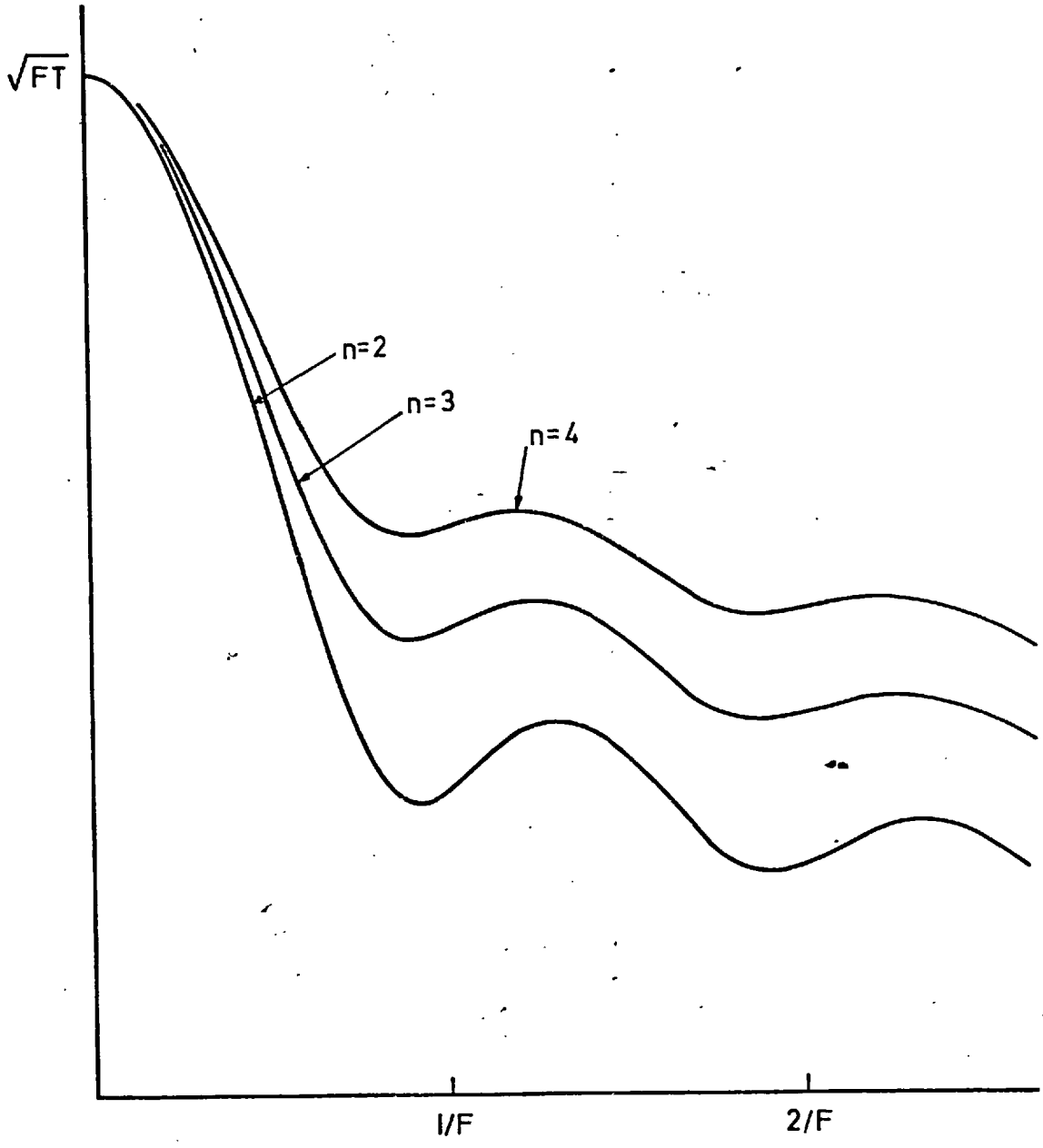


Fig.3.5 Compressed pulse envelope-power law signal matched filter

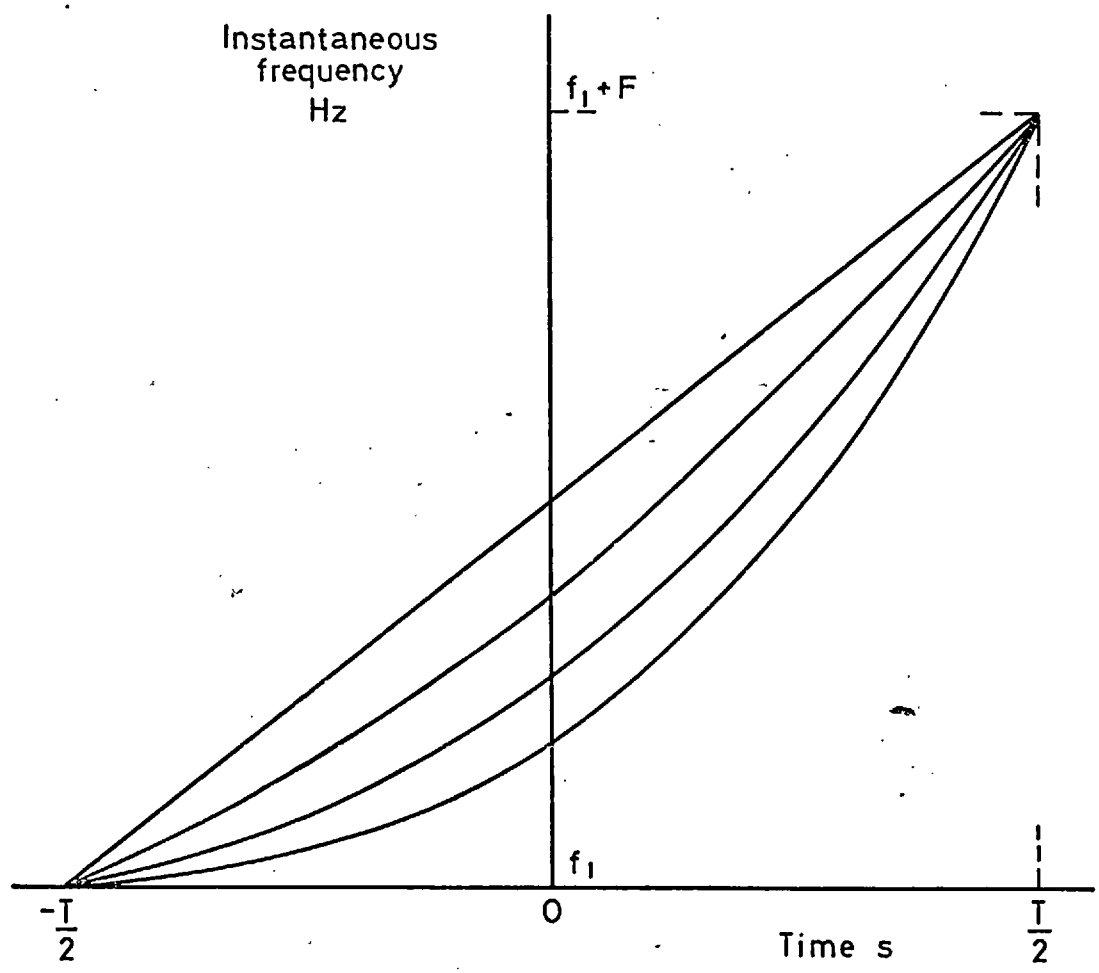


Fig. 3.6 Modified power law signals–frequency vs time

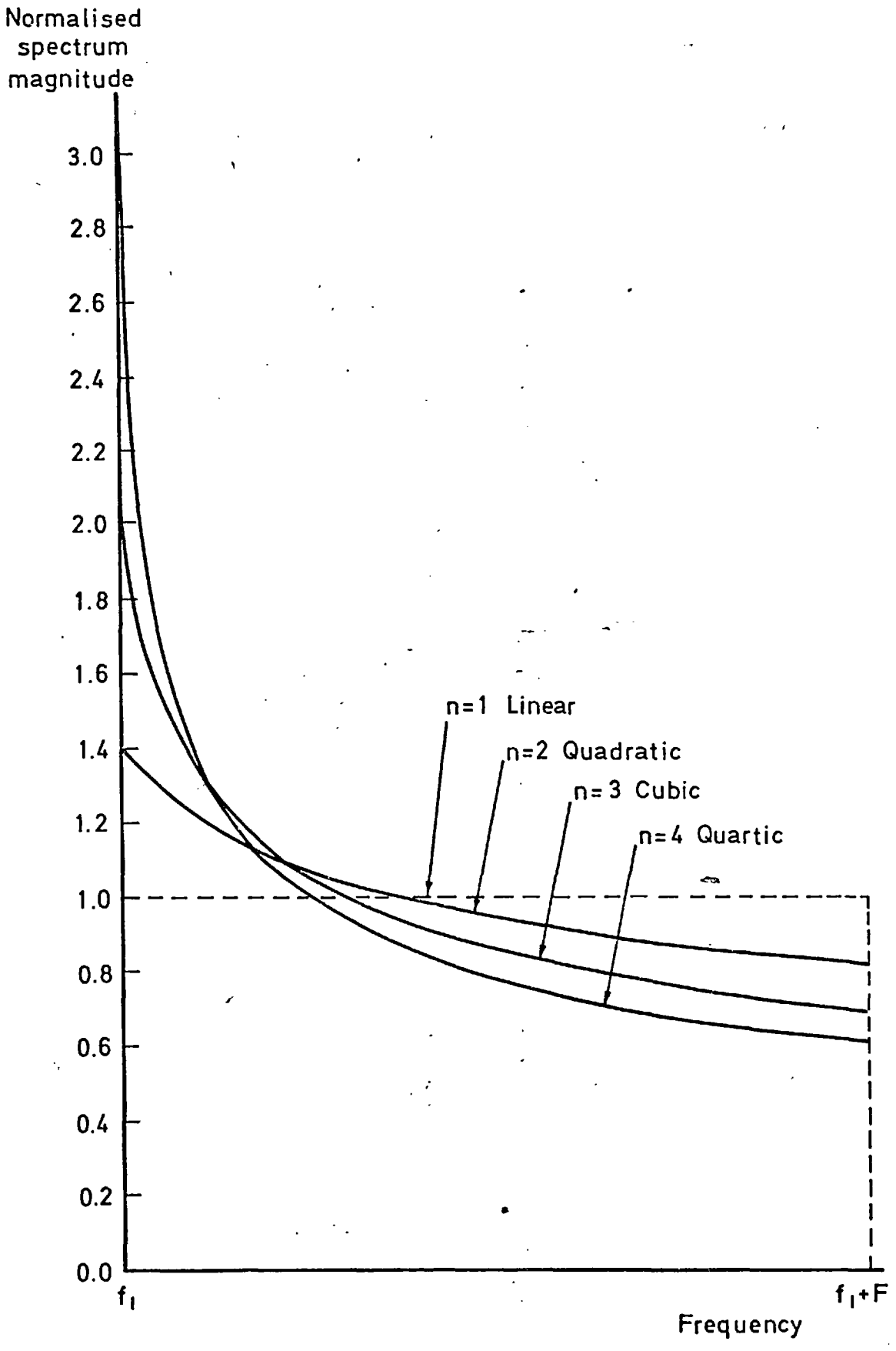


Fig.3.7 Modified power law signals — stationary phase spectra

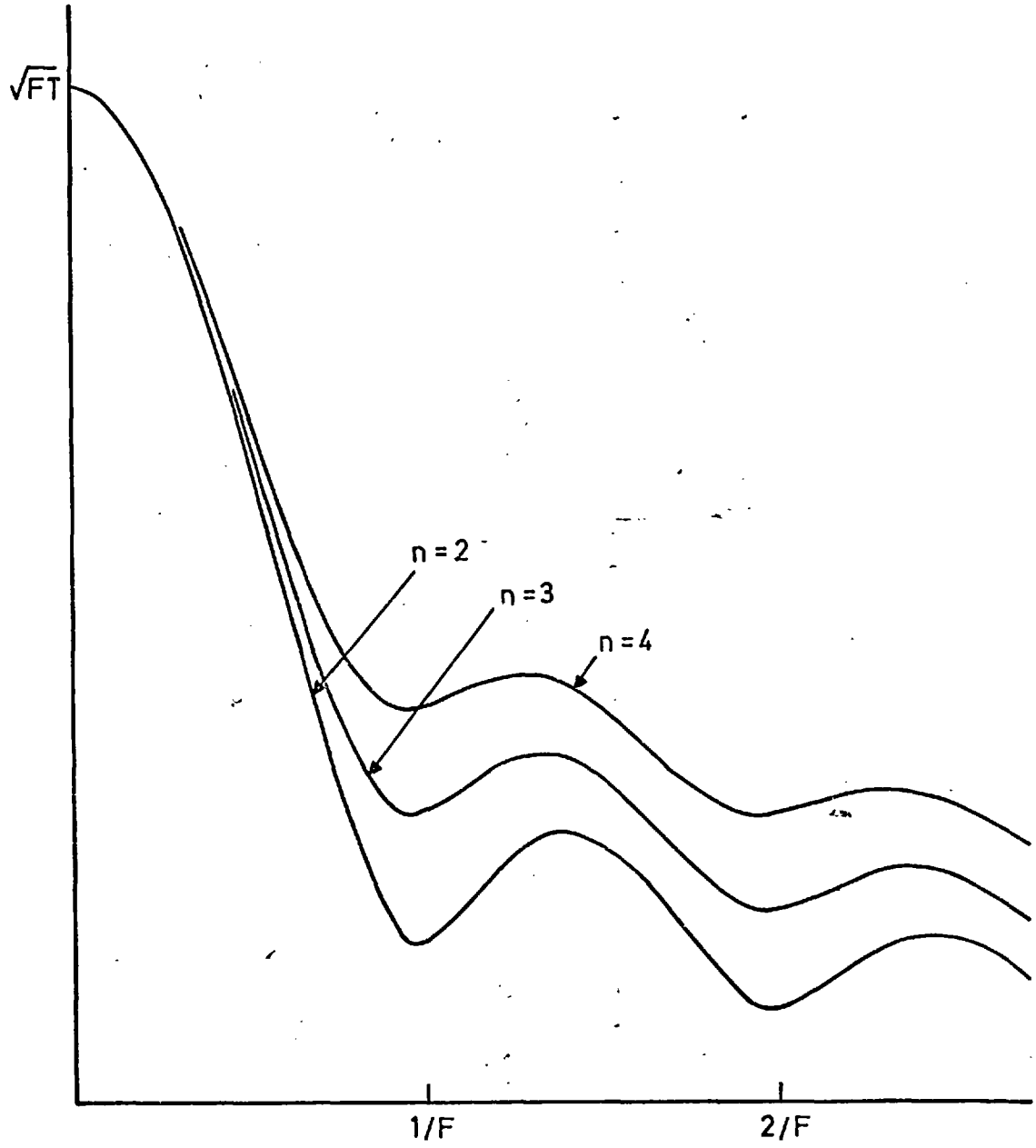


Fig.3.8 Compressed pulse envelope - modified power law signal - matched filter

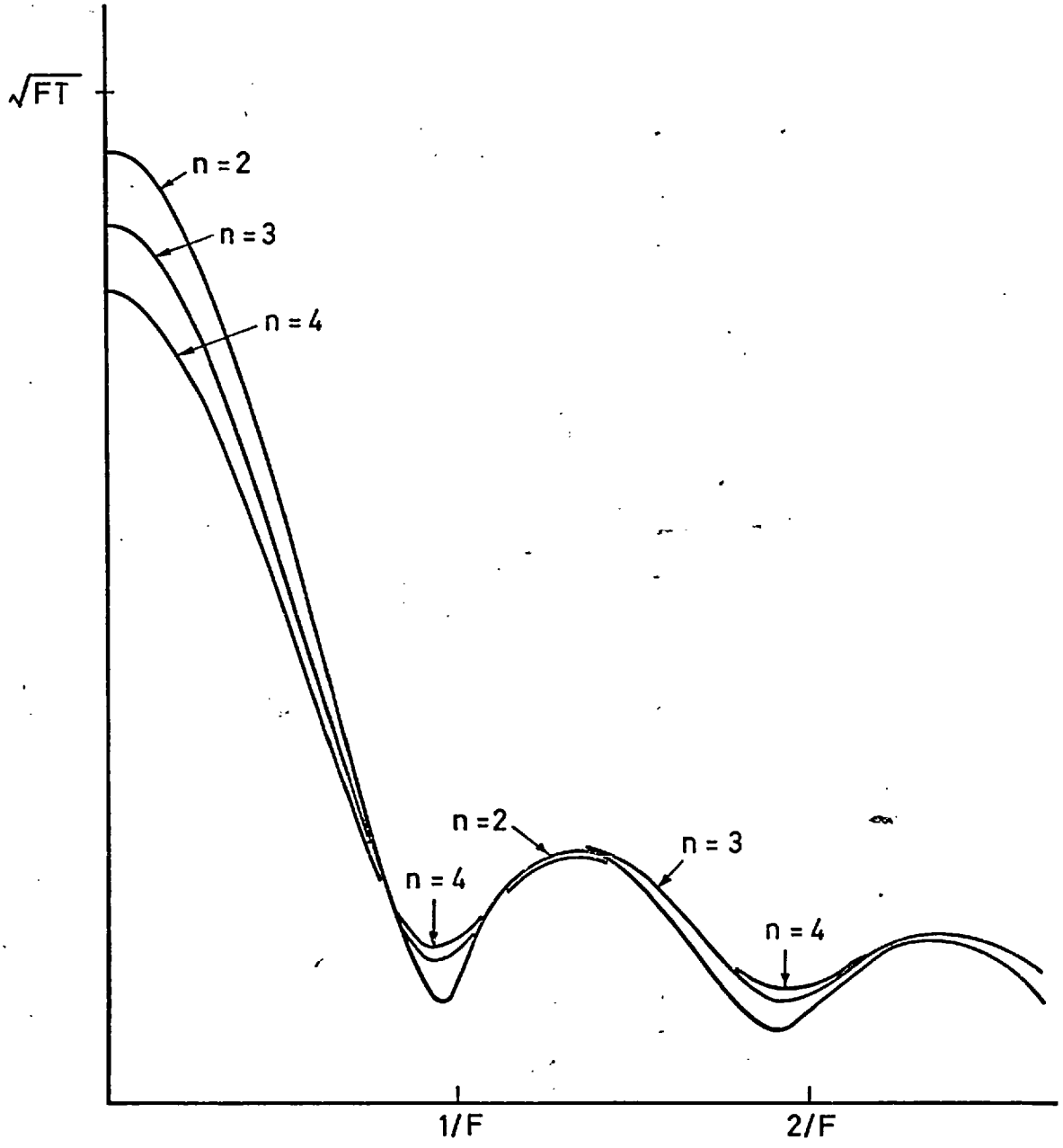


Fig. 3.9 Compressed pulse envelope - power law signal - all pass filter

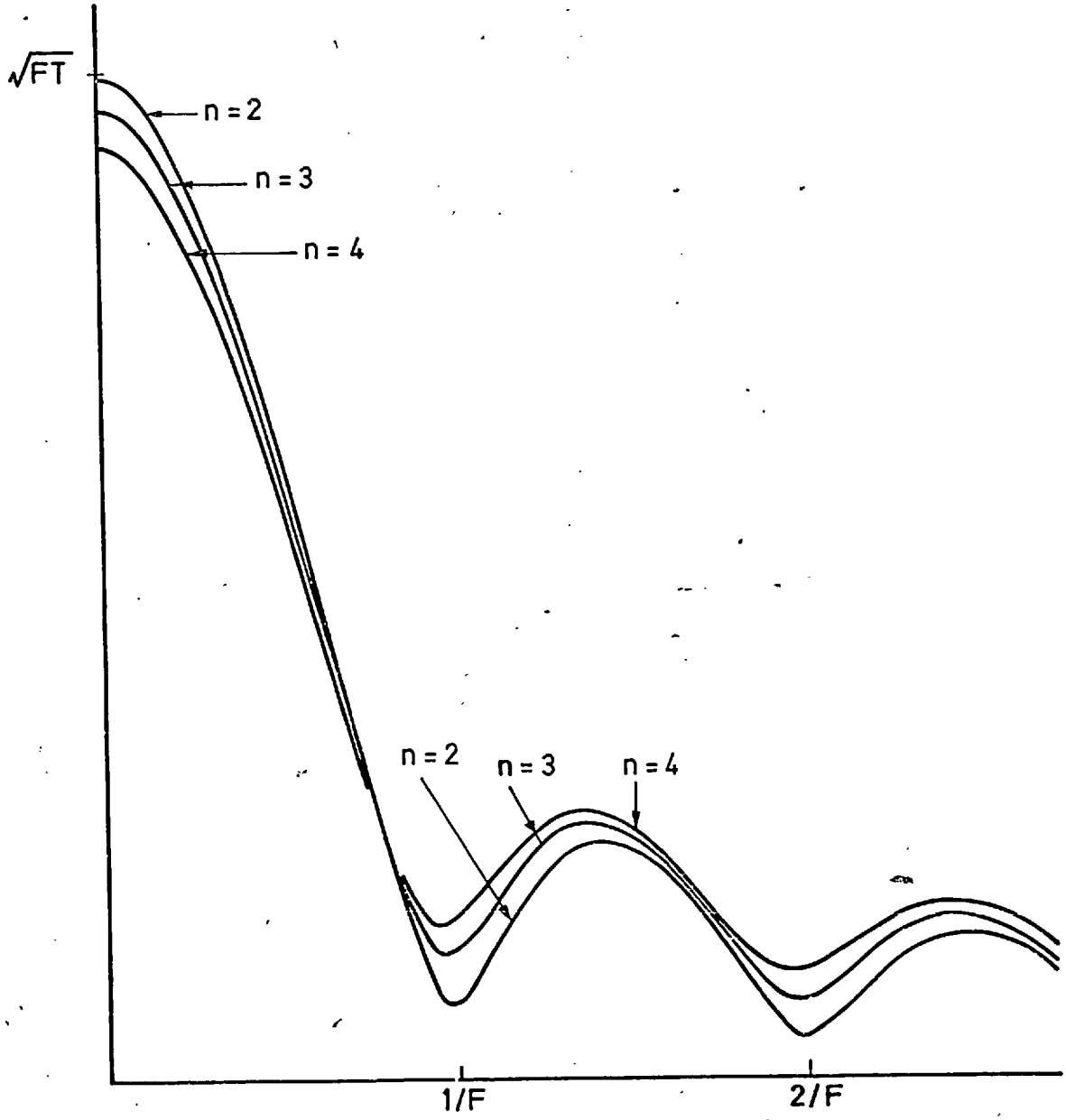


Fig.3.10 Compressed pulse envelope-modified power law signal-all pass filter

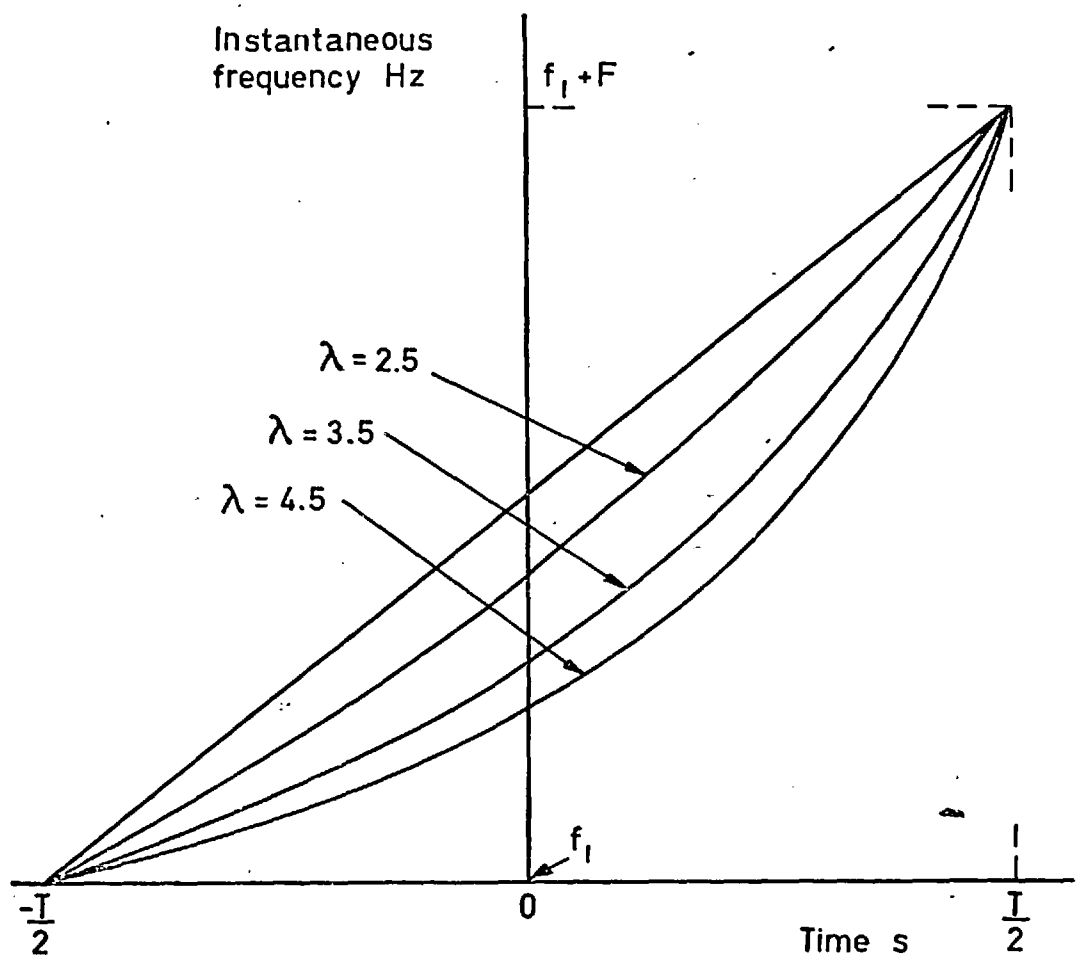


Fig.3.11 Logarithmic phase signals - frequency vs time

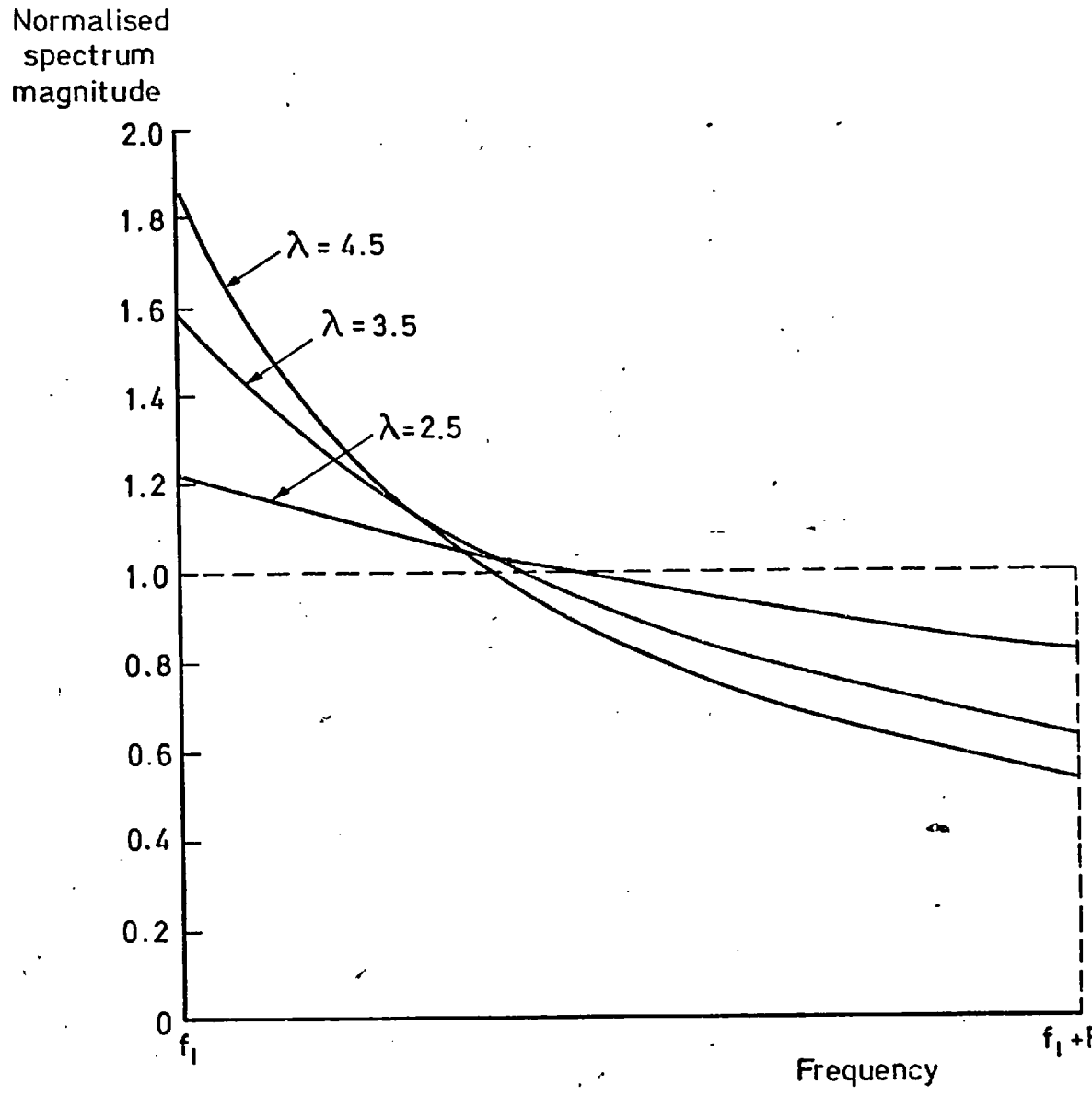


Fig.3.12 Logarithmic phase signals - stationary phase spectra

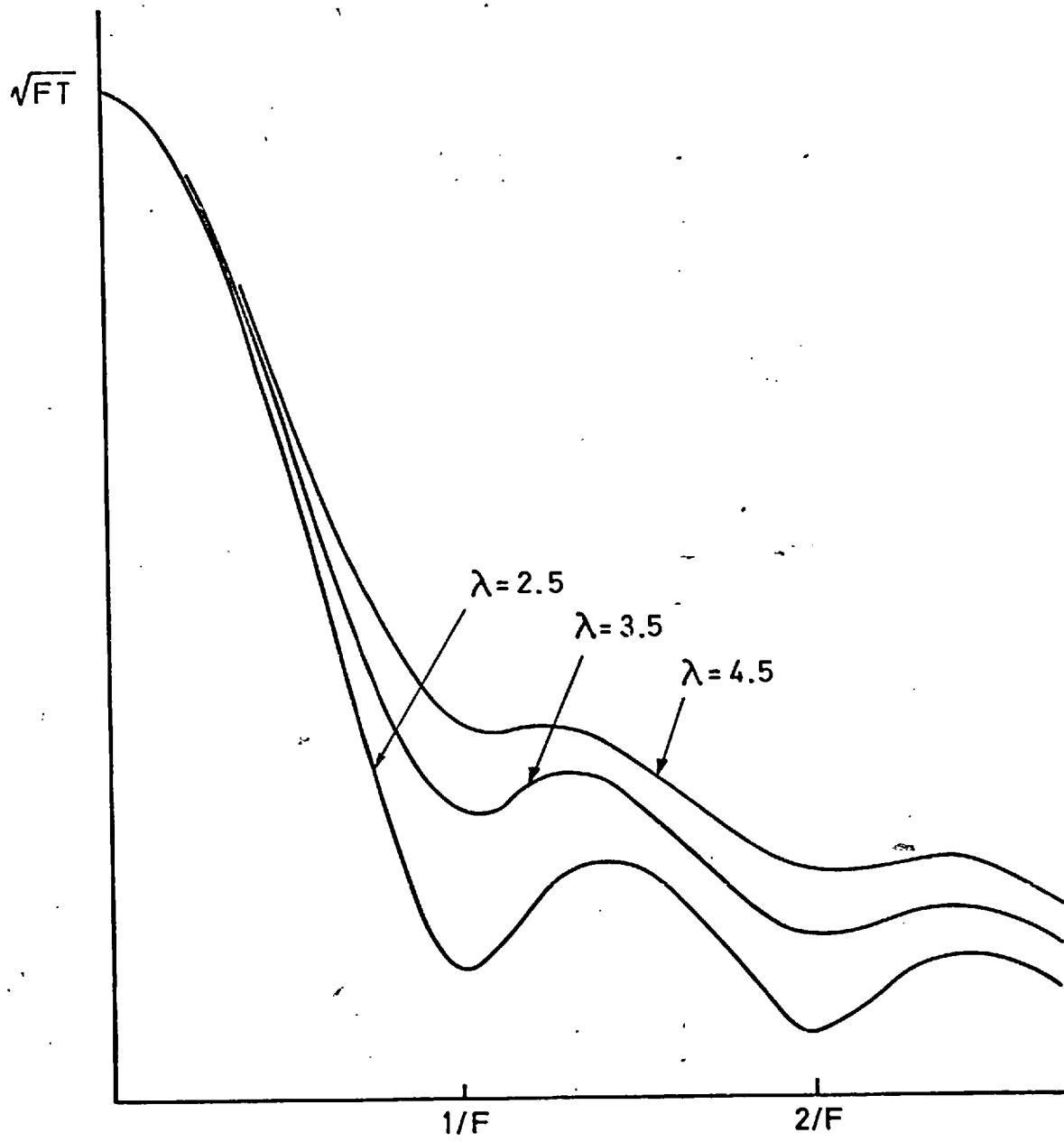


Fig. 3.13 Compressed pulse envelope-logarithmic phase signal-matched filter

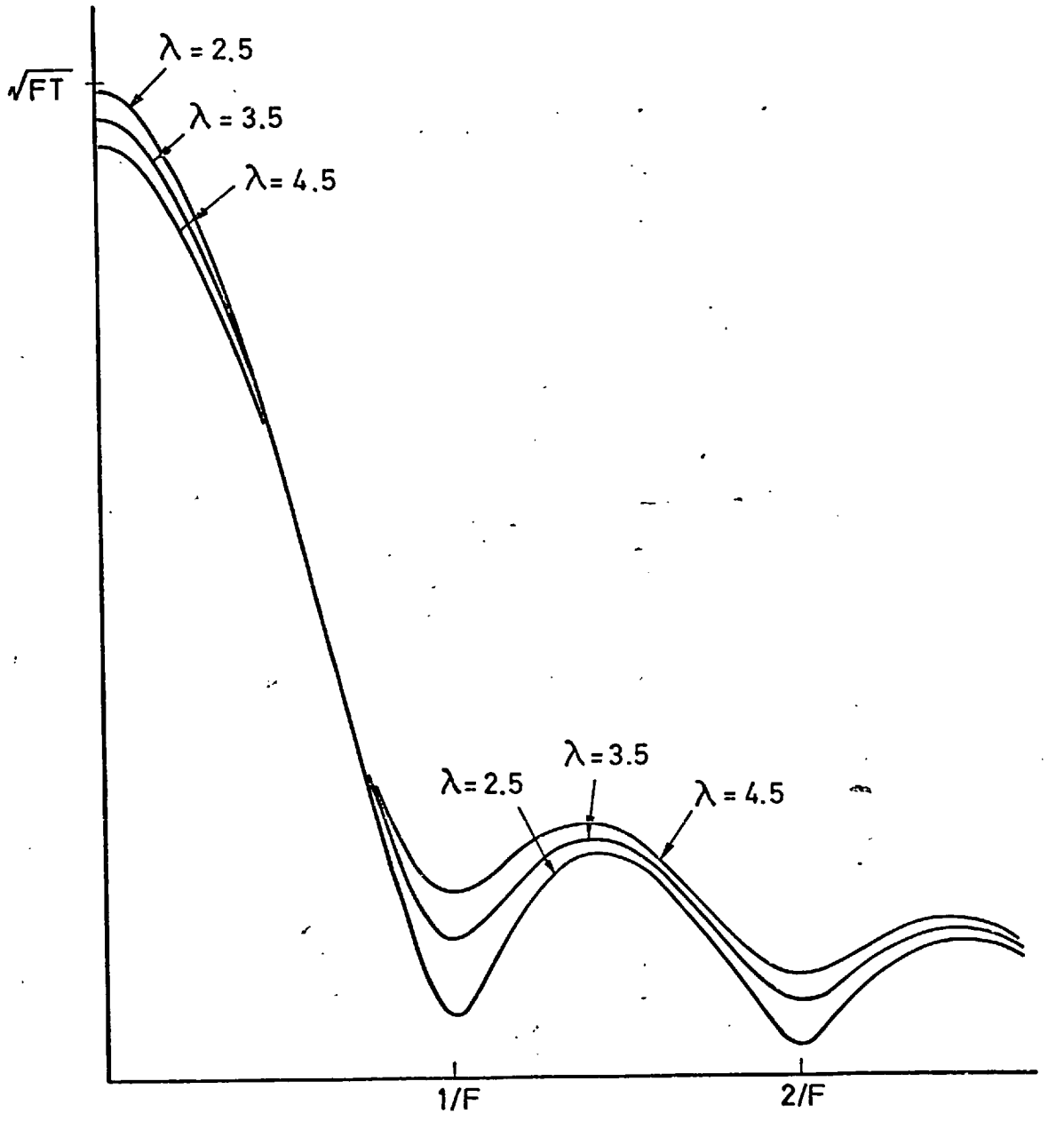


Fig.3.14 Compressed pulse envelope-logarithmic phase signal-all pass filter

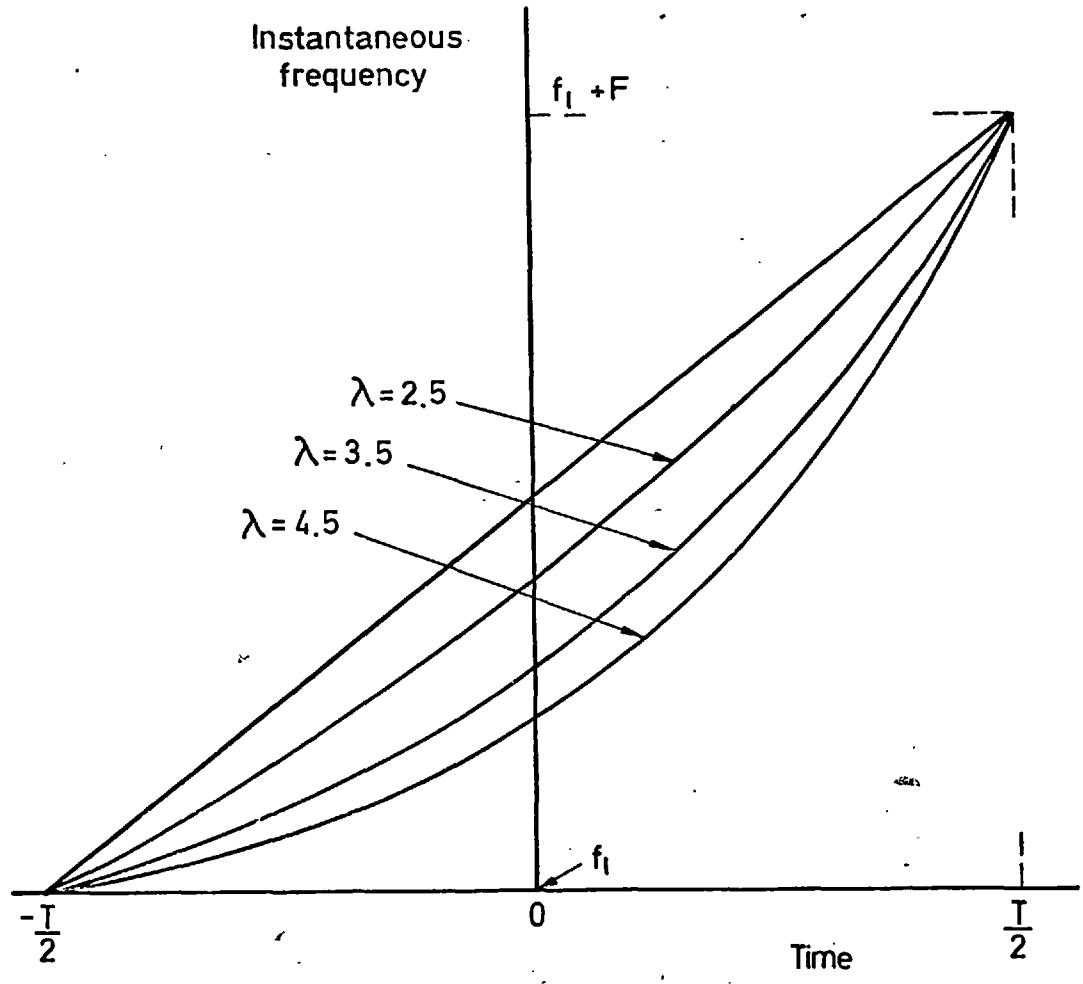


Fig.3.15 Exponential phase signals - frequency vs time

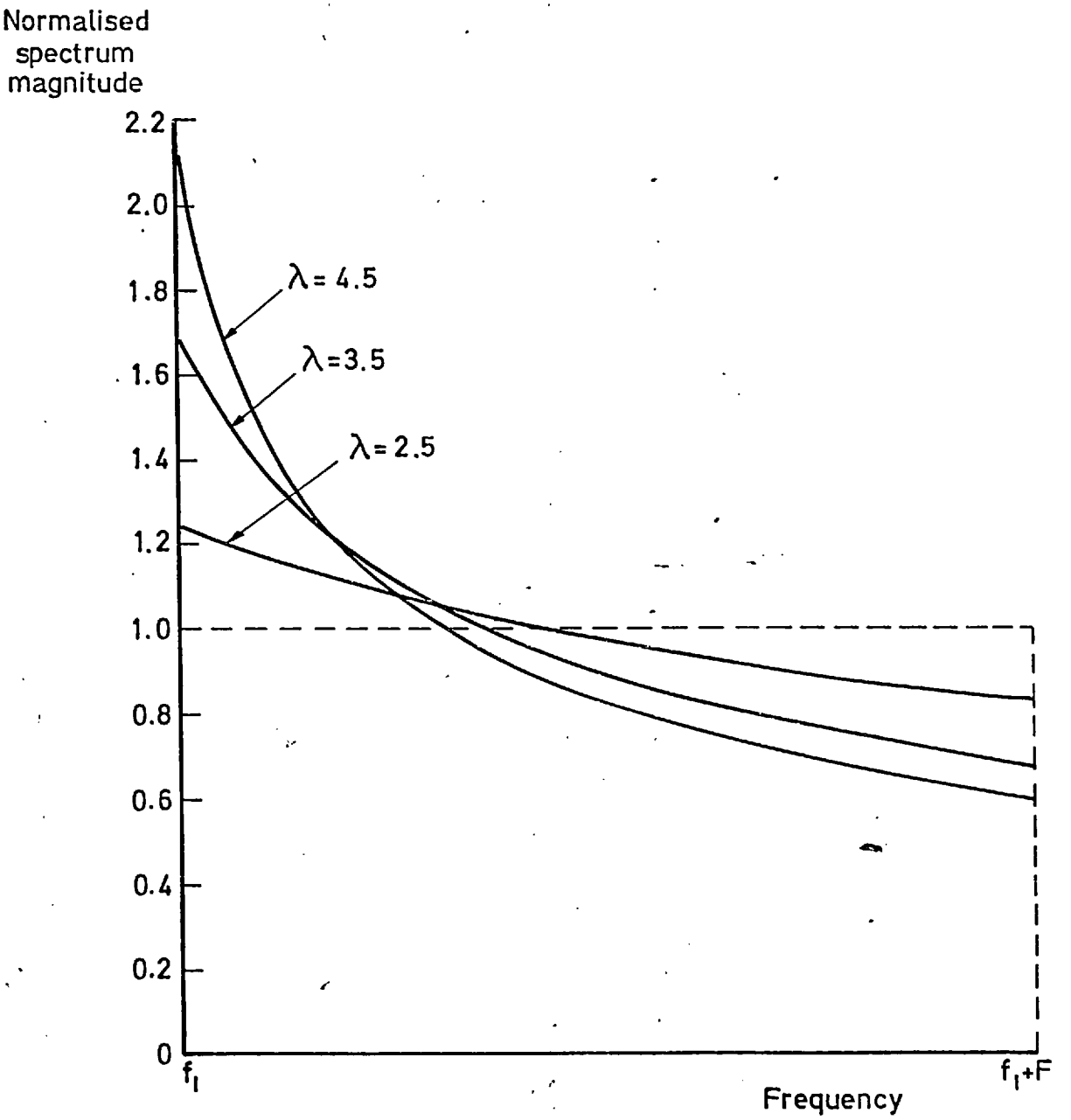


Fig.3.16 Exponential phase signals-stationary phase spectra

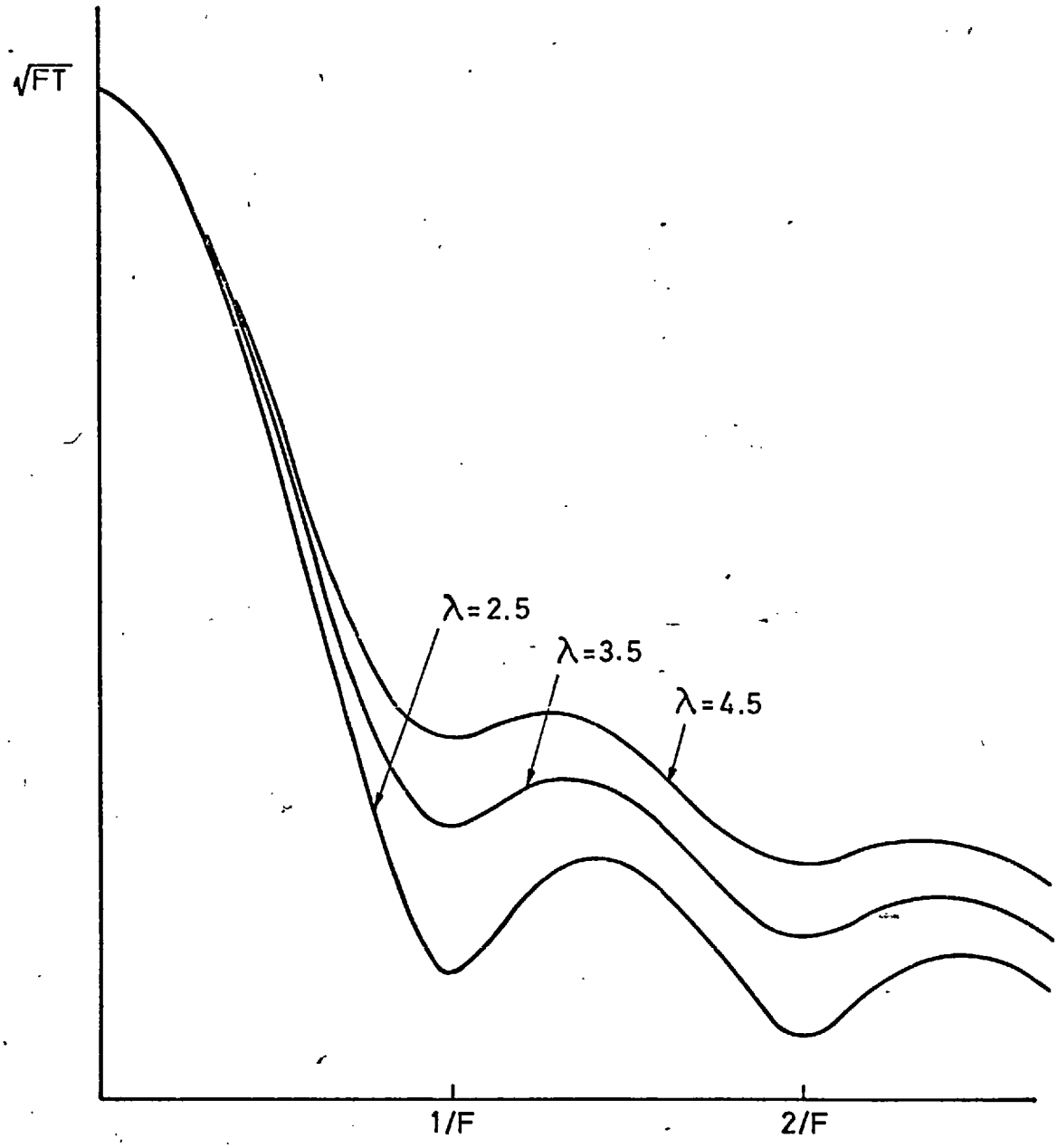


Fig. 3.17 Compressed pulse envelope - exponential phase signal - matched filter

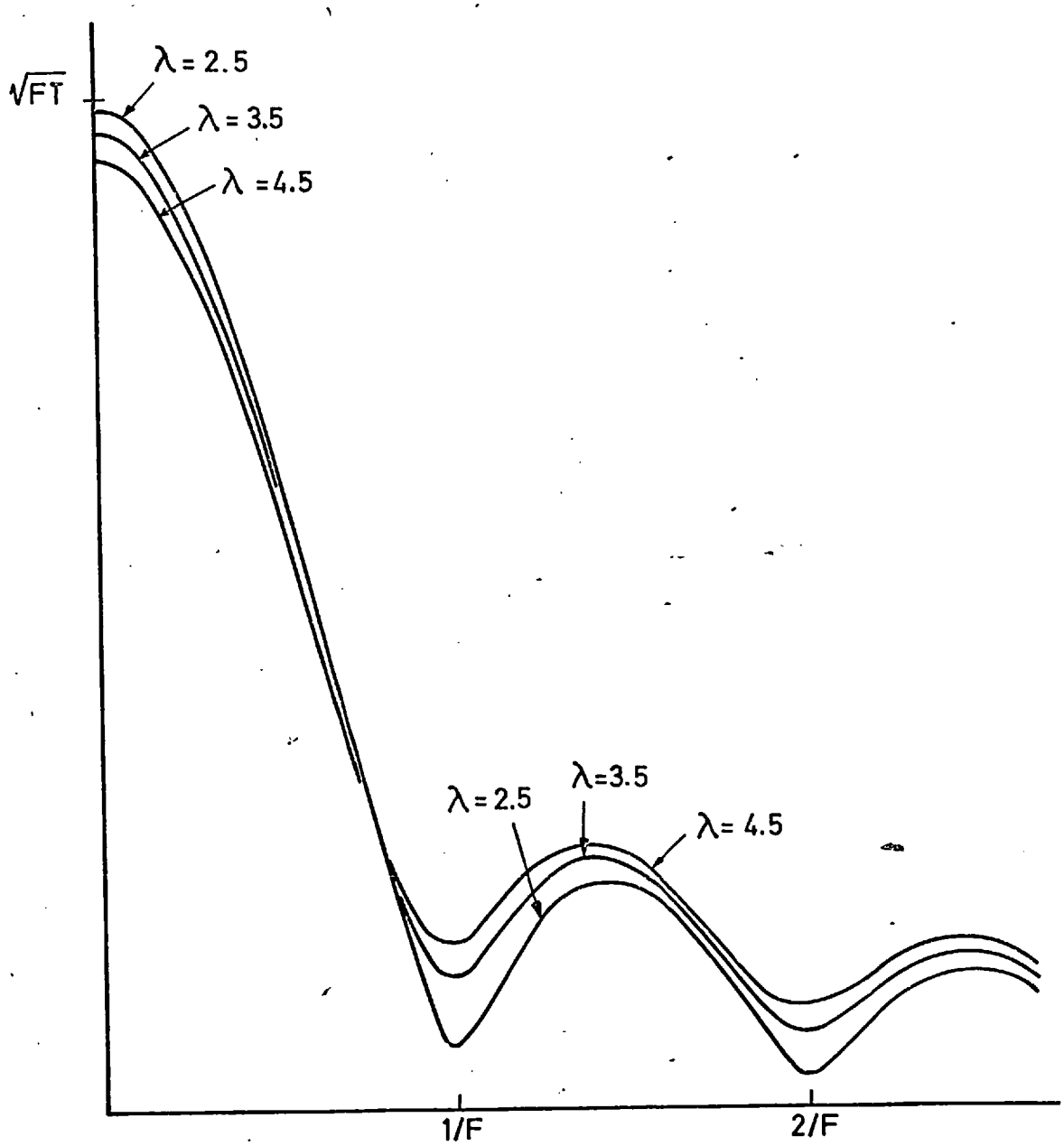


Fig.3.18 Compressed pulse envelope - exponential phase signal - all pass filter

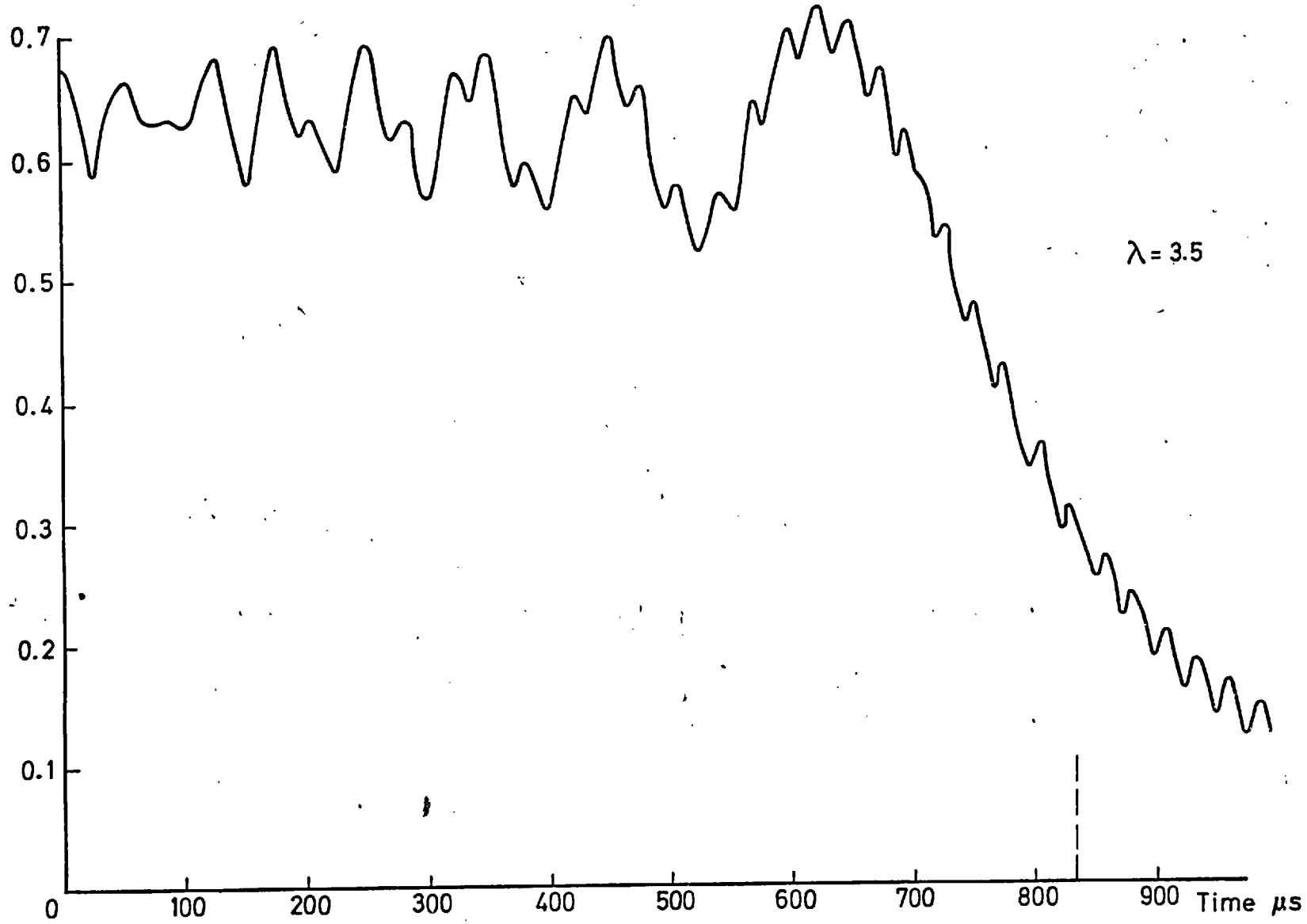


Fig.3.19 Dispersed pulse envelope - logarithmic phase signal-matched filter

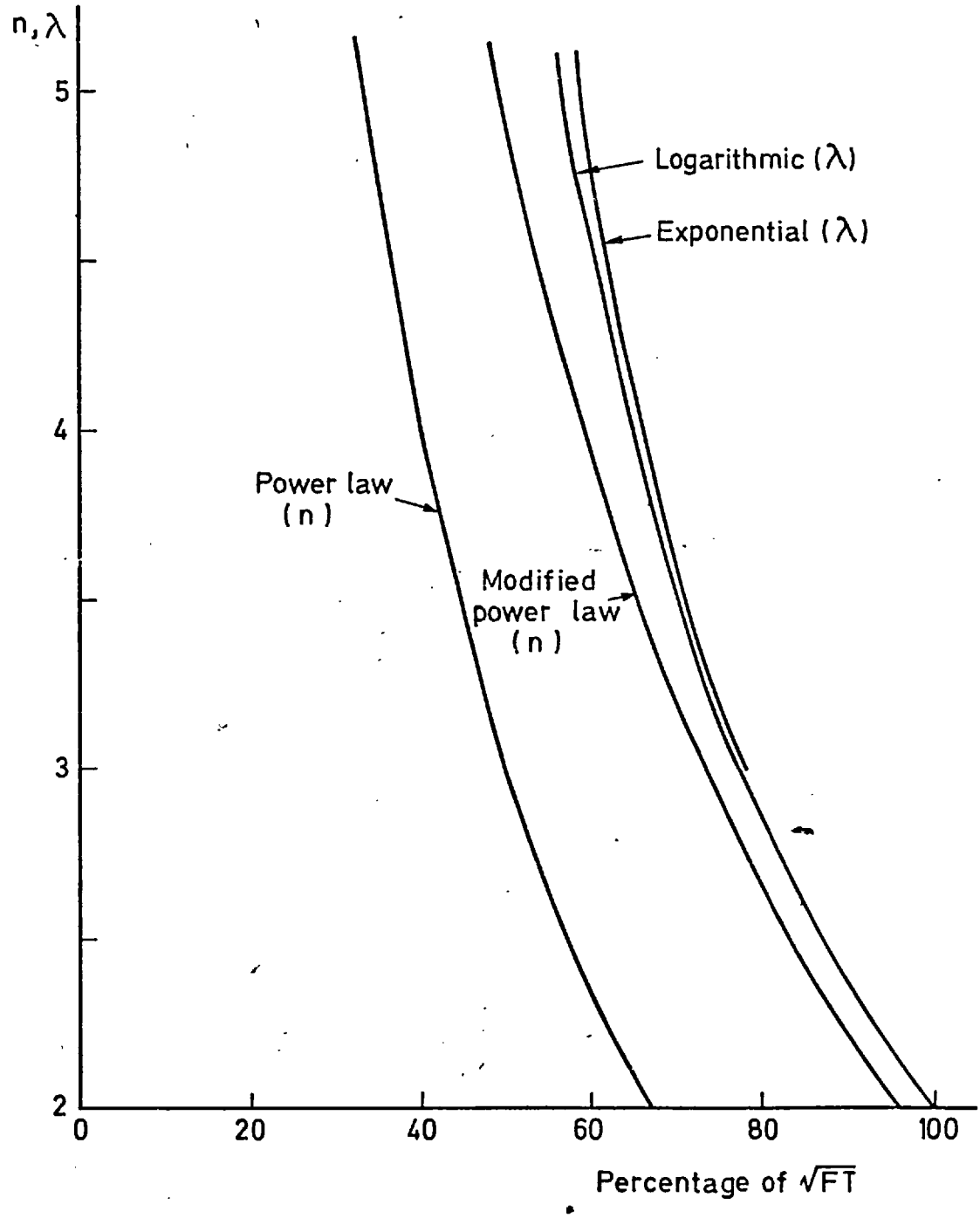


Fig.3.20 Nonlinear FM signals-delay area to be synthesised as a percentage of linear chirp filter area

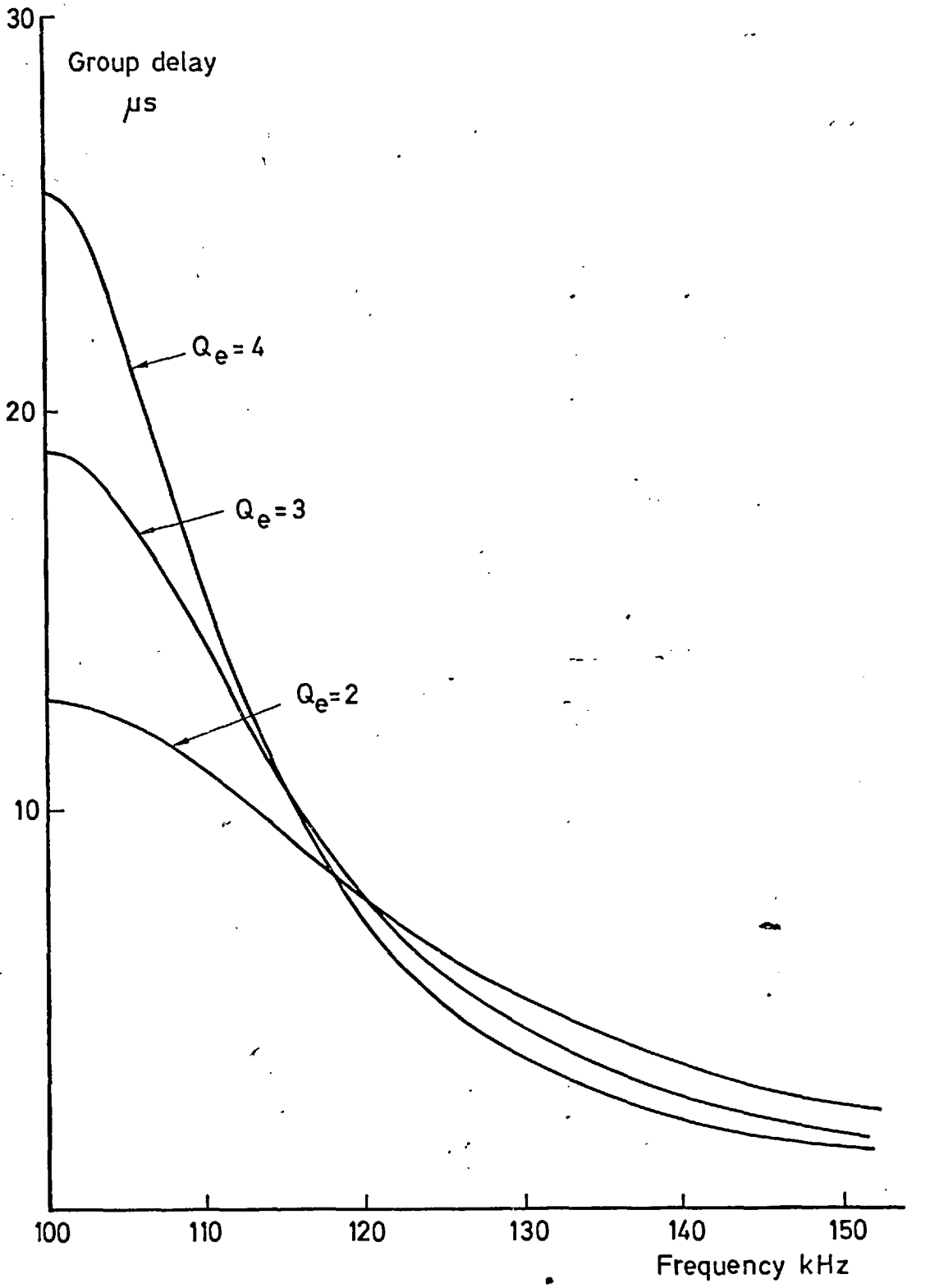


Fig.4.1 Group delay of second order all pass section using approximate expression

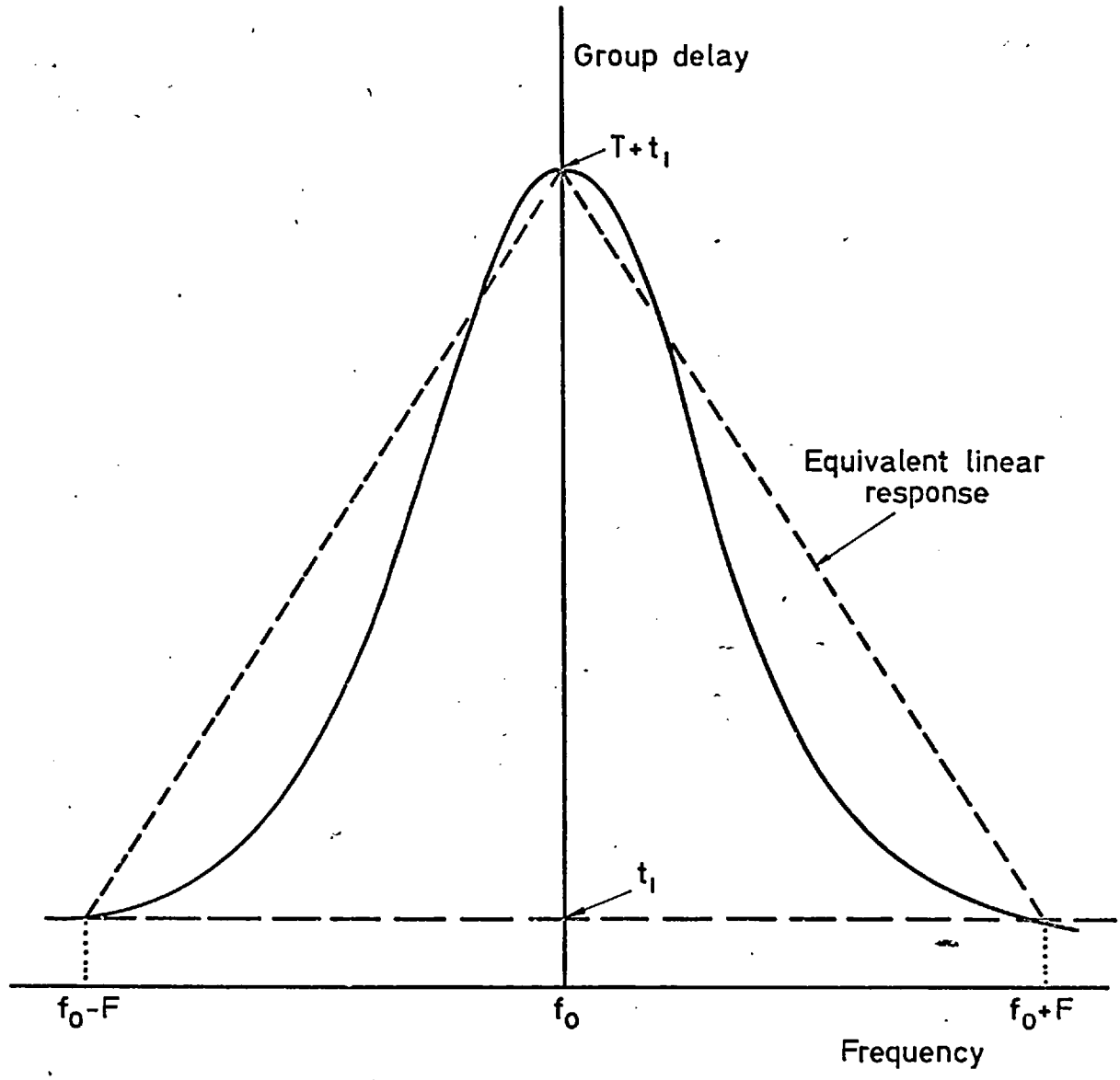


Fig.4.2 Illustration of dispersive delay response using cascaded identical sections.

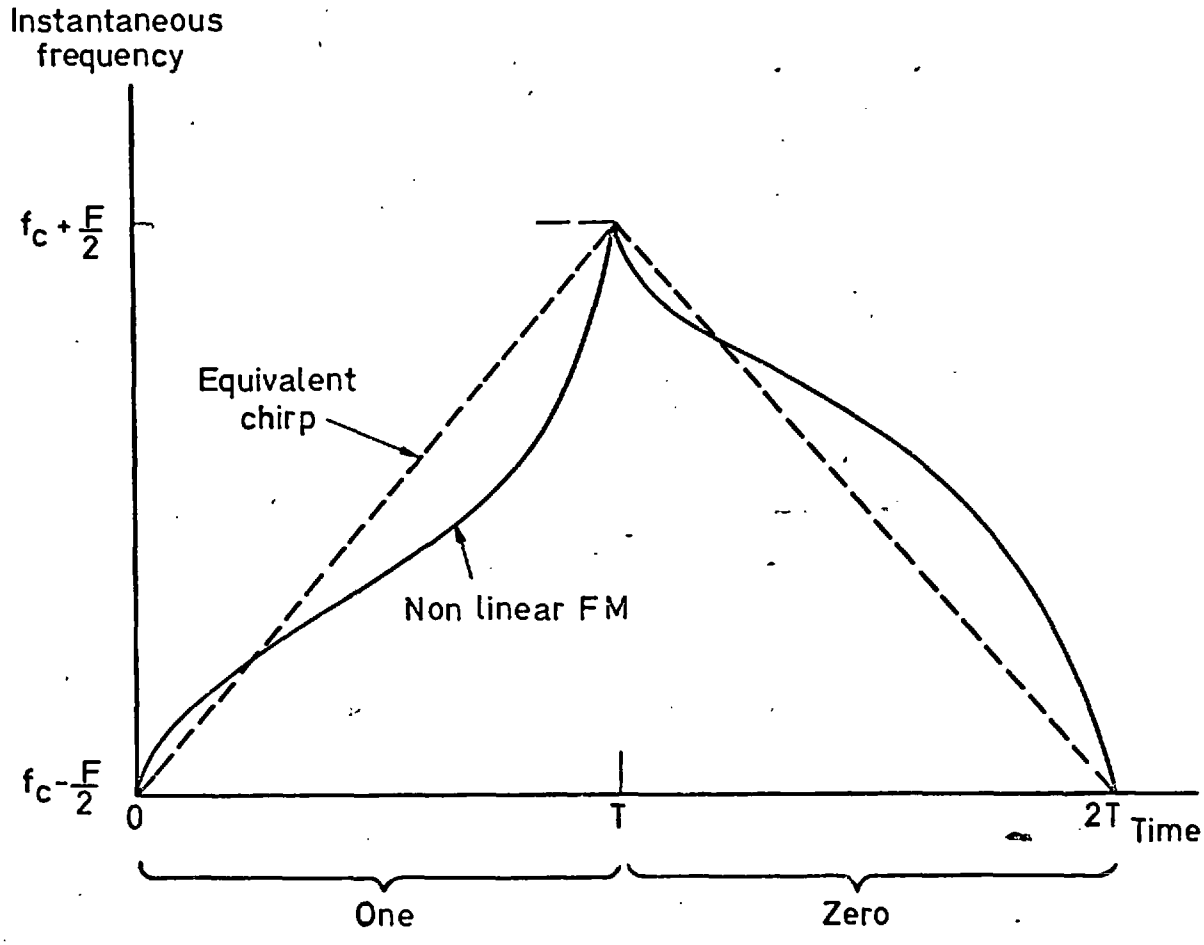


Fig. 4.3 Instantaneous frequency of a {1,0} bit pattern (before demodulator)

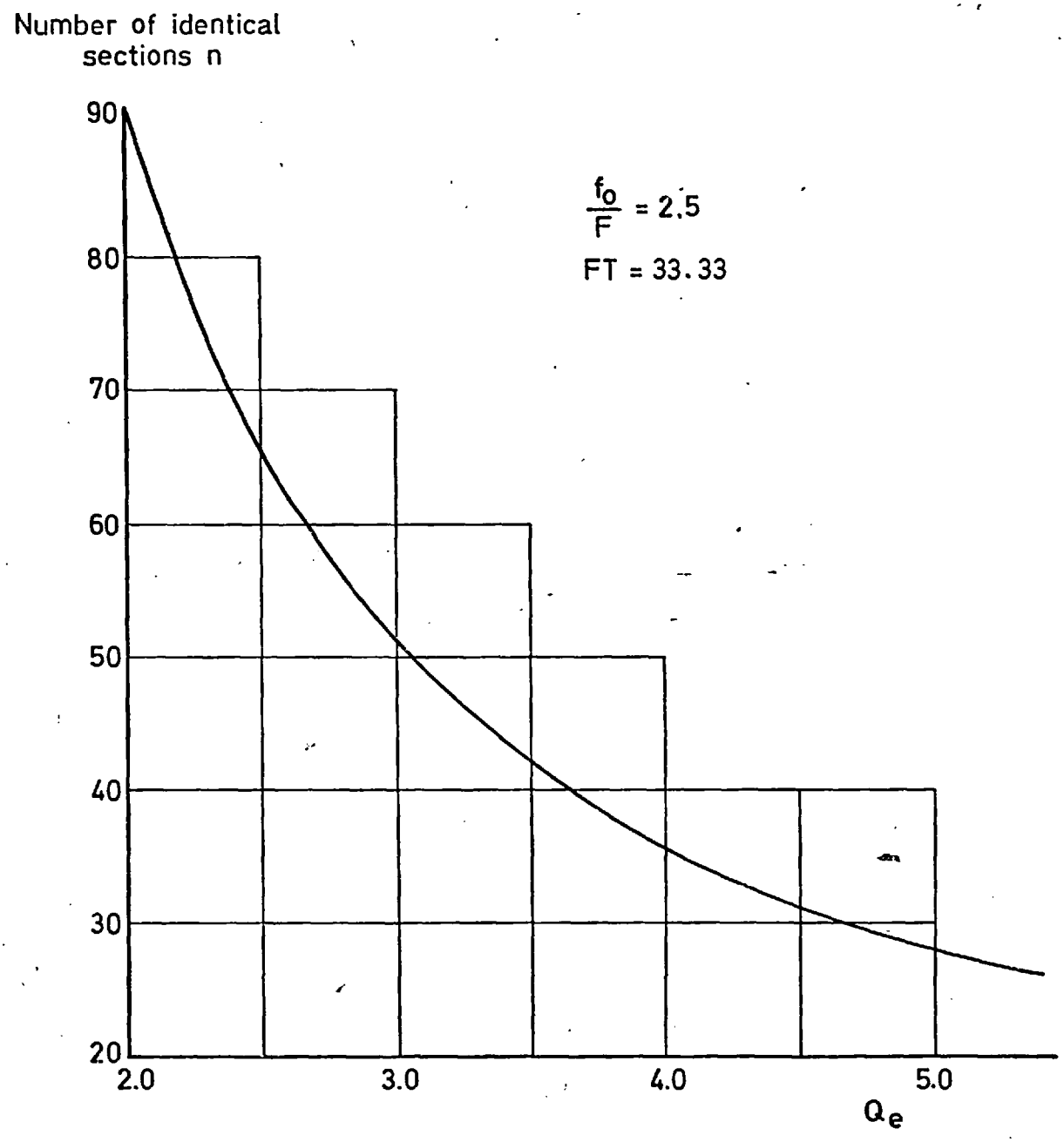


Fig.4.4 Relationship between the number of identical sections and their Q_e factor

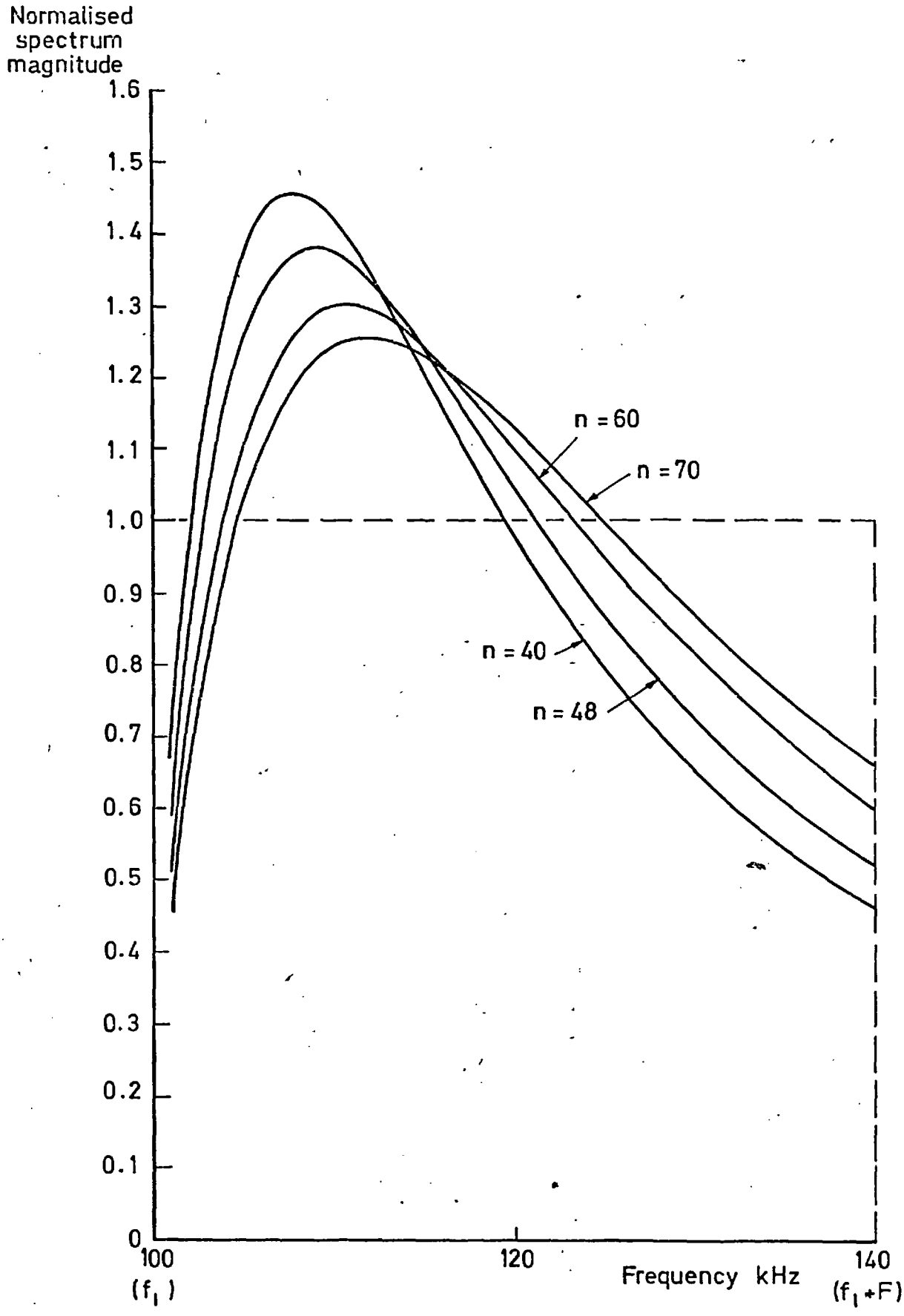


Fig. 4.5 Stationary phase spectra of signals matched to identical section dispersive filter

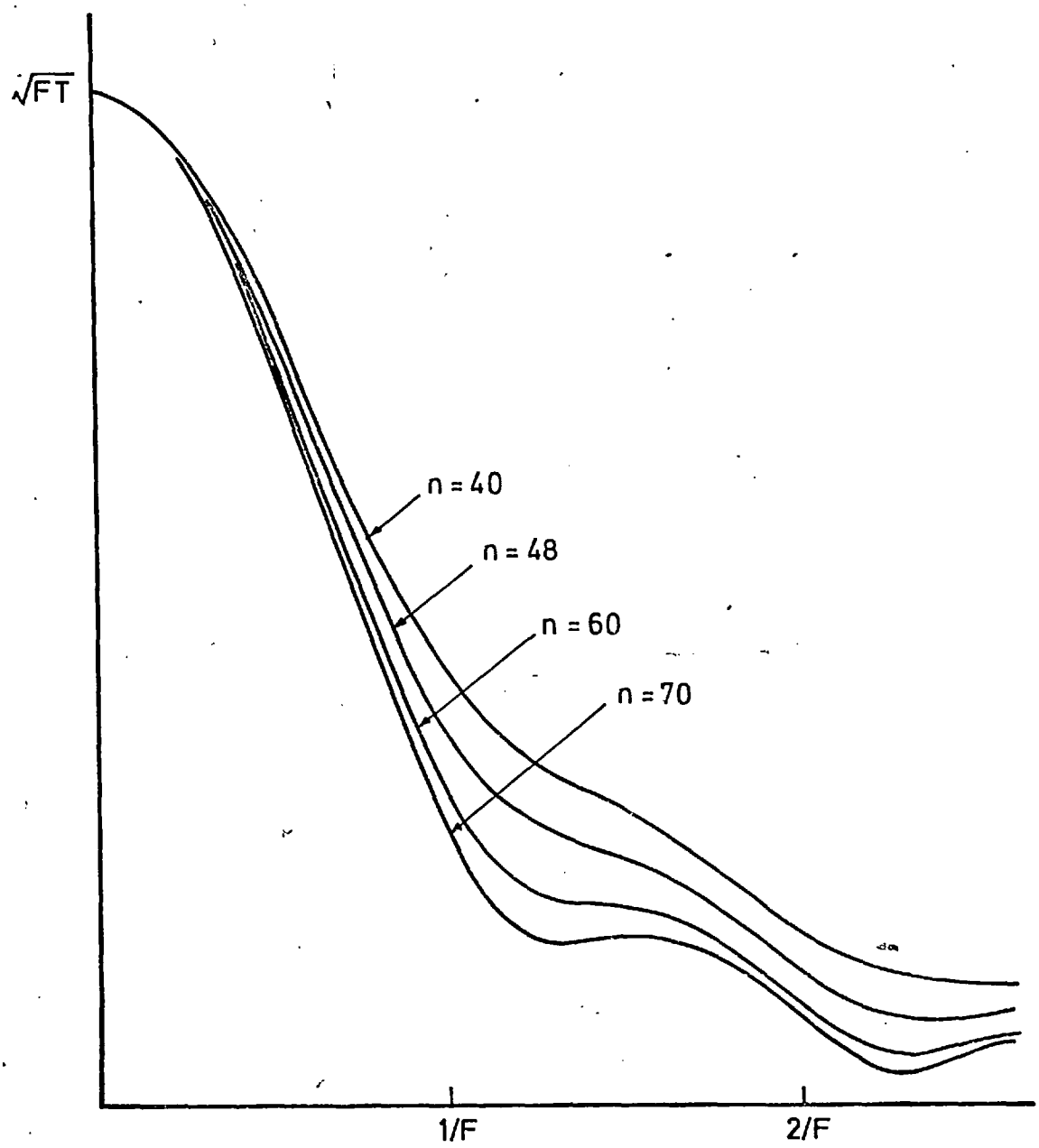


Fig.4.6 Compressed pulse envelope - identical section dispersive system - matched filter

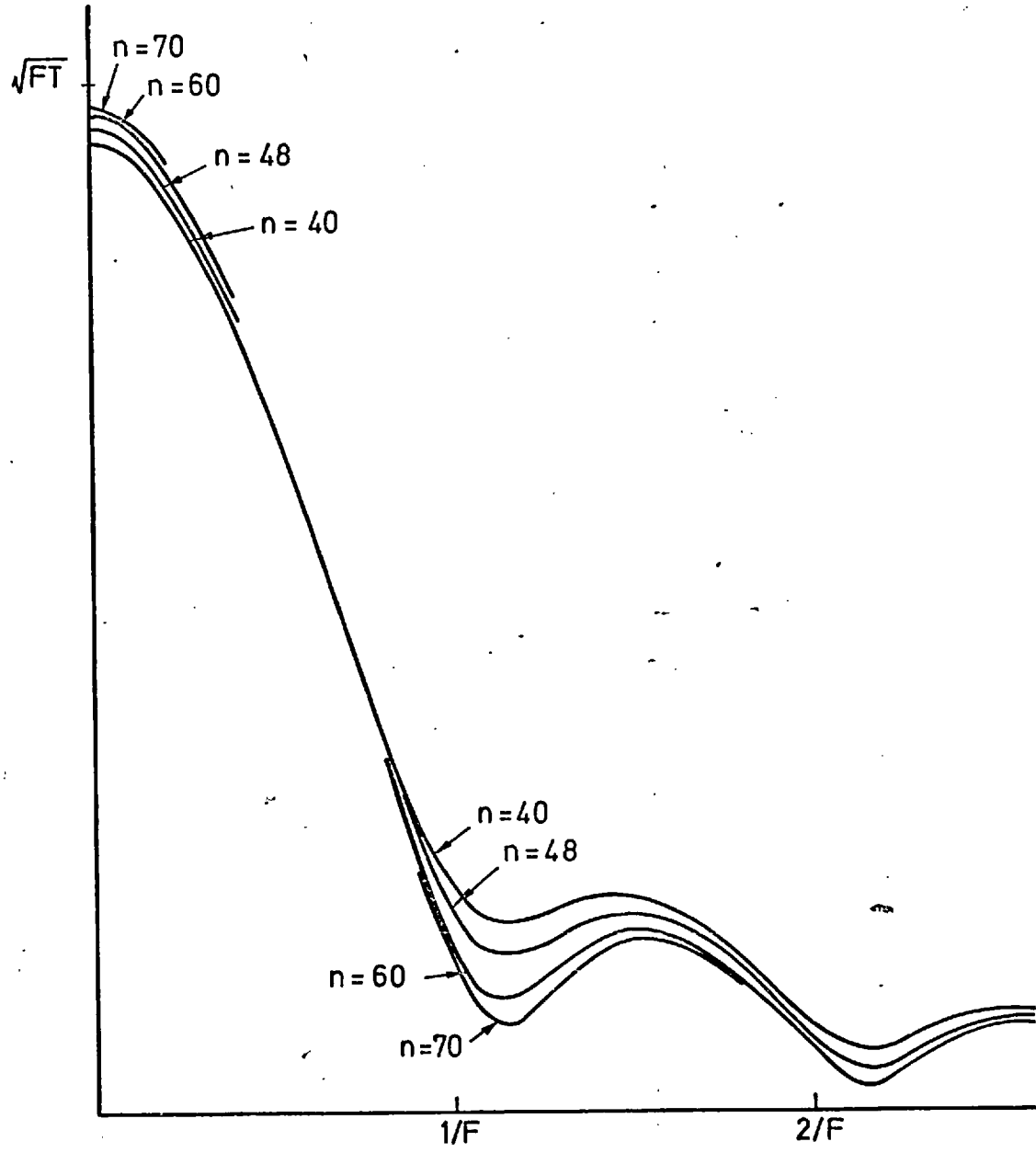


Fig.4.7 Compressed pulse envelope - identical section dispersive system - all pass filter

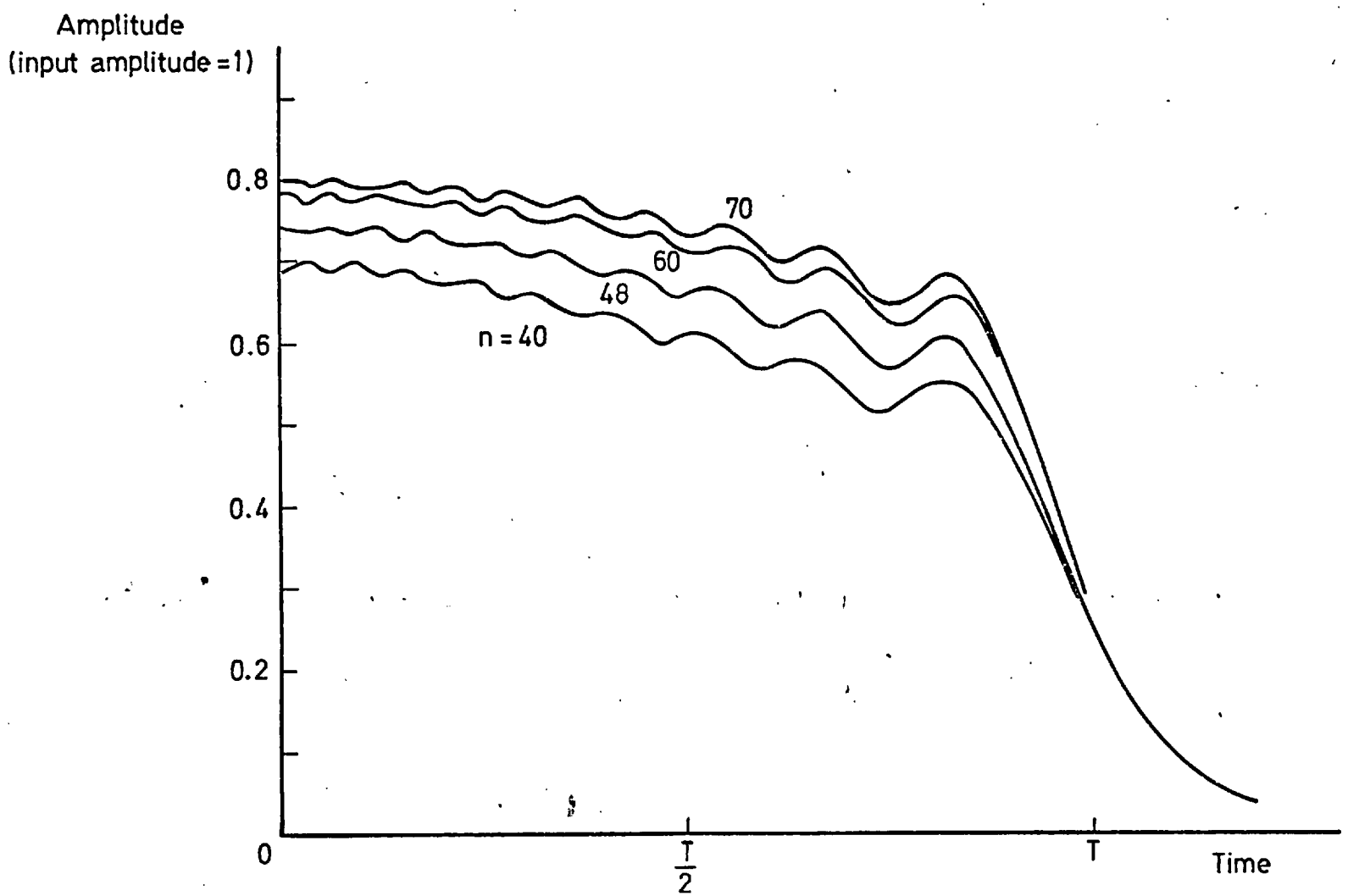


Fig.4.8 Dispersed pulse - identical section dispersive system - matched filter

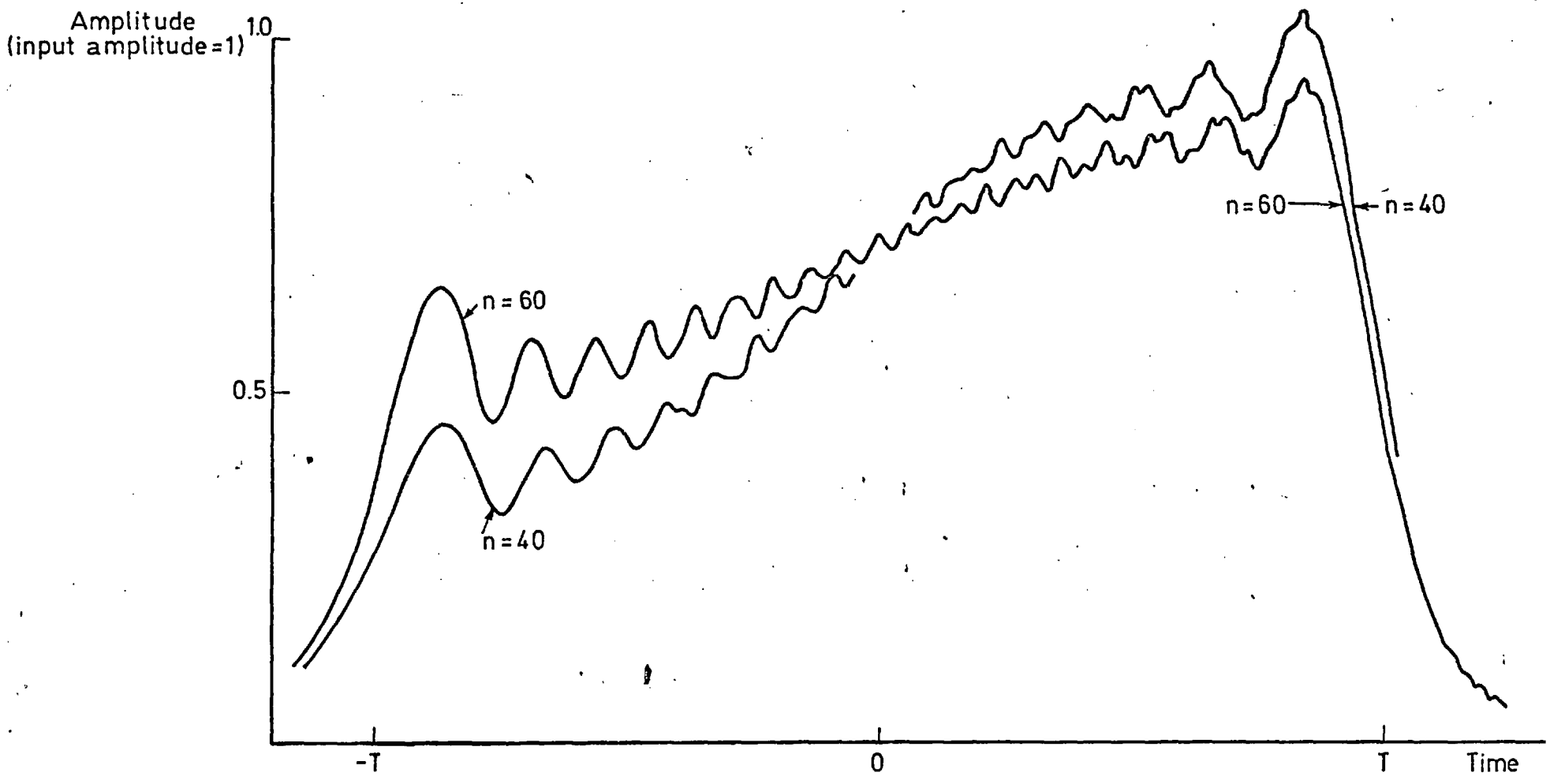


Fig.4.9 Dispersed pulse - identical section dispersive system - all pass filter (n=40,60)

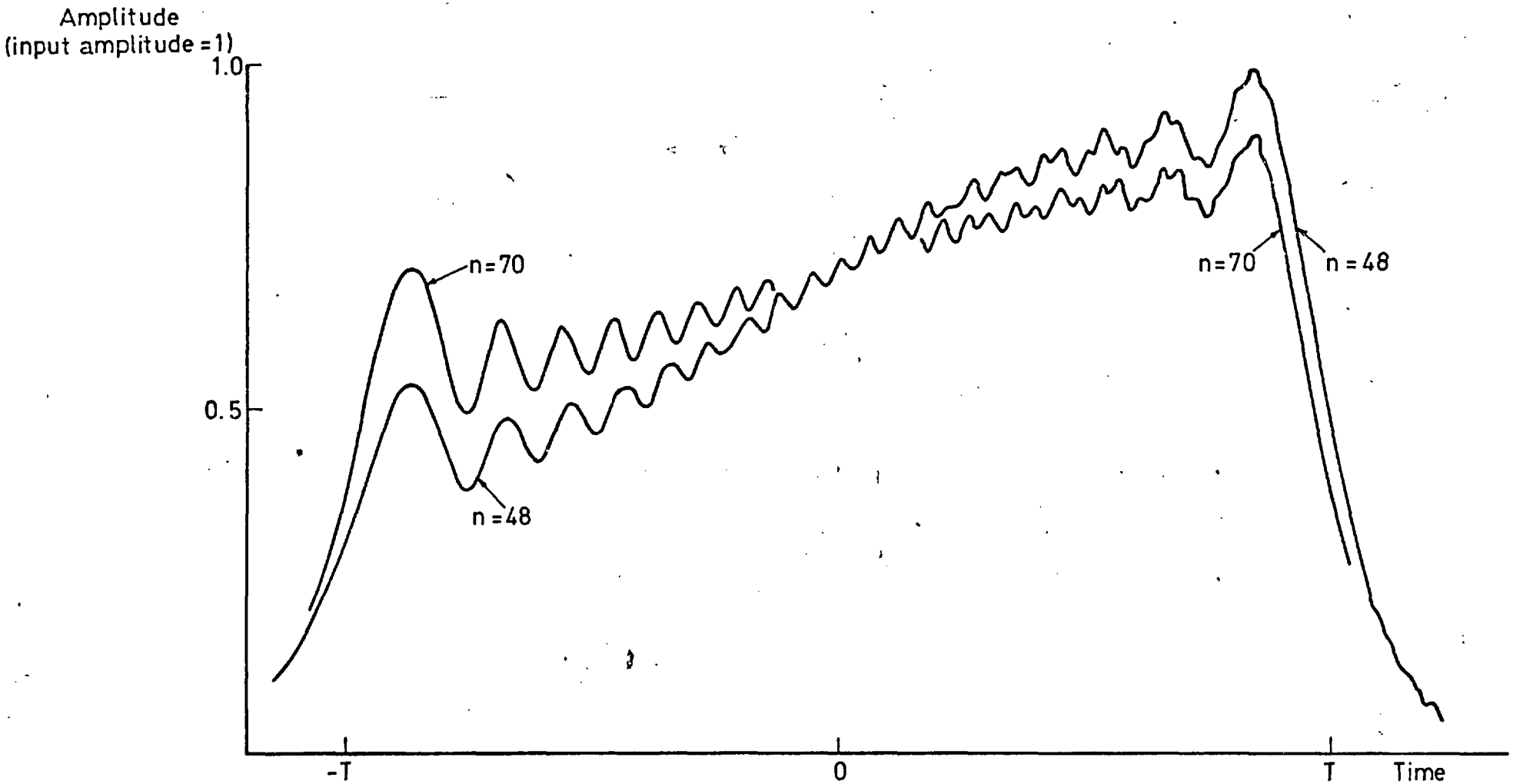


Fig. 4.10 Dispersed pulse - identical section dispersive system - all pass filter (n = 48, 70)

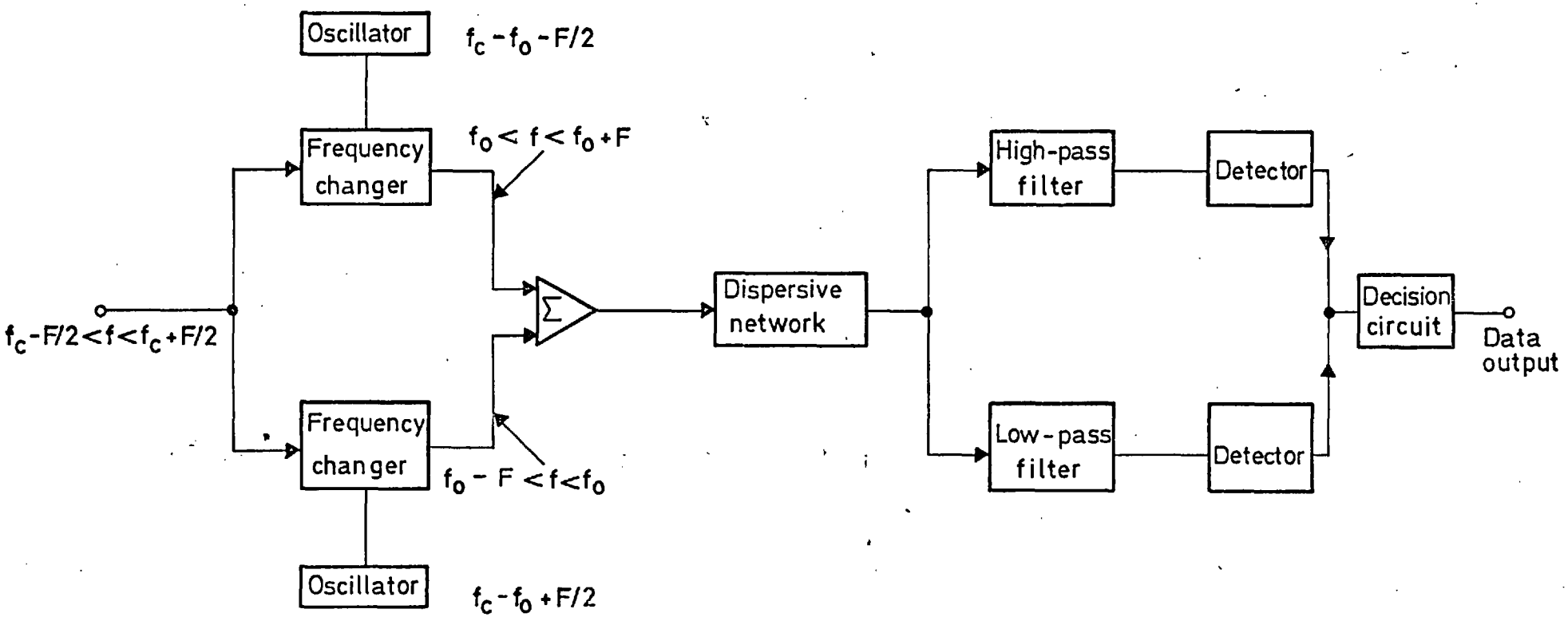


Fig.4.11 Block diagram of complete demodulator

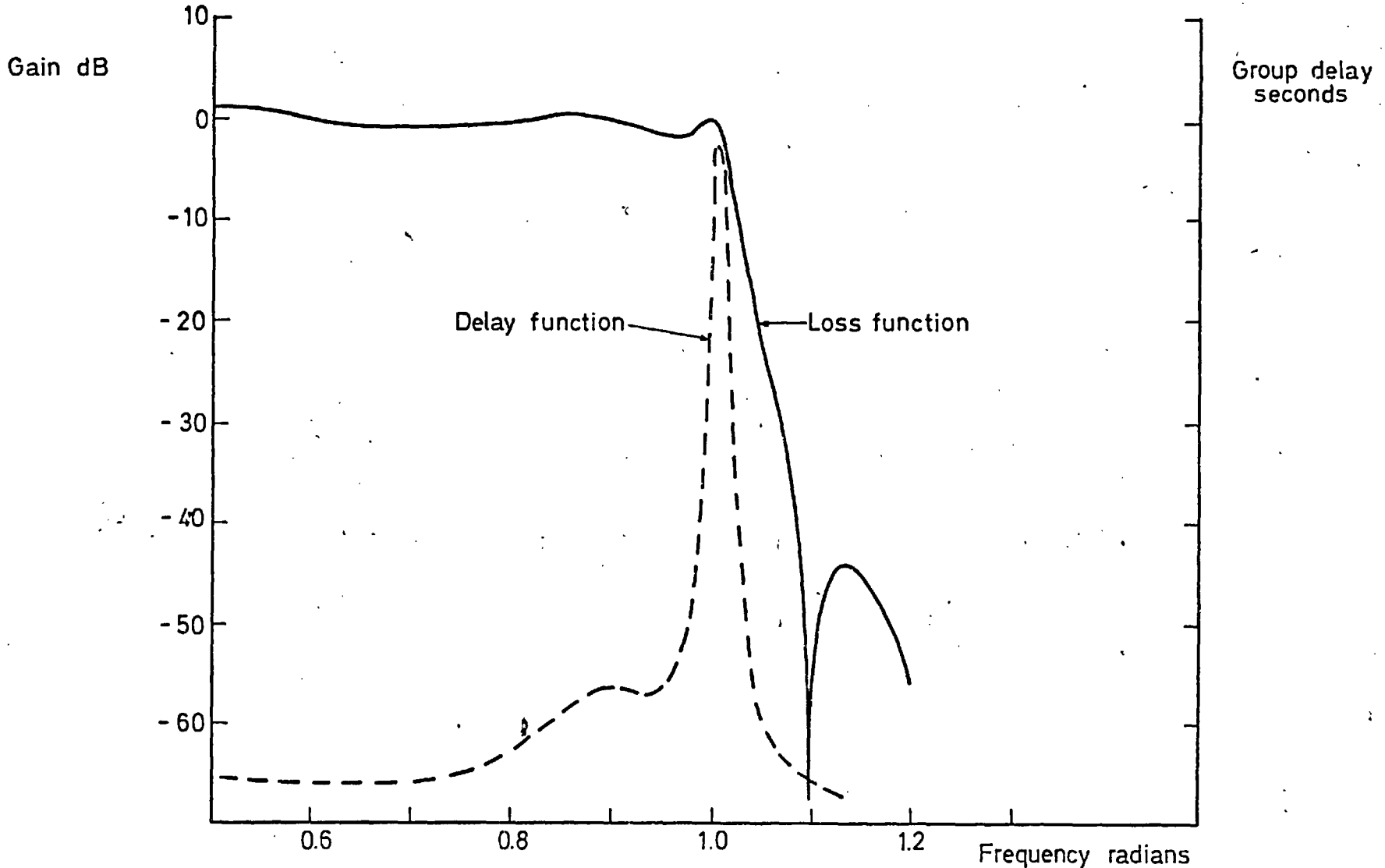


Fig.4.12 Magnitude and delay response of 7th order low pass elliptic function filter

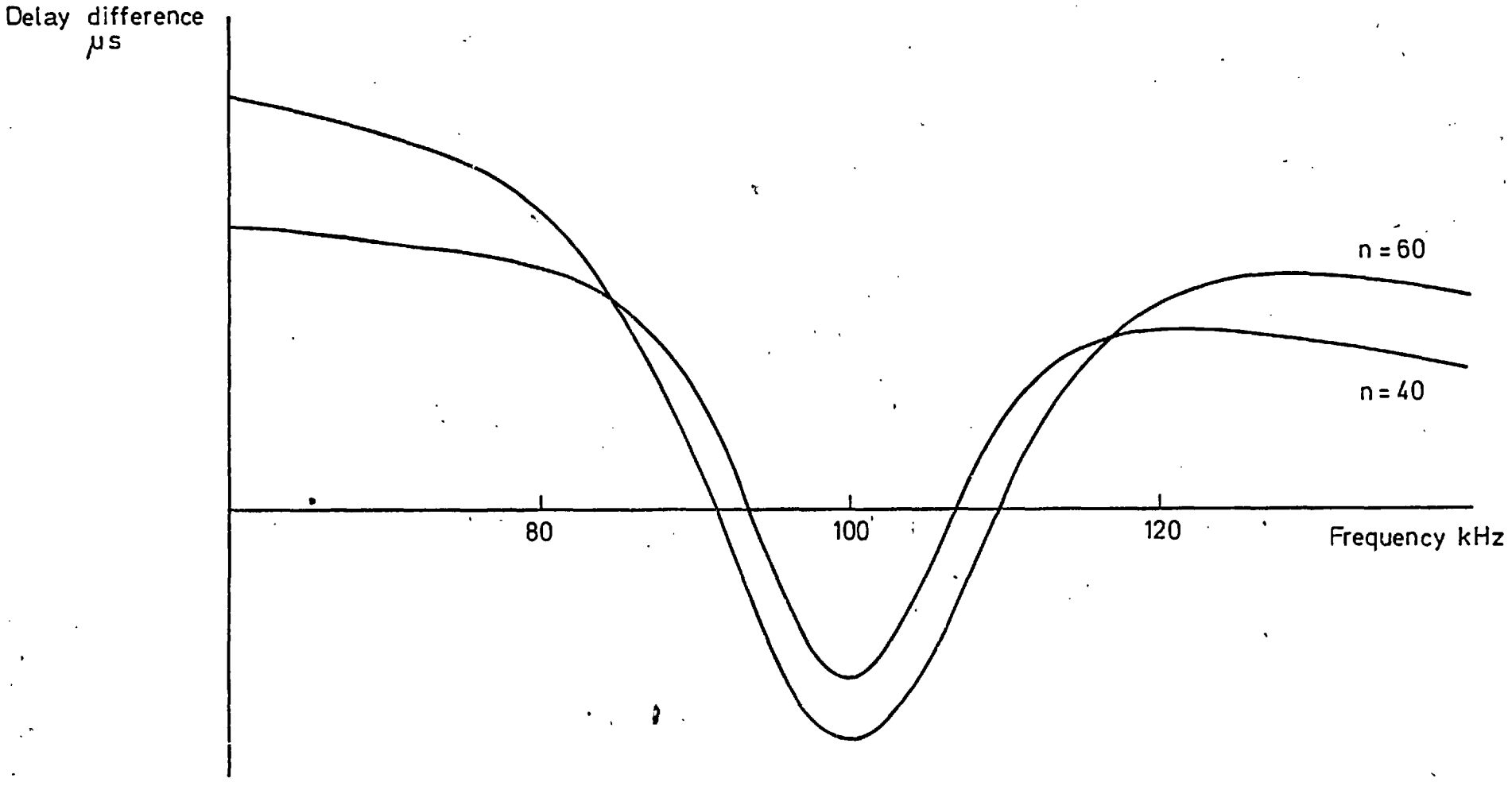


Fig.4.13 Group delay difference between exact and simplified expressions

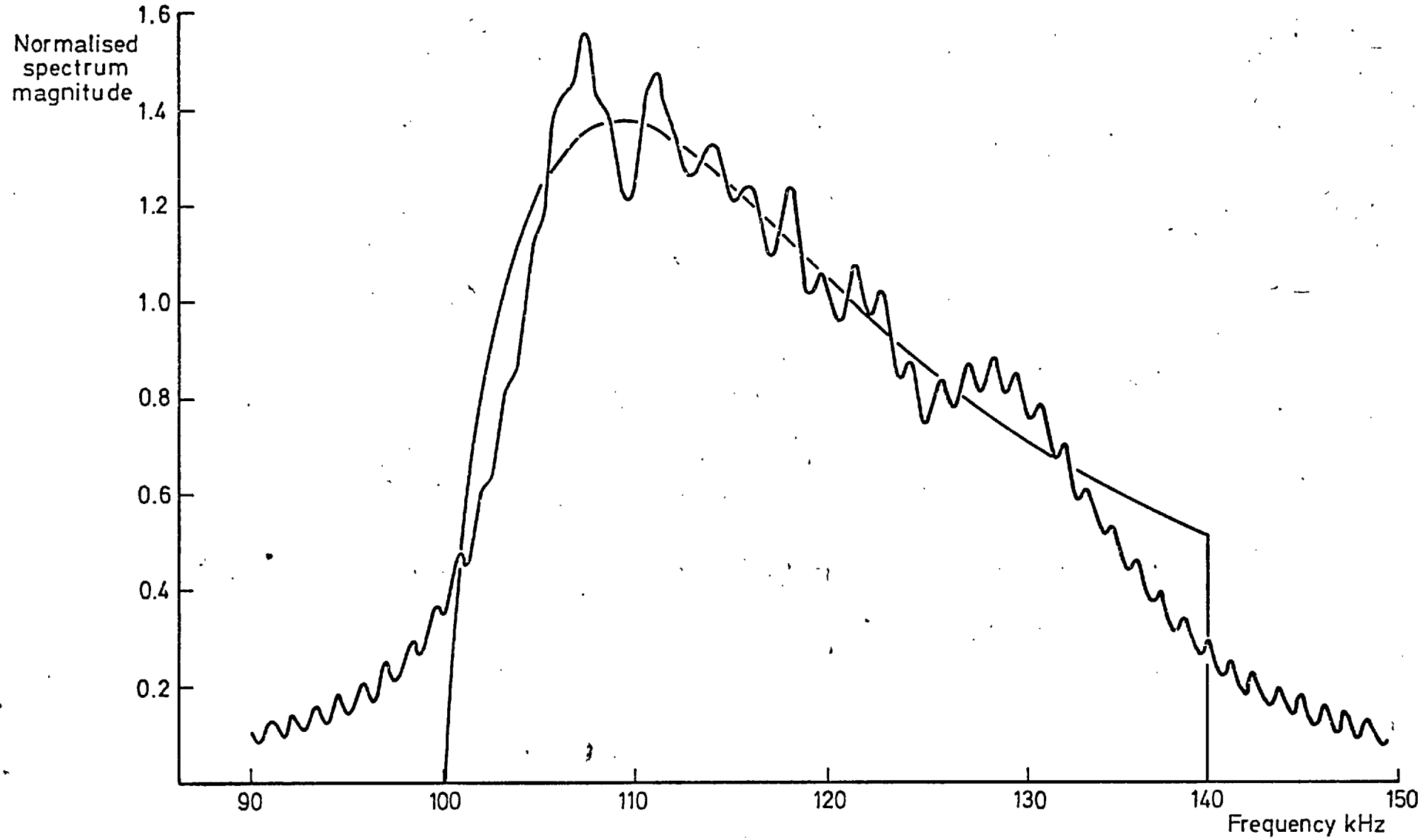


Fig.4.14 Identical section dispersive system (n = 48) - exact spectrum

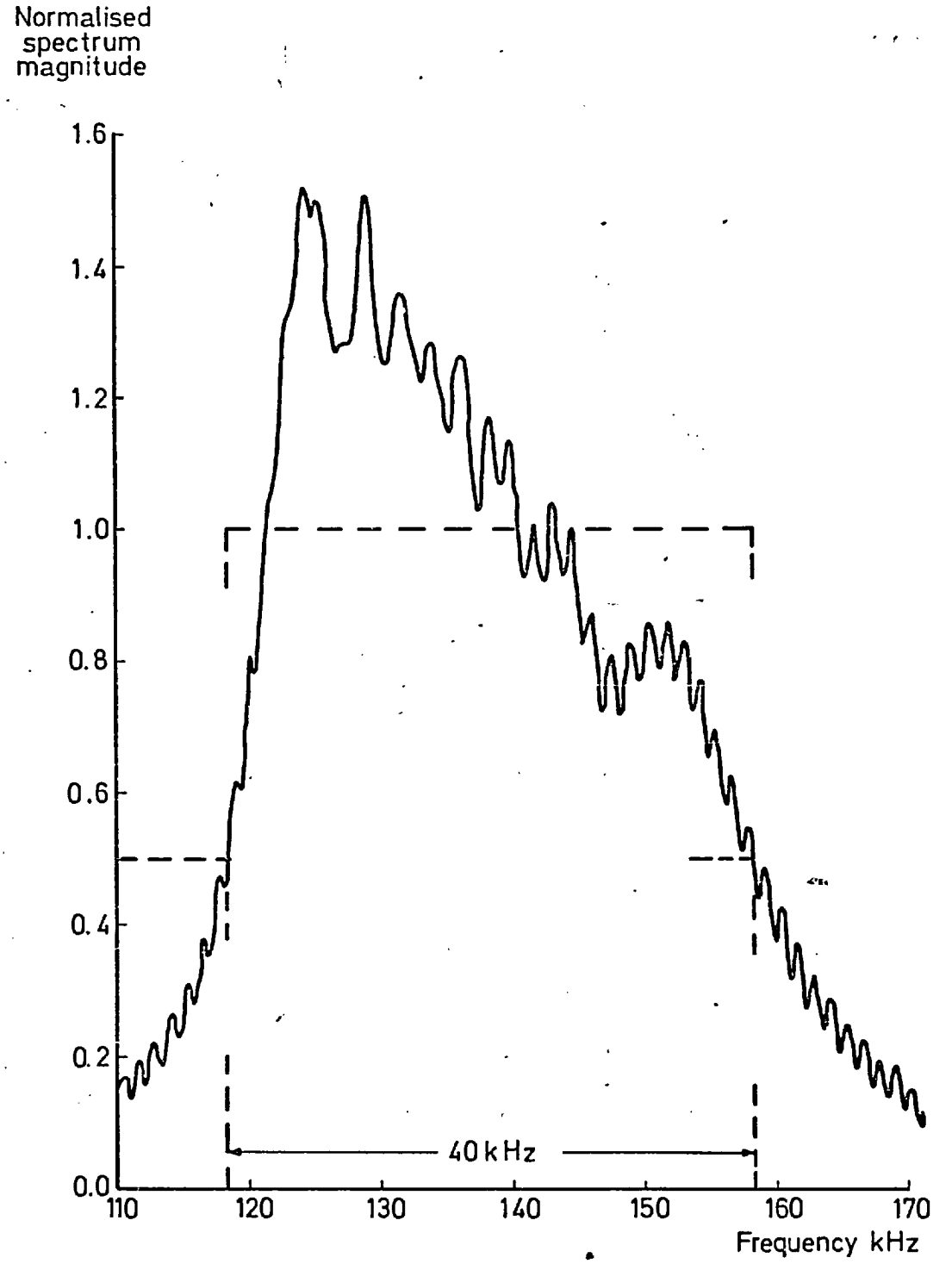


Fig.4.15 Identical section dispersive system
FT = 38.88, F = 46.66, n = 56

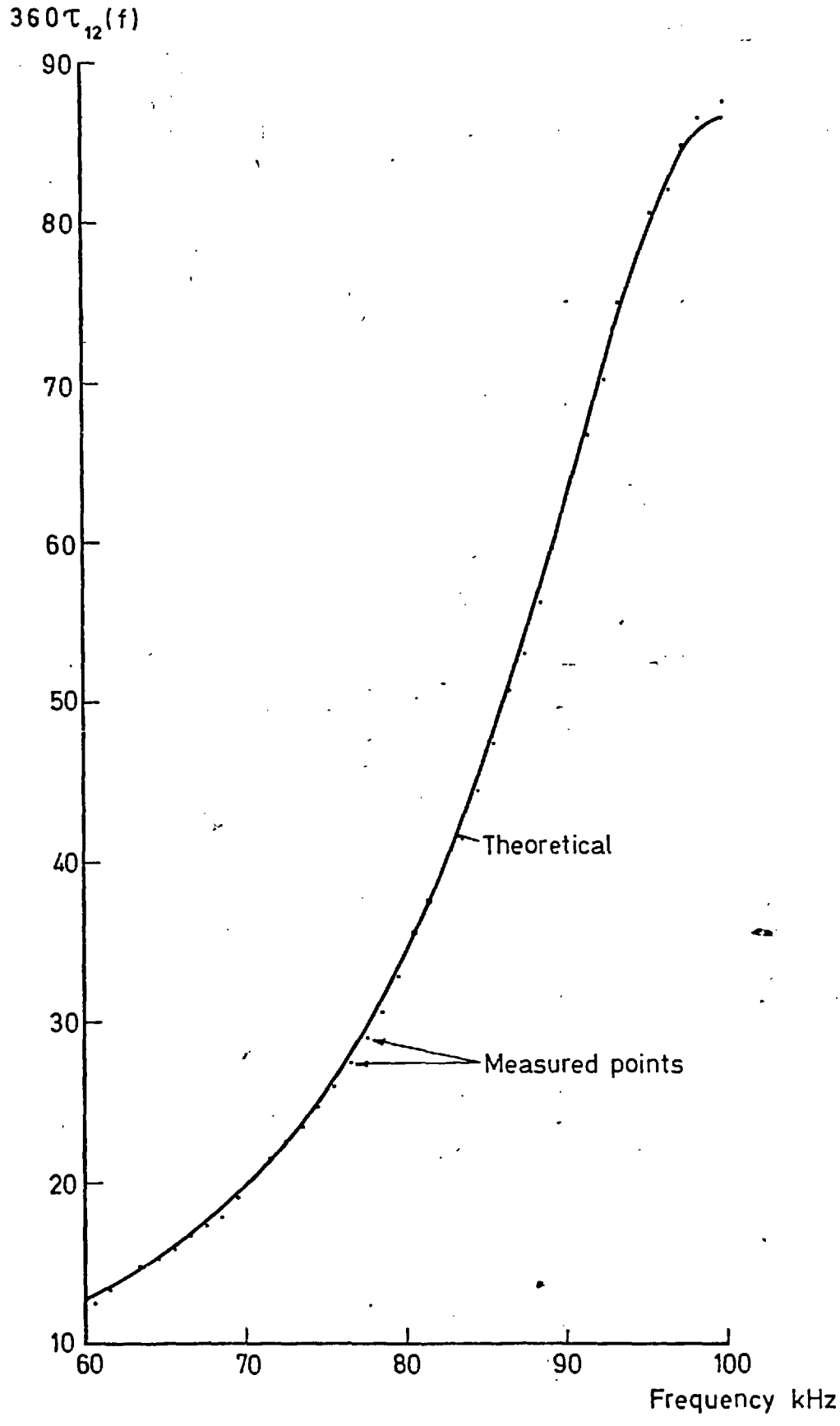


Fig 5.1 Comparison of measured and theoretical delay response of 12 section network

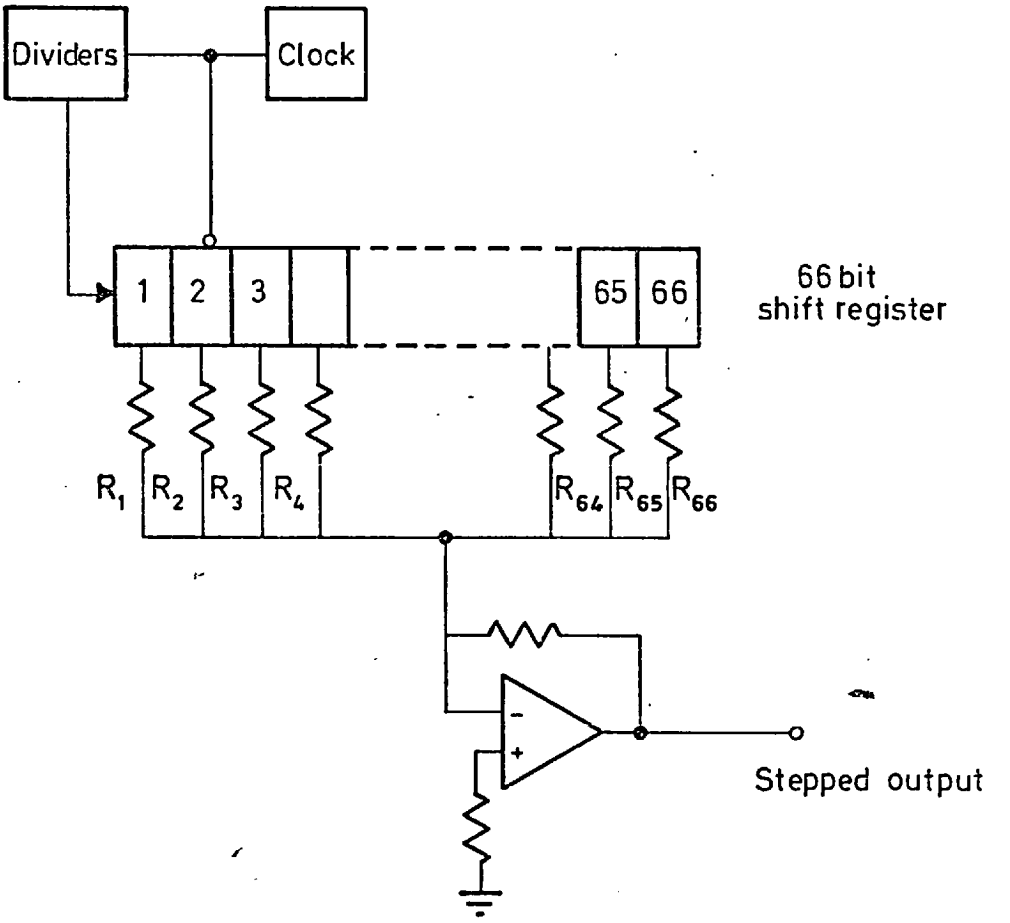


Fig.5.2 Technique for generation of stepped modulating waveform

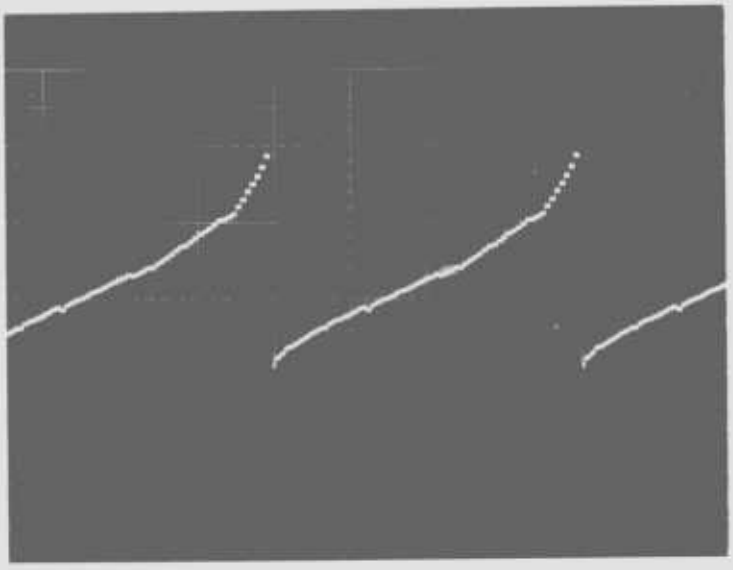


FIG.5.3 – OSCILLOSCOPE PHOTOGRAPH OF
STEPPED MODULATING WAVEFORM

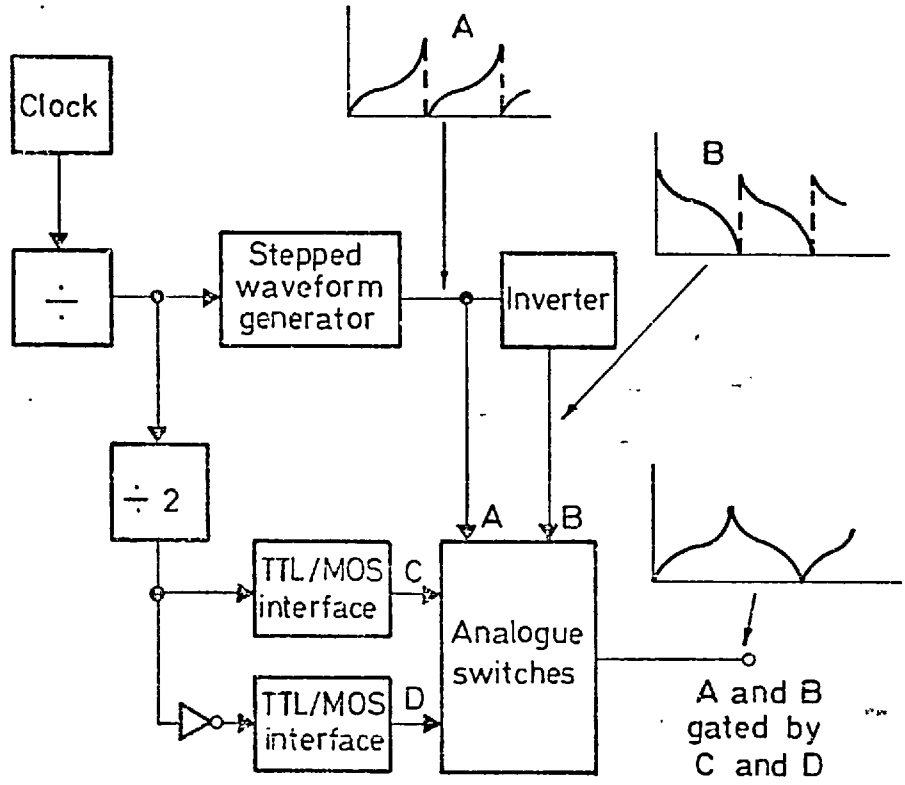


Fig.5.4 Block diagram of {1,0} sequence generator

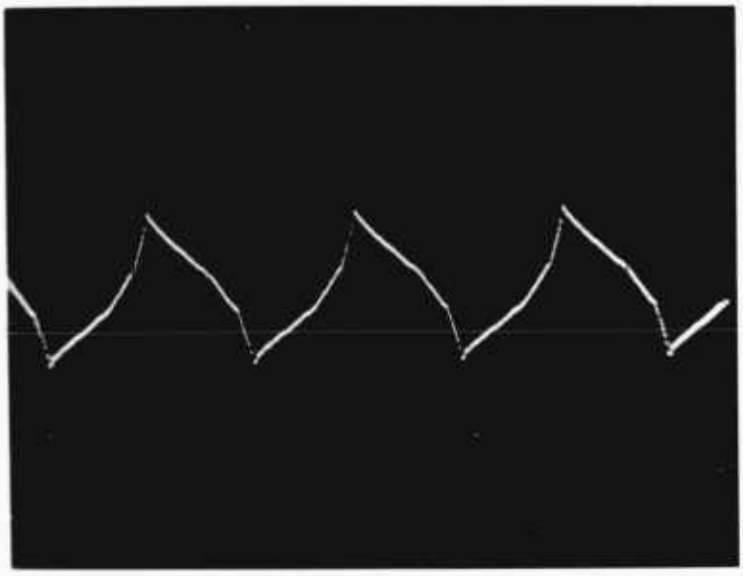


FIG.5.5 - OSCILLOSCOPE PHOTOGRAPH OF {1 ,0}
MODULATING WAVEFORM

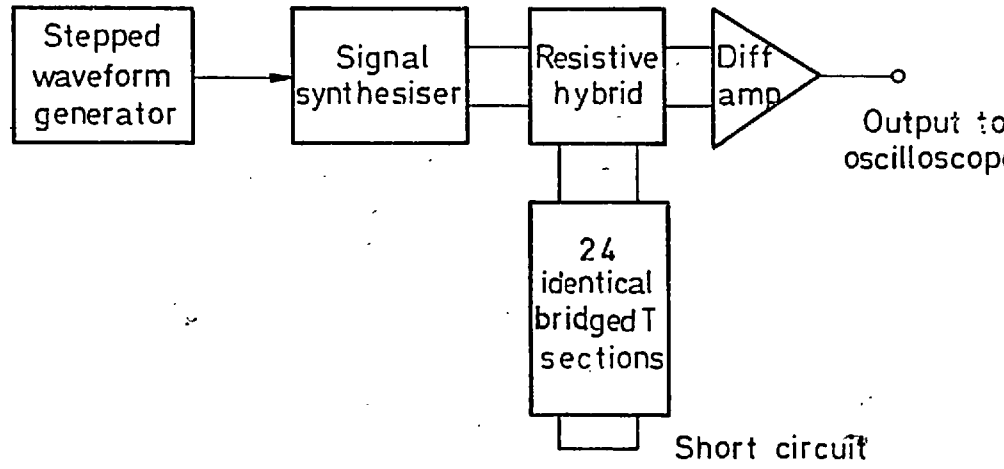


Fig.5.6 Experimental arrangement for demonstration of pulse compression



Fig.5.7.a
Compressed pulses
in 60 < f < 100 kHz



Fig.5.7.b
Compressed pulses
in 100 < f < 140 kHz



Fig.5.7.c
Expanded view of
compressed pulse
in 60 < f < 100 kHz

FIG.5.7 – OSCILLOSCOPE PHOTOGRAPHS OF COMPRESSED PULSES

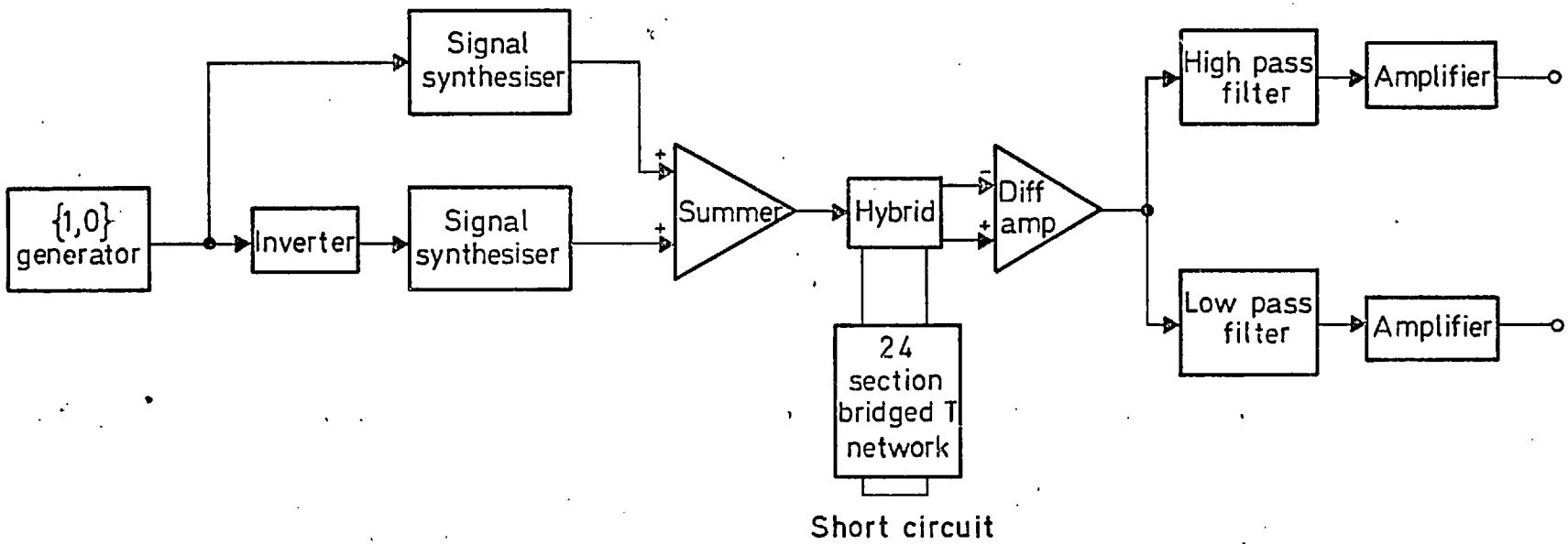
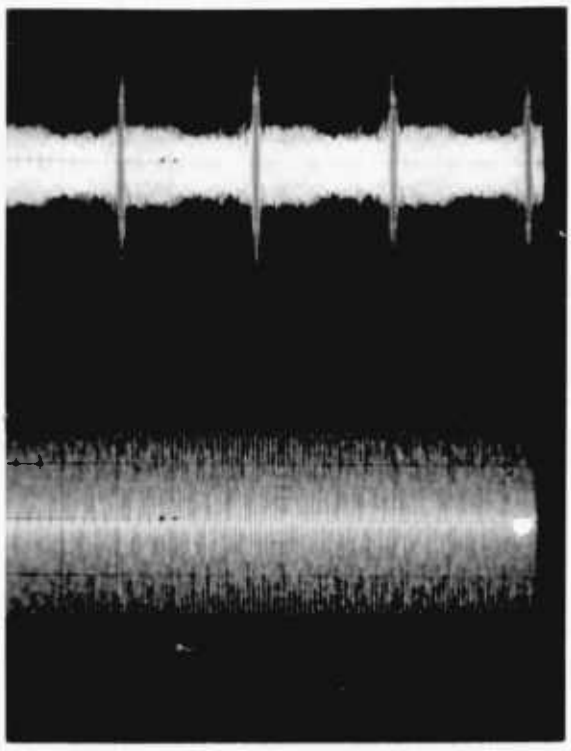


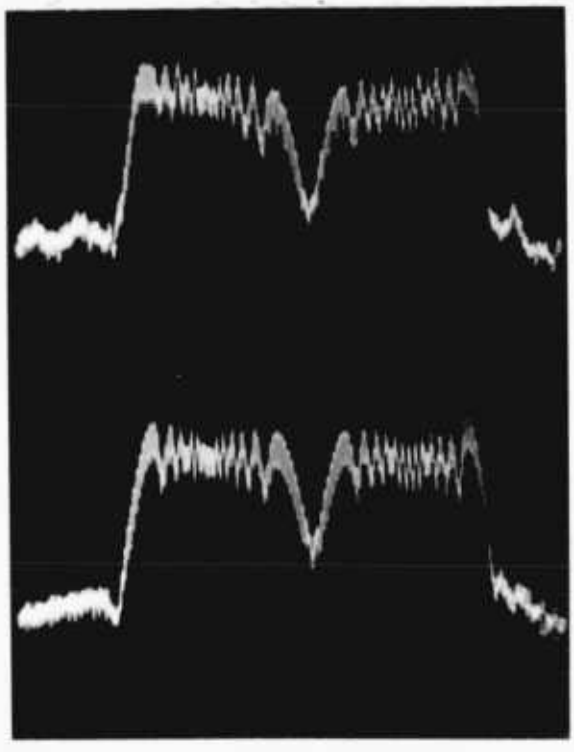
Fig.5.8 Block diagram of experimental arrangement for demonstrating complete system



Output signal

Fig.5.9.a

Input signal

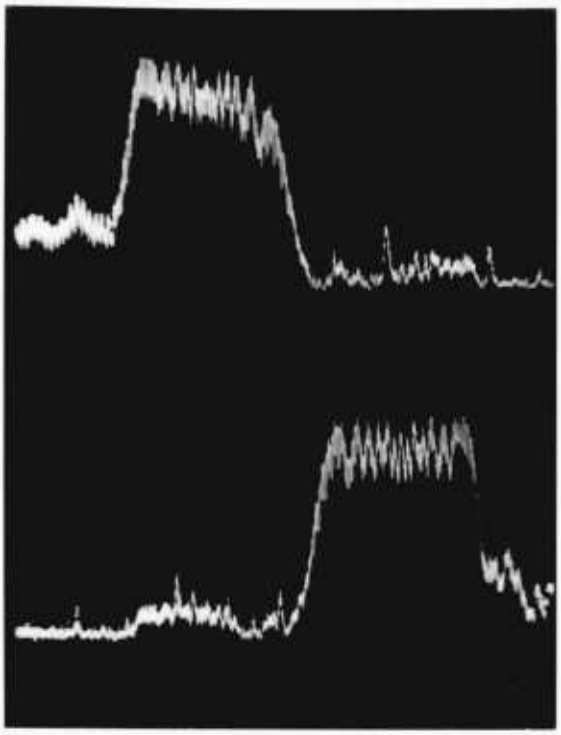


Output spectra

Fig.5.9.b

Input spectra

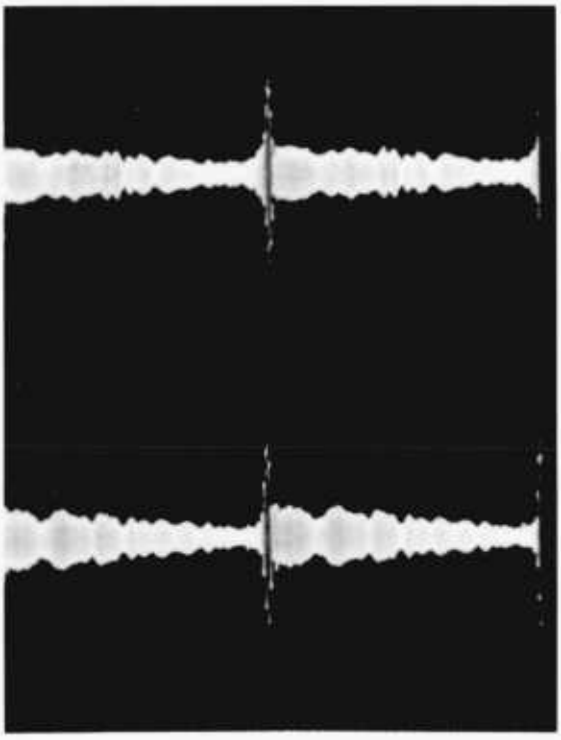
FIG.5.9 – OSCILLOSCOPE PHOTOGRAPHS OF SIGNALS AND SPECTRA AT INPUT AND OUTPUT OF DISPERSIVE NETWORK



Spectrum at
output of
low pass filter

Fig.5.10.a

Spectrum at
output of
high pass filter

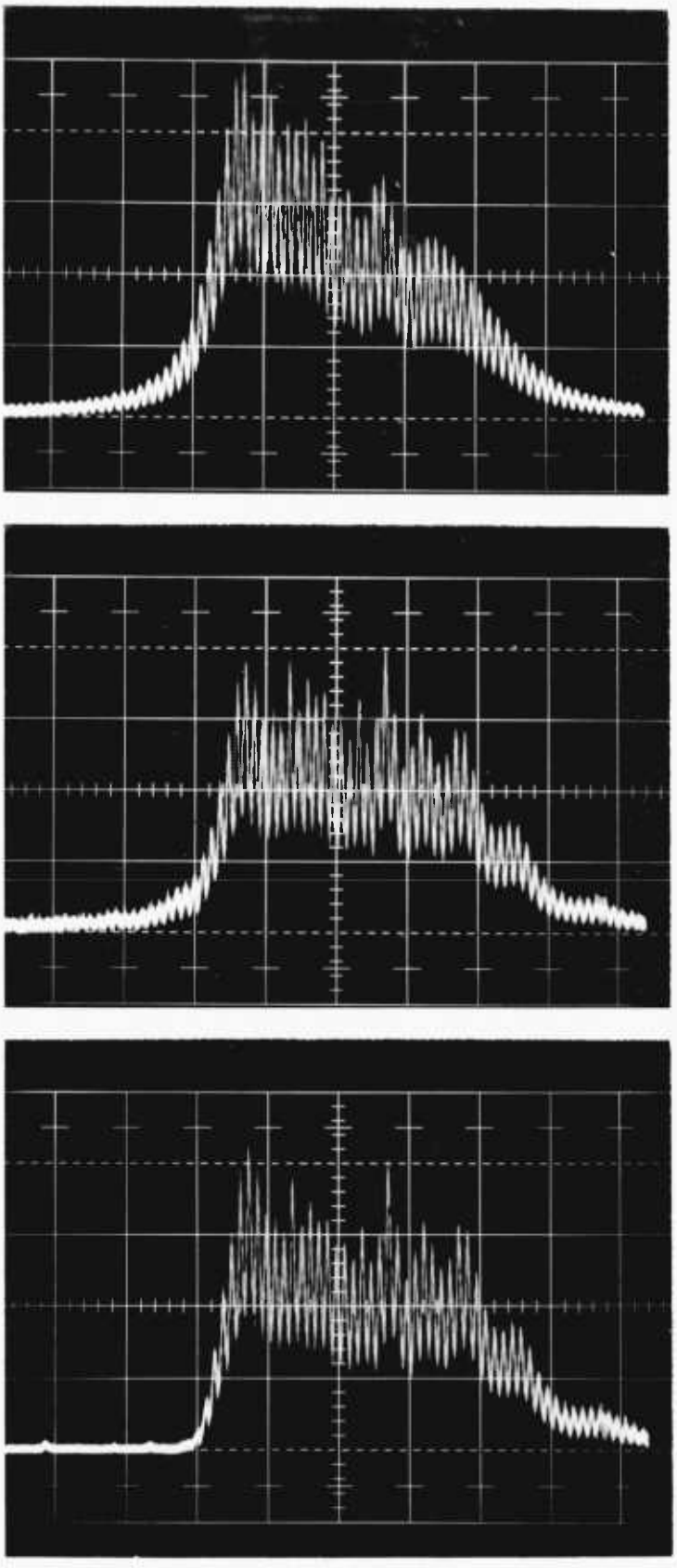


Signal at
output of
low pass filter

Fig.5.10.b

Signal at
output of
high pass filter

FIG.5.10 - OSCILLOSCOPE PHOTOGRAPHS OF SIGNALS AND SPECTRA AT OUTPUT OF CHANNEL FILTERS



Spectrum at input to dispersive network

Spectrum at output of dispersive network

Spectrum at output of high pass filter

FIG.5.11 – OSCILLOSCOPE PHOTOGRAPHS OF SPECTRA OF UNIDIRECTIONAL SIGNALS AT INPUT AND OUTPUT OF DISPERSIVE NETWORK AND HIGH PASS FILTER

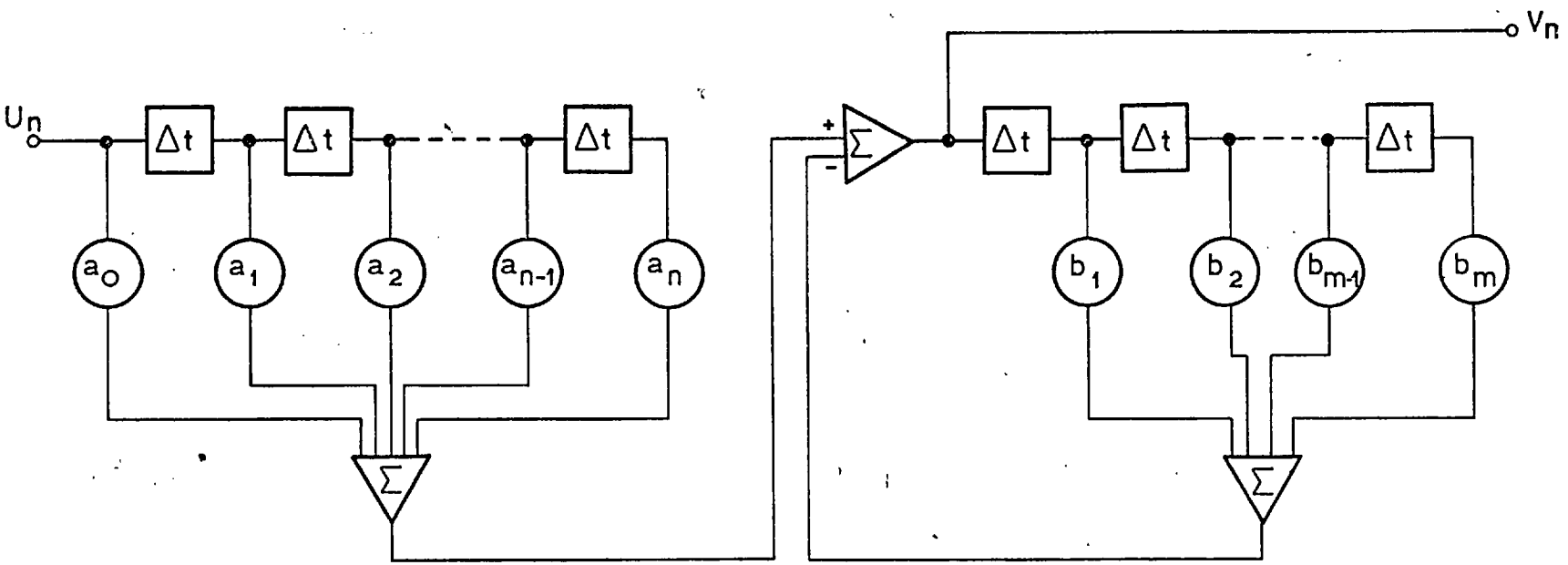


Fig.6.1 Layout of generalised digital filter - direct form

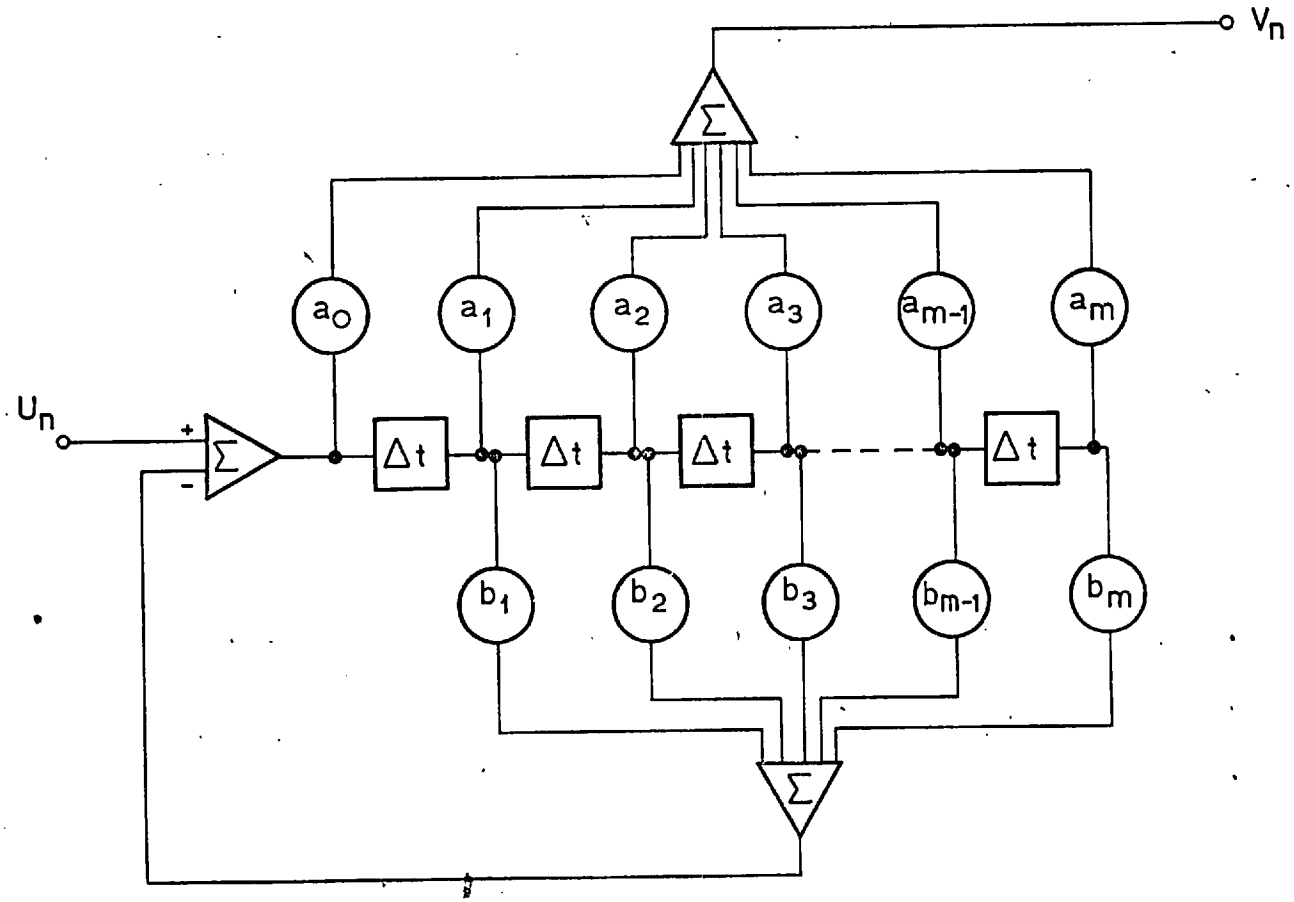


Fig.6.2 Recursive realisation of generalised digital filter

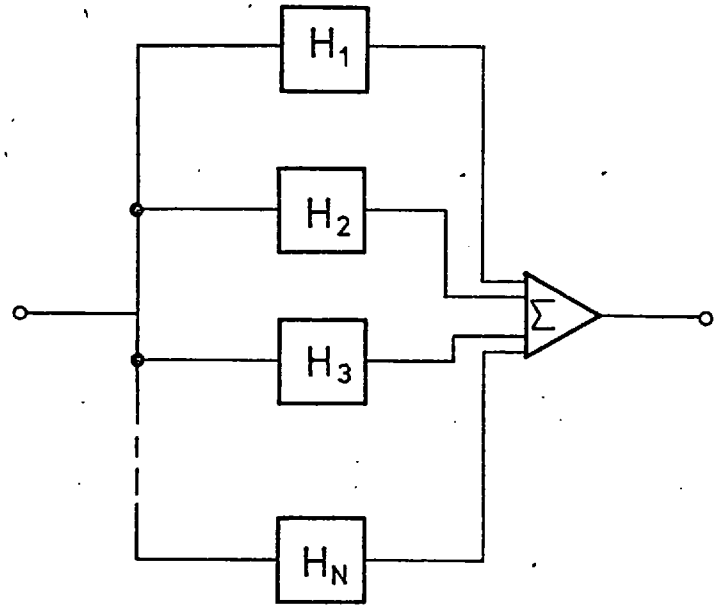


Fig.6.3a Digital filter -parallel form

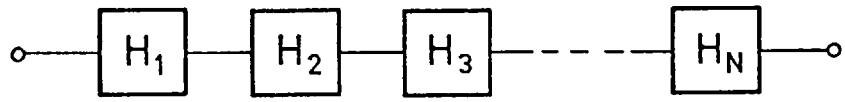


Fig.6.3b Digital filter - cascade form

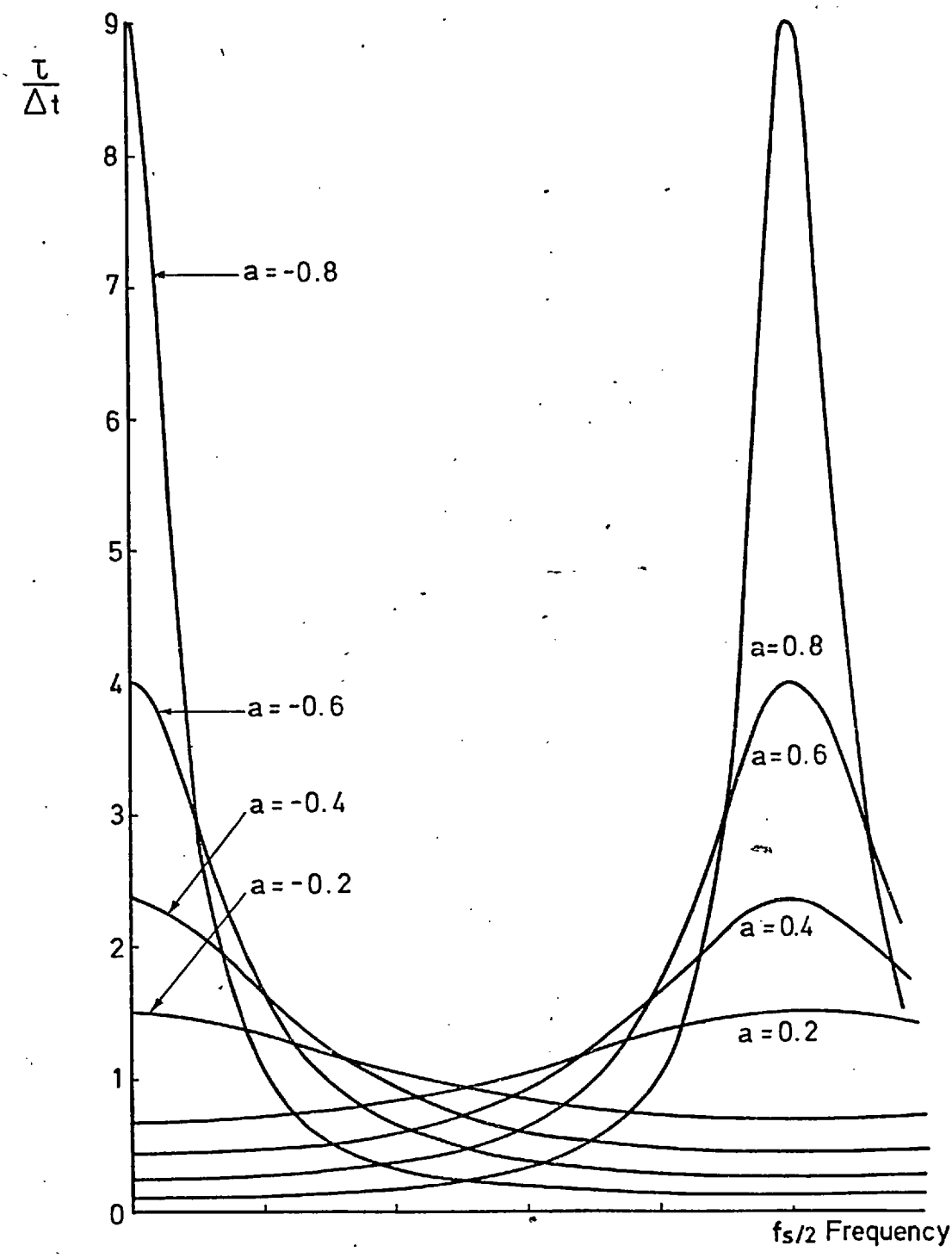


Fig.6.4 Group delay response of first order digital all pass delay network

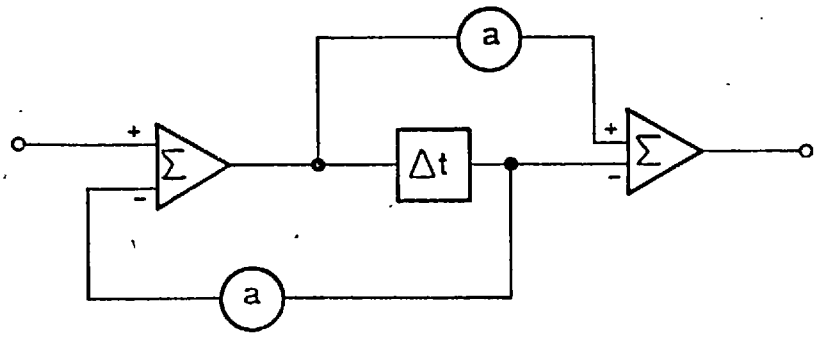


Fig.6.5a

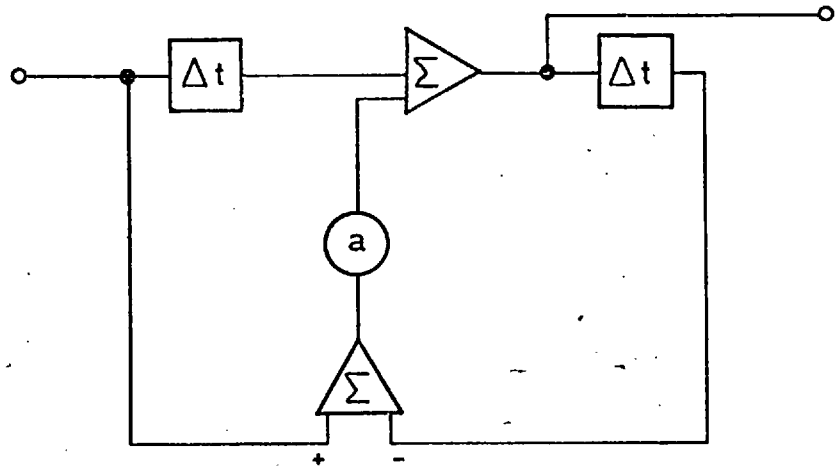


Fig.6.5b

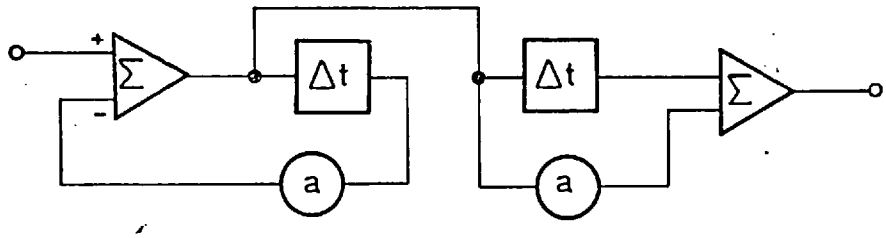


Fig.6.5c

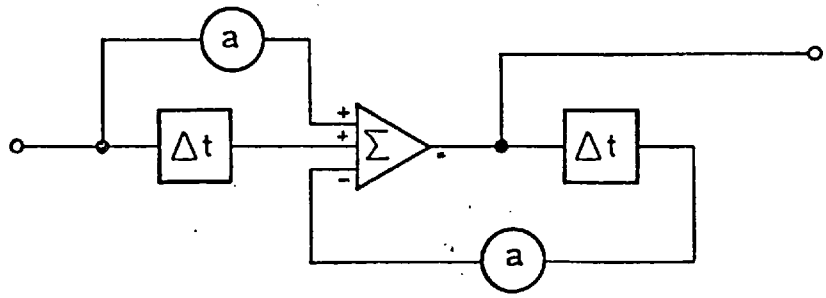


Fig.6.5d

Fig.6.5 Different realisations of first order digital delay network

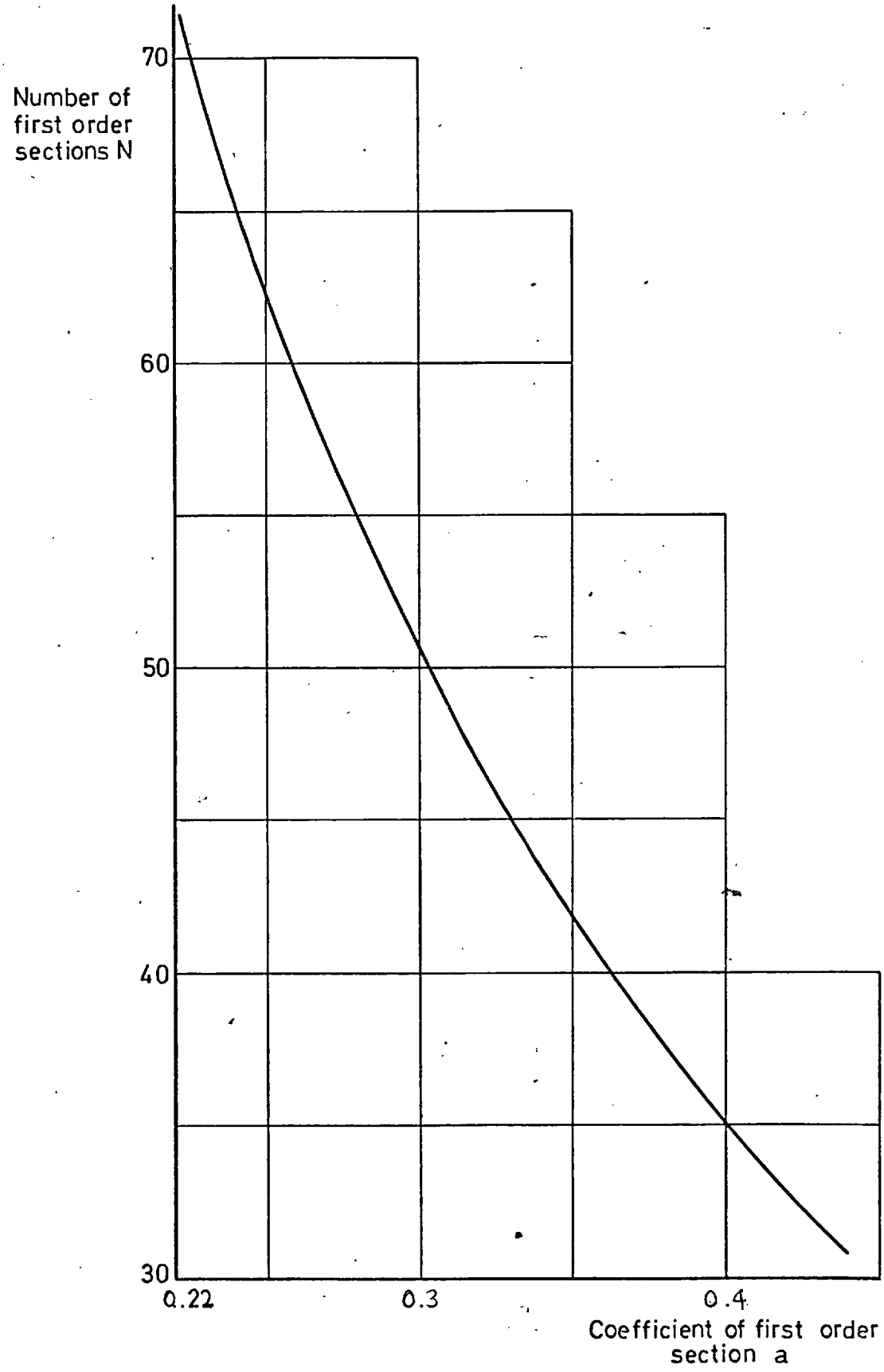


Fig.6.6 Relationship between number of identical sections and coefficient of each one

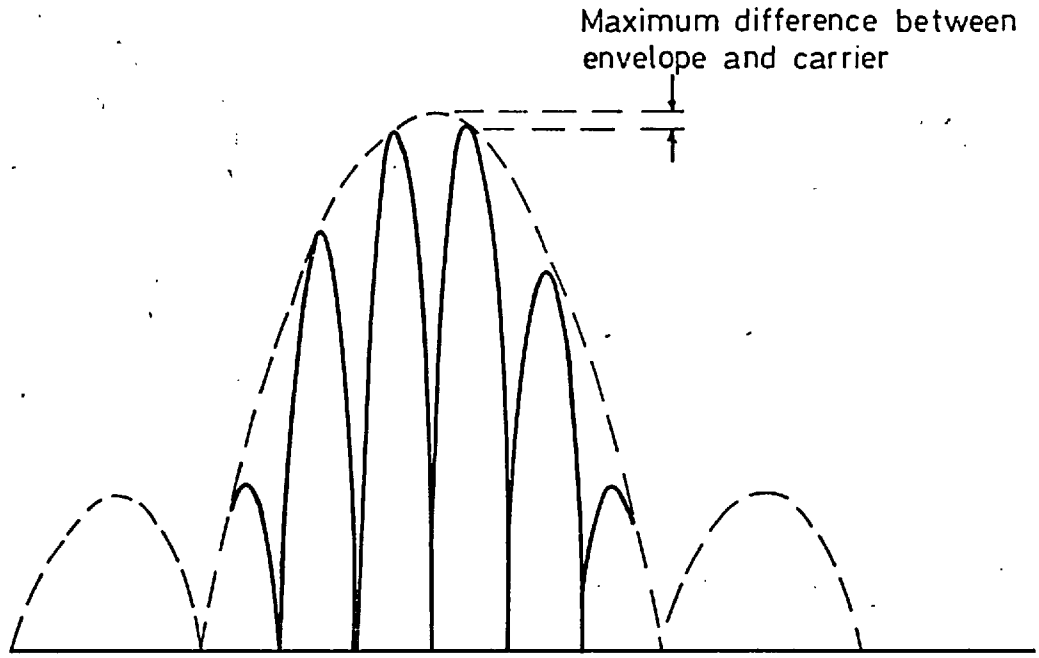


Fig.6.7a

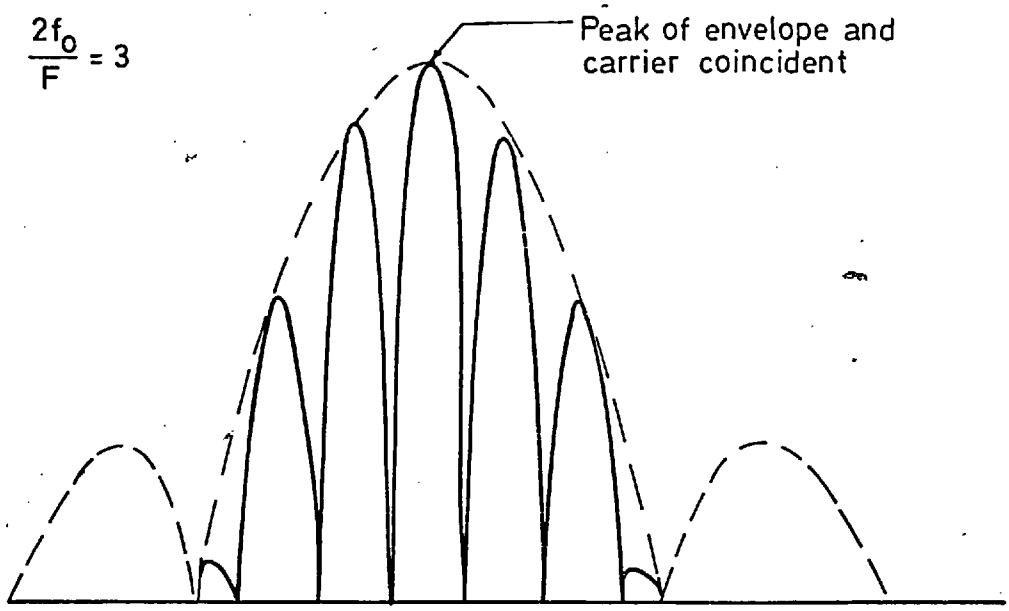


Fig.6.7b

Fig.6.7 Demonstration of maximum "jitter" on rectified output

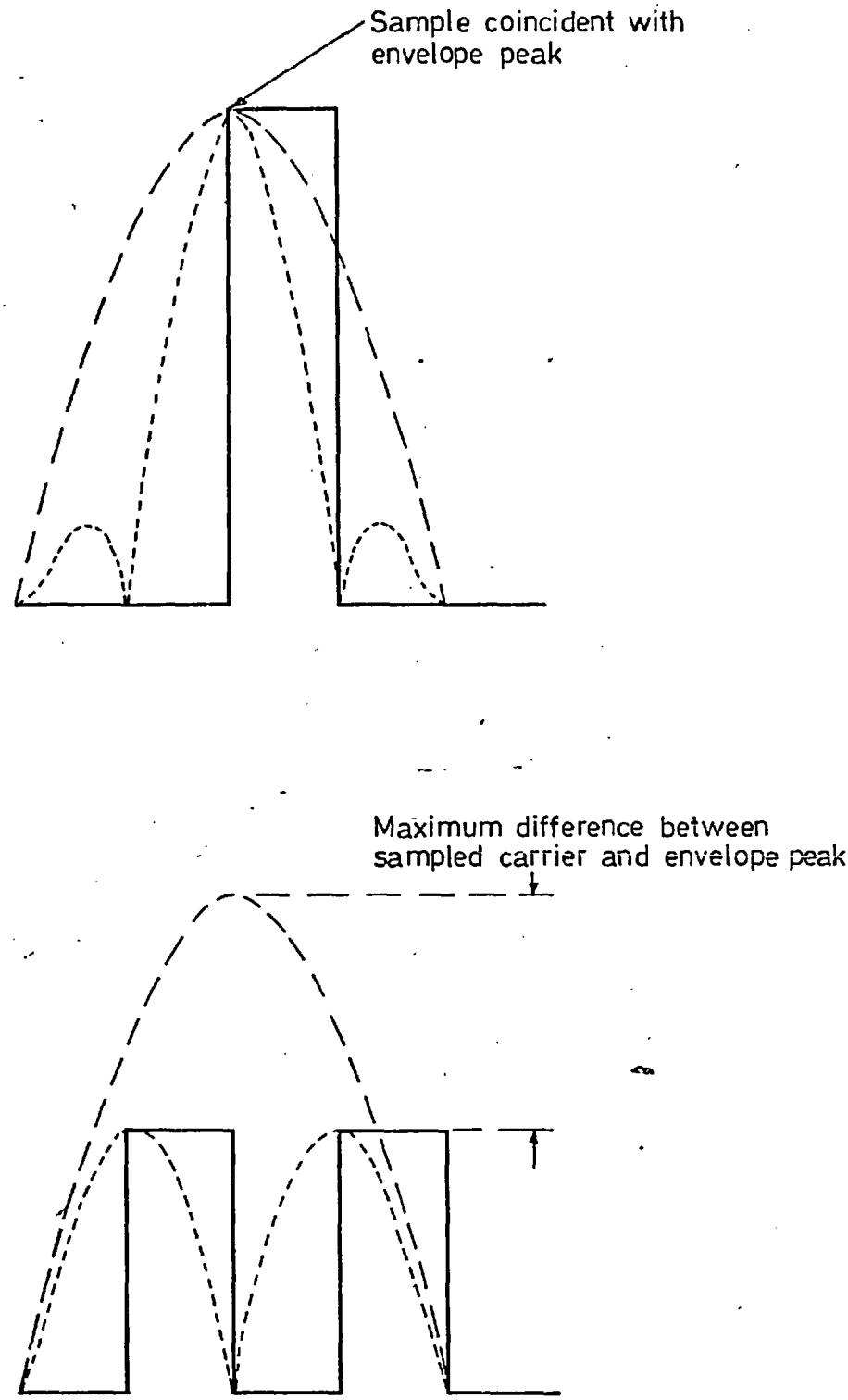


Fig.6.8 Demonstration of maximum "jitter" for sampled system with $2f_0/F=1$

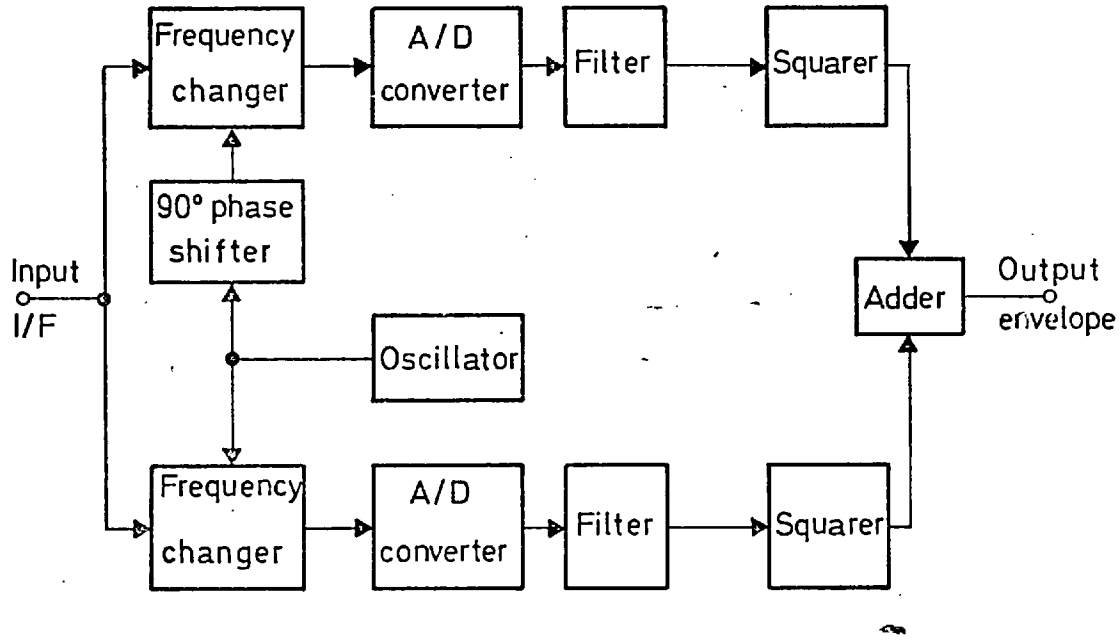


Fig.6.9 Scheme for obtaining output envelope

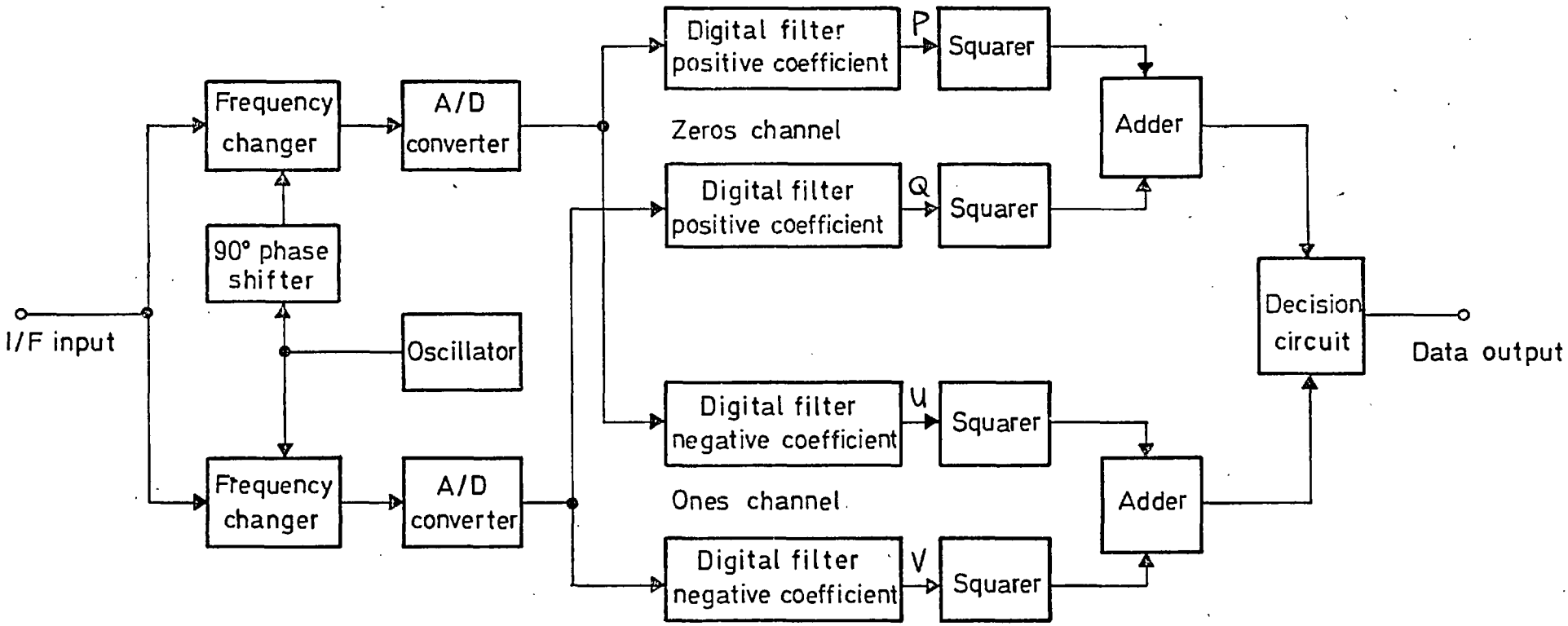


Fig.6.10 Complete digital filter pulse compression demodulator

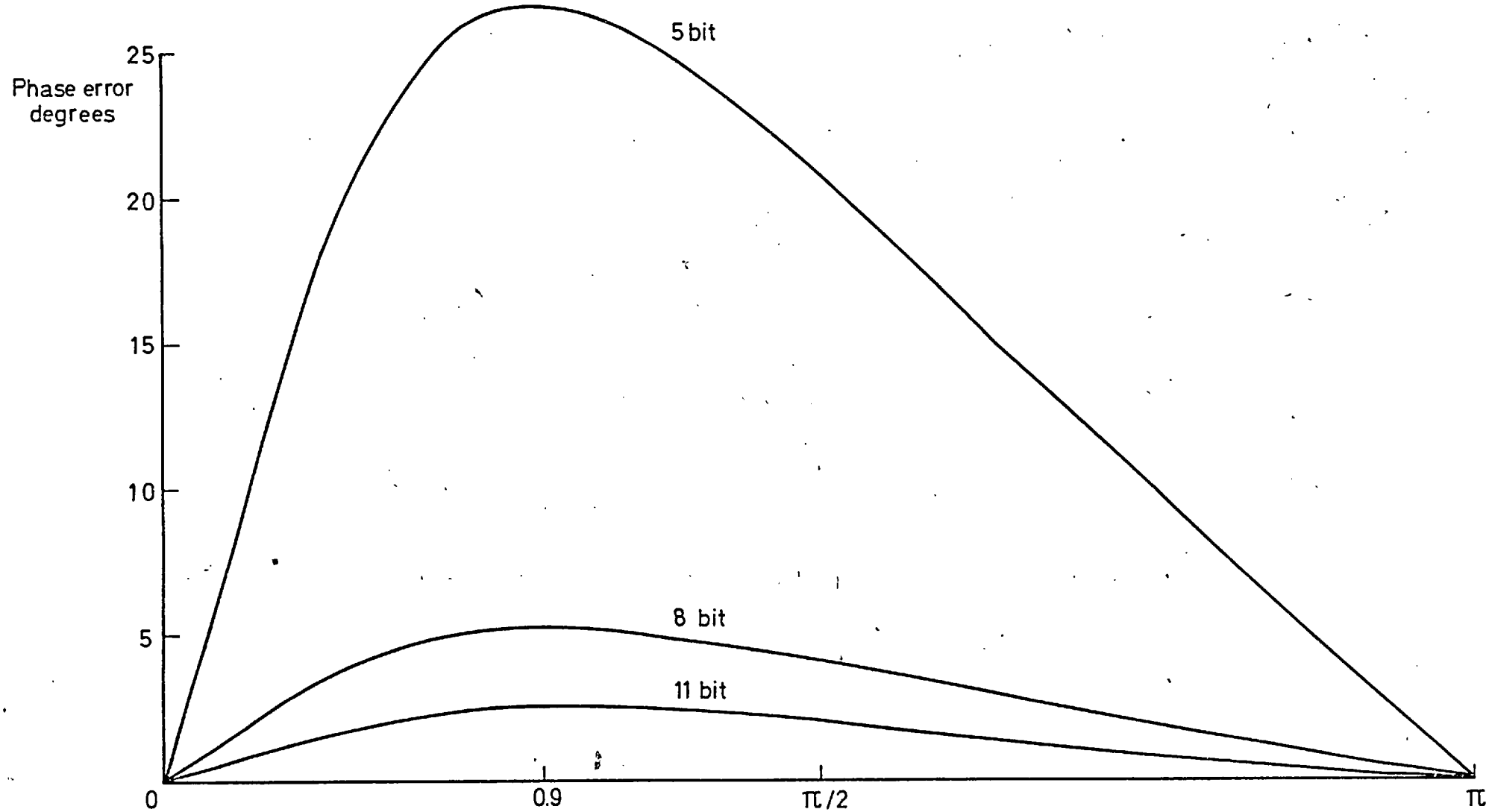


Fig.6.11 Overall phase error of 42 sections for various coefficient word lengths

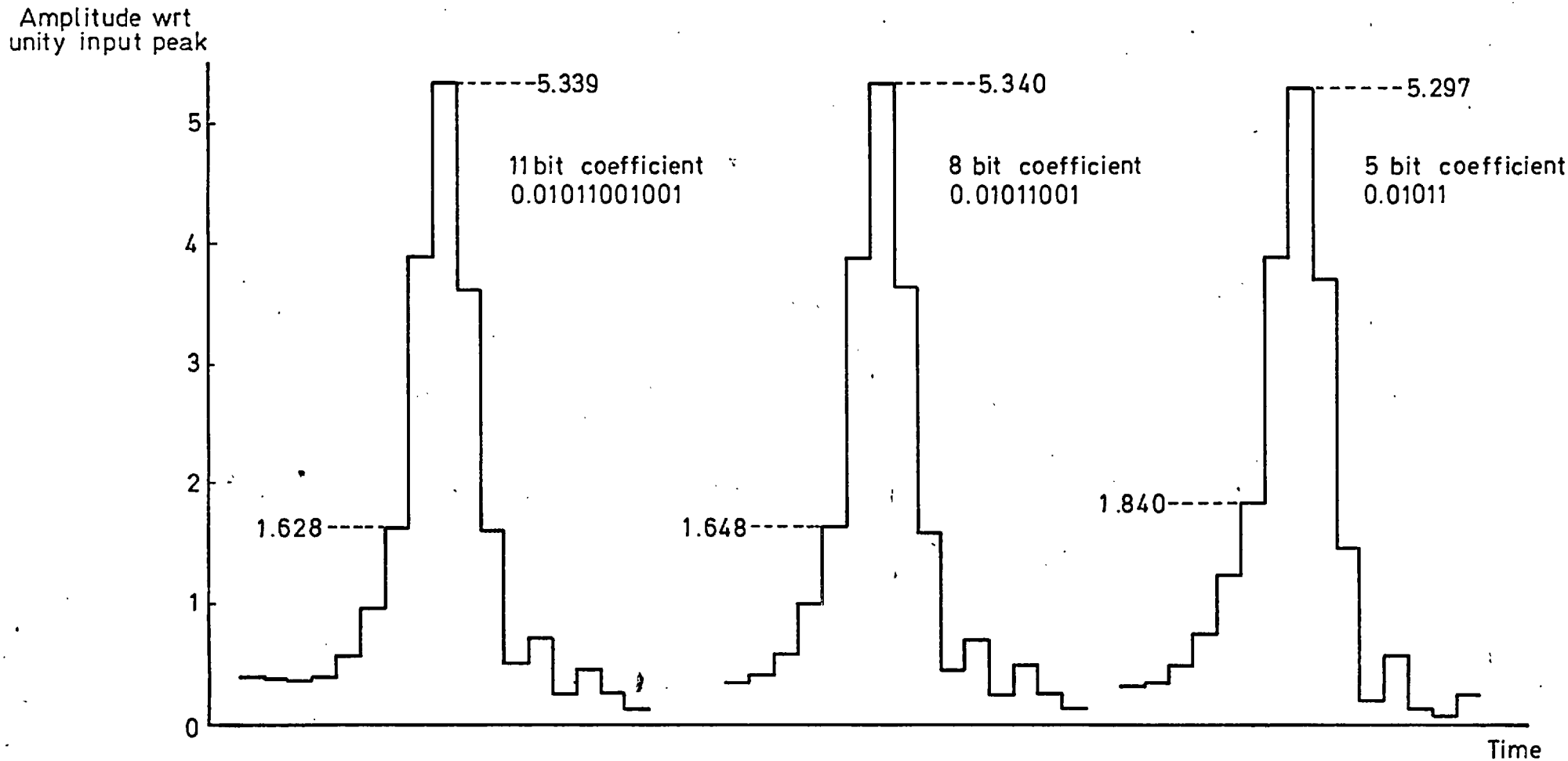


Fig.6.12 Effect of coefficient quantisation on compressed pulse envelope
(N = 42, a = 0.34860, 14 bit binary 0.01011001001111)

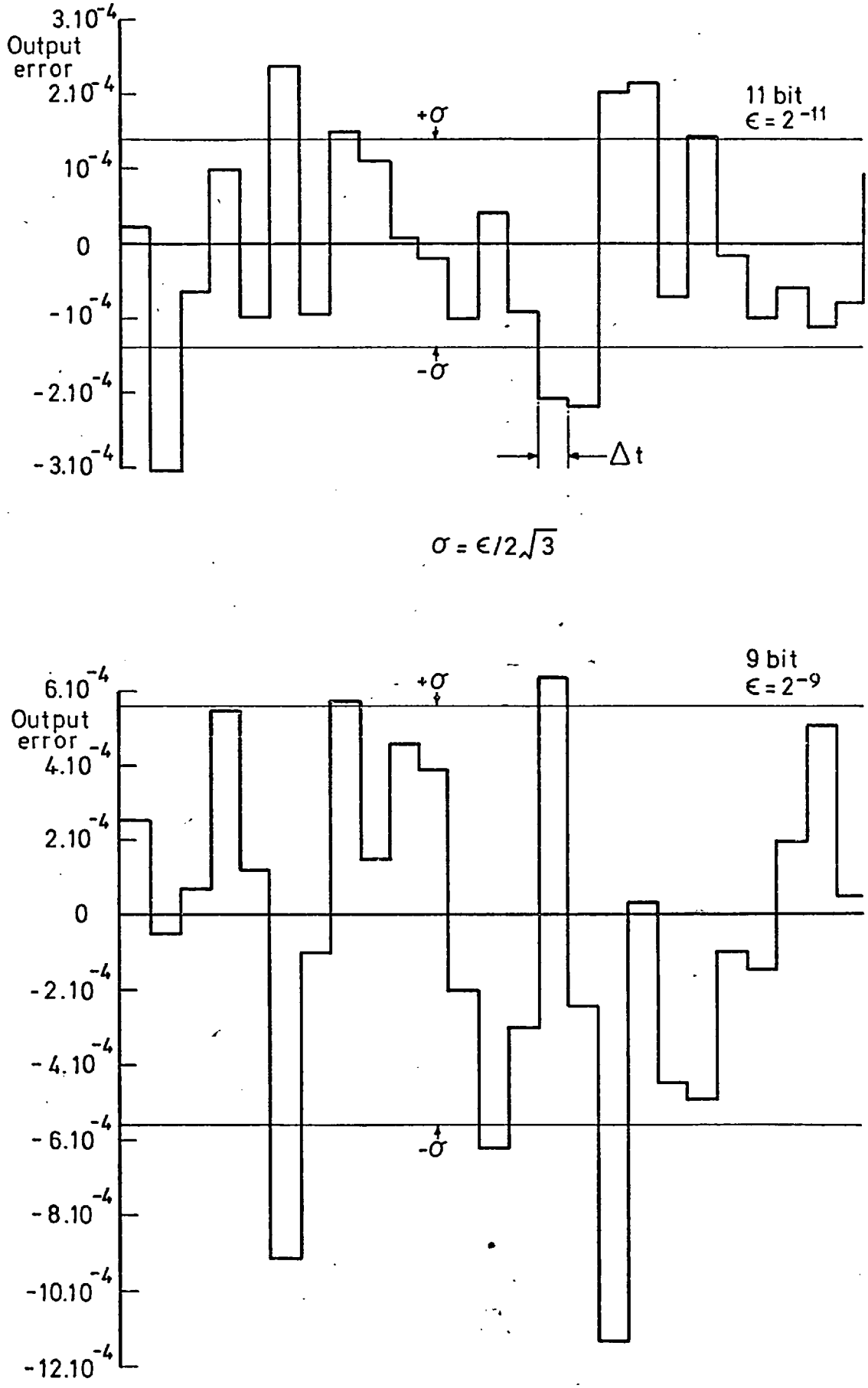


Fig. 6.13 Typical output errors for 9 and 11 bit input quantisation (exact filtering) (N = 30, a = 0.445362)

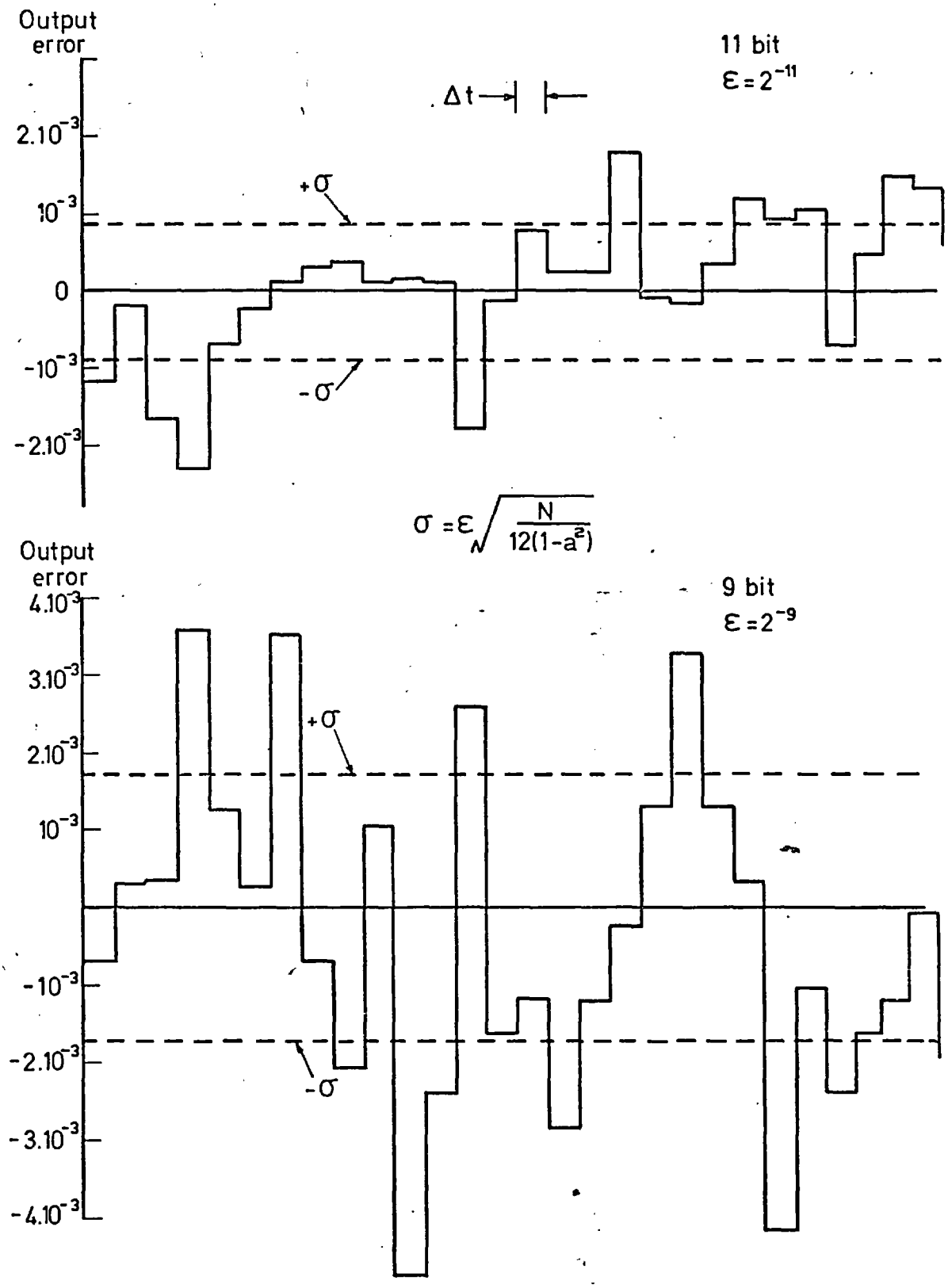


Fig.6.14 Typical output errors for 9 and 11 bit multiplier rounding (N=30, a=0.445362)

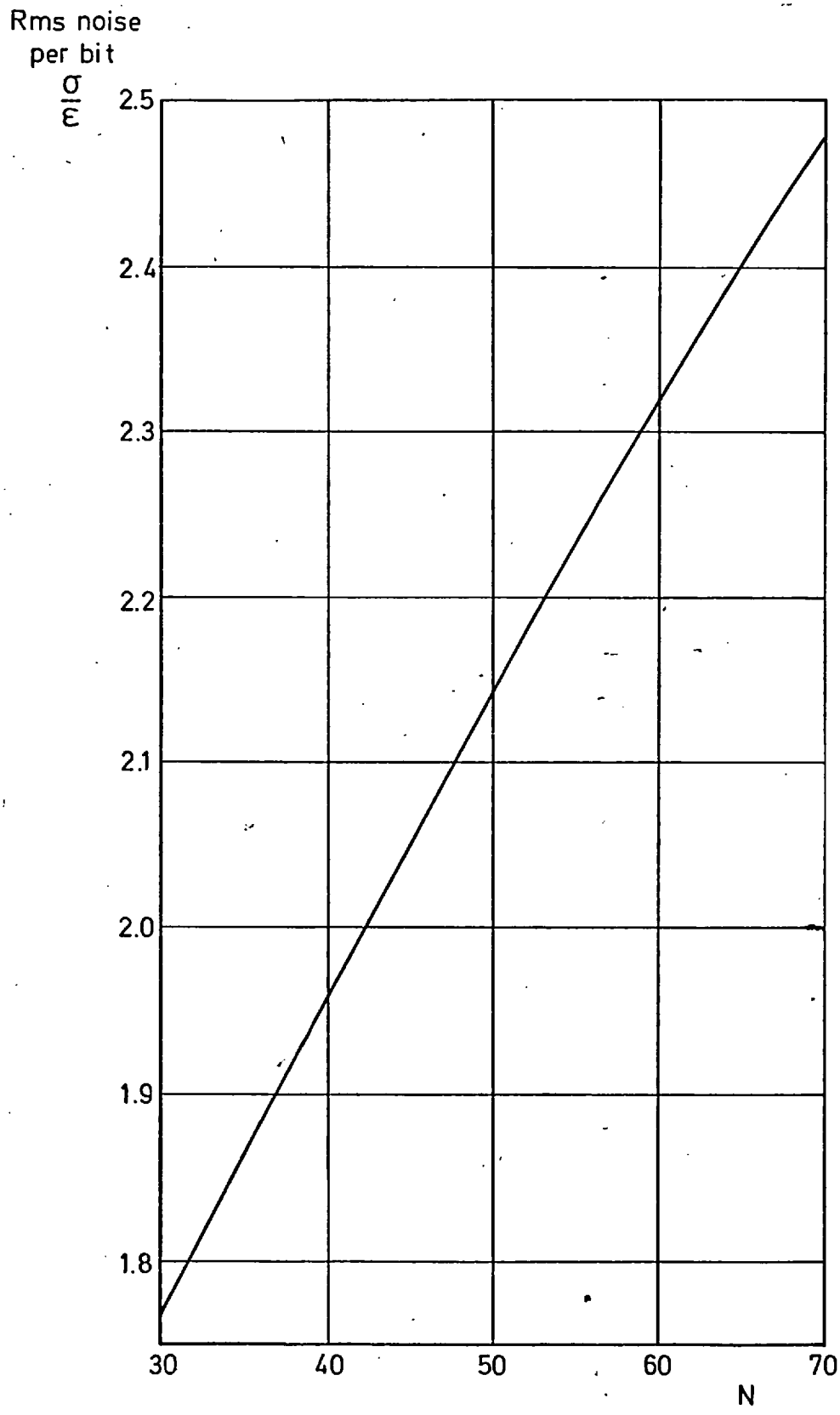


Fig.6.15 Multiplicative round off error – RMS output noise as a function of number of identical sections

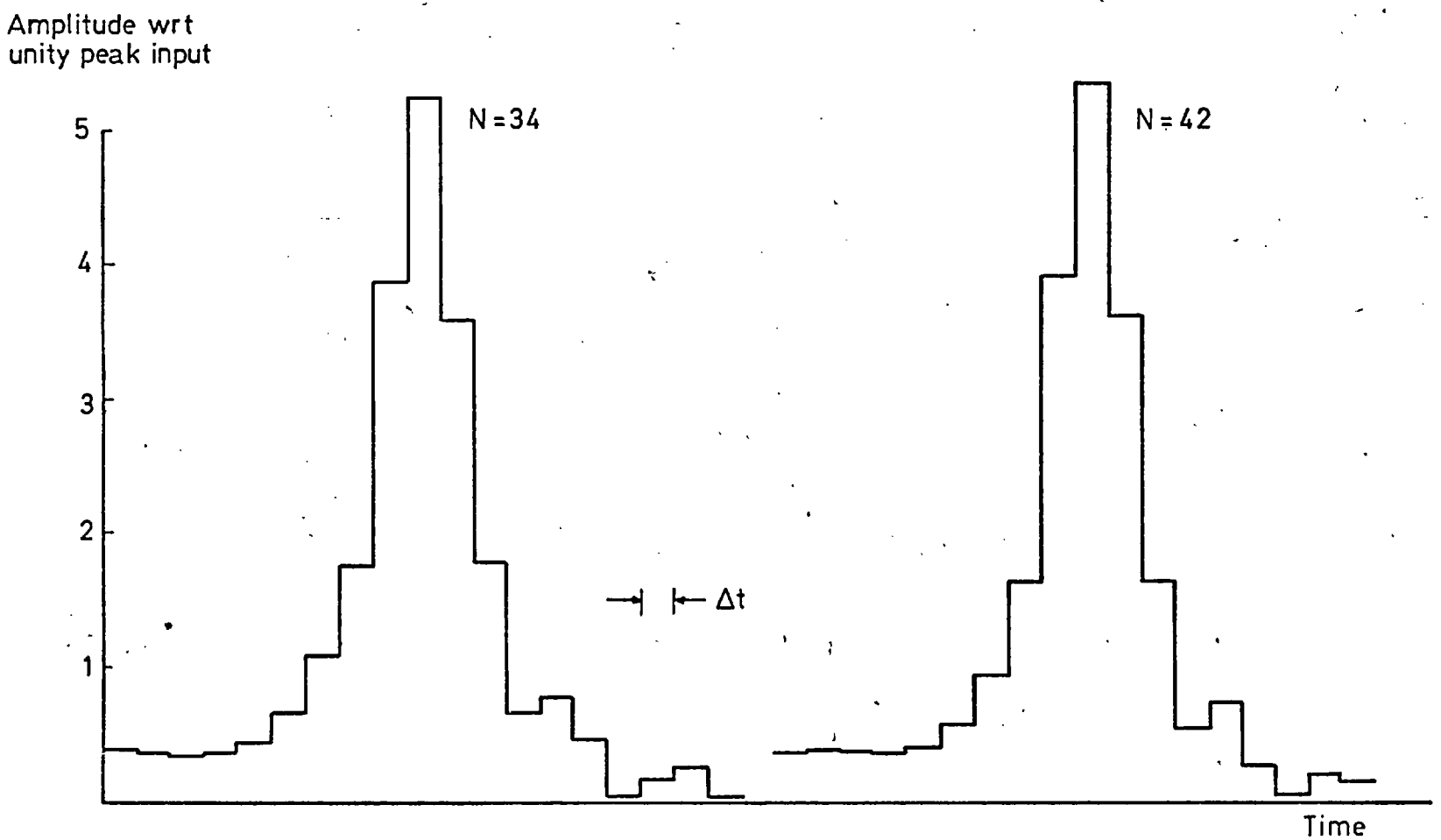


Fig.6.16 Compressed pulse envelopes - exact computation, no quantization
($\phi_{in}(t=o)=0$)

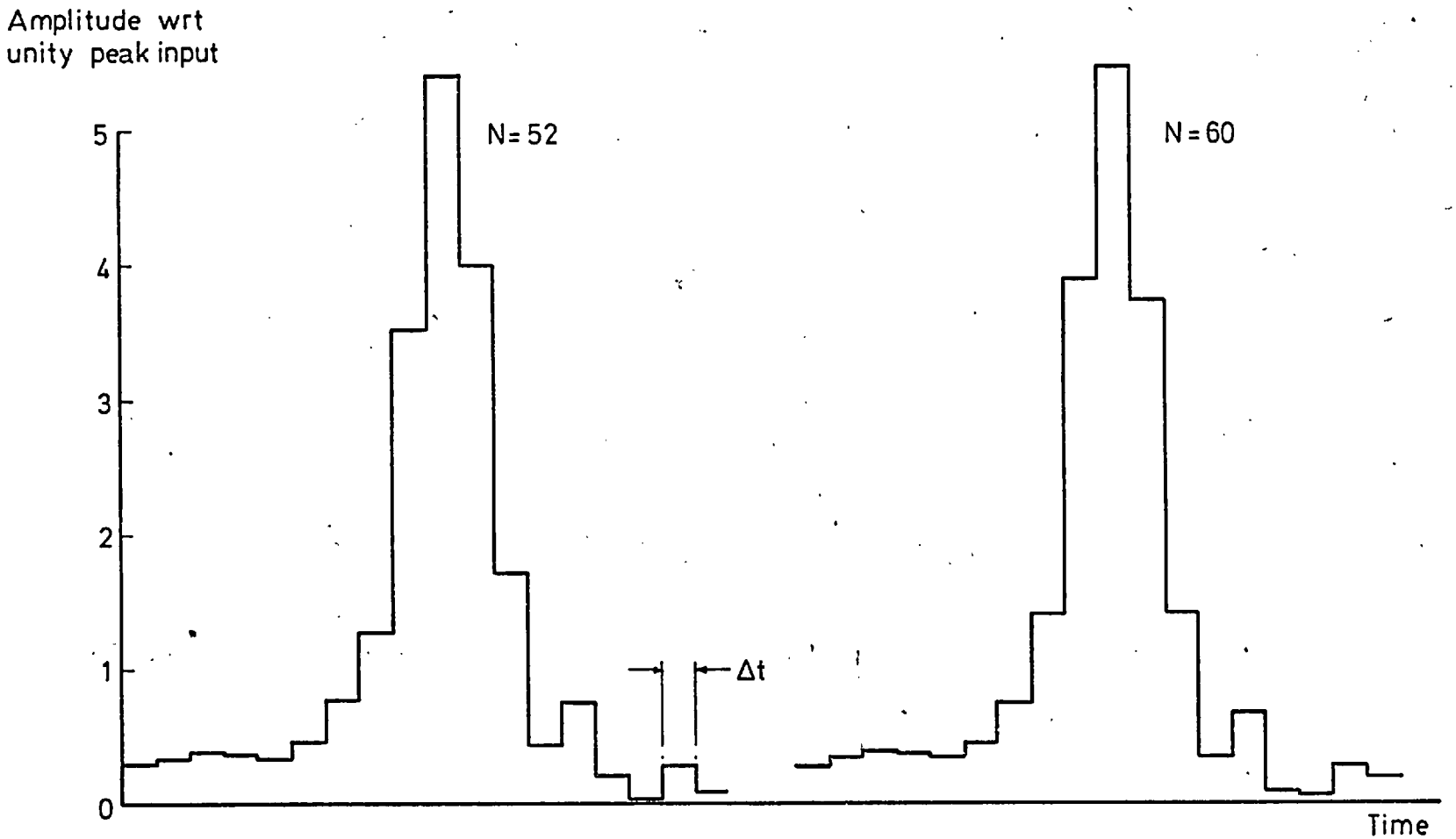


Fig.6.17 Compressed pulse envelopes - exact computation, no quantization
($\phi_{in}(t=o)=0$)

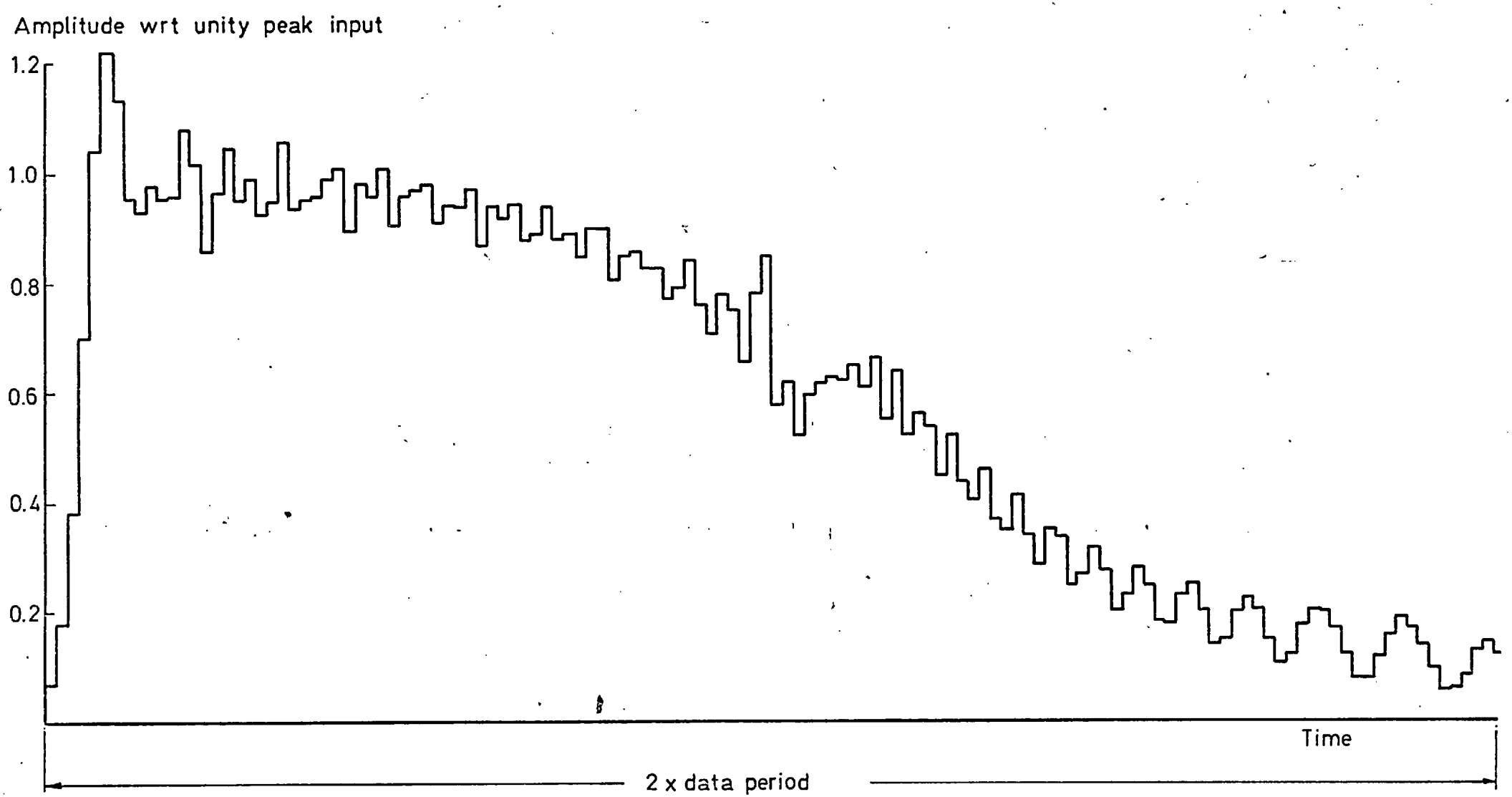


Fig.6.18 Dispersed pulse envelope - digital system N = 34

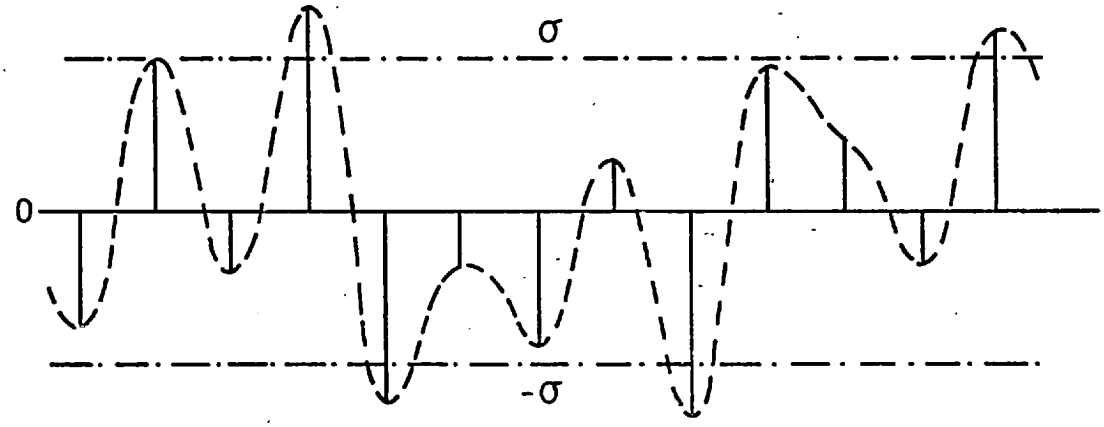


Fig.6.19 Uniform gaussian noise containing no frequencies higher than F, synthesised from random samples

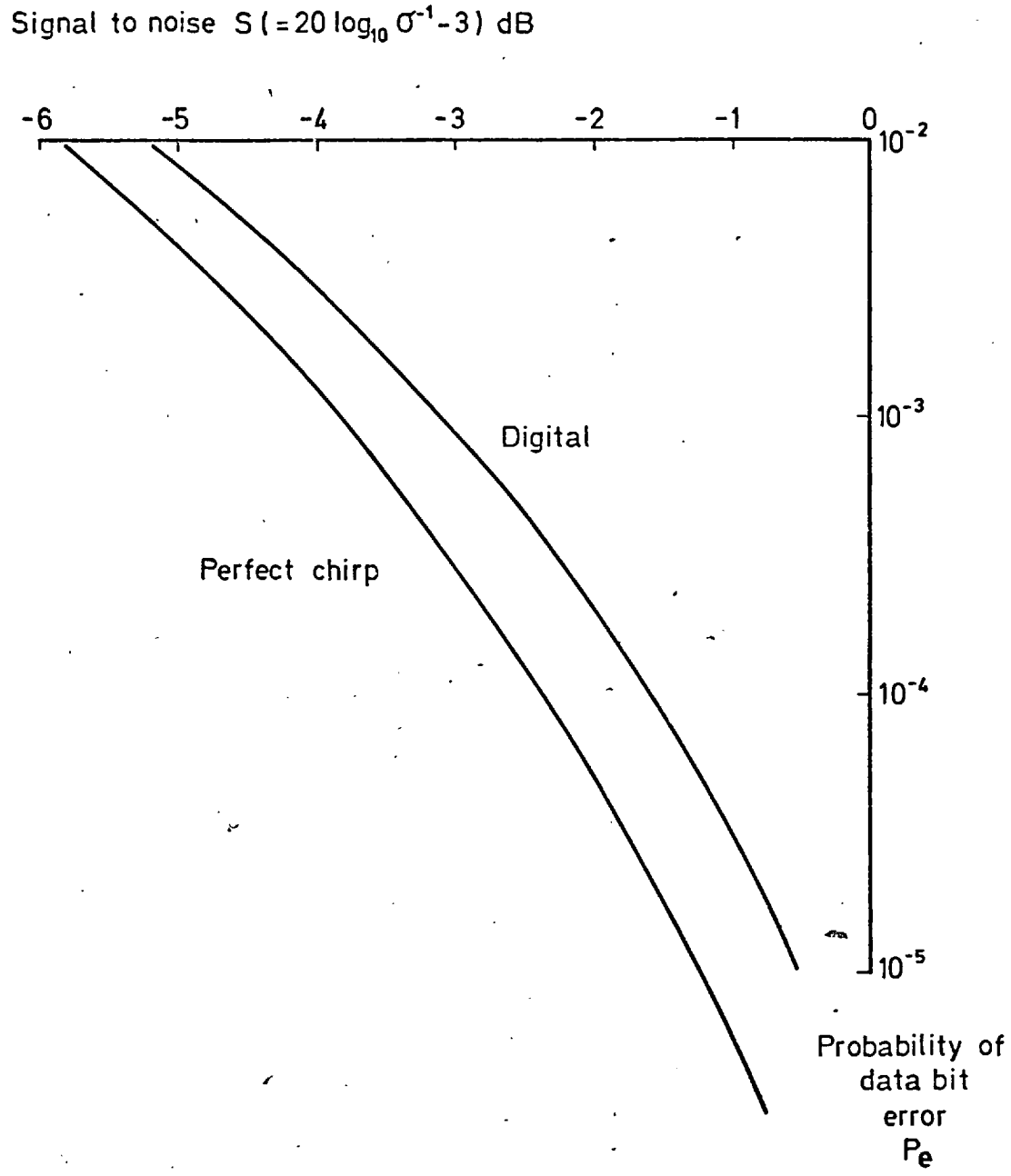


Fig.6.20 Error probability for 42 section digital system (synchronised) FT=33.33

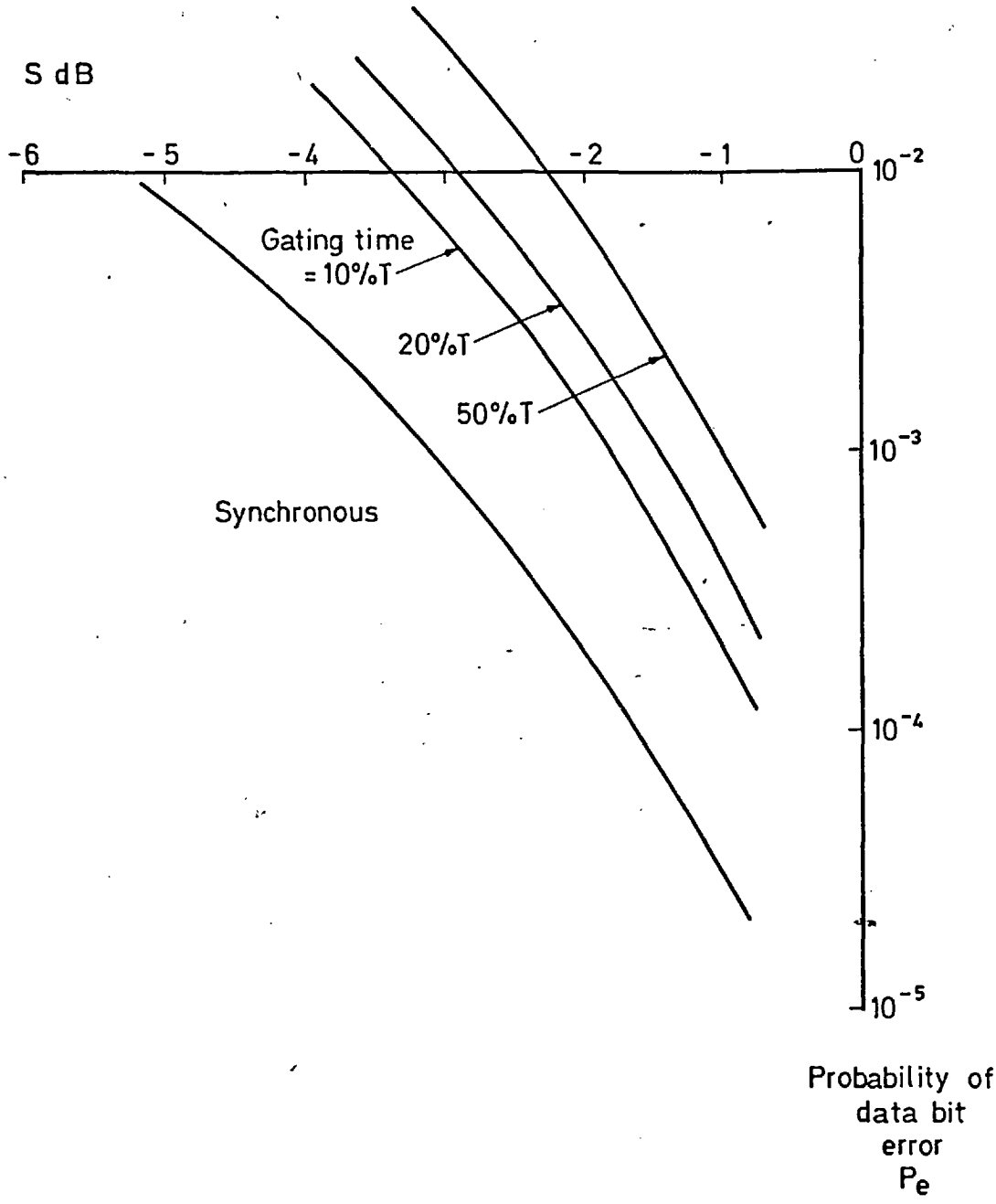


Fig.6.21 Error probability for various gating times (N=42).

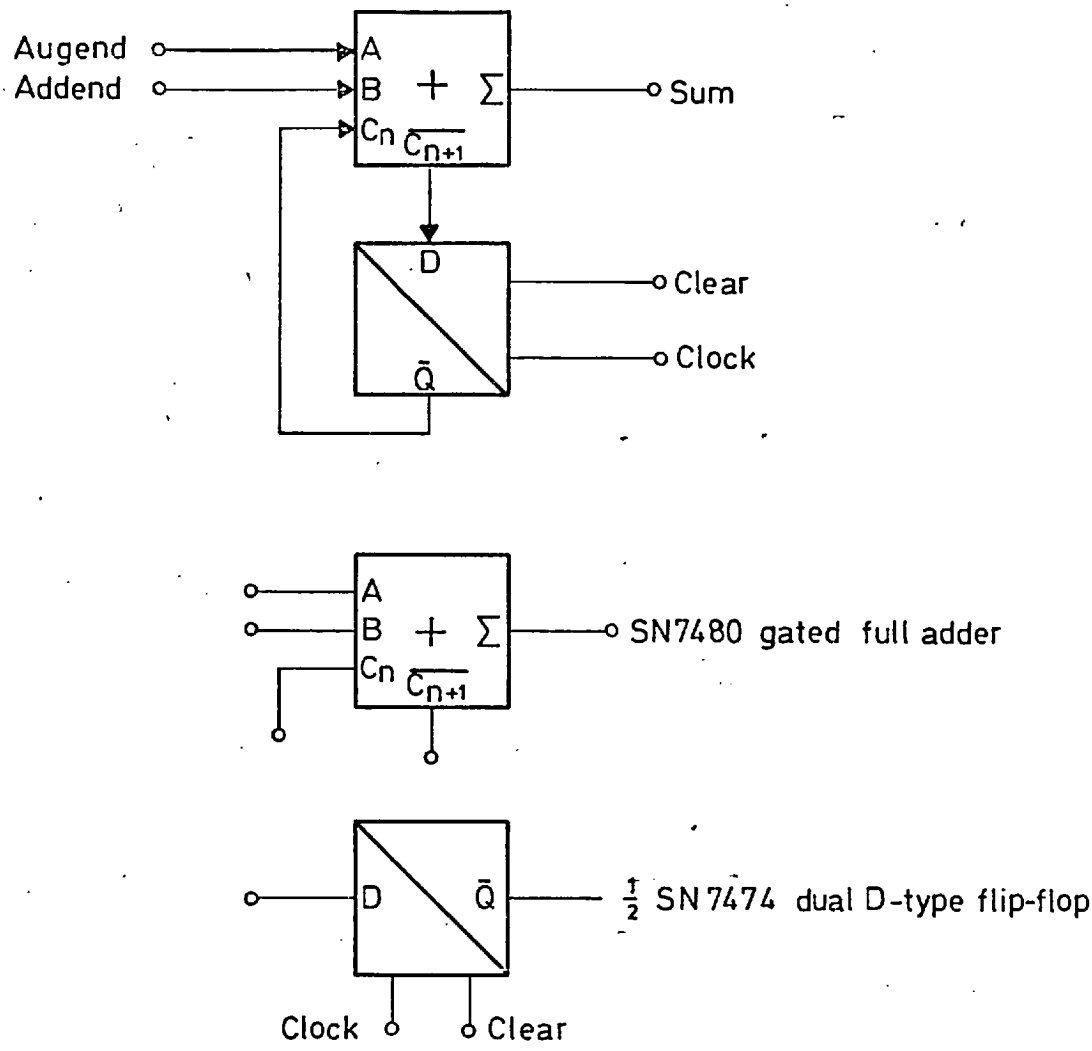


Fig. 7.1 Practical serial adder

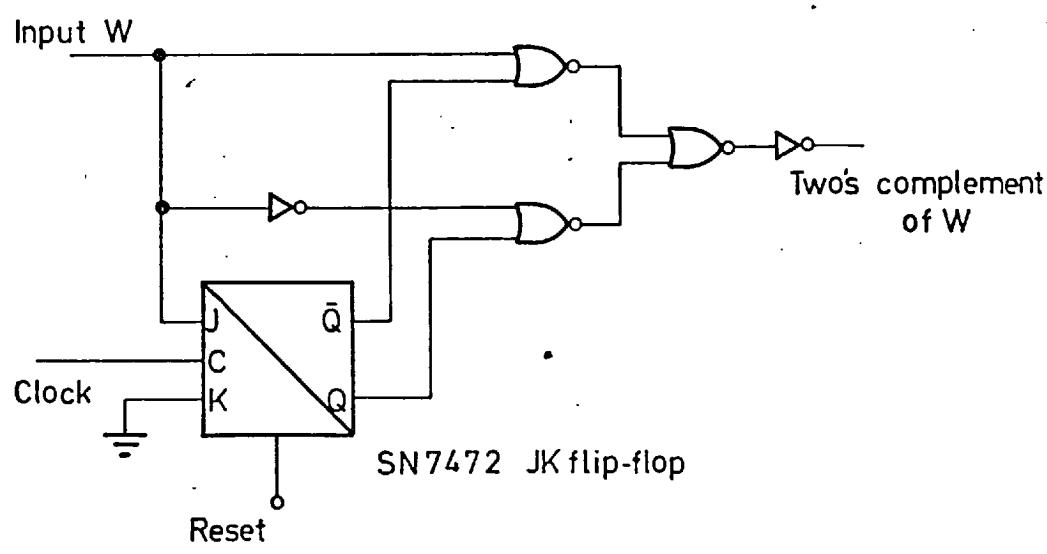


Fig. 7.2 Practical two's complementer

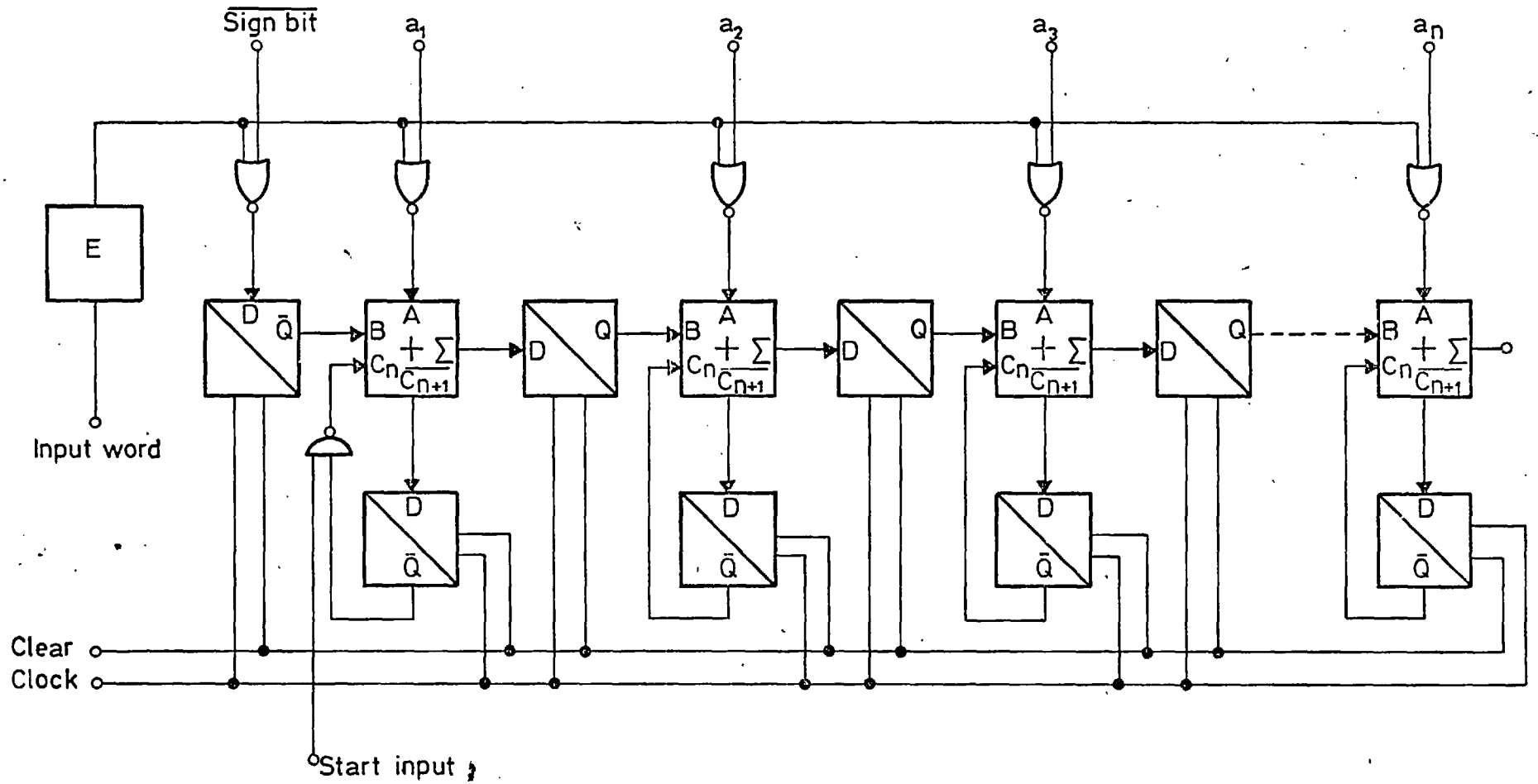


Fig.7.3 Serial/parallel multiplier scheme

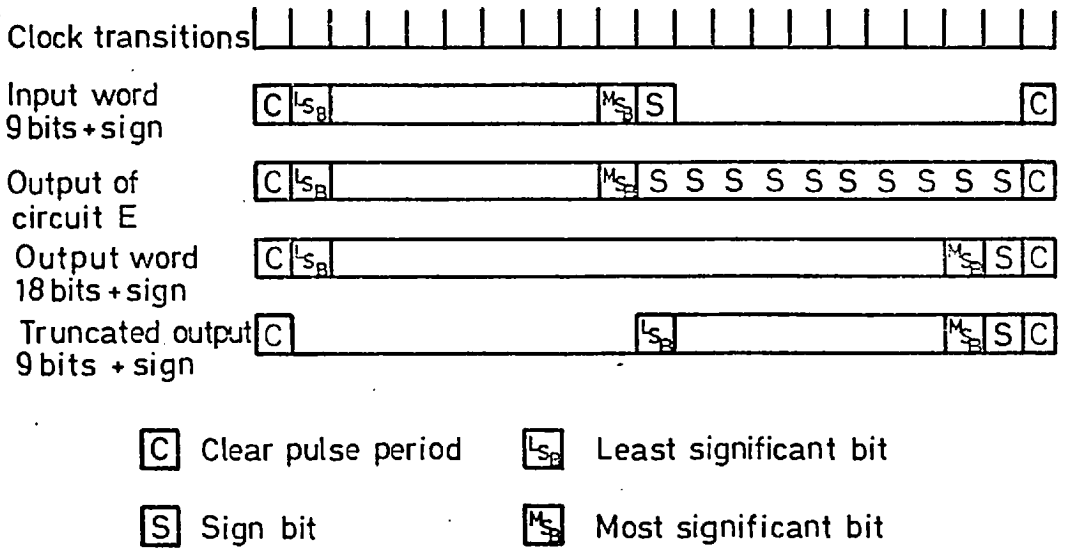


FIG 7.4 Timing diagram for serial/parallel multiplier

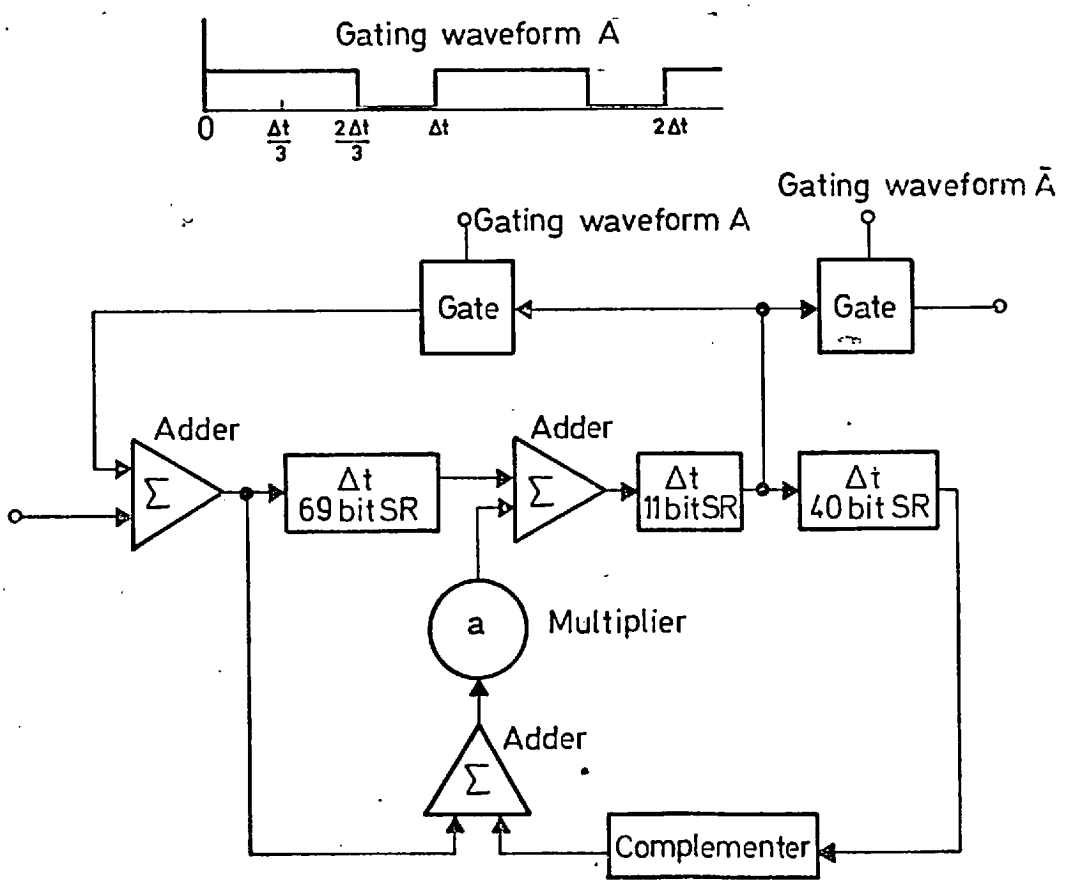


Fig.7.5 Multiplexed or recirculating first order digital delay section

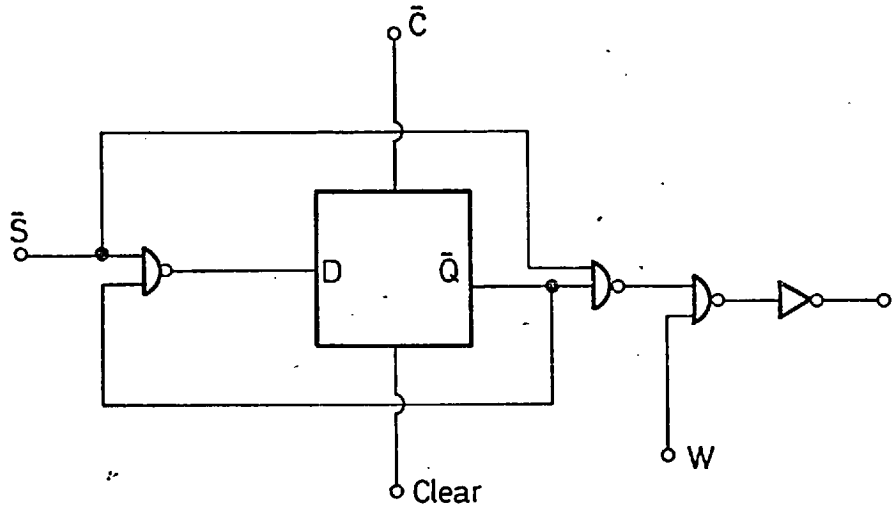
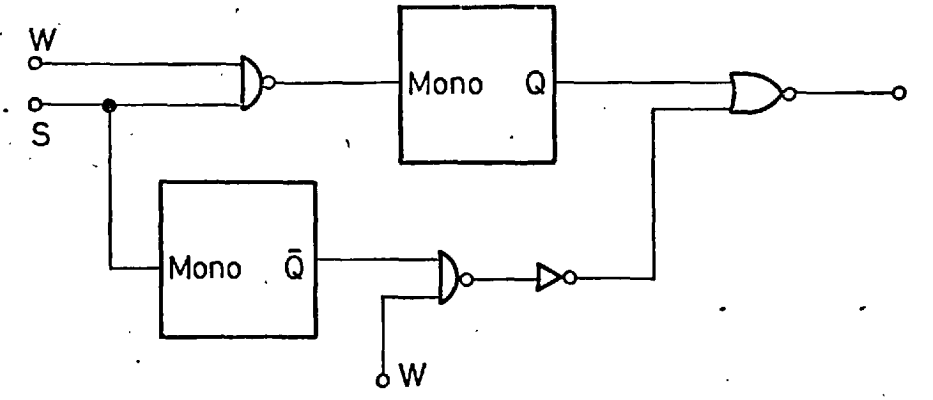
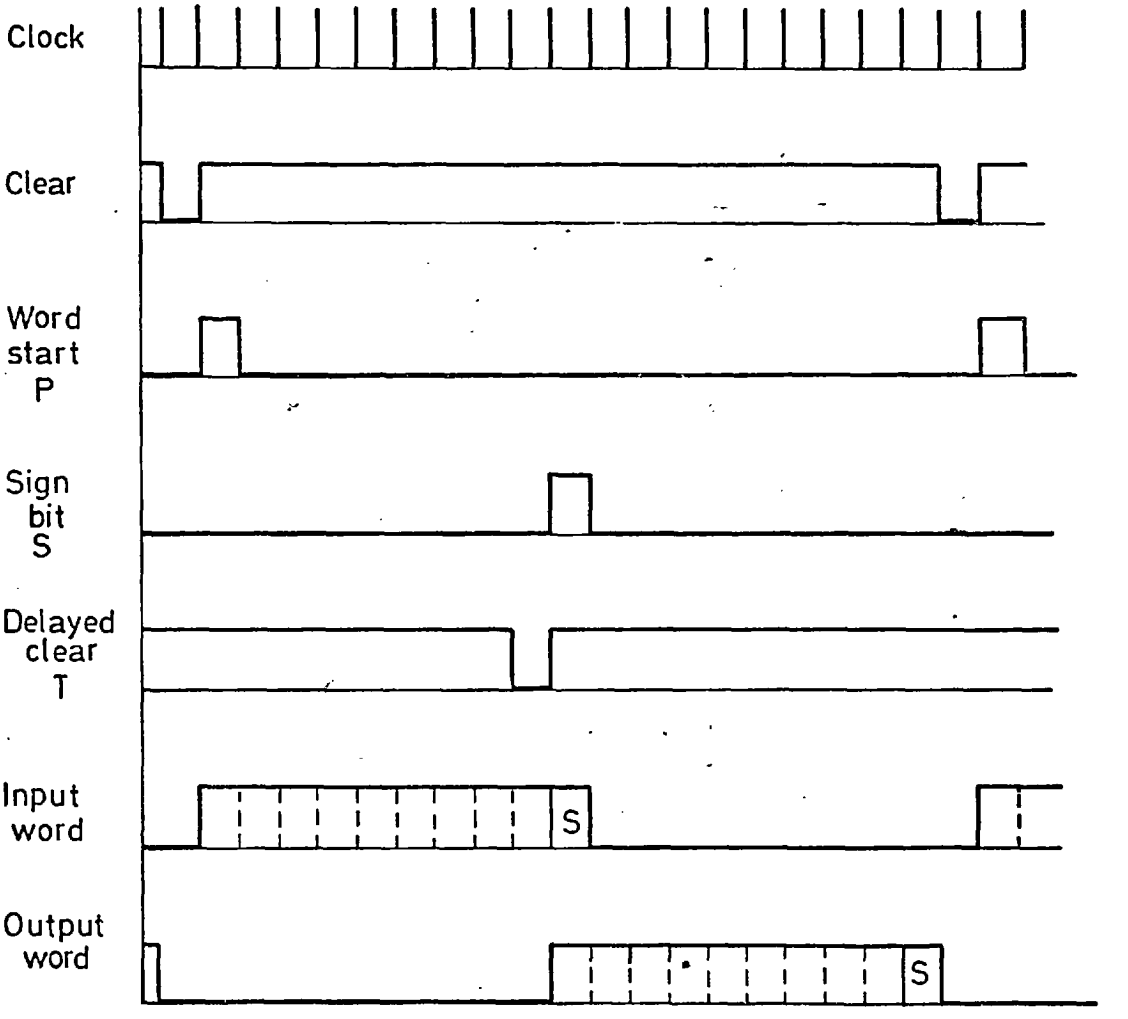


Fig. 7.6 Multiplier truncation circuit



(a) Circuit E



(b) Control waveforms

Fig.7.7 Multiplier sign bit detection and extension circuit (E) and control waveforms

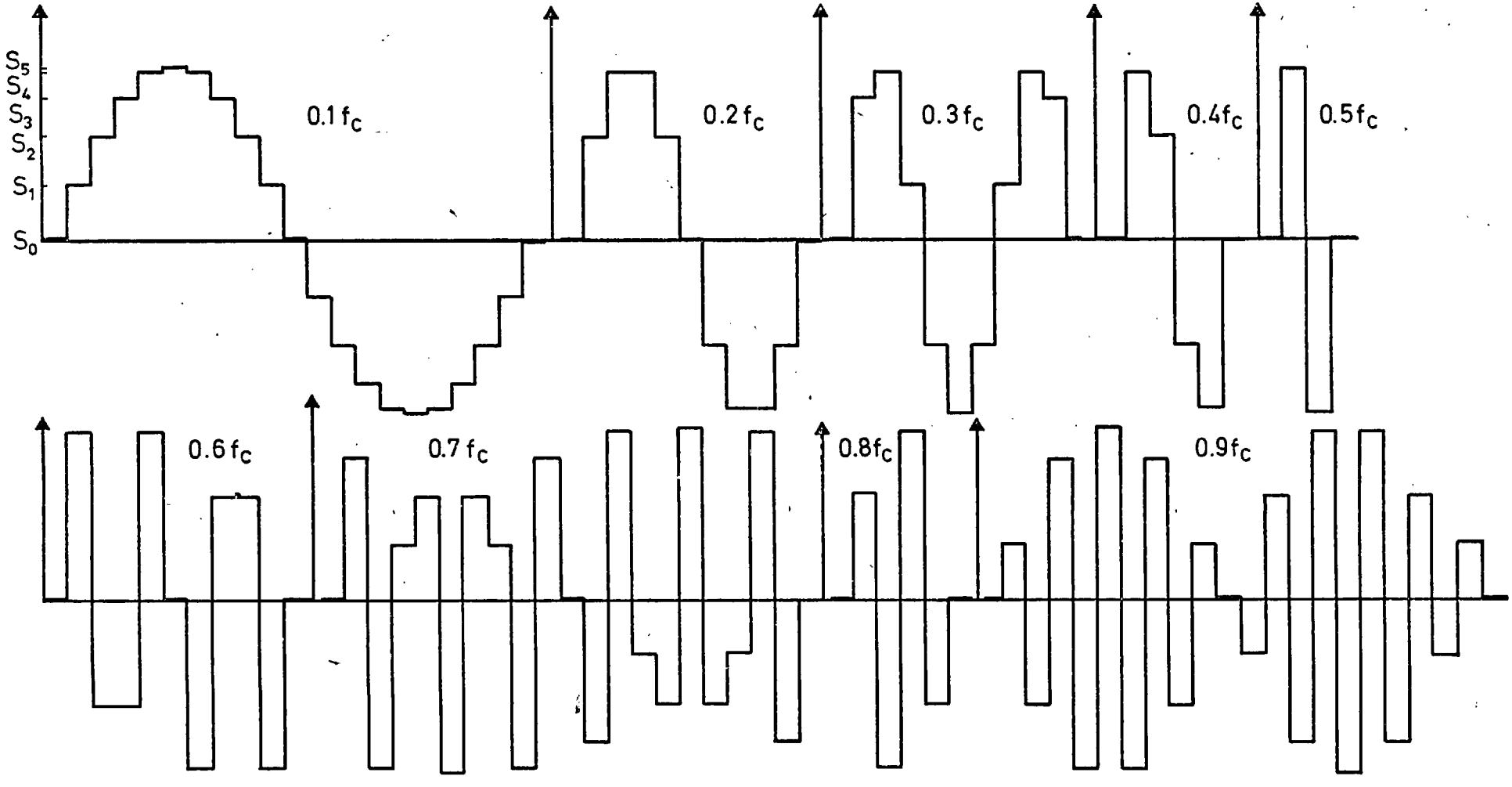


Fig.7.8 Sample sequences generated by test signal generator

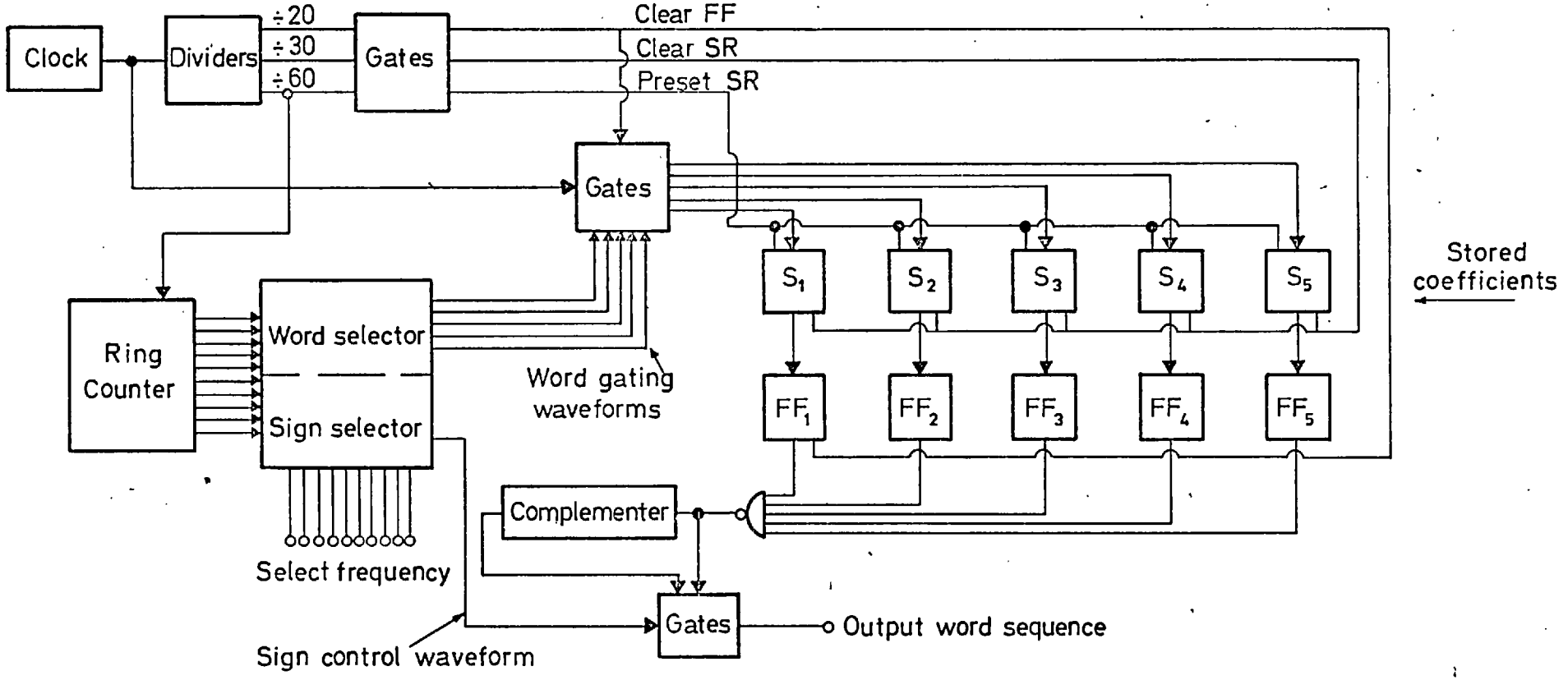


Fig.7.9 Block diagram of test signal generator

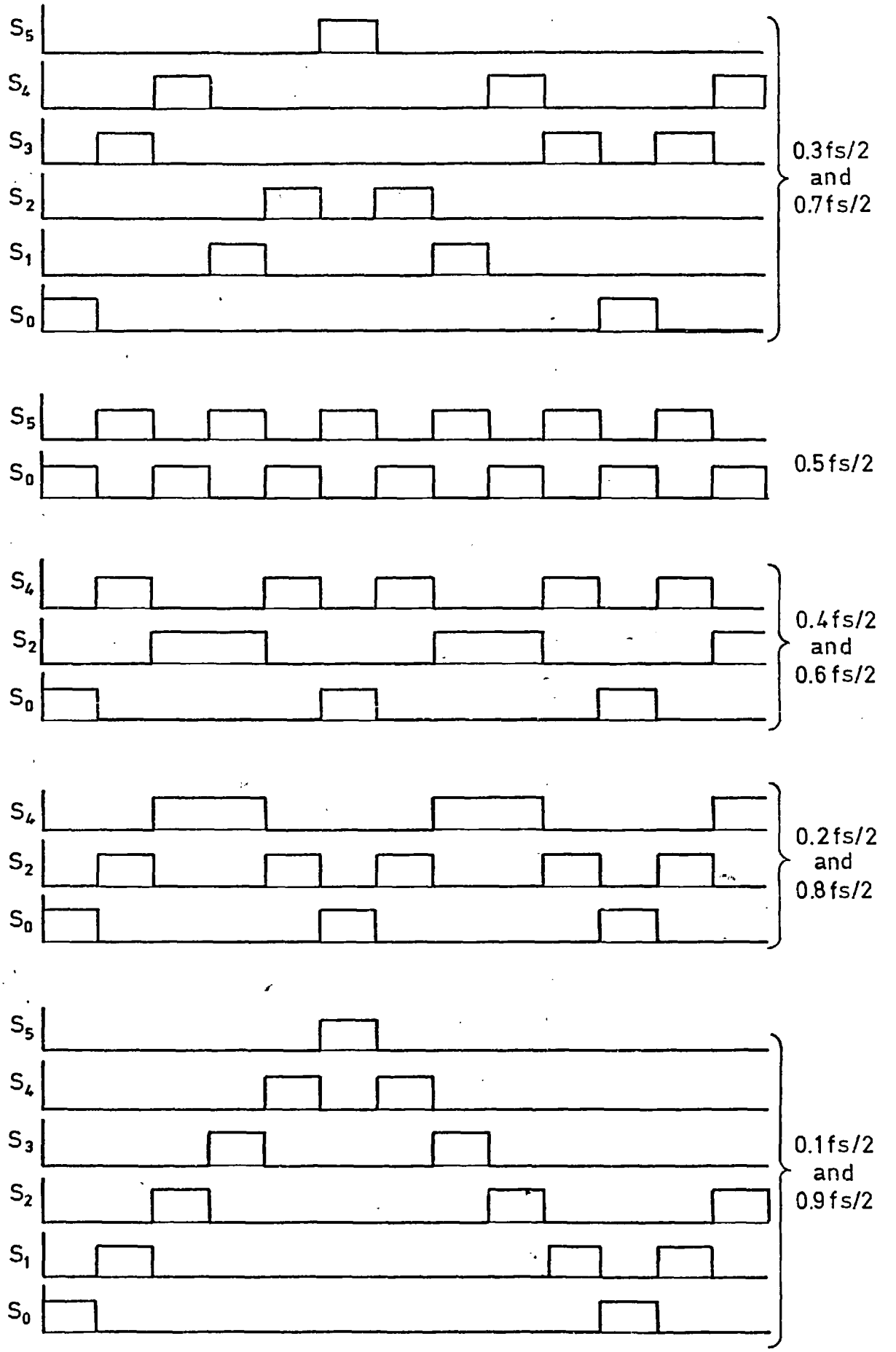


Fig.7.10 Test signal generator – word gating waveforms

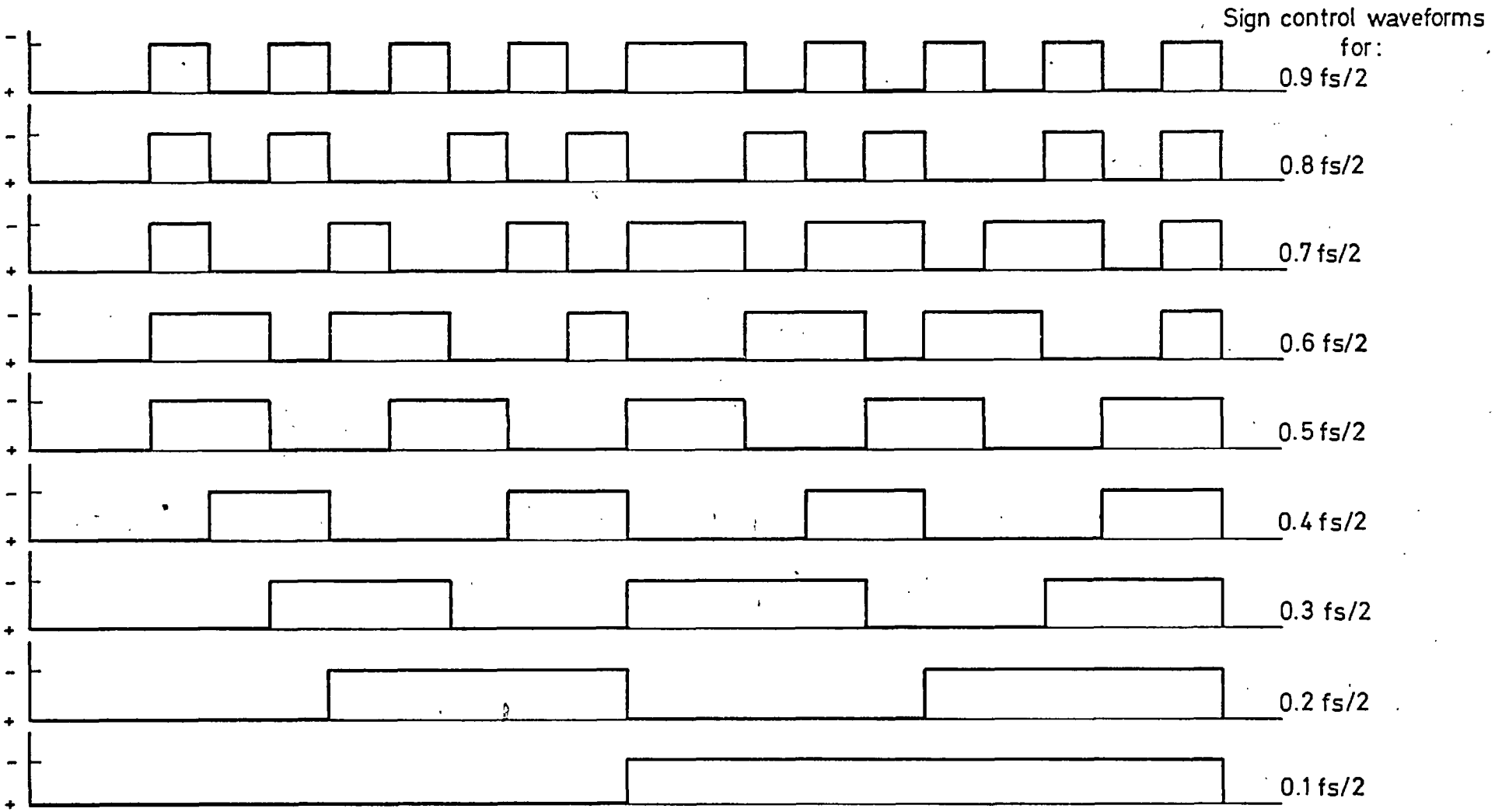


Fig. 7.11 Test signal generator - word sign control waveforms

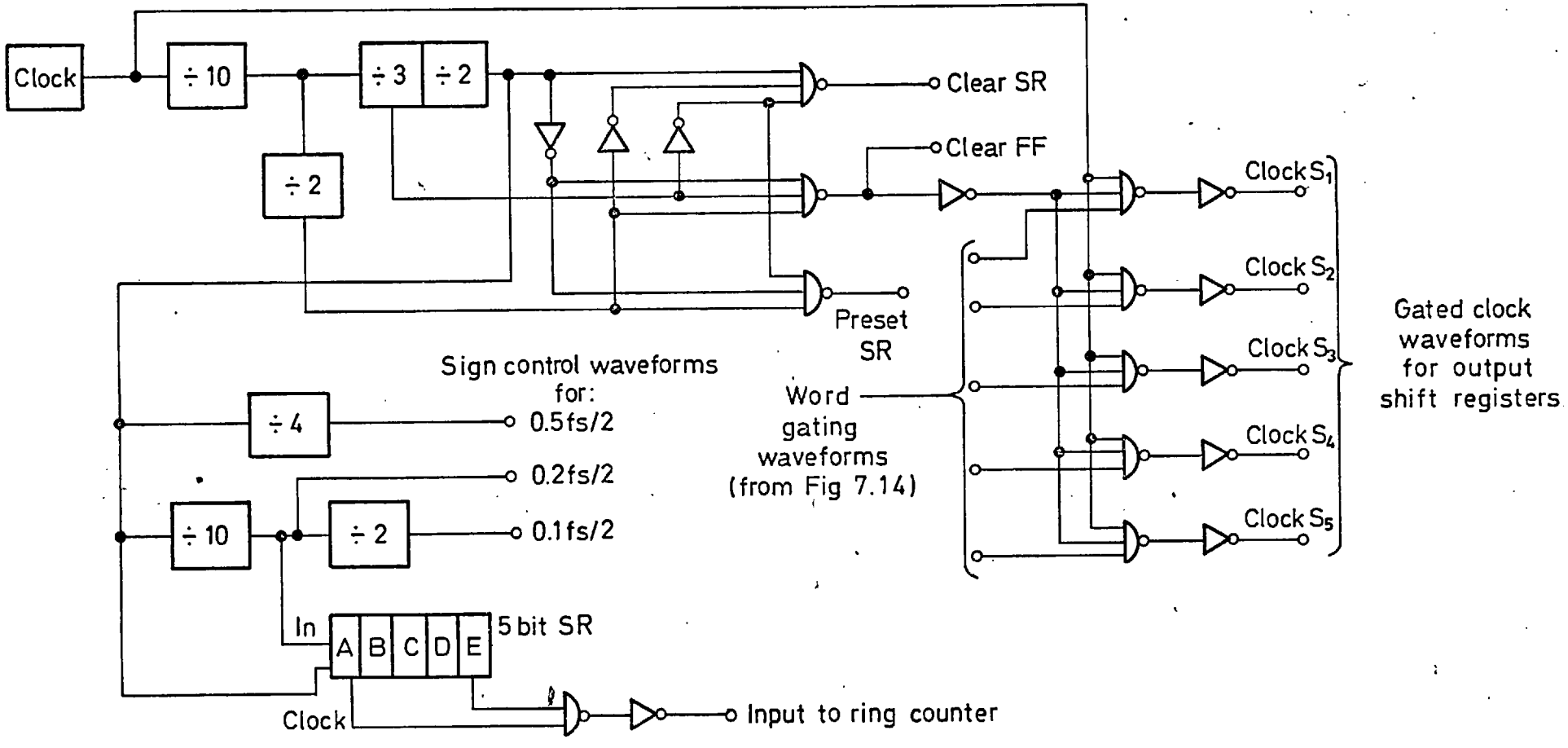


Fig.7.12 Test signal generator - timing and control waveform circuit

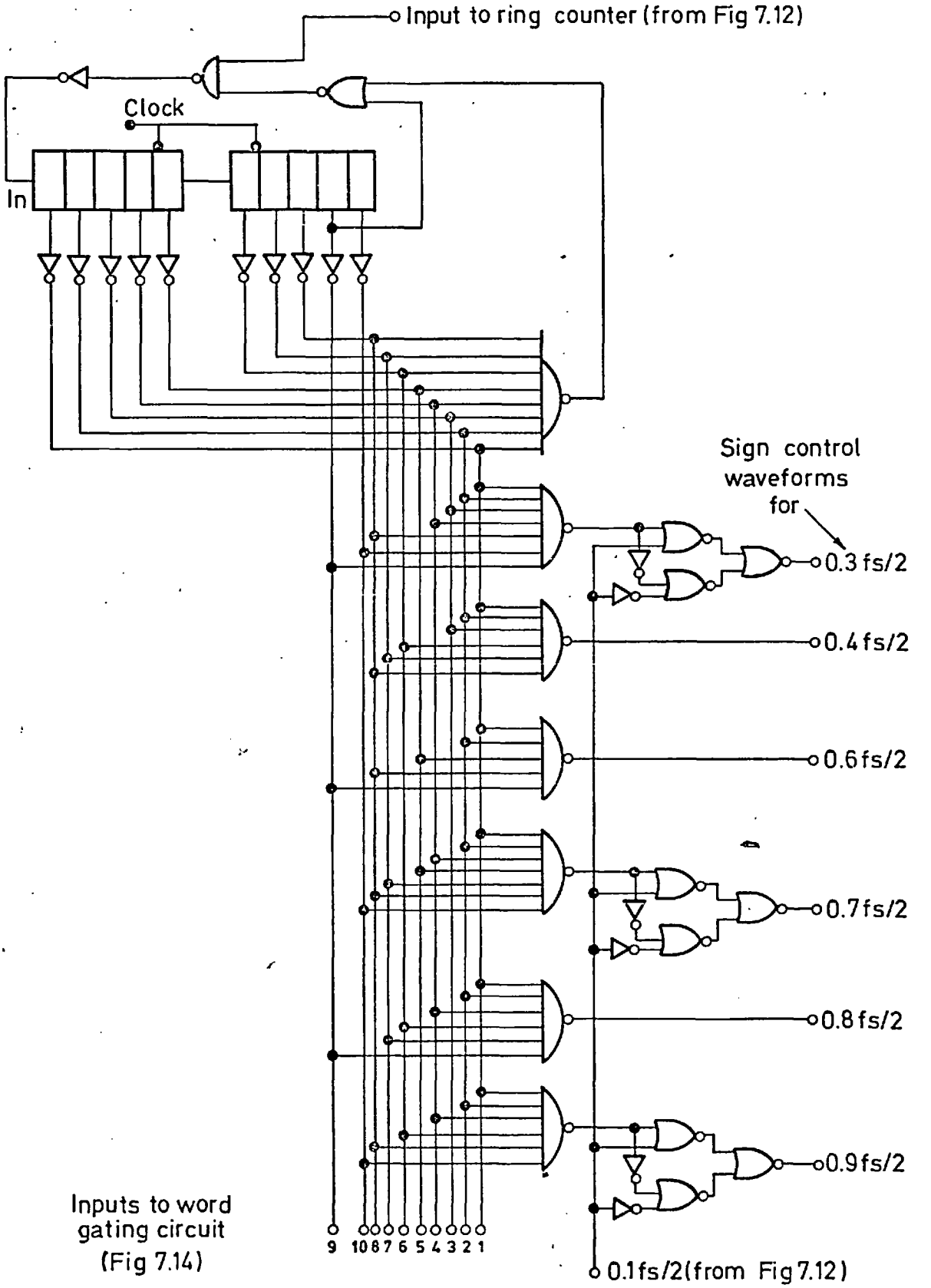


Fig.7.13 Test signal generator - sign control circuit

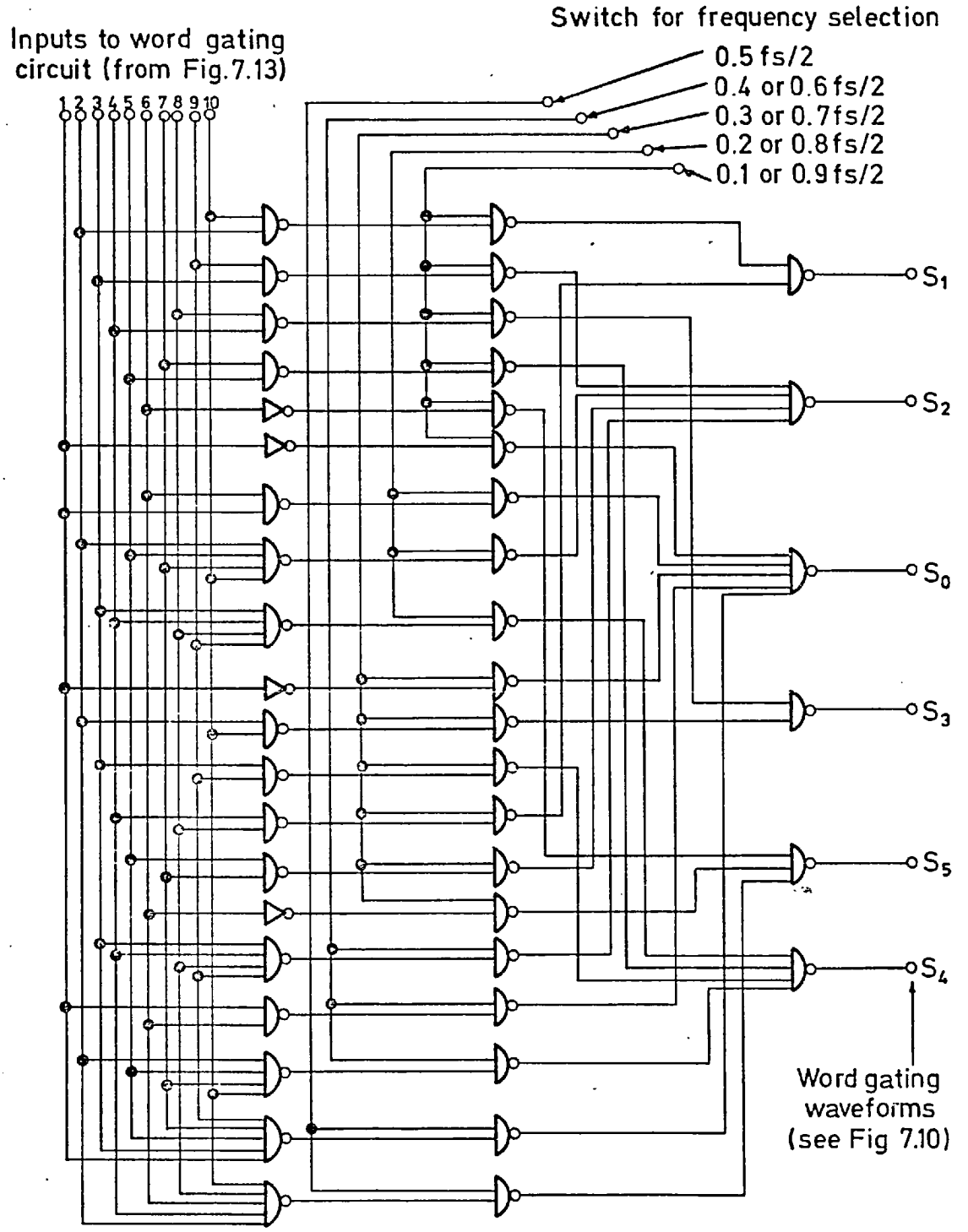


Fig.7.14 Test signal generator - word gating waveform circuit

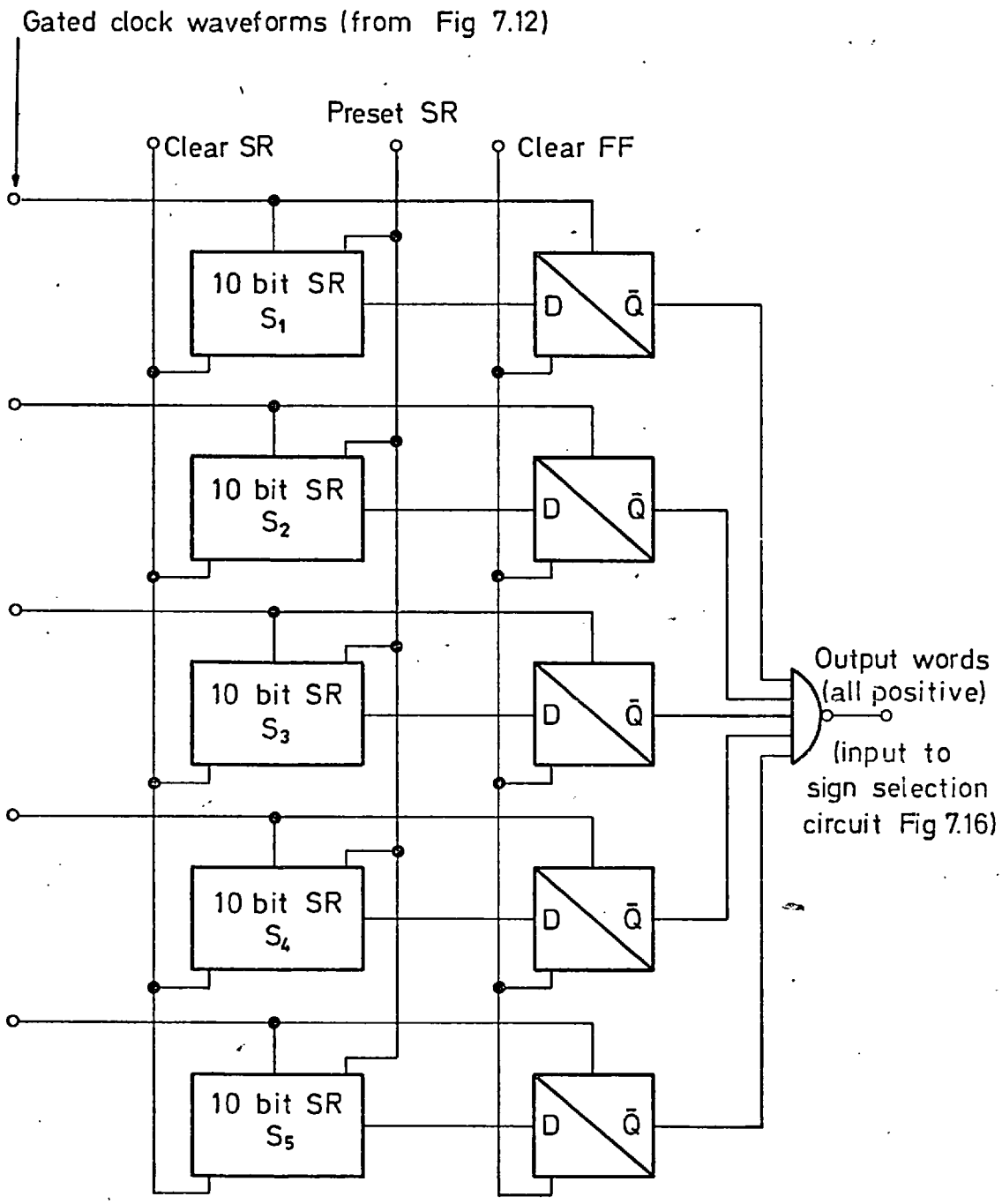


Fig.7.15 Test signal generator - stored samples and output shift registers

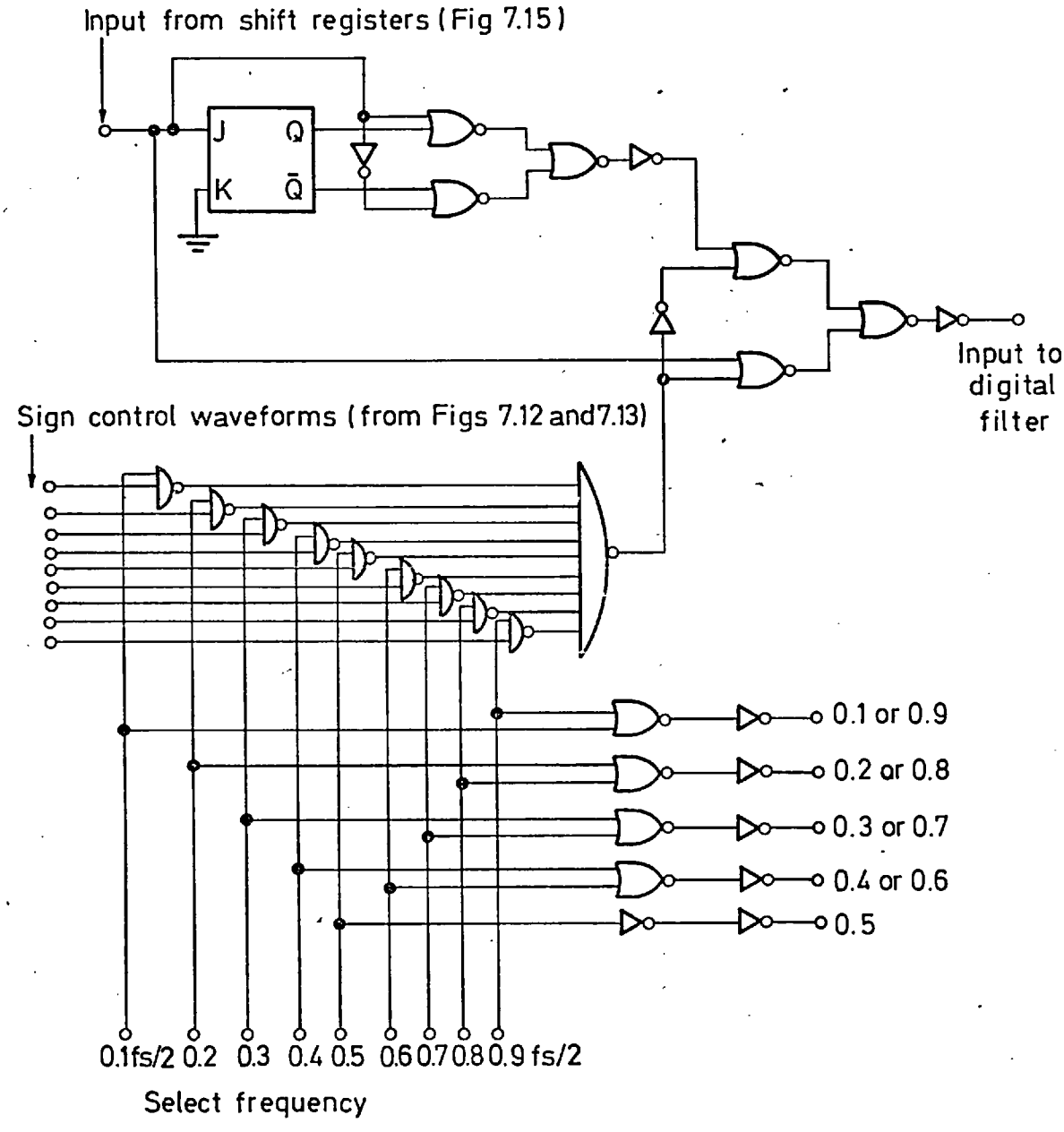


Fig 7.16 Test signal generator - sign selection circuit

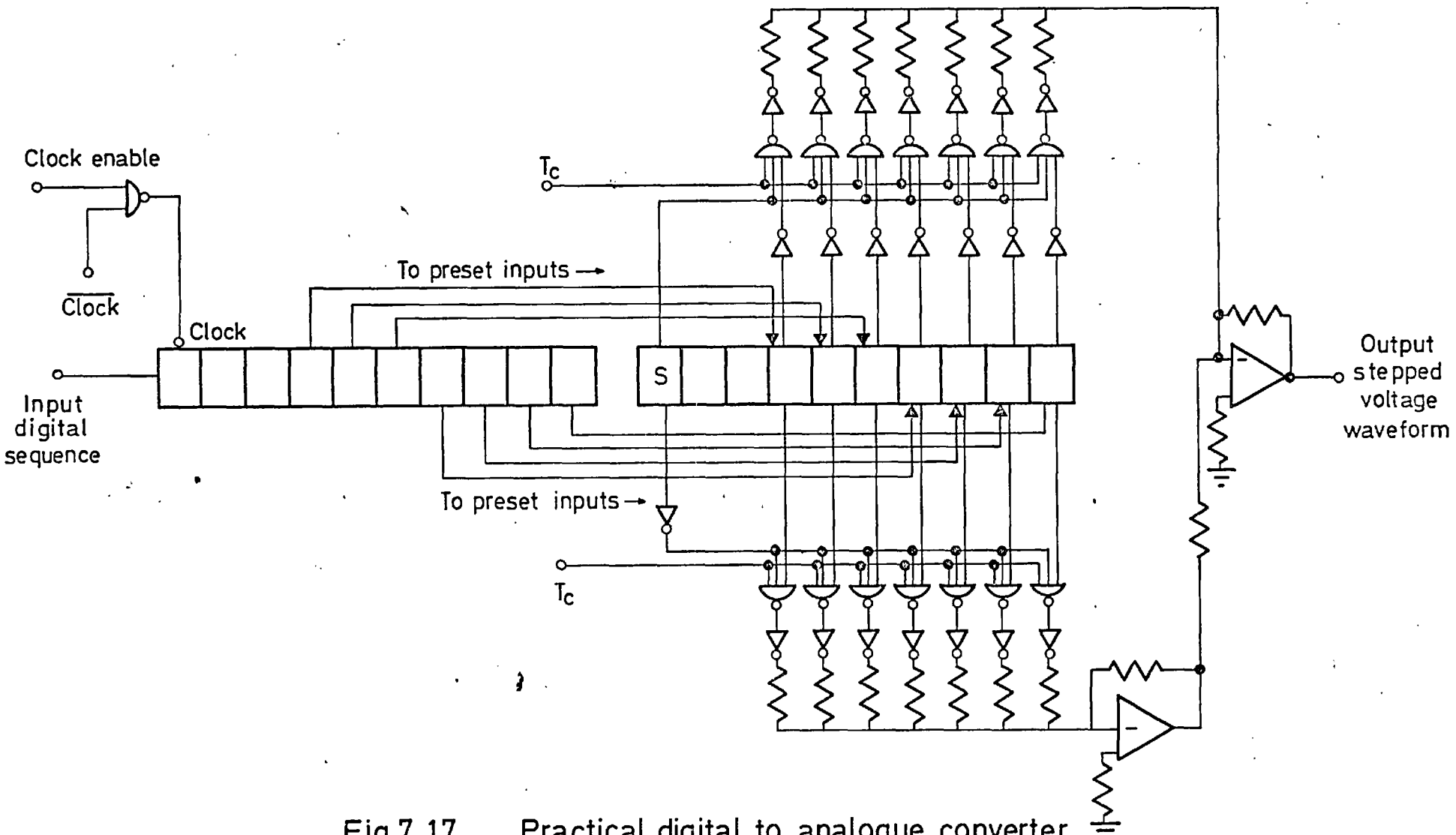
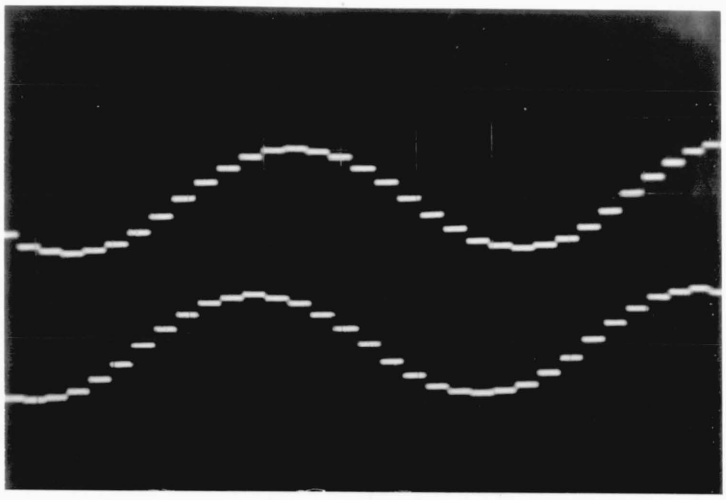


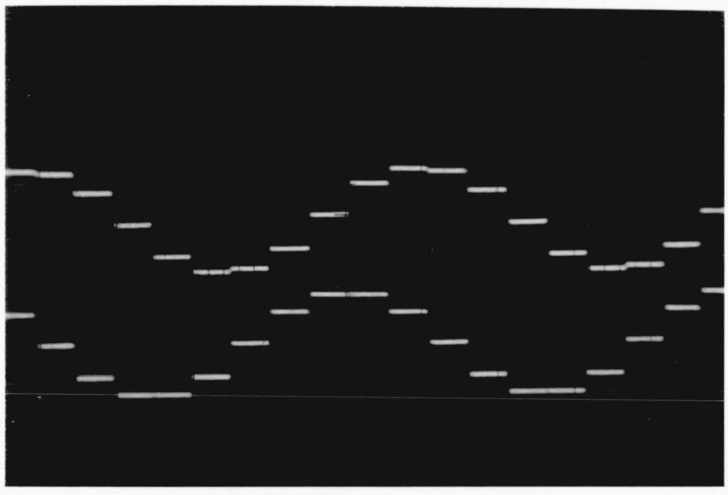
Fig.7.17 Practical digital to analogue converter



Output

$f = 0.1\ f_s/_2$

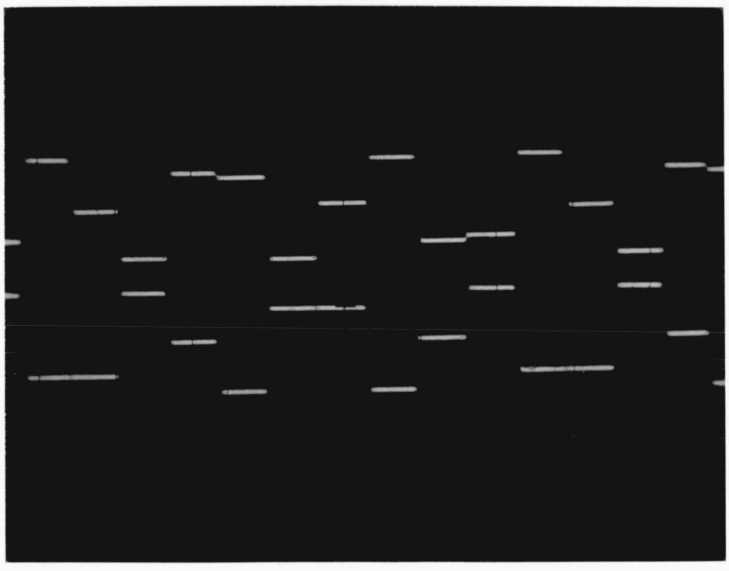
Input



Output

$f = 0.2\ f_s/_2$

Input



Output

$f = 0.6\ f_s/_2$

Input

FIG.7.18 - OSCILLOSCOPE PHOTOGRAPHS OF FILTER RESPONSE TO CONSTANT FREQUENCY SAMPLED WAVEFORMS FROM TEST SIGNAL GENERATOR

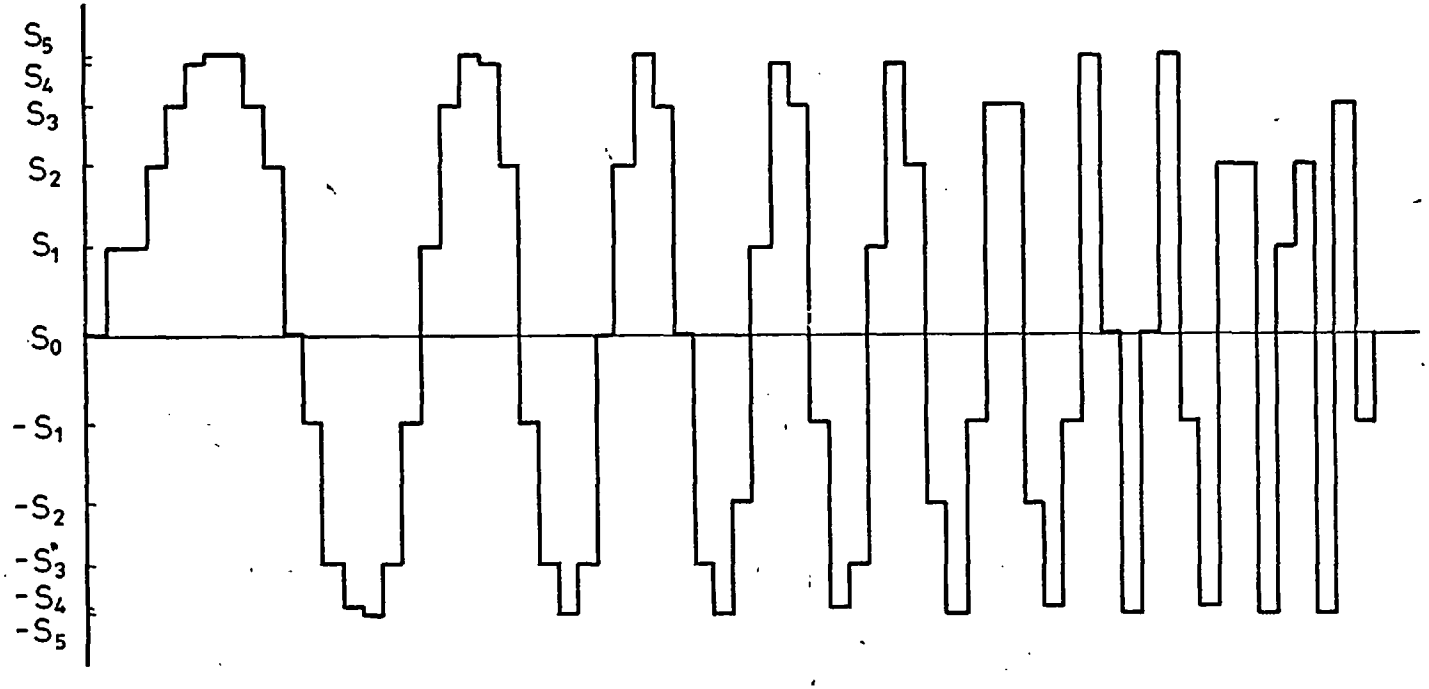


Fig. 7.19 Approximate sampled waveform generated as input to digital pulse compression filter

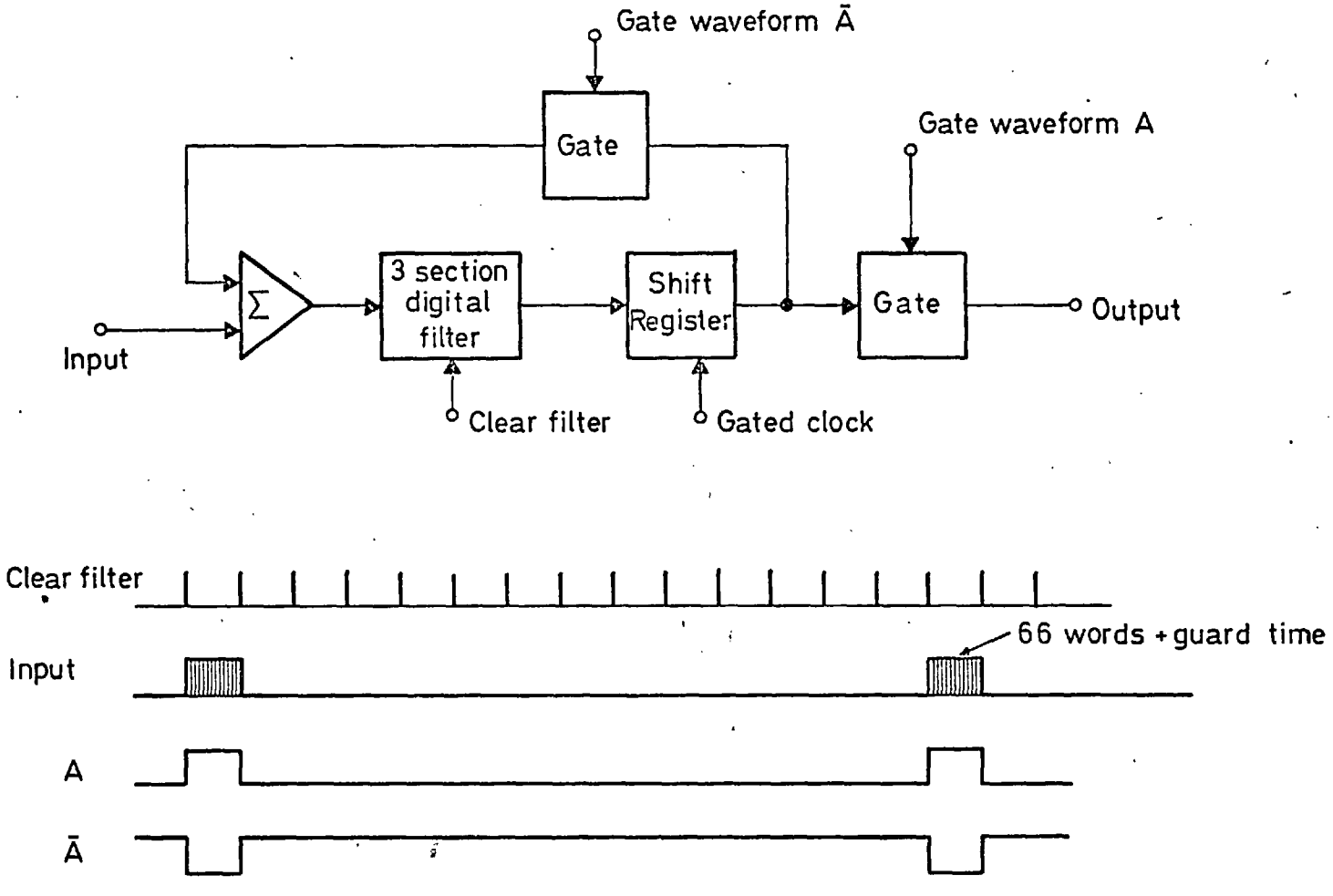


Fig.7.20 Simulation of 42 section filter using 14 times recirculation, with control waveforms

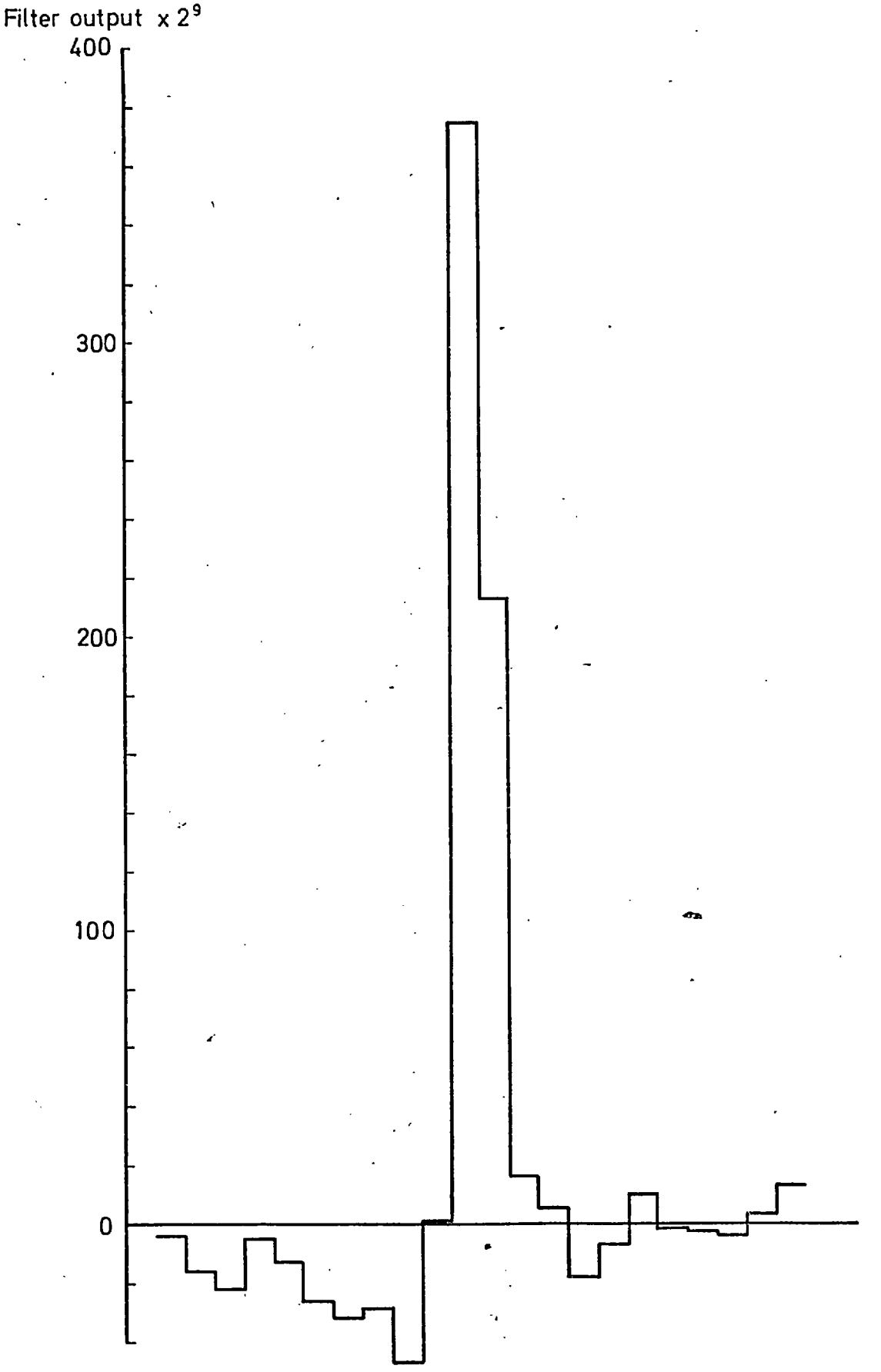
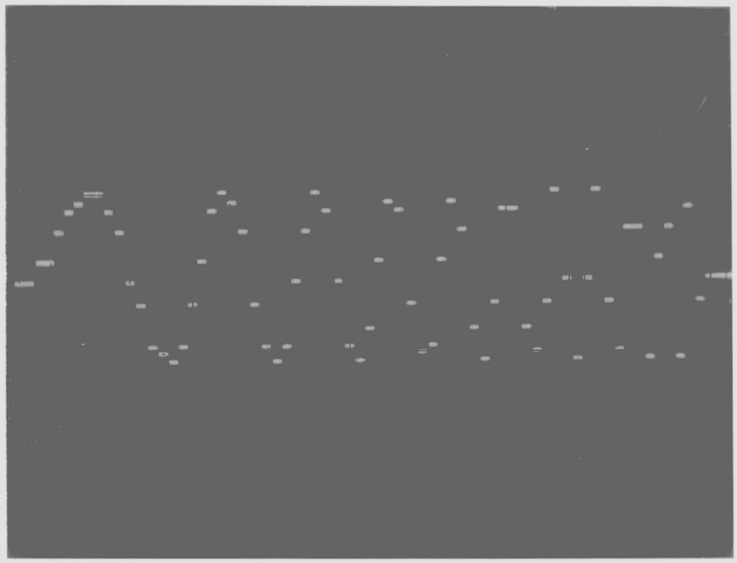
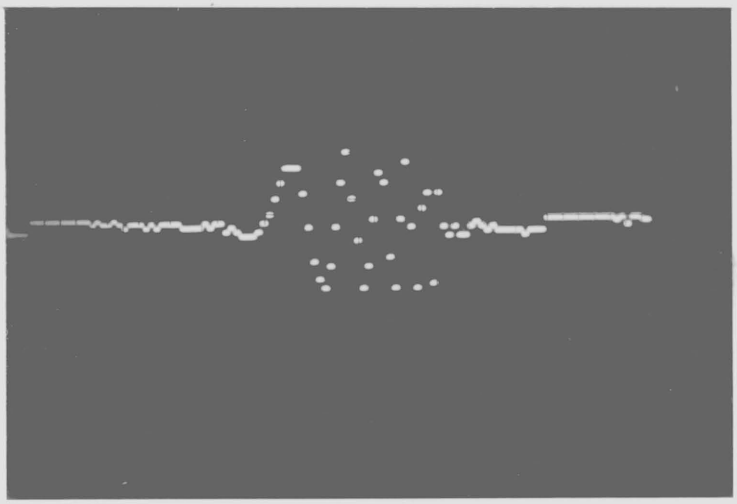


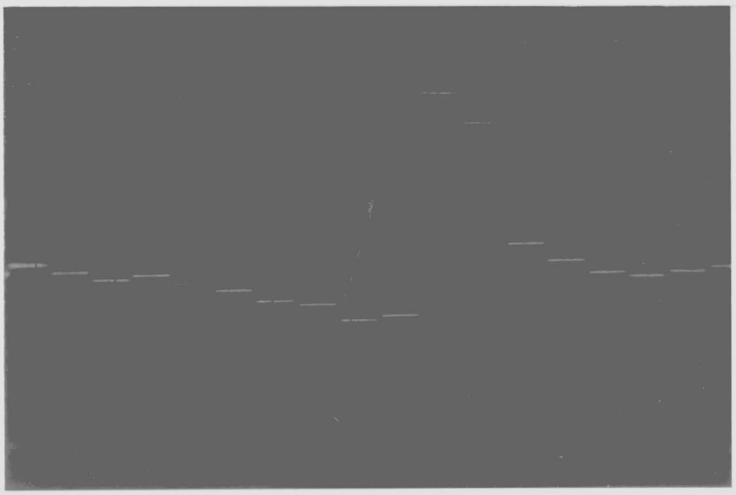
Fig.7.21 Output from 42 sections - response to approximated swept waveform (Fig 7.19) (computed response - true truncation)



Input
(cf. Fig.7.19)



Output from
21 sections



Output from
42 sections
(cf. Fig.7.23)

FIG.7.22 - OSCILLOSCOPE PHOTOGRAPHS OF APPROXIMATE SWEEP AND COMPRESSED PULSE

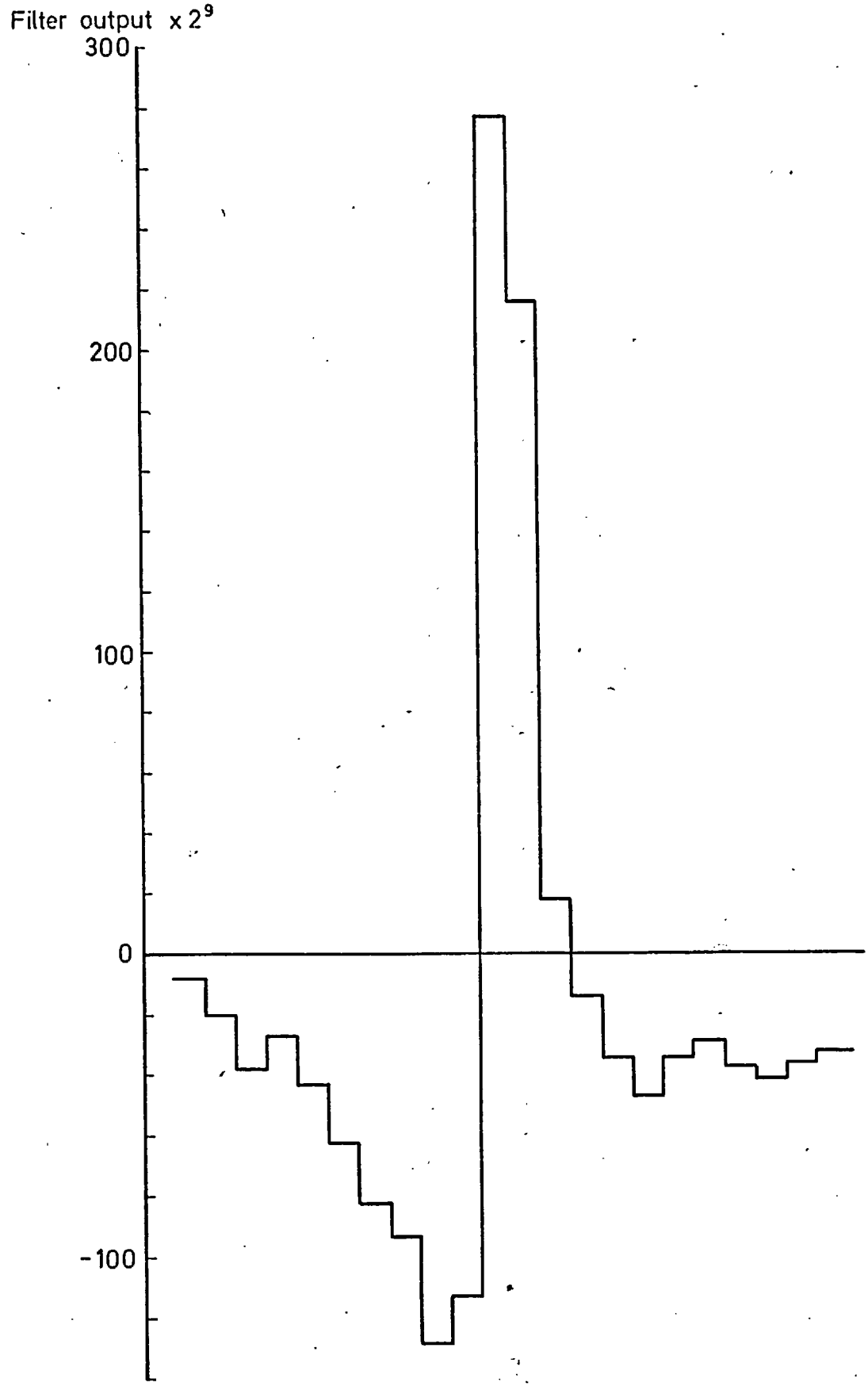
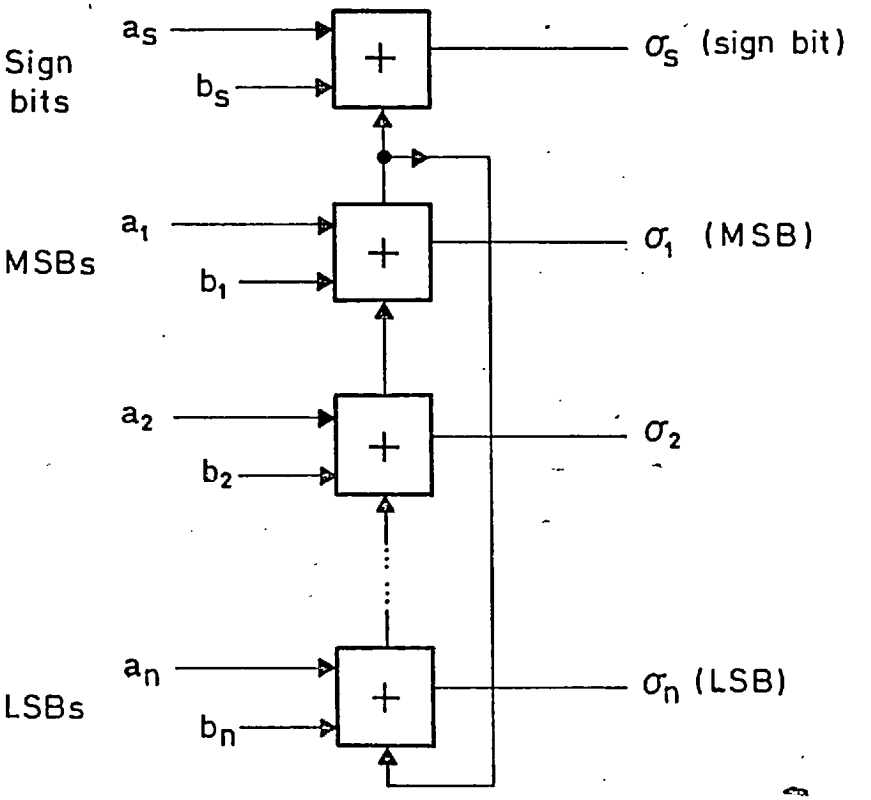
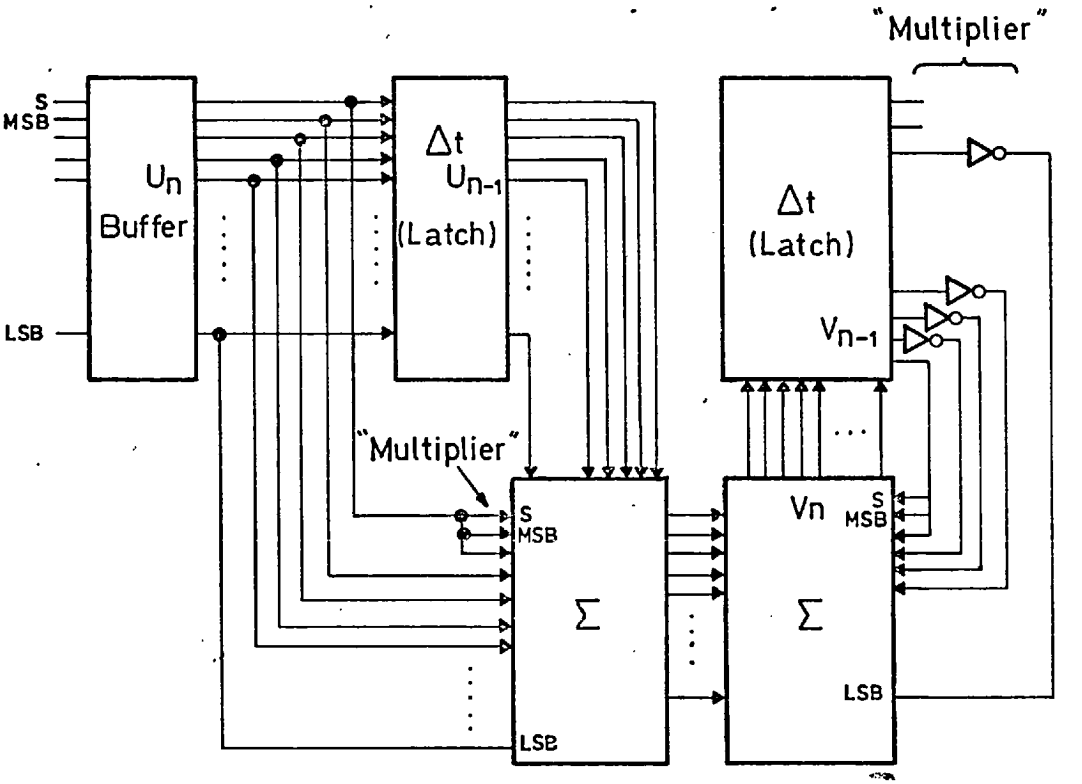


Fig.7.23 Output from 42 sections - response to approximated swept waveform (Fig 7.19) (computed response -2's complement truncation)



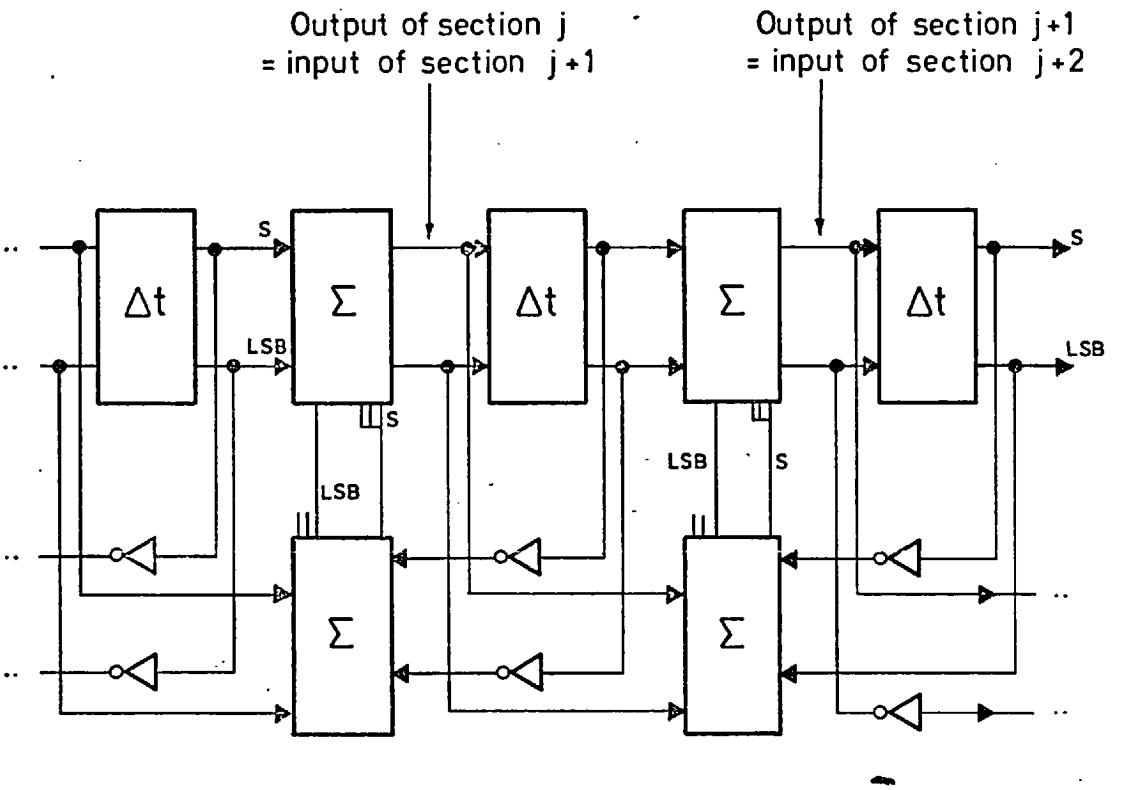
$$\sigma_S \cdot \sigma_1\ \sigma_2 \ldots \sigma_n = a_S \cdot a_1\ a_2 \ldots b_n + b_S\, b_1\, b_2 \ldots b_n$$

Fig.8.1 One's complement parallel adder



$$V_n = U_{n-1} + a(U_n - V_{n-1})$$

Fig.8.2a Single section first order digital delay, a = 0.25 using parallel one's complement arithmetic



N sections comprise 2N adders (Σ) and
N+1 delays (Δt)

Fig. 8.2b Two sections within cascade arrangement illustrating sharing of delay units

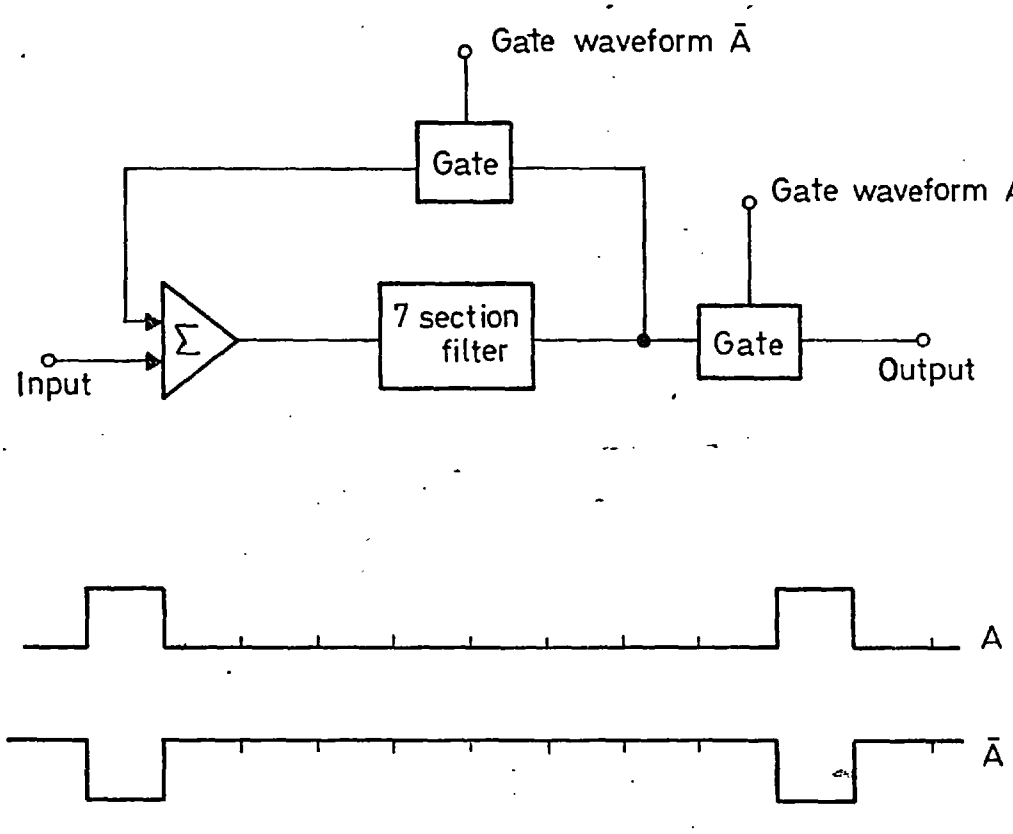


Fig.8.3 Recirculation scheme for 63 section response with 9 times recirculation

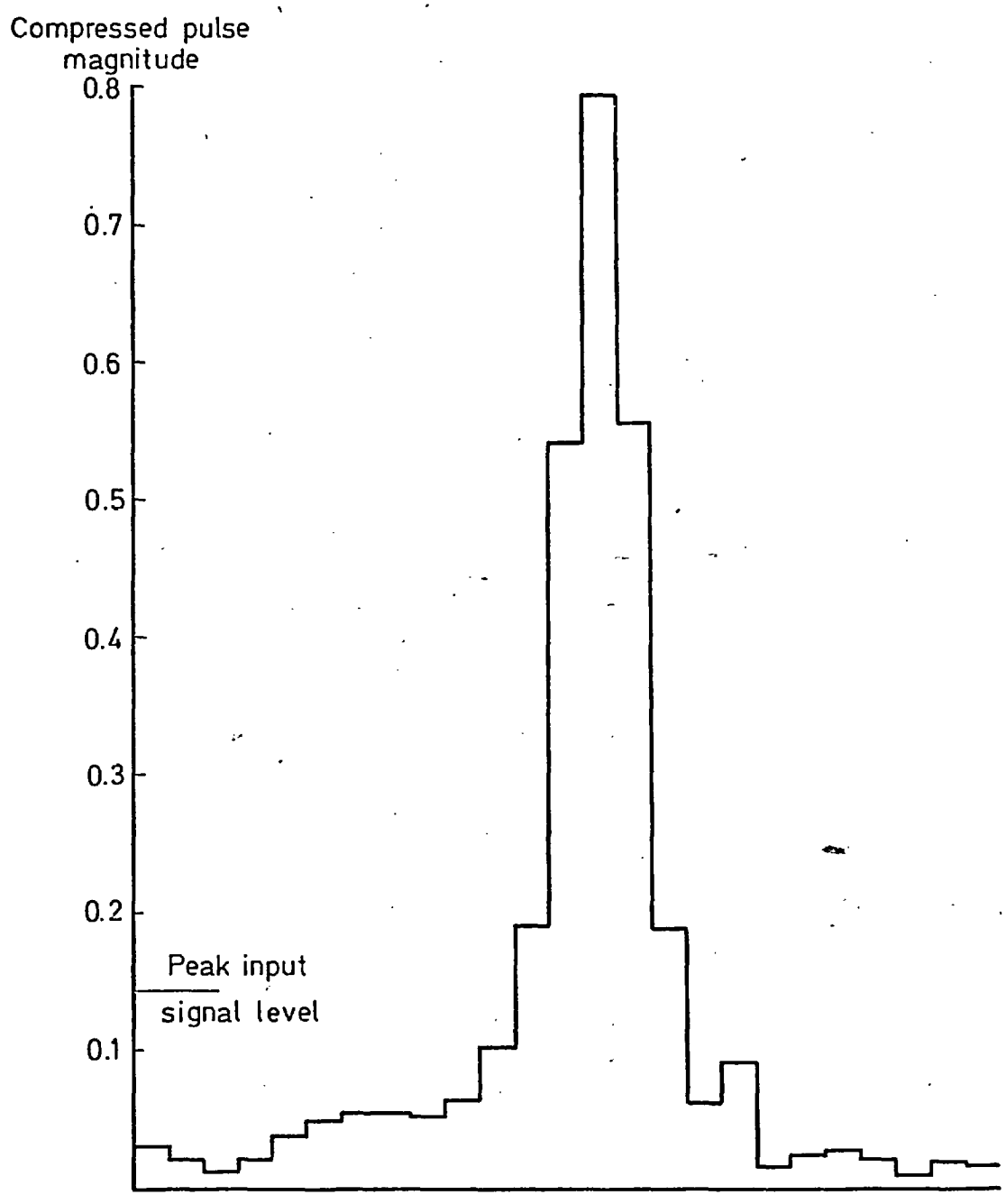


Fig. 8.4 Compressed pulse envelope for
N = 63 a = 0.25

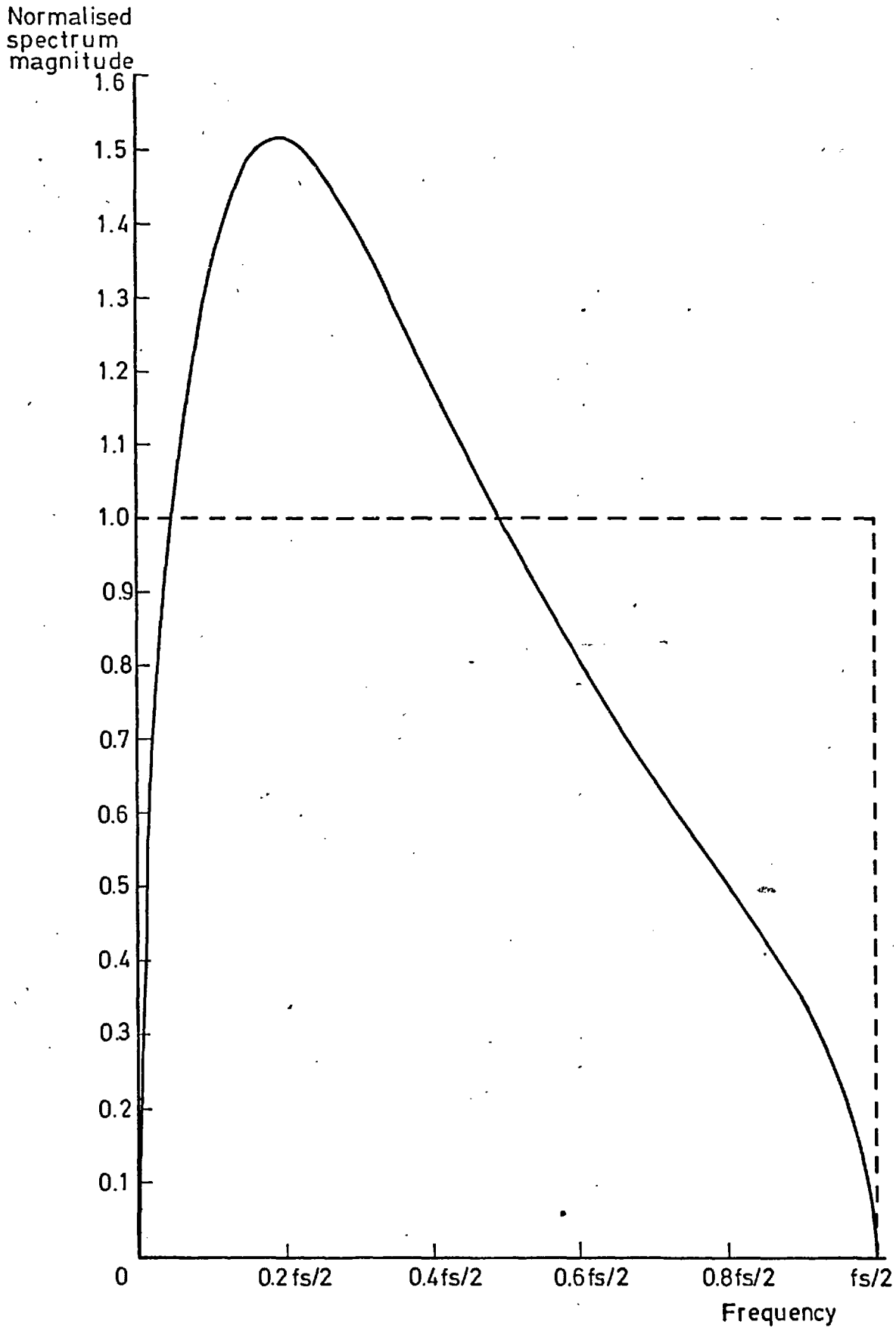


Fig.D.1 Stationary phase spectrum of signal matched to 42 section digital filter response

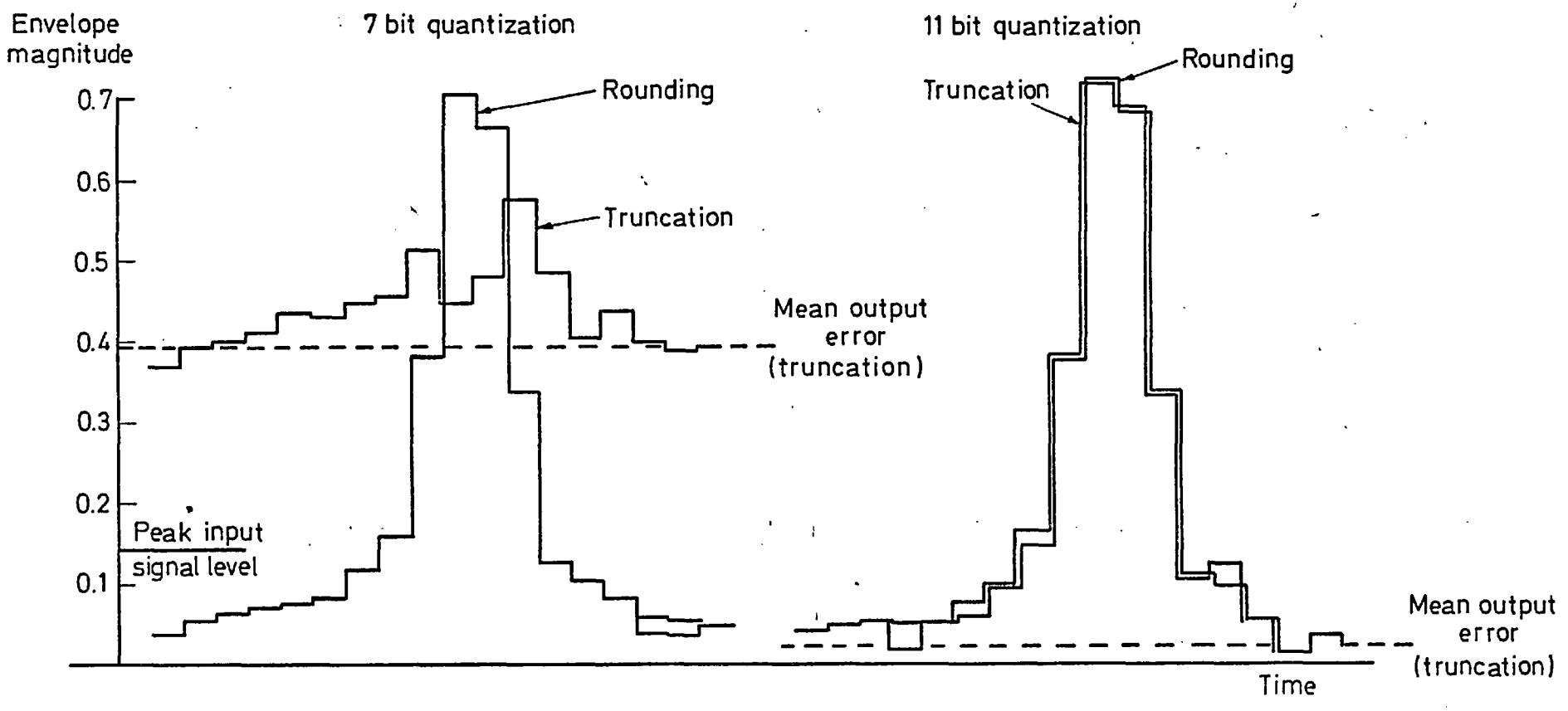
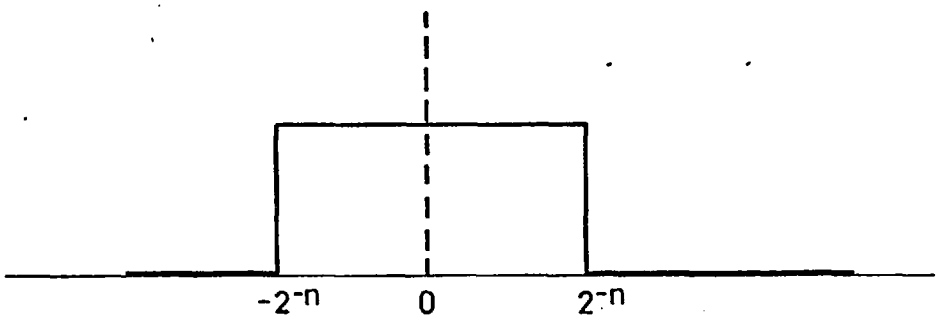
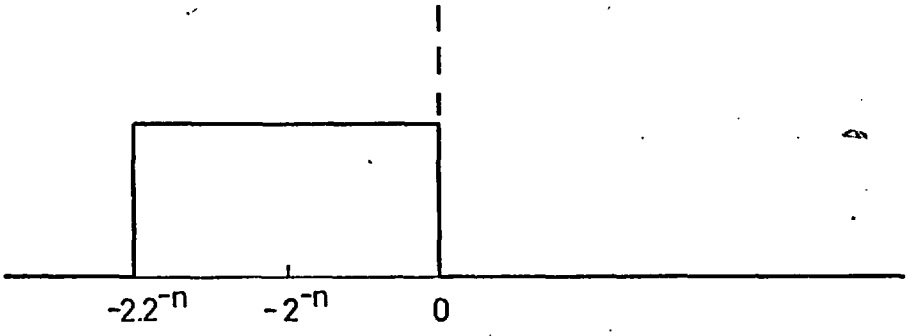


Fig.F.2 Compressed pulse envelopes (N=50) showing effect of rounding and truncation with 7 and 11 bit quantization



(A) Rounding



(B) Truncation

Fig. F.1 Probability density functions of multiplier errors for (A) rounding and (B) two's complement truncation

REFERENCES

1 J.R.KLAUDER, A.C.PRICE, S DARLINGTON, W.J.ALBERSHEIM, "The Theory and Design of Chirp Radars", BSTJ, Vol.39, No.4, July 1960.

2 B.M.OLIVER, "Not with a Bang, but a Chirp", Bell Laboratories Internal Memorandum, 1951.

3 G.W.BARNES, "Chirp Modulation for digital radio links between aircraft and synchronous satellites", RAE Tech Memo RAD 873, Jan 1969.

4 G.F.GOTT, "A study of Chirp Modulation techniques", Ph.D Thesis, University of Nottingham, Oct 1966.

5 C.E.COOK, M.BERNFELD, "Radar Signals", Academic Press, 1967.

6 D.O.NORTH, "Analysis of factors which determine signal-to-noise discrimination in radar", RCA Labs Rept PTR-6C, 1963.

7 D.H.FORGAN, "A study of Chirp Modulation techniques for satellite communication", Ph.D Thesis, University of Nottingham, Oct 1970.

8 J.G.LAWTON, "Comparison of binary data transmission systems", Proc. Second Natl. Conf. on Military Electronics, pp54-61, 1958.

9 J.E.MAY, JR, "Guided wave ultrasonic delay lines", in Physical Acoustics, Principles and Methods, Vol.1, Pt.A pp111-167, Academic Press, N.Y., 1964.

10 G.A.COQUIN and R.TSU, "Theory and performance of perpendicular diffraction delay lines", Proc. IEEE, Vol.53, pp581-591, 1965.

11 W.S.MORTLEY, "Pulse compression by dispersive gratings in crystal quartz", Marconi Review, Vol.28, p159, 1965.

12 F.J.MUELLER and R.L.GOODWIN, "A wideband microwave compressive receiver", IRE Intern. Conv. Record, Pt.3, pp103-119, 1962.

13 A.J.LAMBELL, "A tapped delay line compression network for linear FM signals", IEE Conf. Pub. No.20, p35, 1966.

14 Several methods summarised in Ref.5, Ch.14, pp491-501.

15 G.L.MATTHAEI, "Acoustic surface wave transversal filters", IEEE Trans on Circuit Theory, Vol. CT-20, No.5, pp459-470, Sept 1973.

16 R.C.WILLIAMSON and H.I.SMITH, "The use of surface-elastic-wave reflection gratings in large time-bandwidth pulse-compression filters", IEEE Trans on Microwave Theory and Techniques, Vol. MTT-21, No.4, pp195-203, April 1973.

17 Several methods summarised in Ref.5, Ch.14, pp501-

18 P.S.BRANDON et al, "The design and applications of dispersive networks and the associated weighting filters", Marconi Rept. No. RD/G1686, June 1964 (Ministry of Aviation Agreement KH/B/01235/CB14(b)2).

19 L.STORCH, "Synthesis of constant time delay ladder networks using Bessel polynomials", Proc. IRE, Vol.42, No.11, pp1666-1675, Nov 1954.

20 W.E.THOMSON, "Delay networks having maximally-flat frequency characteristics", Proc. IEE Vol.96, Pt.III, pp487-490, Nov 1949.

21 G.SZENTIRMAI, "The problem of phase equalization", IRE Trans, Vol. CT-6, pp272-277, Sept 1959.

22 S.DARLINGTON, "Network synthesis using Tchebycheff Polynomial series", BSTJ, Vol.32, p613, 1952.

23 B.D.RAKOVICH and D.M.RABRENOVICH, "Method of synthesis of phase-correcting networks", Proc. IEE, Vol.115, No.1, pp57-67, Jan 1968.

24 S.HELLERSTEIN, "Synthesis of all-pass delay equalizers", IRE Trans Circuit Theory, Vol. CT-8, pp215-222, Sept 1961.

25 G.C.TEMES and J.A.C.BINGHAM, "Iterative Chebyshev Approximation Technique for Network Synthesis", IEEE Trans Circuit Theory, Vol.14, No.1, pp31-37, March 1967.

26 T.R.O'MEARA, "Linear Slope delay filters for compression", PROC. IRE (Corres), Vol.48, pp1916-1918, Nov 1960.

27 M.K.WARD, "Low-pass linear slope delay filters for compression", Proc. IEEE (Corres) Vol.53, pp497-498, May 1965.

28 J.VALAND, "On the Linear-Slope Delay Approximation", Proc. IEEE (Letters) Vol.55, pp2059-2060, Nov 1967.

– "Addendum to 'On the Linear-Slope Delay Approximation' ", Proc. IEEE (Letters) Vol. , pp748-750, April 1968.

29 R.L.CRANE, "All-pass Network Synthesis", IEEE Trans on Circuit Theory, Vol. CT- , pp474-478, Dec 1968.

30 A.G.J.HOLT and J.P.GRAY, "Active all-pass sections", Proc. IEEE (Corres) Vol. 114, No.12, p1871, Dec 1967.

31 T.DELIYANNIS, "RC active all-pass sections", Electronics Letters, Vol.5, No.3, p59, Feb 1969.

32 W.F.LOVERING, "Analog computer simulation of transfer functions", Proc. IEEE (Corres), Vol.53, p306, Mar 1965.

33 V.G.K.MURTI and K.VENKATARAMANI, "Analog computer simulation of all-pass functions", Proc. IEEE, Vol.56, p206, Feb 1968.

34 J.E.B.PONSONBY, "Active all-pass filter using a differential operational amplifier", Electronics Letters, Vol.2, pp134-135, Apr 1966.

35 R.GENIN, "Realization of an all-pass transfer function using operational amplifiers", Proc. IEE (Letters), Vol.56, pp1746-1747, Oct 1968.

36 G.S.MOSCHYTZ, "A general all-pass network based on the Sallen-key circuit", IEEE Trans on Circuit Theory, Vol. CT-19, pp392-394, July 1972.

37 A.BUDAK and D.M.PETRELA, "Frequency limitations of active filters using operational amplifiers", IEEE Trans on Circuit Theory, Vol. CT-19, No.4, pp322-328, July 1972.

38 V.A.KISEL, "Phase-correcting circuits using delay lines", Elektrosiyaz, 1965.

39 C.P.ASH, Ph.D Thesis, Nottingham University, 1973.

40 J.J.KROSZCZYNSKI, "Pulse compression by means of linear period modulation", Proc. IEEE, Vol.57, No.7, pp1260-1266, July 1969.

ACKNOWLEDGEMENTS

The author is indebted to the following people for their assistance and encouragement: to Mr W A Johnson, Head of Airborne Communications Division in Radio Department, RAE at the time when the project was started, to Mr G May and Mr G W Barnes then of Radio Department whose wide knowledge and experience were invaluable in the early stages of the project, to Mr P Moore of Radio Department who assisted in the construction of the circuitry and who suffered frequent changes with equanimity, to present bosses Mr R L Dommett and Mr G J Herring of Special Weapons Department who provided the essential impetus to the completion, to Mrs R Lunt and Mrs M Davis of RAE for a superb typing job, to unnamed tracing pool staff for the Figures and finally to Mr R A King of Imperial College for technical guidance and not least for unbelievable patience over the years.